NASA CR-114485
ASRL TR 166-3
Available to the Public

DYNAMIC NONLINEAR ELASTIC STABILITY OF HELICOPTER ROTOR BLADES IN HOVER AND IN FORWARD FLIGHT

Peretz Friedmann
Pin Tong

May 1972

AEROELASTIC AND STRUCTURES RESEARCH LABORATORY
DEPARTMENT OF AERONAUTICS AND ASTRONAUTICS
MASSACHUSETTS INSTITUTE OF TECHNOLOGY
CAMBRIDGE, MASSACHUSETTS 02139

Prepared for
AMES DIRECTORATE
U.S. ARMY AIR MOBILITY RESEARCH AND DEVELOPMENT LABORATORY
AMES RESEARCH CENTER
MOFFETT FIELD, CALIFORNIA
Contract No. NAS2-6175

1. Report No.	2. Government Accession No.	3. Recipient's Catalog No.
NASA CR-114485		

4. Title and Subtitle	5. Report Date
DYNAMIC NONLINEAR ELASTIC STABILITY OF HELICOPTER ROTOR BLADES IN HOVER AND IN FORWARD FLIGHT	May 30, 1972
	6. Performing Organization Code

7. Author(s)	8. Performing Organization Report No.
PERETZ FRIEDMANN AND PIN TONG	ASRL TR 166-3
	10. Work Unit No.

9. Performing Organization Name and Address	11. Contract or Grant No.
Aeroelastic and Structures Research Laboratory Department of Aeronautics and Astronautics Massachusetts Institute of Technology Cambridge, Massachusetts 02139	NAS2-6175
	13. Type of Report and Period Covered
12. Sponsoring Agency Name and Address	Contractor Report
Ames Directorate, U.S. Army Air Mobility Research and Development Laboratory Ames Research Center, Moffett Field, California 94035	14. Sponsoring Agency Code

15. Supplementary Notes

Technical Monitor: Dr. R.A. Ormiston,
Ames Directorate, U.S. Army Air Mobility Research and Development Laboratory, Ames Research Center, Moffett Field, California 94035

16. Abstract

Equations for large amplitude coupled flap-lag motion of hingeless elastic helicopter blades are consistently derived. Only torsionally-rigid blades excited by quasi-steady aerodynamic loads are considered. The nonlinear equations of motion in the time and space variables are reduced to a system of coupled nonlinear ordinary differential equations with periodic coefficients, using Galerkin's method for the space variables. The nonlinearities present in the equations are those arising from the inclusion of moderately large deflections in the inertia and aerodynamic loading terms.

The resulting system of nonlinear equations has been solved, using an asymptotic expansion procedure in multiple time scales. The stability boundaries, amplitudes of nonlinear response, and conditions for existence of limit cycles are obtained analytically. Thus, the different roles played by the forcing function, parametric excitation, and nonlinear coupling in affecting the solution can be easily identified, and the basic physical mechanism of coupled flap-lag response becomes clear.

The effect of forward flight is obtained with the requirement of trimmed flight at fixed values of the thrust coefficient C_T.

A considerable amount of numerical results are presented.

Next, the general nonlinear equations of motion for a hingeless gelicopter blade, having flap-lag and torsional degrees of freedom, are consistently derived, and the various approximations involved in obtaining the elastic, inertia, and aerodynamic loads are clearly stated. The torsional degree of freedom is represented by elastic root torsion.

This system of equations is specialized for the case of coupled flap-lag-pitch blade motion in hovering flight. Using Galerkin's method with one elastic mode for each degree of freedom, the spatial variables are eliminated. Both linearized and completely nonlinear equations are obtained. The stability of the coupled flap-lag-pitch motions is investigated. Divergence and flutter boundaries, obtained from the solution of the linearized system, are presented.

The effect of the torsional degree of freedom on the flap-lag type of instability is investigated. Similarly, the effect of the lag degree of freedom on the pitch-flap type of instability is also considered. Numerical results illustrating these effects are given.

17. Key Words (Suggested by Author(s))	18. Distribution Statement
Helicopter Aeroelasticity Rotor Blade Dynamics Nonlinear Structural Dynamics Nonlinear, Blade Stability Rotor Blade Flutter Nonlinear Flutter Dynamic Stability Perturbation Methods Multiple Time Scaling	Unclassified, Unlimited

19. Security Classif. (of this report)	20. Security Classif. (of this page)	21. No. of Pages	22. Price*
Unclassified	Unclassified	297	$3.00

* For sale by the National Technical Information Service, Springfield, Virginia 22151

FOREWORD

This research was conducted by the Aeroelastic and Structures Research Laboratory, Department of Aeronautics and Astronautics, Massachusetts Institute of Technology, Cambridge, Massachusetts under Contract No. NAS2-6175, supervised by Dr. R.A. Ormiston of the Ames Directorate, U.S. Army Air Mobility Research and Development Laboratory, Ames Research Center, Moffett Field, California.

The authors wish to express their appreciation to Dr. R.A. Ormiston for his useful comments and suggestions.

The authors are deeply indebted to Professors R.H. Miller, N.D. Ham, T.H.H. Pian and E.A. Witmer for their extremely helpful advice and constructive criticism in the course of this study.

The digital computations were carried out at the MIT Information Processing Center.

CONTENTS

CONTENTS CONTINUED

CONTENTS CONTINUED

CONTENTS CONTINUED

CONTENTS CONTINUED

CONTENTS CONCLUDED

LIST OF ILLUSTRATIONS

LIST OF ILLUSTRATIONS CONTINUED

LIST OF ILLISTRATIONS CONCLUDED

SYMBOLS

a	Two-dimensional lift-curve slope
$\underset{\sim}{a}$	Acceleration vector in inertial space
a_o, a_1, a_2	Terms in perturbation expansion of χ_1
a_{o2}, a_{31}, a_{41}, a_{51}, a_{61}	Quantities used in the solution of the $0(\epsilon)$ equations
a_x, a_y, a_z	Components of $\underset{\sim}{a}$ in $\underset{\sim}{i}$, $\underset{\sim}{j}$, $\underset{\sim}{k}$ directions, respectively
$\bar{A}$	Tip loss coefficient
A_o	Amplitude in the solution of $0(\epsilon^{1/2})$ perturbed equations
$\bar{A}_o$, $\tilde{A}_o$	Modified values of A_o as defined in Section 5
A_i	Value of A_o at $\psi_o = 0$
A_{F1T}, A_{L1T}, A_{T1}	Generalized aerodynamic forces in flap, lag, and feathering equation when the torsional degree of freedom is included in the analysis
A_{Li}, A_{Fi}	Generalized aerodynamic force in the ith lagging and flapping mode, respectively
b	Half-chord nondimensionalized with respect to R
b_o, b_1, b_2	Terms in the perturbation expansion of χ_2
$b_\theta = \frac{32\theta}{\sigma a}$	Pitch-angle combination used in inflow calculation
$\bar{B}$	Tip-loss coefficient

$\bar{B}^i$	Generalized masses defined in Appendix M
c	Chord of the blade
$c_1, c_2, c_4, c_6,$ $c_7, c_{11}, c_{17}, c_{12}$	Quantities defined in Eqs. 3.25 and G.79
$C_T = \frac{T_h}{\rho_A(\pi R^2)(\Omega R)^2}$	Thrust coefficient
$C_H = \frac{H}{\rho_A(\pi R^2)(\Omega R)^2}$	Horizontal-force coefficient
$\tilde{C}_1$	Defined in Appendix F.3
C_{d_o}	Profile-drag coefficient
C_i	Element of a matrix required for calculation of the static quantities, defined in Eqs. N.10-N.12
$\bar{C}_i$	Quantity defined in Appendix B
$C(k)$	Theodorsen's lift deficiency function
C_p	Coefficient of proportionality in derivation
C_{DP}	Drag coefficient associated with equivalent flat-plate area of the helicopter
$d_1, d_2, D_1, D_2, \bar{D}_1, \bar{D}_2$	Quantities defined in Appendix H used for Cases C and D
dF_c	Elemental centrifugal force used in Appendix K
dF_{cy}	Component of dF_c in the y direction

dM_{prop}	Propeller moment per unit span used in Appendix K
$\tilde{D}_1$	Defined in Appendix F.3
D_p	Parasite drag, due to equivalent flat-plate area
D_{TOT}	Total drag
e_o	Distance at root between elastic axis (E.A.)
e_1	See Fig. 1
e_A	Distance between area centroid of tensile member and E.A.
$\tilde{E}_1$	Defined in Appendix F.3
E_{c1}, E_{c2}, $\bar{E}_{c1}$, $\bar{E}_{c2}$	Expressions associated with the elastic coupling effect, see Appendix L
$(EI)_y$	Bending stiffness in flapwise direction
$(EI)_z$	Bending stiffness for inplane bending
f	Equivalent flat-plate area
F_{SN}	Static nonlinear part of the flap equation, Eq. N.13

F_{o1}, F_{o2}, $\bar{F}_o$	Functions and quantities used in the perturbation solution for Case D
$\tilde{F}_1$	Quantity defined in Appendix F
$F_o(\psi_o, \theta_c)$, $F_o(\theta_1, \psi_o)$, $F_1(\psi_o, \theta_{c1}, a_o, b_o)$, $F_2(\psi_o, a_o, b_o)$	Functions used in the perturbation scheme defined in relations (G.10, G.11, G.15, G.49, G.50)
F^i	Flapping coefficients defined in Appendix C
F_{NL}	Nonlinear part of the flap equation, Eq. O.4
$F^{**}_{\chi_2}$, $F^{*}_{\chi_2}$, F_{χ_2}, F_{χ_1}, F^{**}_{ϕ}, F^{*}_{ϕ}, F_{ϕ}	Flutter derivatives associated with the flap equations defined in Appendix N; superscripts A and I on these quantities denote the aerodynamic and inertia part, respectively
g	Acceleration of gravity
g_o	Value of g_1^o at $\theta = \theta_c$
g_{o1}, g_{o2}	Terms in the perturbation expansion of g_1^o
g_1^o	Static value of generalized first flapping coordinate for $\mu = 0$
$\tilde{g}_1^o$	Static value of generalized first flapping coordinate for $\mu \neq 0$, used in trim calculation
g_{1c}, g_{1s}	Cosine and sine components of "flapping coefficients" for the hingeless blade
$g(x)$	Function determining spanwise variation of λ_{1c}

g_k	Generalized coordinate, kth normal flapping mode
g_{D1}, g_{D2}	Defined in Eqs. 3.25, damping coefficients
$\bar{g}_{D1}$, $\bar{g}_{D2}$, $\bar{g}_{D3}$	Equivalent damping terms in flap lag and feathering degrees of freedom defined in Appendix N.
g_{D10}, g_{D20}	Values of g_{D1} and g_{D2} at $\theta = \theta_c$
g_{SF}, g_{SL}	Dimensional structural damping coefficient in flap and lag, respectively
$\tilde{G}_1$	Quantity defined in Appendix F
h_1^o	Static value of generalized first lag
h_m	Generalized coordinate, mth normal inplane
H	Horizontal force
H_{o1}, H_{o2}, $\bar{H}_o$	Functions and quantities used in perturbation solution for Case D
$H_o(\psi_o,\theta_c)$, $H_o(\psi_o,\theta_1)$, $H_1(\psi_o,\theta_c, a_o, b_o)$, $H_2(\psi_o,\theta_c, a_o, b_o)$	Functions defined in Appendix G
i	$= \sqrt{-1}$

$\underset{\sim}{i}, \underset{\sim}{j}, \underset{\sim}{k}, \underset{\sim}{i}_1, \underset{\sim}{j}_1, \underset{\sim}{k}_1,$ $\underset{\sim}{i}_2, \underset{\sim}{j}_2, \underset{\sim}{k}_2,$ $\underset{\sim}{I}_1, \underset{\sim}{I}_2, \underset{\sim}{I}_3, \underset{\sim}{J}_1, \underset{\sim}{J}_2, \underset{\sim}{J}_3,$ $\underset{\sim}{K}_1, \underset{\sim}{K}_2, \underset{\sim}{K}_3$	Unit vectors for the various coordinate systems defined in Section 8.3.2.
i_1, i_2	Quantities used in the calculation of the divergence boundaries
$I = \frac{I_f}{I_b} =$	Inertia ratio
I_o	Polar moment of inertia of the whole blade
I_b	Mass moment of inertia of elastic part of the blade about its root, defined in Appendix B
I_f	Feathering moment of inertia of the whole blade
I_E	Equivalent feathering moment of inertia, Eq. 9.26
$J_1(\psi_o, \theta_c),$ $J_2(\psi_o, a_o)$	Functions defined in Appendix G
k_o	Polar radius of gyration of cross-sectional mass about its center of gravity
$K_1(\psi_o, \theta_c), K_2(\psi_o, a_o)$	Functions defined in Appendix G
K_E	Equivalent torsional stiffness, Eq. N.23

$\bar{K}_E$	K_E/I_E
K_ϕ	Torsional spring representing control system stiffness
ℓ	Length of blade capable of elastic deflection
L	Lift per unit span from unsteady two-dimensional wing theory
L_1, L_2	Linear differential operators defined in Appendix G
L^i	Lagging coefficients defined in Appendix C
$\underset{\sim}{L}_A$	Aerodynamic loading vector per unit span
L_Q	Quasi-steady part of L
L_{NL}	Nonlinear part of lag equation, Eq. O.5
L_{NS}	Static nonlinear part of lag equation, Eq. N.14
L_{yT}, L_{zT}, L_{xT}	Aerodynamic force per unit length in the y, z, and x directions, respectively, in the presence of the torsional degree of freedom
L_{Z_2}, L_{Y_2}	Components of $\underset{\sim}{L}_A$ in $\underset{\sim}{J}_2$ and $\underset{\sim}{K}_2$ directions
L_R	Lift of the whole rotor

$L^{**}_{\chi_1}$, $L^{*}_{\chi_1}$, L_{χ_1}, L_{χ_2}, L^{**}_{ϕ}, L^{*}_{ϕ}, L_{ϕ}	Flutter derivatives associated with the lag equation, defined in Appendix N; subscripts A and I on these quantities denote the aerodynamic and inertia part, respectively.
m	Mass of blade per unit length
m_T	Total mass of helicopter
M	Aerodynamic moment per unit span from unsteady two-dimensional wing theory
M_a	Component of aerodynamic torque loading per unit length in the $\underset{\sim}{i}$ direction
M_m, M_ℓ	Pitching and rolling moment, respectively, for one blade
M_{ma}, $M_{\ell a}$	Average values of M_m, M_ℓ per revolution
M_{mr}, $M_{\ell r}$	Pitching and rolling moments on the whole rotor
$\underset{\sim}{M}_P$	Moment vector about point represented by pitch bearing per unit length of the blade
$M_{P_{i_1}}$	Component of $\underset{\sim}{M}_P$ about feathering axis $\underset{\sim}{i}_1$ axis
M_{x_2}	Component of $\underset{\sim}{M}_A$ in the $\underset{\sim}{I}_2$ direction
$\underset{\sim}{M}_A$	Aerodynamic moment loading about E.A.
$\bar{M}_{L_i}$, $\bar{M}_{F_i}$	Generalized mass for the ith lag or flap mode, respectively; defined in Appendix B

M_R	Total bending moment at blade root
$M_{T.F.A.}$	Total feathering moment about feathering axis at blade root
$M(\Lambda)$	Matrix defined in Appendix G
$(M_\eta)_{ik\ell}$, $(M_\gamma)_{imr}$	Defined in Appendix B
n_b	Number of blades
$N_1(a_o, b_o)$, $N_2(a_o, b_o, a_1, b_1)$	Functions defined in Appendix G
p	General complex frequency
$\underset{\sim}{p}$	Total loading vector per unit length
$p_1, p_2 \cdots p_{30}$	Quantities used in the perturbation method defined in Appendix G
p_x, p_y, p_z	Resultant total loading per unit length in the x,y,z directions, respectively
p_{xI}, p_{yI}, p_{zI}	Resultant inertia loading per unit length in the x,y,z directions
$\overline{P}_{ikm}$	Quantity defined in Appendix B

q_{il}	Resultant torque loading per unit length in the feathering axis direction ($\underset{\sim}{i}_1$ direction, Fig. 29)
q_x, q_y, q_z	Resultant torque loadings per unit length in the x, y, z directions, respectively
$Q_1(a_o, b_o)$, $Q_2(a_o, b_o, a_1, b_1)$	Functions defined in Appendix G
r_R	Position vector of blade cross-section center of gravity, in the deformed state, in the rotating coordinate system
$\underset{\sim}{r}_E$	Position vector of a point on the blade elastic axis in the deformed state
R	Blade radius
$[R_1] \ldots [R_6]$	Various coordinate transformation matrices defined in Appendix I
s	Variable associated with phase-plane analysis
s_1, s_2	Roots of characteristic equation for linearized phase-plane analysis
S_{ij}	Elements of a matrix associated with the calculation of the linear static equilibrium position of the blade

t	Time
T	Tension in the blade in the x direction
T_1, T_2, T_3	Coefficients defined in the equations
T_h	Thrust of the rotor
T_{NL}	Nonlinear part of the torsional equation, Eq.
T_{SN}	Static nonlinear part of the feathering equation, defined in Eq. N.15
T^1, T^2, T^3	Quantities defined by Eqs. M.19 through M.21
$T^{**}_{N\chi_1}$, $T^{**}_{N\chi_2}$, $T^{**}_{N\phi}$	Quantities used in the nonlinear equations defined in Eqs. O.1 through O.3)
$T^{**}_{\chi_1}$, $T^{*}_{\chi_1}$, T_{χ_1}	Flutter derivatives associated with the feathering equation, defined in Appendix N.
$T^{**}_{\chi_2}$, $T^{*}_{\chi_2}$, T_{χ_2}	Superscripts A and I on these quantities denote
T^{**}_{ϕ}, T^{*}_{ϕ}, T_{ϕ}	the aerodynamic and inertia part, respectively
u, v, w	x,y,z displacement of a point on the elastic axis of the blade
$\hat{u}$, $\hat{v}$, $\hat{w}$	Displacements of a point on the elastic axis in the x,y,z directions, respectively, when $\Phi = 0$
U	Airstream velocity with respect to the blade at station x.
$\underset{\sim}{U}$	Airflow velocity vector relative to the blade at station x_o
U_p	Component of U perpendicular to x-y plane (hub plane), positive downward (Fig. 2)

U_T	Component of U in the x-y plane tangent to a circle having a radius x
U_{X_2}, U_{Y_2}, U_{Z_2}	Components of U in the $\underset{\sim}{I}_2$, $\underset{\sim}{J}_2$ and $\underset{\sim}{K}_2$ directions, respectively
v_e	Elastic part of the displacement of a point located on the elastic axis of the blade in the $\underset{\sim}{j}$ direction, defined in Fig. 27a
v_{e2}	Elastic displacement of a point on the elastic axis used in Appendix I
v_i	Induced velocity
v_r	Amplitude ratio at critical condition, Eq. 5.23
$\underset{\sim}{v}_{EA}$	Velocity of a point on the elastic axis of the blade
V	Velocity of forward flight of the whole rotor
$\underset{\sim}{V}_a$	Velocity of air
w_e	Elastic part of the displacement of a point located on the elastic axis of the blade in the $\underset{\sim}{k}$ direction, approximately. See Fig. 27a.
w_{e2}	Elastic part of the displacement of a point on the elastic axis used in Appendix I
x,y,z	Rotating orthogonal coordinate system (Fig. 1)

$x_o = x - e_1$ — Running spanwise coordinate for part of the blade free to deflection elastically; x_1 - same, dummy variable

x_1, y_1, z_1 — Coordinates of the blade cross-sectional center of gravity in its deformed position

x_I — Blade cross-sectional mass center-of-gravity offset from the elastic axis, shown in Fig. 28. Positive for c.g. before E.A.

x_A — Blade cross-sectional aerodynamic center offset from elastic axis, shown in Fig. 28. Positive for A.C. before E.A.

$\bar{x}_A = x_A/bR$

X_1, X_2 — Coefficients in perturbation expansion of X_H

X_H — Coupling term in flap equation

X_{H_o} — Value of X_H at $\theta = \theta_c$

$X(\xi,\eta)$ — Function used in phase-plane investigation of condition for suppressing secular terms

Y_1, Y_2 — Coefficients in the perturbation expansion of Y_G

Y_G — Coupling term in lag equation

Y_{G_o} — Value of Y_G at $\theta = \theta_c$

$\Upsilon(\xi,\eta)$	Function used in phase-plane investigation of condition for suppressing the secular terms

Greek Symbols

$\alpha_1,\alpha_2,\alpha_3,\bar{\alpha}_3$	Quantities defined in Appendix G
α_R	Angle of attack of the whole rotor
β	Inclination of feathering axis with respect to the hub plane measured in a vertical plane, (angle of built-in coning, shown in Fig. 27a
$\beta_1,\beta_2,\beta_3,\bar{\beta}_3$	Quantities defined in Appendix G
β_p	Angle of preconing, shown in Fig. 27b
γ	Locke number ($\gamma = 2\rho\frac{bR^5a}{I_b}$)
γ_m	mth inplane bending mode
γ_F	Flight path angle with respect to horizontal
δ	Quantity used in phase-plane investigation of condition for suppressing secular terms
ε	Perturbation parameter
$\tilde{\varepsilon}$	Perturbation quantity in uniformly valid expansion

ε_D	Symbolic quantity having the same order of magnitude like the displacements v and w
ζ, η	Coordinates attached to the blade cross section origin located at elastic axis, η coincides with the blade chord, ζ perpendicular to the blade chord, shown in Fig. 28. η also used in the phase-plane investigation for suppressing the secular terms.
$\eta_{11}, \eta_{12}, \eta_{21}, \eta_{22}$	Coefficients in the perturbation expansion of damping
$\eta_1(1)$	η_1 at $\bar{x}_o = 1$
$\tilde{\eta}_1(1)$	Quantity defined in Appendix F
η_k	kth flapwise normal bending mode
η_{SF_i}, η_{SL_i}	Structural damping coefficients defined in Appendix B

θ	Pitch angle measured from x,y plane
θ_c	Critical value of collective pitch
θ_1, θ_2	Coefficients in perturbation expansion of θ
θ_o	Constant part of collective pitch
θ_{1c}, θ_{1s}	Cyclic pitch component, multiplied by cos ψ, sin ψ, respectively
$\kappa_{2\theta 1}$, $\kappa_{2\lambda 1}$	Constants defined by Eqs. G.80 and G.81
$\kappa_1, \kappa_2 \ldots \kappa_{10}$	Quantities used in the perturbation method defined in Appendix G
$\lambda_H = \sqrt{\frac{C_T}{2}}$	Value of inflow ratio in hover
λ_{ap}	Approximate expression defined in Eq. D.9
λ	Inflow ratio, induced velocity over disk, positive down, nondimensionalized with respect to ΩR
λ_{1c}	$= \bar{\lambda}_{1c}\, g(x)$ first cosine component of λ
$\bar{\lambda}_{1c}$	Constant part of λ_{1c}
λ_o	Steady state part of λ constant over disc
λ_{oc}	Value of λ_o at critical condition
λ_1, λ_2	Coefficients in perturbation expansion of λ
μ	Advance ratio
μ_o, μ_1	Coefficients used in the perturbation expansion of the advanced ratio

ν	Quantity of order one, or less, used to characterize the closeness of ω_c to $\frac{1}{2}$ or 1
$\nu_6, \nu_5, \ldots \nu_o$	Coefficients of the characteristic equation used in Section 10
ξ	Coordinate used in the phase plane investigation of the condition for suppressing the secular term
ξ_o	Defined in Appendix H
π_1, π_2	Quantities used in the derivation of the conditions for suppressing the secular term
ρ	Quantity associated with limit cycle amplitude used in the investigation of the condition for suppressing the secular term
ρ_o	Value of ρ at $\psi_o = 0$
$\rho_{\ell.c.}$	Value of ρ for stable limit cycle
ρ_A	Density of air
$\rho(x,\eta)$	Mass of blade per unit area used in Appendix K
$\sigma = \frac{2bRn_b}{\pi R}$	Solidity ratio
ϕ	Quantity used in phase plane investigation of condition for suppressing the secular term

$\bar{X}_2, \tilde{X}_2$	Quantities defined in Eq. 5.95 and page
X_1, X_2	Amplitudes of oscillation about equilibrium position for flap and lag, respectively
ψ	Azimuth angle of blade ($\psi = \Omega t$) measured from straight aft position
$\psi_o, \psi_1, \ldots \psi_n$	Time scales used in multiple time-scale expansion
ω_c	Flutter frequency
$(\omega_c)_{1,2}$	Flutter frequencies used in the complete linearized flap-lag-pitch problem
ω_{Fi}, ω_{Li}	Natural frequency of the ith flap or lag mode
$\bar{\omega}_{F1N}, \bar{\omega}_{L1N}$	Nonrotating flap and lag frequencies, respectively, nondimensional with respect to Ω
$\omega_{F10}, \omega_{L10}$	Unperturbed value of first flap and lag natural frequency, respectively
Ω	Speed of rotation

Special Symbols

$\overline{(\ )}$	Nondimensionalized quantity unless otherwise stated, lengths associated with elastic bending properties, nondimensionalized with respect to ℓ; all others with respect to R; frequencies with respect to Ω; mass properties with respect to I_b
$(\ )'$	Differentiation with respect to $\overline{x}_o$
$\overset{*}{(\ )}$	Differentiation with respect to ψ
$(\ )^*$	Complex conjugate of the quantity in brackets
$\overset{*}{\widetilde{(\ )}}$	Derivative of the product in the bracket
$(\ )_R$, $(\ )_I$	Subscripts R and I denote, respectively, the real and imaginary part of the appropriate quantity
$\underset{\sim}{(\ )}$	The symbol $\sim$ beneath a quantity denotes a vector or a matrix
$\underset{\sim}{(\ )}^{-1}$	Denotes the inverse of a matrix
$[\ ]^T$	Transpose of a matrix [ ]

SECTION 1

INTRODUCTION

1.1 General

A helicopter blade in forward flight is exposed to a severe aeroelastic environment. Periodic, unsteady airloads act upon the blade due to a combination of forward flight and rotation of the blade. Strong inertia, including Coriolis forces, due to the relatively large speed of rotation further complicate the problem. Therefore, the aeroelastic stability and the response of the blade are of extreme importance for both flutter calculation and vibration level estimation. Vibration level predictions are required for both the linear and the nonlinear range of blade motion in order to evaluate the fatigue life of the blade and the blade supporting structure. The nonlinearities are those arising from the inclusion of moderately large deflections in the inertia and aerodynamic loading terms. Therefore, during the last thirty years, a considerable amount of work associated with helicopter blade dynamic and aeroelastic problems has been done.

A good review and an elementary description of the various dynamic and aeroelastic problems associated with VTOL vehicles, in general, and helicopter blades, in particular, have been given recently by Loewy in Ref. 32. A considerable amount of the work done up to 1964, in the general area of helicopter blade dynamic response and flutter, has also been reviewed with a considerable amount of detail by Bielawa (Ref. 35). In this report, no attempt will be made to repeat the reviews given in Refs. 32 and 35. The only references cited will be those pertinent to the problem being treated.

This report is divided, essentially, into three distinct and almost independent parts:

(a) The first part, composed of Sections 1 through 7, deals with the somewhat controversial problem of flap-lag-type instability of torsionally-rigid, hingeless helicopter blades. This type of instability is analyzed in the nonlinear range of blade

motion in both hover and in forward flight. The main purpose of this part is the identification of the physical mechanism of the instability and the determination of the respective roles of the forcing function, parametric excitation, and nonlinear coupling in affecting the coupled flap-lag response.

(b) The second part, composed of Section 8, presents a consistent derivation of the general nonlinear equations of motion for a hingeless helicopter blade, having flap-lag and torsional degrees of freedom. The torsional degree of freedom is represented by elastic root torsion; thus distributed torsion and built-in twist are not treated. All second-order terms (in terms of the displacements) in the flap and lag equations are retained, while third-order terms are neglected. In the feathering equation, some important nonlinear effects are included by retaining third-order terms. The main purpose of this section is to emphasize the various approximations involved in obtaining the elastic, inertia, and aerodynamic loads.

Hopefully, these equations will serve as a starting point for future work in this field.

(c) The third part, Sections 9 through 11, is devoted to the investigation of the stability of coupled flap-lag-pitch blade motion. This treatment is limited to the case of hovering flight. Due to the novel aspects of the various effects included in the equations of motion, both divergence and flutter boundaries had to be obtained from the linearized equations of motion.

The main purpose of this part is to illustrate how the stability boundaries obtained in the first part of this report are affected by the addition of the torsional degree of freedom.

Each part of this report will have its own introductory section in which the pertinent literature will be surveyed.

1.2 Introduction to the Flap-Lag Stability Problem

1.2.1 Brief Review of Past Work

In the first part of this report, the flap-lag-type instability of torsionally-rigid hingeless blades in the nonlinear range of blade motion will be treated. This problem was first treated by Young (Ref. 1) with a restrictive analytical approach. Modal equations of motion were obtained, but the numerical results were evaluated for a blade represented by a centrally-hinged, spring-restrained, equivalent model. Young concluded that the triggering mechanism of the flap-lag-type instability is the lag degree of freedom.

Hohenemser (Ref. 2) treated the same problem, using a somewhat unconventional numerical integration scheme. Due to the various approximations made in Ref. 2, the results presented there are of a qualitative nature.

A good treatment of the linear stability of the blade in hover has been made recently by Ormiston and Hodges (Ref. 3). In this work, both the centrally-hinged, spring-restrained and modal-elastic representation of a hingeless blade were used. Stability boundaries for the linear case were obtained.

The linearized equations of motion in flap lag, at high values of advance ratio, were treated by Hall (Ref. 4). Using a rigid, offset hinged, spring-restrained representation of the blade, multivariable Floquet theory was applied to investigate the stability of blade motion. Reverse flow effects were included. The trim conditions associated with the variation of μ were vaguely mentioned without specifying what they were or how they were satisfied. The primary purpose of the Ref. 4 work was the investigation of the blade response in the presence of a simple control system; a stability investigation in the aeroelastic sense was not intended.

The flap-lag instability and response for both articulated and hingeless blades was also treated by Elman (Ref. 5). Reverse flow and stall effects were included in this work. Unfortunately, the description of the theoretical part of this work was very brief.

The transient nonlinear flap-lag motion of a fully-articulated rotor blade was also treated by Jenkins in Ref. 38. Reverse flow effects were included; two-dimensional stall and compressibility effects could also be accounted for, but were not used in the numerical calculations. The equations of motion were solved using direct numerical integration. The physical explanation of the mechanism of the instability was not attempted due to the purely numerical nature of this work.

The perturbation method in multiple time scales (Ref. 6) has been first applied to the nonlinear flap-lag problem by Tong (Refs. 7 and 8).

1.2.2 Objectives of the Present Study

A preliminary study of the nonlinear flap-lag probem has been made in Ref. 41 using numerical integration. The main purpose of Ref. 41 is to gain some physical insight into the problem before applying the perturbation method.

In the present report, a consistent system of equations representing the flap-lag motion of a hingeless elastic blade with moderate nonlinearity has been derived. Modes are assumed and the spatial variables are eliminated, using Galerkin's method. The resulting system of equations is solved using the perturbation method in multiple time scales (Refs. 7 and 8). For some cases, results were also obtained by direct numerical integration.

The effect of forward flight is studied with the additional requirement that the helicopter should be in trim, i.e., the thrust coefficient is kept constant during the increase in the advance ratio; thus the effect of forward flight on a fixed configuration can be obtained. The effects associated with the trim requirement were disregarded in the other works dealing with forward flight, except, possibly, in Ref. 4.

SECTION 2

BASIC ASSUMPTIONS

The rotor blade can be considered to be a thin flexible beam attached to the hub at its inboard end and free at its outboard end. Figure 1 describes the geometry of the problem.

The large deflections will have only a small effect on the tension in the blade due to elastic effects, because one of its ends is free (in fact it can be shown that this is a third-order effect in terms of deflections); therefore, a linear treatment of the elastic restoring forces can be considered adequate. Such a theory has been derived by Houbolt (Ref. 10). It is very similar to the usual engineering beam theory.

It is assumed that the blade is initially straight, with its elastic axis coincident with the x-axis. The blade is torsionally rigid. It has a pitch setting of θ and it can bend in both the y and the z directions. The cross section of the blade is assumed to be symmetrical about the major principal axis.

A quasi-steady two-dimensional aerodynamic strip theory is used as justified by Miller (Ref. 11) and apparent mass effects are neglected. This means that in the usual unsteady aerodynamic expressions, Theodorsen's lift deficiency function $C(k) = 1$. Stall, compressibility, and reversed flow effects are neglected; thus, the aerodynamic load is applicable to moderately large advance ratios.

Periodicity and spanwise variation of rotor inflow is restricted to the first cosine component:

$$\lambda = \lambda_0 + \bar{\lambda}_{1c}\, g(x) \cos\psi \tag{2.1}$$

In deriving the equations of motion, an x, y, z coordinate system (see Fig. 1) rotating with the shaft of the helicopter and attached to the blade is used.

SECTION 3

THE EQUATIONS OF MOTION

3.1 Brief Derivation of the Equations of Motion

A brief derivation of the equations of motion is given below. A more complete and detailed derivation is given in Sec. 8. The equations of dynamic equilibrium of a blade undergoing only bending in flap and lag can be taken from Ref. 10:

$$\frac{\partial^2}{\partial x_o^2}\left\{\left[(EI)_y\cos^2\theta+(EI)_z\sin^2\theta\right]\frac{\partial^2 w}{\partial x_o^2}+\left[(EI)_z-(EI)_y\right]\sin\theta\cos\theta\frac{\partial^2 v}{\partial x_o^2}\right.$$
$$\left.-Te_A\sin\theta\right\}-\frac{\partial}{\partial x_o}\left[T(x_o)\frac{\partial w}{\partial x_o}\right]=p_z$$

$$\frac{\partial^2}{\partial x_o^2}\left\{\left[(EI)_z-(EI)_y\right]\sin\theta\cos\theta\frac{\partial^2 w}{\partial x_o^2}+\left[(EI)_y\sin^2\theta+\right.\right. \tag{3.1}$$
$$\left.\left.(EI)_z\cos^2\theta\right]\frac{\partial^2 v}{\partial x_o^2}-Te_A\cos\theta\right\}-\frac{\partial}{\partial x_o}\left[T(x_o)\frac{\partial v}{\partial x_o}\right]=p_y$$

where p_z and p_y, which are given in Eqs. 3.3 and 3.4, include the pertinent aerodynamic and inertial forces.

For present purposes, it is assumed that the elastic axis, area centroid, aerodynamic center, center of gravity, and feathering axis of the blade are all coincident. The offset between these points in the cross section of the blade is important only when one considers the torsional degree of freedom also.

For moderate angles of pitch setting, the elastic coupling due to pitch setting was neglected. This effect was included in the coupled flap-lag pitch equations treated in the last part of this study. Reference 3 illustrates, in detail, the importance of this effect, which is strongly stabilizing. As pointed out in Appendix L, a consistent treatment of this effect requires a more sophisticated treatment of the elastic mode shape than the one used in this study. Therefore,

the elastic coupling will be neglected in order to be able to study conveniently the destabilizing aerodynamic and inertial flap-lag coupling terms. In a practical sense, this assumption is a limiting case of reduced elastic coupling which can occur for hingeless rotor blades with nonuniform stiffness distribution.

$$\frac{\partial^2}{\partial x_o^2}\left[(EI)_y \frac{\partial^2 w}{\partial x_o^2}\right] - \frac{\partial}{\partial x_o}\left[T(x_o)\frac{\partial w}{\partial x_o}\right] = p_z$$

$$\frac{\partial^2}{\partial x_o^2}\left[(EI)_z \frac{\partial^2 v}{\partial x_o^2}\right] - \frac{\partial}{\partial x_o}\left[T(x_o)\frac{\partial v}{\partial x_o}\right] = p_y \qquad (3.2)$$

The loading terms in the z and y direction, with nonlinearities accurate up to third order in displacements can be written as

$$p_z = L_z - \Omega^2 m \overset{**}{w} - g_{SF}\overset{*}{w}\Omega \qquad (3.3)$$

$$p_y = L_y - m\Omega^2\left[\overset{**}{v} - (e_o + v) + 2\overset{*}{v}\right] - g_{SL}\Omega\overset{*}{v} \qquad (3.4)$$

$$p_x = -\frac{\partial T}{\partial x_o} = m\Omega^2\left(x_o + e_1 + 2\overset{*}{v}\right) \qquad (3.5)$$

The last terms in Eqs. 3.3 and 3.4 represent viscous-type of structural damping.

The boundary conditions for a hingeless blade can be taken as

$$w(0,t) = \frac{\partial w(0,t)}{\partial x_o} = \frac{\partial^2 w(\ell,t)}{\partial x_o^2} = \frac{\partial^3 w(\ell,t)}{\partial x_o^3}$$

$$v(0,t) = \frac{\partial v(0,t)}{\partial x_o} = \frac{\partial^2 v(\ell,t)}{\partial x_o^2} = \frac{\partial^3 v(\ell,t)}{\partial x_o^3} \qquad (3.6)$$

Next, in order to apply Galerkin's method, the displacements u, v, w of the beam are expressed in terms of the normal modes of the beam in flap and lag

$$w = \ell \eta_k(x_0)\, q_k(t) = \sum_k \ell \eta_k(x_0)\, q_k(t) \tag{3.7}$$

$$v = -\ell \gamma_m(x_0)\, h_m(t) \tag{3.8}$$

$$u \cong -\frac{1}{2} \int_0^{x_0} \left[\left(\frac{\partial w}{\partial x_1} \right)^2 + \left(\frac{\partial v}{\partial x_1} \right)^2 \right] dx_1 \tag{3.9}$$

Equation 3.9 represents the shortening effect or inboard movement of a mass point on the blade due to bending, under the assumption that the blade is inextensible.

Note, that whenever repeated indices are used in this report, the summation convention is always implied, unless otherwise stated.

The substitution of Eqs. 3.7 through 3.9 into Eqs. 3.3 through 3.5 and 3.2, together with the application of Galerkin's method on the resulting system of equations, yields after a considerable amount of algebraic manipulation

$$\bar{M}_{Fi}\, \ddot{q}_i + \bar{g}_{SFi}\, \dot{q}_i + \bar{M}_{Fi}\, \bar{\omega}_{Fi}^2\, q_i = 2\, \bar{P}_{ikm}\, q_k\, h_m + \frac{\ell^2}{\Omega^2 I_b} \int_{\bar{A}}^{\bar{B}} L_z\, \eta_i\, d\bar{x}_0 \qquad i = 1, 2, \ldots N \tag{3.10}$$

$$\bar{M}_{Li}\, \ddot{h}_i + \bar{g}_{SLi}\, \dot{h}_i + \bar{M}_{Li}\, \bar{\omega}_{Li}^2\, h_i = \left[2\, S_{imr} - 2 (\bar{M}_\gamma)_{imr} \right] \dot{h}_m h_r - 2 (\bar{M}_\eta)_{ike}\, \dot{q}_k\, q_e - \bar{e}_o\, \bar{C}_i - \frac{\ell^2}{\Omega^2 I_b} \int_{\bar{A}}^{\bar{B}} L_y\, \gamma_i\, d\bar{x}_0 \qquad i = 1, 2, \ldots M \tag{3.11}$$

In obtaining Eqs. 3.10 and 3.11, the boundary conditions, Eqs. 3.6, and the orthogonality relations for rotating beams, given in Appendix A have been

used. The various quantities $\bar{M}_{Fi}$, $\bar{P}_{ikm}$ ... etc., used above are defined in Appendix B and represent generalized masses.

Next, the aerodynamic loading terms will be evaluated. The loading term in the z-direction can be obtained from Miller and Ellis (Ref. 11) or from Bisplinghoff (Ref. 12).

$$L_z = a\rho b R U_T \left(U_T \theta - U_p\right) \tag{3.12}$$

The aerodynamic load in the y-direction (see Fig. 2)

$$L_y = -\rho a b R \left[U_p \left(U_T \theta - U_p\right) + \frac{C_{d_o}}{a} U_T^2\right] \tag{3.13}$$

where the velocities U_p, U_T can be written as

$$U_p = \Omega R \left(\lambda + \mu \frac{\partial w}{\partial x_o} \cos\psi\right) + \dot{w}^* \Omega \tag{3.14}$$

$$U_T = \Omega R \left(\mu \sin\psi + \bar{x}\right) + \Omega \dot{v}^* \tag{3.15}$$

The expressions for the aerodynamic loads given above represent aerodynamic loads, for moderate angles of collective pitch θ. The nonlinearities originating from these expressions are due to the retention of the second-order terms due to large deflections in the appropriate relations for $U_T U_P$, U_T^2, and U_P^2.

The reference plane used in evaluating relations in Eqs. 3.12 through 3.15, for a hingeless blade, is the hub plane. Therefore, in an exact formulation, the terms associated with the cyclic pitch variation should also appear in these equations. Keeping in mind that the primary aim of this report is the evaluation of the nonlinear effects associated with large displacements, and the determination of the respective roles of parametric excitation* and forcing due to forward flight, it was decided to treat the effect of cyclic pitch variation only in a later part of this investigative effort which will also include the torsional effects.

*Note that in this study, the term parametric excitation, stands for the effect of the time dependent coefficients in the equations of motion.

The substitution of Eqs. 3.7 through 3.9, 3.14 and 3.15 into Eqs. 3.12 and 3.13 will yield the appropriate expressions for L_z and L_y. A further integration will give the generalized aerodynamic loads required for Eqs. 3.10 and 3.11:

$$A_{Fi} = \frac{\ell^2}{\Omega^2 I_b} \int_{\bar{A}}^{\bar{B}} L_z \eta_i \, d\bar{x}_o \tag{3.16}$$

$$A_{Li} = -\frac{\ell^2}{\Omega^2 I_b} \int_{\bar{A}}^{\bar{B}} L_y \gamma_i \, d\bar{x}_o \tag{3.17}$$

The complete expressions for A_{Fi}, A_{Li} are given in Appendix C where the various flap coefficients F^1 ... F^{20} and lag coefficients L^1 ... L^{19} are also defined.

Using Eqs. 3.10, 3.11, 3.16, and 3.17, the final form of the general equations of motion, for an arbitrary number of modes, can be written in compact form

$$\bar{M}_{Fi} \ddot{g}_i^* + \bar{g}_{SFi} \dot{g}_i^* + \bar{M}_{Fi} \bar{\omega}_{Fi}^2 g_i = 2 \bar{P}_{ikm} g_k \dot{h}_m^* + A_{Fi}$$

$$i = 1, 2, \ldots, N \tag{3.18}$$

$$\bar{M}_{Li} \ddot{h}_i^* + \bar{g}_{SLi} \dot{h}_i + \bar{M}_{Li} \bar{\omega}_{Li}^2 h_i = \left[2 \bar{S}_{imr} - 2 (\bar{M}_\gamma)_{imr} \right] \dot{h}_m^* h_r$$

$$- 2 (\bar{M}_\eta)_{ike} \dot{g}_k^* g_e - e_o \bar{C}_i + A_{Li}$$

$$i = 1, 2, \ldots, M \tag{3.19}$$

3.2 Equations of Motion for the Two-Mode Case

The solution for the system of equations derived in the previous section for an arbitrary number of modes is very difficult and complex. Therefore, in this report only one elastic mode in each degree will be considered.

The static equilibrium condition in hover ($\mu = 0$, with all time derivatives equal to zero) denoted by g_1^o, h_1^o, will be used as the natural equilibrium state of the system.

$$g_1^o = \frac{1}{\bar{M}_{F1}\bar{\omega}_{F1}^2}\frac{\gamma}{2}\left(\frac{\ell}{R}\right)\left(F^1\theta - F^2\lambda_o\right) \tag{3.20}$$

$$h_1^o = \frac{1}{\bar{M}_{L1}\bar{\omega}_{L1}^2}\left\{\frac{\gamma}{2}\left(\frac{\ell}{R}\right)\left[\lambda_o\left(L^1\theta - L^2\lambda_o\right) + \frac{C_{do}}{a}L^4\right] - \bar{e}_o\bar{C}_1\right\} \tag{3.21}$$

In the following, the lower indices on the various L^i and F^i coefficients will be dropped. By expressing

$$\begin{aligned} g_1 &= g_1^o + \chi_1 \\ h_1 &= h_1^o + \chi_2 \end{aligned} \tag{3.22}$$

and considering only the case $\lambda_{\overline{1c}} = 0$, Eqs. 3.18, 3.19 and 3.20 through 3.22 become

$$\begin{aligned} &\overset{**}{\chi}_1 + \left(g_{D1} + C_1F^9\mu\sin\psi\right)\overset{*}{\chi}_1 + \left[\bar{\omega}_{F1}^2 + C_2\mu\cos\psi\left(F^6 - \frac{\ell}{R}F^{14}\overset{*}{\chi}_2\right)\right]\chi_1 = \\ &C_2\left[\left(2\theta F^2 - \lambda_o F^3\right) - 2\left(\frac{\ell}{R}\right)F^{11}\theta\overset{*}{\chi}_2\right]\mu\sin\psi + \\ &\overset{*}{\chi}_2\left[C_4\chi_1 + X_H + C_1\left(\frac{\ell}{R}\right)\theta F^{13}\overset{*}{\chi}_2 + C_1\left(\frac{\ell}{R}\right)F^{15}\overset{*}{\chi}_1\right] \\ &+ C_2 g_1^o\left[-F^6 + \left(\frac{\ell}{R}\right)F^{14}\overset{*}{\chi}_2\right]\mu\cos\psi + \\ &C_2\left[\frac{F^3\theta}{2}\mu^2 - \mu^2F^3\theta\cos 2\psi + \frac{\mu^2}{2}F^7\left(g_1^o + \chi_1\right)\sin 2\psi\right] \end{aligned} \tag{3.23}$$

$$\begin{aligned} &\overset{**}{\chi}_2 + g_{D2}\overset{*}{\chi}_2 + \bar{\omega}_{L1}^2\chi_2 = \mu C_6L^2\theta\lambda_o\sin\psi + \mu C_6\left(g_1^o + \chi_1\right)\left(\theta L^{10} - \right. \\ &\left.2\lambda_o L^{11}\right)\cos\psi + \overset{*}{\chi}_1\left[Y_G - C_{11}\chi_1 + C_7\mu\theta L^{18}\sin\psi - 2\mu C_7L^{17}\left(\chi_1 + g_1^o\right)\cos\psi\right. \\ &\left. - C_7\left(\frac{\ell}{R}\right)\left(L^{18}\chi_1 + \theta L^{19}\overset{*}{\chi}_2\right)\right] - \\ &\mu C_7\overset{*}{\chi}_2\left[\left(g_1^o + \chi_1\right)\theta L^{16}\cos\psi\right] + \\ &C_6\left[\theta\frac{\mu^2}{2}L^{17}\sin 2\psi\left(g_1^o + \chi_1\right) + 2\frac{C_{do}}{a}\mu L^1\sin\psi\right] \end{aligned} \tag{3.24}$$

In the lag equations, terms proportional to $(C_{d_o}/a)\mu^2$ have been neglected because they are small quantities. The various quantities used in the last two equations are defined below.

$$C_1 = \frac{\gamma}{2\bar{M}_{F1}}\left(\frac{\ell}{R}\right)^3$$

$$C_2 = \frac{\gamma}{2\bar{M}_{F1}}\left(\frac{\ell}{R}\right)^2$$

$$g_{D1} = \frac{\bar{g}_{SF1}}{\bar{M}_{F1}} + \left(\frac{\ell}{R}\right)^3 \frac{\gamma}{2\bar{M}_{F1}} F^8$$

$$C_4 = 2\,\bar{P}_{111}/\bar{M}_{F1}$$

$$C_6 = \frac{\gamma}{2\bar{M}_{L1}}\left(\frac{\ell}{R}\right)^2$$

$$C_7 = \frac{\gamma}{2\bar{M}_{L1}}\left(\frac{\ell}{R}\right)^3 \qquad (3.25)$$

$$C_{11} = 2(\bar{M}_\eta)_{111}/\bar{M}_{L1}$$

$$C_{17} = -\left[\frac{\bar{S}_{111} - (\bar{M}_\beta)_{111}}{\bar{M}_{L1}}\right] \cong 0$$

$$g_{D2} = \frac{g_{SL1}}{\bar{M}_{L1}} + C_7\, 2\,\frac{C_{d_o}}{a} L^{14} + C_7 L^{13}\lambda_o\theta$$

$$X_H = C_4 g_1^\circ - C_1\left(2\theta F^{10} - F^{11}\lambda_o\right)$$

$$Y_G = -C_{11} g_1^\circ + C_7\left(L^7\theta - 2\lambda_o L^8\right)$$

The equations above are a coupled nonlinear system of Hill-type equations under the influence of periodic forcing. The periodicity of the coefficients of the equations and the periodic forcing are due to forward flight.

The terms g_{D1} and g_{D2} represent the damping present in the system. The damping is partly of aerodynamic origin and partly from structural damping. The damping in the lag degree of freedom is very small; therefore this is the potentially unstable mode.

SECTION 4

SOLUTION FOR THE LINEAR SYSTEM IN HOVER

For the case of hovering flight $\mu = 0$, when Eqs. 3.23 and 3.24 are linearized, the resulting system of equations is simply:

$$\begin{aligned} \overset{**}{\chi}_1 + g_{D_1} \overset{*}{\chi}_1 + \bar{\omega}_{F_1}^2 \chi_1 - X_H \overset{*}{\chi}_2 = 0 \\ \overset{**}{\chi}_2 + g_{D_2} \overset{*}{\chi}_2 + \bar{\omega}_{L_1}^2 \chi_2 - Y_G \overset{*}{\chi}_1 = 0 \end{aligned} \tag{4.1}$$

The critical condition for the complete system (Eqs. 3.23 and 3.24) will be given by the flutter or critical condition of linearized system (Eq. 4.1). The flutter condition is characterized by the existence of a small amplitude oscillation for Eqs. 4.1. Assuming the solution in the form

$$\chi_1 = A_1 e^{p\psi} \quad ; \quad \chi_2 = A_2 e^{p\psi} \tag{4.2}$$

Substitution of Eq. 4.2 into Eq. 4.1 yields the following characteristic equation

$$\left(p^2 + p g_{D_1} + \bar{\omega}_{F_1}^2\right)\left(p^2 + g_{D_2} p + \bar{\omega}_{L_1}^2\right) - p^2 X_H Y_G = 0 \tag{4.3}$$

For a small value of θ, the root of Eq. 4.3 has Real (p) < 0 and the solution is stable. For the critical value $\theta = \theta_c$, the system is neutrally stable. For $\theta > \theta_c$, at least one of the roots of Eq. 4.3 has Real (p) > 0 and the system is unstable.

At $\theta = \theta_c$, there are two solutions to Eq. 4.3 such that p is imaginary

$$p = \pm i\omega_c$$

Then by setting equal to zero the real and imaginary parts of Eq. 4.3, the following relations are obtained

$$\omega_c^2 = \frac{g_{D1}\bar{\omega}_{L1}^2 + g_{D2}\bar{\omega}_{F1}^2}{g_{D1}+g_{D2}} \tag{4.4}$$

and

$$(-\omega_c^2+\bar{\omega}_{F1}^2)(-\omega_c^2+\bar{\omega}_{L1}^2) - \omega_c^2 g_{D1} g_{D2} + \omega_c^2 X_H Y_G = 0 \tag{4.5}$$

Equations similar to Eq. 4.4 and 4.5 have also been obtained by Ormiston (Ref. 3) and Tong (Ref. 7).

From Eqs. 3.25 it can be seen that g_{D2}, X_H , Y_G are all functions of θ and λ_o, while λ_o is also a function of θ. As shown in Appendix D, the relation between the inflow and collective pitch is given by

$$\lambda_o = \frac{\sigma a}{16}\left\{\frac{4}{15 b_\theta^2}\left[(1+b_\theta)^{3/2}(3b_\theta-2)+2\right]-1\right\} \tag{4.6}$$

where

$$b_\theta = \frac{32\theta}{\sigma a} \tag{4.7}$$

Therefore, from Eqs. 4.4 and 4.5 the critical value θ_c can be determined.

SECTION 5

PERTURBATION SOLUTION IN THE NEIGHBORHOOD OF THE CRITICAL CONDITION

5.1 The Multiple Time-Scaling Technique

The multiple time-scaling technique is an extension of the two variable expansions introduced by Cole (Ref. 6), Cole and Kevorkian (Ref. 13) and Kevorkian (Ref. 14).

In the use of a perturbation method, one may encounter terms of type $t^n \sin t$, $t^n \cos t$, which means that the solution will be unbounded for $t \to \infty$. These terms (which show the singular nature of the problem) are called secular terms: from a physical point of view one does not expect unbounded solutions; from a mathematical point of view, it means that the perturbation series break down for large t. By introducing an additional time scale, $t_1 = \varepsilon t$, where ε is some small positive parameter, the original differential equation is changed into what is formally a partial differential equation. This can be exploited in various ways to examine how the solutions grow and how to suppress the secular terms. The multiple time-scaling technique is a further generalization of the two time-scale expansions (Ref. 15) by introducing additional time scales $t_n = \varepsilon^n t$ to achieve greater flexibility. In particular, all possible secular terms can be avoided and a uniformly valid asymptotic expansion in the time domain is obtained.

The multiple time-scaling technique has been extensively used in treating the nonlinear panel flutter problem (Refs. 16 through 18). It has been applied first to the nonlinear helicopter blade-flutter problem by Tong (Refs. 7 and 8).

5.2 The Perturbation Expansion

Let $\varepsilon > 0$ be some small parameter representing the perturbed state of the system relative to the critical condition denoted by subscript "c". The following expansion can be established in the vicinity of the critical condition. Let

$$\chi_1 = \varepsilon^{1/2} a_0 + \varepsilon a_1 + \varepsilon^{3/2} a_2 + \ldots$$

$$\chi_2 = \varepsilon^{1/2} b_0 + \varepsilon b_1 + \varepsilon^{3/2} b_2 + \ldots \qquad (5.1)$$

be the expansion of the dependent variables.

The various other parameters of the problem can be expanded as

$$\mu = \mu_0 \varepsilon^{1/2} + \mu_1 \varepsilon + \ldots$$

$$\theta = \theta_c + \theta_1 \varepsilon + \theta_2 \varepsilon^{3/2} + \ldots$$

$$\lambda_0 = \lambda_{0c} + \lambda_1 \varepsilon + \lambda_2 \varepsilon^{3/2} + \ldots$$

$$g_{D1} = g_{D10} + \eta_{11} \varepsilon + \eta_{12} \varepsilon^{3/2} + \ldots$$

$$g_{D2} = g_{D20} + \eta_{21} \varepsilon + \eta_{22} \varepsilon^{3/2} + \ldots$$

$$g_1^{\circ} = g_0 + g_{01} \varepsilon + g_{02} \varepsilon^{3/2} + \ldots \qquad (5.2)$$

$$X_H = X_{H0} + X_1 \varepsilon + X_2 \varepsilon^{3/2} + \ldots$$

$$Y_G = Y_{G0} + Y_1 \varepsilon + Y_2 \varepsilon^{3/2} + \ldots$$

$$\bar{\omega}_{F1}^2 \equiv \omega_{F10}^2$$

$$\bar{\omega}_{L1}^2 \equiv \omega_{L10}^2$$

This particular expansion scheme has been chosen so that the $0(\varepsilon^{1/2})$ perturbed equations will be a system of ordinary differential equations with constant coefficients.

In addition, the multiple time scales will be introduced, using the following relations

$$\psi_m = \varepsilon^m \psi \qquad m = 0, 1, 2, \ldots \qquad (5.3)$$

where the ψ_m's are chosen as the new independent variables. Then

$$(\,)^{*} = \frac{d}{d\psi} = \frac{\partial}{\partial \psi_0} + \varepsilon \frac{\partial}{\partial \psi_1} + \ldots$$

$$(\,)^{**} = \frac{d^2}{d\psi^2} = \frac{\partial^2}{\partial \psi_0^2} + 2\varepsilon \frac{\partial^2}{\partial \psi_0 \partial \psi_1} + \ldots \qquad (5.4)$$

Some of the perturbed parameters in Eq. 5.2 are not independent, being related to θ_1 or θ_c. The various pertinent relations are given below.

$$\lambda_{0c} = \frac{\sigma_a}{16}\left\{\frac{4}{15 b_{\theta c}^2}\left[(1+b_{\theta c})^{3/2}(3b_{\theta c}-2)+2\right]-1\right\} \qquad (5.5)$$

$$\lambda_1 = \frac{\theta_1}{\theta_c}\sigma_a\left\{\frac{(1+b_{\theta c})^{1/2}}{8} - \frac{1}{30 b_{\theta c}^2}\left[(1+b_{\theta c})^{3/2}(3b_{\theta c}-2)+2\right]\right\} =$$

$$= \frac{\theta_1}{\theta_c}\sigma_a\left\{\frac{(1+b_{\theta c})^{1/2}}{8} - \left(1+\frac{16\lambda_{0c}}{\sigma_a}\right)\right\} \qquad (5.6)$$

where

$$b_{\theta c} = \frac{32\,\theta_c}{\sigma_a}$$

$$g_0 = \frac{c_2}{\omega_{F10}^2}\left(F^1\theta_c - F^2\lambda_{oc}\right)$$

$$g_{01} = \frac{c_2}{\omega_{F10}^2}\left(F^1\theta_1 - F^2\lambda_1\right)$$

$$X_{H0} = c_4 g_0 - c_1\left(2\theta_c F^{10} - F^{11}\lambda_{oc}\right)$$

$$X_1 = c_4 g_{01} - c_1\left(2\theta_1 F^{10} - F^{11}\lambda_1\right)$$

$$Y_{G0} = -c_{11} g_0 + c_7\left(L^7\theta_c - 2\lambda_{oc}L^8\right) \qquad (5.7)$$

$$Y_1 = -c_{11} g_{01} + c_7\left(L^7\theta_1 - 2\lambda_1 L^8\right)$$

$$g_{D20} = \frac{\bar{g}_{SL1}}{\bar{M}_{L1}} + c_7\left(2\frac{c_{do}}{a}L^{14} + L^{13}\lambda_{oc}\theta_c\right)$$

$$\eta_{21} = c_7 L^{13}\left(\lambda_1\theta_c + \lambda_{oc}\theta_1\right)$$

In a similar manner, expressions for λ_2, X_2, g_{02}, Y_2, η_{22}, etc., could also be evaluated. These expressions would be important only if one would consider expansions of order higher than $0(\varepsilon^{3/2})$ and will not be required in this report.

It is important now to associate the mathematical perturbation parameter ε, which represents basically the ratio between the two time scales used in the problem, with physical parameters affecting the rotor blade dynamics. For this purpose, a distinction between the two cases must be made:

Case 1: Hovering Flight -- $\mu = 0$ (i.e., $\mu_1 = 0$)

From Eqs. 5.2 through 5.7, it can be seen that θ_1 has been undetermined and is, in fact, a free parameter. Without loss of generality, it can be taken as $\theta_1 = \pm 1$, so that

$$\varepsilon = \frac{\theta - \theta_c}{\theta_1} = |\theta - \theta_c| \tag{5.8}$$

i.e., for this case, the perturbation parameter ε is equal to the absolute value of the difference between the actual collective pitch setting of the blade in the flight condition being investigated, and the critical value of the collective pitch θ_c.

Case 2: Forward Flight -- $\mu \neq 0$ (i.e., $\mu_0 \neq 0$, or $\mu_1 \neq 0$)

For this case, one may have ε associated with μ. Depending on the value of ω_c, one can have either: (a) $\mu_0 = 1$ and $\mu_1 = 0$ or (b) $\mu_1 = 1$ and $\mu_0 = 0$. Thus

(a) $\mu = \varepsilon^{1/2}$

or

(b) $\mu = \varepsilon$

which will be discussed in detail later.

For the cases with forward flight, Eq. 5.6 is no longer valid. For these cases, the inflow is evaluated from the usual relation given in Gesow and Myers (Ref. 19)

$$\lambda_0 = \mu \tan \alpha_R + \frac{C_T}{2\sqrt{\mu^2 + \lambda_0^2}} \tag{5.9}$$

while λ_1 and θ_1 are evaluated from

$$\lambda_1 = \frac{\lambda_0 - \lambda_{0c}}{\varepsilon} \tag{5.10}$$

$$\theta_1 = \frac{\theta - \theta_c}{\varepsilon}$$

5.3 The Perturbed Equations of Motion

Substituting Eqs. 5.1 through 5.4 into Eqs. 3.23 and 3.24 and requiring terms of the same order in ε to satisfy Eqs. 3.23 and 3.24 separately yields the somewhat lengthy system of equations written out in detail in Appendix G, Eqs. G.1 through G.3. This general system of equations is specialized below according to the various cases mentioned in the previous section.

For hovering flight, $\mu = 0$ (i.e., $\mu_o = \mu_1 = 0$), Eqs. G.1 through G.3 reduce to:

Equations of $O(\varepsilon^{1/2})$:

$$L_1(a_0, b_0) = 0$$
$$L_2(a_0, b_0) = 0 \tag{5.11}$$

Equations of $O(\varepsilon)$:

$$L_1(a_1, b_1) = Q_1(a_0, b_0)$$
$$L_2(a_1, b_1) = N_1(a_0, b_0) \tag{5.12}$$

Equation of $O(\varepsilon^{3/2})$:

$$L_1(a_2, b_2) = Q_2(a_0, b_0, a_1, b_1)$$
$$L_2(a_2, b_2) = N_2(a_0, b_0, a_1, b_1) \tag{5.13}$$

where the operators L_1, L_2 and the expressions Q_1, N_1, Q_2 and N_2 are defined in Eqs. G.4 through G.9 of Appendix G.

For the case of forward flight with $\mu = \mu_o \varepsilon^{1/2}$ ($\mu_1 = 0$), the equations are:

Equations of $O(\varepsilon^{1/2})$:

$$L_1(a_0, b_0) = \mu_o F_0(\psi_0, \theta_c)$$
$$L_2(a_0, b_0) = \mu_o H_0(\psi_0, \theta_c) \tag{5.14}$$

Equations of $O(\varepsilon)$:

$$L_1(a_1, b_1) = \mu_o F_1(\psi_0, \theta_c, a_0, b_0) + \mu_o^2 J_1(\psi_0, \theta_c) + Q_1(a_0, b_0) \tag{5.15}$$

$$L_2(a_1, b_1) = \mu_o H_1(\psi_0, \theta_c, a_0, b_0) + \mu_o^2 K_1(\psi_0, \theta_c) + N_1(a_0, b_0) .$$

Equations of $O(\varepsilon^{3/2})$:

$$L_1(a_2,b_2) = \mu_0 F_1(\psi_0,\theta_c,a_1,b_1) + \mu_0 F_0(\theta_1,\psi_0) + \mu_0 F_2(\psi_0,a_0,b_0) + \mu_0^2 J_2(\psi_0,a_0) + Q_2(a_0,b_0,a_1,b_1)$$

$$L_2(a_2,b_2) = \mu_0 H_1(\psi_0,\theta_c,a_1,b_1) + \mu_0 H_0(\psi_0,\theta_1) + \mu_0 H_2(\psi_0,\theta_c,a_0,b_0) + \mu_0^2 K_2(\psi_0,a_0) + N_2(a_0,b_0,a_1,b_1) \quad (5.16)$$

where the expressions F_o, H_o, F_1, J_1, H_1, K_1, F_2, J_2, H_2, K_2 are defined in Eqs. G.10 through G.18 of Appendix G.

For the case of forward flight with $\mu = \mu_1\varepsilon$ ($\mu_o = 0$), the equations are:

Equations of $O(\varepsilon^{1/2})$:

$$L_1(a_0,b_0) = 0$$
$$L_2(a_0,b_0) = 0 \quad (5.17)$$

Equations of $O(\varepsilon)$:

$$L_1(a_1,b_1) = \mu_1 F_0(\psi_0,\theta_c) + Q_1(a_0,b_0)$$
$$L_2(a_1,b_1) = \mu_1 H_0(\psi_0,\theta_c) + N_1(a_0,b_0) \quad (5.18)$$

Equations of $O(\varepsilon^{3/2})$:

$$L_1(a_2,b_2) = \mu_1 F_1(\psi_0,\theta_c,a_0,b_0) + Q_2(a_0,b_0,a_1,b_1)$$
$$L_2(a_2,b_2) = \mu_1 H_1(\psi_0,\theta_c,a_0,b_0) + N_2(a_0,b_0,a_1,b_1) \quad (5.19)$$

In Eqs. 5.11 through 5.19, the terms F_o, H_o, J_1, K_1 represent forcing functions; F_1, F_2, H_1, H_2 represent parametric excitation functions, while Q_1, N_1, Q_2, N_2 represent nonlinear coupling.

5.4 Solution of the Perturbed Equations and the Conditions for Suppressing the Secular Terms

In this section, the equations derived previously will be treated in detail. For convenience, the various cases will be classified in the following manner:

Case A -- Hovering flight $\mu = 0$ (i.e., $\mu_o = \mu_1 = 0$)

Case B -- General forward flight case, $\mu = \mu_o \varepsilon^{1/2}$ (i.e., $\mu_1 = 0$) and $\omega_c \neq 1/2 + \varepsilon\nu$ or $\omega_c \neq 1 + \varepsilon\nu$

Case C -- Forward flight case, with $\omega_c = 1/2 + \varepsilon\nu$, for this case $\mu = \mu_1 \varepsilon$ (i.e., $\mu_o = 0$)

Case D -- Forward flight case, with $\omega_c = 1 + \varepsilon\nu$, for this case $\mu = \mu_o \varepsilon^{1/2}$ (i.e., $\mu_1 = 0$)

In these relations ν is a quantity of order one or smaller, which will be specified in the analysis. The reason for this classification will become apparent within the context of this section.

5.4.1 Solution for Case A

This case represents hovering flight ($\mu = 0$). The equations which must be solved are Eqs. 5.11 through 5.13. First, the solution to the equation of $0(\varepsilon^{1/2})$ will be obtained. As represented by Eq. 5.11, these equations are identical to the linear system (Eq. 4.1), treated previously in Section 4. Since the damped branches are stable, only the harmonically oscillating branches must be considered, which can be represented by

$$\begin{Bmatrix} a_o \\ b_o \end{Bmatrix} = A_o \begin{Bmatrix} v_r \\ 1 \end{Bmatrix} e^{i\omega_c \psi_o} + (A_o)^* \begin{Bmatrix} (v_r)^* \\ 1 \end{Bmatrix} e^{-i\omega_c \psi_o} =$$

$$= 2\,\mathrm{Real}\left(A_o \begin{Bmatrix} v_r \\ 1 \end{Bmatrix} e^{i\omega_c \psi_o} \right) \tag{5.20}$$

where $(\,)^*$ denotes the complex conjugate; A_o is a function of $\psi_1, \psi_2, \ldots$, etc., but not of ψ_o. In analogy to Section 4, the values of ω_c and θ_c are determined from

$$\omega_c^2 = \frac{\omega_{L10}^2 + \dfrac{g_{D20}}{g_{D10}} \omega_{F10}^2}{1 + \dfrac{g_{D20}}{g_{D10}}} \tag{5.21}$$

$$\frac{g_{D10}\, g_{D20}\, (\omega_{F10}^2 - \omega_{40}^2)^2}{(g_{D10} + g_{D20})^2} + g_{D10}\, g_{D20}\, \omega_c^2 = \omega_c^2 X_{H0}\, Y_{G0} \tag{5.22}$$

The quantity v_r, determined from Eqs. 5.11 is given by

$$v_r = \frac{X_{H0}\, i\omega_c}{-\omega_c^2 + g_{D10} i\omega_c + \omega_{F10}^2} \tag{5.23}$$

This quantity represents the ratio between the flap and lag amplitudes. It can be shown that

$$|v_r| = \sqrt{\frac{g_{D20}\, X_{H0}}{g_{D10}\, Y_{G0}}} \tag{5.24}$$

Next, the equations of $0(\varepsilon)$ must be solved. The solution of Eqs. 5.12 is composed of two parts: the solution of the homogeneous system and the particular solution which is obtained by the method of undetermined coefficients. The homogeneous solution would have importance only if the equations of $0(\varepsilon^2)$ were also considered. This being not the case, the particular solution would be sufficient. Then

$$\begin{Bmatrix} a_1 \\ b_1 \end{Bmatrix} = 2\,\mathrm{Real}\left(A_0^2 \begin{Bmatrix} \alpha_2 \\ \beta_2 \end{Bmatrix} e^{i 2\omega_c \psi_0} + A_0 (A_0)^* \begin{Bmatrix} \alpha_3 \\ \beta_3 \end{Bmatrix} \right) \tag{5.25}$$

where the quantities α_2, β_2, α_3, β_3 are defined in Eqs. G.19 and G.21.

Finally, the $0(\varepsilon^{3/2})$ equations are treated, substituting Eqs. 5.20 and 5.25 into Eq. 5.13 and using Eq. 5.26

$$2\,\mathrm{Real}\,(A e^{i\omega t})\, 2\,\mathrm{Real}\,(B e^{i\alpha t}) = 2\,\mathrm{Real}\,[A B\, e^{i(\alpha+\omega)t} + (A)^* B\, e^{i(\alpha-\omega)t}] \tag{5.26}$$

yield the following relations

$$L_1(a_2, b_2) = 2\,\text{Real}\left\{\left[p_1 \frac{\partial A_0}{\partial \psi_1} + p_3 A_0 + p_{15}(A_0)^* A_0^2\right] e^{i\omega_c \psi_0} + \right.$$

$$\left. + (\ldots\ldots)\, e^{i3\omega_c \psi_0}\right\} \tag{5.27}$$

$$L_2(a_2, b_2) = 2\,\text{Real}\left\{\left[p_2 \frac{\partial A_0}{\partial \psi_1} + p_4 A_0 + p_{16}(A_0)^* A_0^2\right] e^{i\omega_c \psi_0}\right.$$

$$\left. + (\ldots\ldots)\, e^{i3\omega_c \psi_0}\right\} \tag{5.28}$$

where the quantities p_1, p_2, p_3, p_4, p_{15}, and p_{16} are defined in Eqs. G.21 of Appendix G. The terms p_{15}, p_{16} in Eqs. 5.27 and 5.28 represent the nonlinear coupling terms.

5.4.2 Solution for Case B

This case represents the general forward flight case $\mu = \mu_o \varepsilon^{1/2}$ and $\omega_c \neq 1/2 + \varepsilon\nu$ or $\omega_c \neq 1 + \varepsilon\nu$.

The solution to Eq. 5.14 ($0(\varepsilon^{1/2})$ equations) is given by Eq. 5.20 with an additional part representing the particular solution. Thus,

$$\begin{Bmatrix} a_o \\ b_o \end{Bmatrix} = 2\,\text{Real}\left(A_o \begin{Bmatrix} v_r \\ 1 \end{Bmatrix} e^{i\omega_c \psi_0} + \mu_o \begin{Bmatrix} a_{o2} \\ b_{o2} \end{Bmatrix} e^{i\psi_0}\right) \tag{5.29}$$

where a_{o2}, b_{02} are defined in Appendix G.

The solution to Eq. 5.15 ($0(\varepsilon)$ equations) is given by

$$\begin{Bmatrix} a_1 \\ b_1 \end{Bmatrix} = 2\,Real\left(A_0^2 \begin{Bmatrix} \alpha_2 \\ \beta_2 \end{Bmatrix} e^{i2\omega_c\psi_0} + \mu_0 (A_0)^* \begin{Bmatrix} a_{13} \\ b_{13} \end{Bmatrix} e^{i(1-\omega_c)\psi_0} \right.$$

$$\left. + \mu_0 A_0 \begin{Bmatrix} a_{14} \\ b_{14} \end{Bmatrix} e^{i(1+\omega_c)\psi_0} + \mu_0^2 \begin{Bmatrix} a_{15} \\ b_{15} \end{Bmatrix} e^{i2\psi_0} \right)$$

$$+ \quad A_0 (A_0)^* \begin{Bmatrix} \bar{\alpha}_3 \\ \bar{\beta}_3 \end{Bmatrix} + \mu_0^2 \begin{Bmatrix} a_{16} \\ b_{16} \end{Bmatrix} \qquad (5.30)$$

where the a_{13}, b_{13}, a_{14}, b_{14}, a_{15}, b_{15}, $\bar{\alpha}_3$, $\bar{\beta}_3$, a_{16}, b_{16} are given in Eqs. G.31 through G.35 of Appendix G.

Finally, when Eqs. 5.29 and 5.30 are substituted into Eqs. 5.16 [$0(\varepsilon^{3/2})$ equations] lengthy expressions occur which can be written as

$$L_1 (a_2, b_2) = 2\,Real \left\{ \left[p_1 \frac{\partial A_0}{\partial \psi_1} + p_3 A_0 + p_{21} \mu_0^2 A_0 + p_{15} (A_0)^* A_0^2 \right] e^{i\omega_c\psi_0} + \right.$$

$$(\ldots\ldots)\, e^{i\psi_0} + (\ldots)\, e^{i3\psi_0} + e^{i3\omega_c\psi_0} (\ldots\ldots) +$$

$$+ (\ldots)\, e^{i(2-\omega_c)\psi_0} + (\ldots)\, e^{i(2+\omega_c)\psi_0} + (\ldots)\, e^{i(1+2\omega_c)\psi_0} +$$

$$\left. (\ldots)\, e^{i(1-2\omega_c)\psi_0} + \ldots \text{ constant terms} \right\} \qquad (5.31)$$

$$L_2(a_2,b_2) = 2\,\mathrm{Real}\left\{\left[p_2\frac{\partial A_0}{\partial \psi_1} + p_4 A_0 + p_{22}\mu_0^2 A_0 + p_{16}(A_0)^* A_0^2\right]e^{i\omega_c\psi_0} + (\ldots)e^{i\psi_0} + (\ldots)e^{i3\psi_0} + (\ldots)e^{i3\omega_c\psi_0} + (\ldots)e^{i(2-\omega_c)\psi_0} + (\ldots)e^{i(2+\omega_c)\psi_0} + (\ldots)e^{i(1+2\omega_c)\psi_0} + (\ldots)e^{i(1-2\omega_c)\psi_0} + \text{const. terms}\right\} \tag{5.32}$$

where the quantities p_{21}, p_{22} are defined in Eqs. G.44 and G.45 of Appendix G.

5.4.3 Solution for Case C

This is a forward flight case with $\omega_c = 1/2 + \varepsilon\nu$ and $\mu \neq 0$ where ν is a quantity of 0(1) or smaller which will be specified later. From Eq. 5.30 it can be seen that the expressions for a_{13}, b_{13} (and their conjugates) become very large for $\omega_c = 1/2 + \varepsilon\nu$, because $\underset{\sim}{M}(1 - \omega_c)$ of Eq. G.32 is near singular. This situation can be corrected by requiring that $\mu_o = 0$, then $\mu = \mu_1\varepsilon$. For this case, the solution is obtained by solving Eqs. 5.17 through 5.19. Proceeding analogously to the previous cases, the solution to the $0(\varepsilon^{1/2})$ equation is again given by Eq. 5.20, while the solution to the $0(\varepsilon)$ equations, Eq. 5.18 is given by

$$\begin{Bmatrix} a_1 \\ b_1 \end{Bmatrix} = 2\,\mathrm{Real}\left(A_0^2\begin{Bmatrix}\alpha_2\\ \beta_2\end{Bmatrix}e^{i2\omega_c\psi_0} + A_0(A_0)^*\begin{Bmatrix}\alpha_3\\ \beta_3\end{Bmatrix} + \mu_1\begin{Bmatrix}\alpha_1\\ \beta_1\end{Bmatrix}e^{i\psi_0}\right) \tag{5.33}$$

where the quantities α_1, β_1 are defined in Eq. G.46.

The substitution of Eqs. 5.20 and 5.33 into Eq. 5.19 yields

$$L_1(a_2,b_2) = 2\,Real\left\{\left[p_1\frac{\partial A_0}{\partial \psi_1} + p_3 A_0 + p_{15}(A_0)^* A_0^2\right]e^{i\omega_c\psi_0}\right.$$

$$+ \quad \mu_1 p_5 (A_0)^* e^{i(1-\omega_c)\psi_0} + (\ldots)\, e^{i(1+\omega_c)\psi_0} +$$

$$\left.(\ldots)\, e^{i3\omega_c\psi_0} + \ldots\right\} \tag{5.34}$$

$$L_2(a_2,b_2) = 2\,Real\left\{\left[p_2\frac{\partial A_0}{\partial \psi_1} + p_4 A_0 + p_{16}(A_0)^* A_0^2\right]e^{i\omega_c\psi_0}\right.$$

$$+\mu_1 (A_0)^* p_6 e^{i(1-\omega_c)\psi_0} + (\ldots)\, e^{i(1+\omega_c)\psi_0} +$$

$$\left.(\ldots) e^{i3\omega_c\psi_0} + \ldots\right\} \tag{5.35}$$

The quantities p_5 and p_6 defined in Eqs. G.47 and G.48 are associated with parametric excitation.

5.4.4 Solution for Case D

This is a case with forward flight $\mu = \mu_o \varepsilon^{1/2}$ ($\mu_1 = 0$) and $\omega_c = 1 + \varepsilon\nu$. From the solution of the general forward flight case, Eq. 5.29, it can be see that the expressions a_{o2} and b_{o2} will be nearly singular. This situation can be corrected by assuming that the expressions associated with the forcing $F_o(\psi_o, \theta_c)$ and $H_o(\psi_o, \theta_c)$, Eqs. G.10 are mathematically quantities of $0(\varepsilon)$ which physically means that at the flight condition being investigated θ_c and g_o are small quantities or in other words flight at low values of C_T.

Then, from Eqs. G.10

$$F_o(\psi_o, \theta_c) = \varepsilon\left(F_{o1}\sin\psi_o - F_{o2}\cos\psi_o\right) = \varepsilon \bar{F}_o(\psi_o, \theta_c) \tag{5.36}$$

$$H_o(\psi_o,\theta_c) = \varepsilon\left(H_{o1}\sin\psi_o + H_{o2}\cos\psi_o\right) = \varepsilon\,\bar{H}_o(\psi_o,\theta_c) \tag{5.37}$$

where F_{o1}, F_{02}, H_{o1}, H_{o2} are defined in Eqs. G.49 through G.52, and it is required that these quantities be all of order one.

The equations which must be solved for this case are:

(a) Equations of $0(\varepsilon^{1/2})$ as given by Eq. 5.11

(b) Equations of $0(\varepsilon)$ as given by Eq. 5.15

(c) Equations of $0(\varepsilon^{3/2})$ as given by Eq. 5.16, except that in this case, the term $\mu_o F_o(\psi_o, \theta_c)$ replaces $\mu_o F_o(\theta_1, \psi_o)$ and $\mu_o H_o(\psi_o, \theta_c)$ replaces $\mu_o H_o(\psi_o, \theta_1)$

The solution to this system of equations is given by Eq. 5.20 and

$$\begin{Bmatrix} a_1 \\ b_1 \end{Bmatrix} = 2\,\mathrm{Real}\left(A_o^2 \begin{Bmatrix} \alpha_2 \\ \beta_2 \end{Bmatrix} e^{i2\omega_c\psi_o} + \mu_o (A_o)^* \begin{Bmatrix} \bar{a}_{13} \\ \bar{b}_{13} \end{Bmatrix} e^{i(1-\omega_c)\psi_o} + \mu_o A_o \begin{Bmatrix} \bar{a}_{14} \\ \bar{b}_{14} \end{Bmatrix} e^{i(1+\omega_c)\psi_o} + \mu_o^2 \begin{Bmatrix} \bar{a}_{15} \\ \bar{b}_{15} \end{Bmatrix} e^{i2\psi_o} \right) + A_o (A_o)^* \begin{Bmatrix} \alpha_3 \\ \beta_3 \end{Bmatrix} + \mu_o^2 \begin{Bmatrix} \bar{a}_{16} \\ \bar{b}_{16} \end{Bmatrix} \tag{5.38}$$

where the quantities $\bar{a}_{13}$, $\bar{b}_{13}$, $\bar{a}_{14}$, $\bar{b}_{14}$, $\bar{a}_{15}$, $\bar{b}_{15}$, $\bar{a}_{16}$, $\bar{b}_{16}$ are equal to the same quantities without the bar, when $a_{o2} = b_{02} = 0$. For convenience, the quantities $\bar{p}_{11}$ through $\bar{p}_{14}$ and $\bar{p}_{17}$ through $\bar{p}_{20}$ are given by Eqs. G.53 through G.60.

The substitution of Eqs. 5.20 and 5.38 into the modified equations (Eq. 5.16) yields:

$$L_1(a_2,b_2) = 2\,\mathrm{Real}\left\{\left[p_1 \frac{\partial A_0}{\partial \psi_1} + p_3 A_0 + \bar{p}_{21}\mu_0^2 A_0 + p_{15}(A_0)^* A_0^2 \right] e^{i\omega_c\psi_0} + \left[\frac{\mu_0}{\epsilon} p_9 + \mu_0^3 p_{23} + \mu_0 (A_0)^* A_0 p_{25}\right] e^{i\psi_0} + \mu_0^2 (A_0)^* p_{27} e^{i(2-\omega_c)\psi_0} + \mu_0 A_0^2 (p_{29})^* e^{-i(1-2\omega_c)\psi_0} + (\ldots)\, e^{i3\omega_c\psi_0} + (\ldots)\, e^{i(2+\omega_c)\psi_0} + (\ldots)\, e^{i(1+2\omega_c)\psi_0} + \ldots + \ldots \right\} \tag{5.39}$$

$$L_2(a_2,b_2) = 2\,\mathrm{Real}\left\{\left[p_2 \frac{\partial A_0}{\partial \psi_1} + p_4 A_0 + \bar{p}_{22}\mu_0^2 A_0 + p_{16}(A_0)^* A_0^2 \right] e^{i\omega_c\psi_0} + \left[\mu_0 \frac{p_{10}}{\epsilon} + \mu_0^3 p_{24} + \mu_0 (A_0)^* A_0 p_{26}\right] e^{i\psi_0} + \mu_0^2 (A_0)^* p_{28} e^{i(2-\omega_c)\psi_0} + \mu_0 A_0^2 (p_{30})^* e^{-i(1-2\omega_c)\psi_0} + (\ldots)\, e^{i3\omega_c\psi_0} + (\ldots) e^{i(2+\omega_c)\psi_0} + (\ldots)\, e^{i(1+2\omega_c)\psi_0} + \ldots \right\} \tag{5.40}$$

where $\bar{p}_{21}$, $\bar{p}_{22}$ are equal to p_{21}, p_{22} when $a_{02} = b_{02} = 0$, and the quantities p_{23} through p_{30} are given in Eqs. G.61 through G.68.

5.4.5 Conditions for Suppressing the Secular Terms for the Various Cases Considered

In this section, a general condition for suppressing secular terms of type $\psi_o e^{i\omega_c \psi_o}$ will be derived. As shown below, the condition for suppressing secular terms can be obtained from a relatively simple consideration.

A general case in which secular terms would appear, can be formally written as

$$L_1(a_2, b_2) = \Pi_1 e^{i\omega_c \psi_o}$$
$$L_2(a_2, b_2) = \Pi_2 e^{i\omega_c \psi_o} \tag{5.41}$$

The solution to Eqs. 5.41 can be written as

$$a_2 = \Pi_{10} e^{i\omega_c \psi_o}$$
$$b_2 = \Pi_{20} e^{i\omega_c \psi_o} \tag{5.42}$$

From Eqs. 5.41 and 5.42

$$\begin{bmatrix} -\omega_c^2 + g_{D10} i\omega_c + \omega_{F10}^2 & -X_{H0} i\omega_c \\ -Y_{G0} i\omega_c & -\omega_c^2 + i\omega_c g_{D20} + \omega_{L0}^2 \end{bmatrix} \begin{Bmatrix} \Pi_{10} \\ \Pi_{20} \end{Bmatrix} = \begin{Bmatrix} \Pi_1 \\ \Pi_2 \end{Bmatrix}$$

It has been previously shown in Section 4, that the matrix of the coefficients in the last equation vanishes. Thus, these equations are not independent of each other and the first row of the matrix must be proportional to its second row, denoting the constant of proportionality by C_p:

$$C_p = \frac{\Pi_1}{\Pi_2} = \frac{-\omega_c^2 + g_{D10} i\omega_c + \omega_{F10}^2}{-Y_{G0} i\omega_c} = \frac{-X_{H0} i\omega_c}{-\omega_c^2 + i\omega_c g_{D20} + \omega_{L10}^2} \tag{5.43}$$

From Eqs. 5.43 and 5.23

$$\Pi_1 v_r Y_{G0} + \Pi_2 X_{H0} = 0 \tag{5.44}$$

As shown below, taking the appropriate combination for π_1 and π_2, Eq. 5.44 will give the required condition for suppressing the secular terms for the various cases considered.

Cases A and B

Case B which is the general forward flight case with $\omega_c \neq 1 + \nu\varepsilon$ or $\omega_c \neq 1/2 + \nu\varepsilon$ and $\mu = \mu_o \varepsilon^{1/2}$, will also include Case A as a particular case.

From Eqs. 5.31 and 5.32

$$\pi_1 = p_1 \frac{\partial A_0}{\partial \psi_1} + p_3 A_0 + \mu_o^2 p_{21} A_0 + p_{15} (A_0)^* A_0^2$$

$$\pi_2 = p_2 \frac{\partial A_0}{\partial \psi_1} + p_4 A_0 + \mu_o^2 p_{22} A_0 + p_{16} (A_0)^* A_0^2 \qquad (5.45)$$

From Eqs. 5.44 and 5.45, the condition for suppressing the secular term can be written as

$$\frac{\partial A_0}{\partial \psi_1} = (\kappa_2 + \mu_o^2 \kappa_6) A_0 + \kappa_3 A_0^2 (A_0)^* \qquad (5.46)$$

For the case of hovering flight, Case A, $\mu_o = 0$, ($\mu_1 = 0$) and Eq. 5.46 reduces to

$$\frac{\partial A_0}{\partial \psi_1} = \kappa_2 A_0 + \kappa_3 A_0^2 (A_0)^* \qquad (5.47)$$

Evidently, Eq. 5.47 is not subject to the flutter frequency limitation of Eq. 5.46.

The quantities κ_1, κ_2, κ_3, κ_6 are defined in Eqs. G.69 through G.72.

Case C

For this case, $\omega_c = 1/2 + \varepsilon\nu$ and $\mu = \mu_1 \varepsilon$. Where ν is of order one or smaller, it can be shown that

$$\nu \simeq f(\eta_{21}, g_{D10}, g_{D20}, \omega_{F10}, \omega_{L10}) \tag{5.48}$$

For this case

$$\begin{aligned} \Pi_1 &= p_1 \frac{\partial A_0}{\partial \psi_1} + p_3 A_0 + p_{15} A_0^2 (A_0)^* + \mu_1 p_5 (A_0)^* e^{-i\nu\psi_1} \\ \Pi_2 &= p_2 \frac{\partial A_0}{\partial \psi_1} + p_4 A_0 + p_{16} A_0^2 (A_0)^* + \mu_1 p_6 (A_0)^* e^{-i\nu\psi_1} \end{aligned} \tag{5.49}$$

and from Eqs. 5.44 and 5.49, the condition for suppressing the secular term is

$$\frac{\partial A_0}{\partial \psi_1} = \kappa_2 A_0 + \kappa_3 A_0^2 (A_0)^* + \mu_1 \kappa_5 e^{-i\nu\psi_1} \tag{5.50}$$

where κ_5 is given by Eq. G.73.

Equation 5.50 can be rewritten in a more convenient manner after changing the dependent variable. Let

$$\bar{A}_0 = A_0 e^{i\nu\psi_1} \tag{5.51}$$

Then Eqs. 5.50 and 5.51 yield:

$$\frac{\partial \bar{A}_0}{\partial \psi_1} = \bar{\kappa}_2 \bar{A}_0 + \kappa_3 \bar{A}_0^2 (\bar{A}_0)^* + \mu_1 \kappa_5 (\bar{A}_0)^* \tag{5.52}$$

where

$$\bar{\kappa}_2 = \kappa_2 + i\nu \tag{5.53}$$

It should be mentioned that a case $\omega_c = 2 + \varepsilon\nu$ could also have some practical importance, when the harmonic components of the inflow are considered

together with cyclic pitch variations. In the present report, these effects will not be considered. A partial treatment of this case can be found in Ref. 8.

Case D

For this case, the flutter frequency is close to the forcing frequency $\omega_c = 1 + \varepsilon\nu$ and $\mu = \mu_o \varepsilon^{1/2}$. It can be shown that

$$\nu \cong \frac{1}{2} f(\eta_{21}, g_{D10}, g_{D20}, \omega_{F10}, \omega_{L10}) \tag{5.54}$$

From Eqs. 5.39 and 5.40, it is clear that many terms will contribute secular terms. In addition to $e^{i\psi_o}$, terms of type $e^{i(2-\omega_c)\psi_o}$ and $e^{-i(1-2\omega_c)\psi_o}$ will also yield secular terms. For this case

$$\begin{aligned}
\overline{\Pi_1} = {} & p_1 \frac{\partial A_o}{\partial \psi_1} + p_3 A_o + \overline{p_{21}} \mu_o^2 A_o + p_{15} A_o^2 (A_o)^* + \\
& \left[\frac{\mu_o}{\varepsilon} p_9 + \mu_o^3 p_{23} + \mu_o (A_o)^* A_o \, p_{25} \right] e^{-i\nu\psi_1} \\
& + \mu_o^2 (A_o)^* p_{27} e^{-2i\nu\psi_1} + \mu_o A_o^2 (p_{29})^* e^{i\nu\psi_1}
\end{aligned}$$

$$\begin{aligned}
\overline{\Pi_2} = {} & p_2 \frac{\partial A_o}{\partial \psi_1} + p_4 A_o + \overline{p_{22}} \mu_o^2 A_o + p_{16} (A_o)^* A_o^2 + \\
& + \left[\mu_o \frac{p_{10}}{\varepsilon} + \mu_o^3 p_{24} + \mu_o A_o (A_o)^* p_{26} \right] e^{-i\nu\psi_1} \\
& + \mu_o^2 (A_o)^* p_{27} e^{-2i\nu\psi_1} + \mu_o A_o^2 (p_{29})^* e^{i\nu\psi_1}
\end{aligned} \tag{5.55}$$

From Eqs. 5.44 and 5.55, the condition for suppressing the secular term can be written as

$$\frac{\partial A_0}{\partial \psi_1} = \left(\kappa_2 + \mu_0^2 \bar{\kappa}_6\right) A_0 + \kappa_3 A_0^2 (A_0)^* +$$

$$\left[\mu_0 \frac{\kappa_4}{\varepsilon} + \mu_0^3 \kappa_7 + \mu_0 A_0 (A_0)^* \kappa_8 \right] e^{-i\nu\psi_1}$$

$$+ \mu_0^2 (A_0)^* \kappa_9 e^{-2i\nu\psi_1} + \mu_0 A_0^2 \kappa_{10} e^{i\nu\psi_1}$$

(5.56)

where the quantities κ_4, κ_7, κ_8, κ_9, and κ_{10} are given by Eqs. G.74 through G.78, while $\bar{\kappa}_6$ is equivalent to κ_6 with $a_{o2} = b_{02} = 0$.

Equation 5.56 can be rewritten in a more convenient manner by changing the dependent variable.

Let

$$\tilde{A}_0 = A_0 e^{i\nu\psi_1}$$

(5.57)

Then Eqs. 5.56 and 5.57 yield

$$\frac{\partial \tilde{A}_0}{\partial \psi_1} = \left(\tilde{\kappa}_2 + \mu_0^2 \bar{\kappa}_6\right) \tilde{A}_0 + \kappa_3 \tilde{A}_0^2 (\tilde{A}_0)^* +$$

$$\left[\frac{\mu_0}{\varepsilon} \kappa_4 + \mu_0^3 \kappa_7 + \mu_0 \kappa_8 (\tilde{A}_0)^* \tilde{A}_0 \right] +$$

$$+ \mu_0^2 (\tilde{A}_0)^* \kappa_9 + \mu_0 \tilde{A}_0^2 \kappa_{10}$$

(5.58)

where

$$\tilde{\kappa}_2 = \kappa_2 + i\nu$$

(5.59)

5.5 Stability Analysis and Blade Response Amplitudes for the Various Cases Considered

In this section, the amplitudes of blade response will be determined, and the stability of the motion will be investigated for the various cases considered in the preceding sections. The stability will be investigated using the conditions for suppressing the secular terms, while the amplitudes of blade response will be determined by taking appropriate combinations of the solutions to the perturbed equations of motion.

5.5.1 Case A, Hovering Flight

For this case, $\mu = 0$ and the condition for suppressing the secular term is given by Eq. 5.47. Equation 5.47 can be solved in closed form, taking the solution in the form of (Refs. 17 and 7)

$$A_o = \rho e^{i\varphi} \tag{5.60}$$

where both ρ and ϕ are real.

Substitution of Eq. 5.60 into Eq. 5.47 yields

$$\frac{\partial \rho}{\partial \psi_1} = \kappa_{2R}\rho + \kappa_{3R}\rho^3 \tag{5.61}$$

$$\frac{\partial \varphi}{\partial \psi_1} = \kappa_{2I} + \kappa_{3I}\rho^2 \tag{5.62}$$

where the subscripts R and I denote, respectively, the real and imaginary part of the appropriate quantity.

The solution of Eq. 5.61 can be written as:

$$\rho^2 = \rho_o^2 \Big/ \left\{ e^{-2\kappa_{2R}\psi_1} + \rho_o^2 \frac{\kappa_{3R}}{\kappa_{2R}} \left(e^{-2\kappa_{2R}\psi_1} - 1 \right) \right\} \tag{5.63}$$

From Eqs. 5.62 and 5.63, the solution for ϕ can be written as

$$\varphi = \varphi_o + \kappa_{2I}\psi_1 - \frac{\kappa_{3I}}{2\kappa_{3R}} \ln\left[1 + \rho_o^2 \frac{\kappa_{3R}}{\kappa_{2R}}\left(1 - e^{2\kappa_{2R}\psi_1}\right)\right]$$

(5.64)

where the quantities ρ_o, ϕ_o are the values of ρ and ϕ at $\psi_1 = 0$.

For the case of hovering flight, the solution is given by Eqs. 5.20, 5.25, 5.1, 5.63, and 5.64.

$$\begin{Bmatrix} \chi_1 \\ \chi_2 \end{Bmatrix} = 2\,\text{Real}\left(\varepsilon^{1/2} A_o \begin{Bmatrix} v_r \\ 1 \end{Bmatrix} e^{i\omega_c \psi_o} + \varepsilon A_o^2 \begin{Bmatrix} \alpha_2 \\ \beta_2 \end{Bmatrix} e^{i2\omega_c \psi_o} + \right.$$

$$\left. + \varepsilon A_o (A_o)^* \begin{Bmatrix} \alpha_3 \\ \beta_3 \end{Bmatrix} + \cdots\cdots \right)$$

(5.65)

For the case of hovering, from Eq. 5.8, the perturbation parameter ε is $\varepsilon = |\theta - \theta_c|$, so that the blade response depends only upon the collective pitch setting.

The stability of the blade response can be investigated using Eq. 5.63. The following four cases can occur.

Case 1: $\kappa_{2R} > 0$ and $\kappa_{3R} > 0$

At $\psi_1 = 0$, $\rho = \rho_o$, at some finite time, the denominator of Eq. 5.63 approaches zero. That is $\rho \to \infty$. This clearly represents an unstable case.

Case 2: If both $\kappa_{2R} < 0$ and $\kappa_{3R} < 0$, $\rho^2 \to 0$ as $\psi_1 \to \infty$. This clearly represents a stable situation.

Case 3: If $\kappa_{2R} > 0$ and $\kappa_{3R} < 0$, the exponential terms in Eq. 5.69 tend to zero and

$$\rho_{\psi_1 \to \infty} = \sqrt{-\frac{\kappa_{2R}}{\kappa_{3R}}} \tag{5.66}$$

This case represents a stable limit cycle oscillation.

Case 4: If $\kappa_{2R} < 0$ and $\kappa_{3R} > 0$,

Denoting $$\rho_{\ell.c.} = \sqrt{-\frac{\kappa_{2R}}{\kappa_{3R}}}$$

Eq. 5.63 can be rewritten as

$$\frac{1}{\rho^2} = \left(\frac{1}{\rho_o^2} - \frac{1}{\rho_{\ell.c}^2}\right) e^{-2\kappa_{2R}\psi_1} + \frac{1}{\rho_{\ell.c}^2} \tag{5.67}$$

from the last expression for

$$\frac{1}{\rho_o^2} - \frac{1}{\rho_{\ell.c}^2} < 0 \tag{5.68}$$

The system is unstable and for

$$\frac{1}{\rho_o^2} - \frac{1}{\rho_{\ell.c}^2} > 0 \tag{5.69}$$

the system is stable.

From Eqs. 5.66 and 5.68 for

$$\rho_o^2 > -\frac{\kappa_{2R}}{\kappa_{3R}}$$

the system is unstable, and from Eqs. 5.66 and 5.69 for

$$\rho_o^2 < -\frac{\kappa_{2R}}{\kappa_{3R}}$$

the system is stable.

Thus, in this case, the stability is conditionally dependent upon the relative magnitude of the initial value of ρ_o when compared to $\rho_{\ell.c.}$

From Eqs. G.69, G.70, G.24, G.25, and 5.7, it is clear that κ_{2R} is linearly proportional to θ_1. That is, the origin ($A_o \tilde{\sim} 0$) is unstable above the critical condition ($\theta_1 > 0$) and stable below the critical condition ($\theta_1 < 0$).

5.5.2 Case B -- The General Forward Flight Case

In the general case with forward flight, $\mu = \mu_o \varepsilon^{1/2}$ ($\mu_1 = 0$) without any loss of generality μ_o can be taken as $\mu_o = 1$. Thus, in this case, the perturbation parameter is $\varepsilon = \mu^2$. The flutter frequency for this case can have any value except $\omega_c \neq 1/2 + \varepsilon\nu$ or $\omega_c \neq 1 + \varepsilon\nu$.

The condition for suppressing the secular terms is given by Eq. 5.46. The solution of this equation is identical to the solution of Eq. 5.47 with $\delta_2 + \mu_o^2 \delta_6$ replacing δ_2. In analogy to Eq. 5.63, ρ^2 can be written as

$$\rho^2 = \rho_o^2 \Big/ \left\{ e^{-2(\kappa_{2R}+\mu_o^2\kappa_{6R})\psi_1} + \rho_o^2 \frac{\kappa_{3R}}{\kappa_{2R}+\mu_o^2\kappa_{6R}} \left[e^{-(\kappa_{2R}+\mu_o^2\kappa_{6R})\psi_1} - 1 \right] \right\} \tag{5.70}$$

The various cases for which the stability of the response was investigated in the previous section remain unchanged and are summarized below:

Case 1: $\kappa_{2R} + \kappa_{6R}\mu_o^2 > 0$ and $\kappa_{3R} > 0$ -- the system is unstable

Case 2: $\kappa_{2R} + \mu_o^2\kappa_{6R} < 0$ and $\kappa_{3R} < 0$ -- the system is stable

Case 3: $\kappa_{2R} + \mu_o^2 \kappa_{6R} > 0$ and $\kappa_{3R} < 0$ -- stable limit cycle oscillation with

$$\rho_{\ell.c} = -\sqrt{\frac{\kappa_{2R}+\mu_o^2\kappa_{6R}}{\kappa_{3R}}} \tag{5.71}$$

Case 4: $\kappa_{2R} + \mu_o^2\kappa_{6R} < 0$ and $\kappa_{3R} > 0$ -- this system is conditionally stable

Thus for

$\rho_o^2 < \rho_{\ell.c.}$ the system is stable

and for $\rho_o^2 > \rho_{\ell.c.}$ the system is unstable

From these relations it is clear that the forward flight can influence the stability through the magnitude and sign of κ_{6R}. In addition to this effect, forward flight can also affect the stability of the system by influencing κ_{2R}.

From Eqs. G.22, G.23, G.24, and G.70, it is clear that κ_1 is dependent only upon the critical conditions and κ_2 (with $\eta_{11} = 0$) is composed of two parts, one proportional to θ_1 and one proportional to λ_1.

$$\kappa_2 = (\kappa_{2\theta 1})\theta_1 + (\kappa_{2\lambda 1})\lambda_1 \tag{5.72}$$

where $\kappa_{2\theta 1}$ and $\kappa_{2\lambda 1}$ are given in Eqs. G.80 and G.81. Thus κ_{2R} can be written as

$$\kappa_{2R} = (\kappa_{2\theta_1})_R \theta_1 + (\kappa_{2\lambda_1})_R \lambda_1 = \kappa_{2R}(\theta_1, \lambda_1) \tag{5.73}$$

In forward flight θ_1 must be evaluated from Eq. 5.10. The flight condition is determined by a fixed value of C_T and a known value of μ. For a given flight condition, the values of θ and α_R are evaluated using an approximate trim calculation described in Appendix F. These determine θ_1 by Eq. 5.10. Thus, a change in μ, at a fixed value of C_T, results in a change of θ_1 and λ_1, which has a considerable influence on both the stability and response of the blade.

From Eqs. 5.1, 5.29, and 5.30, the blade response for this case can be written as

$$\begin{Bmatrix} \chi_1 \\ \chi_2 \end{Bmatrix} = 2\,\mathrm{Real}\Bigg(\mu A_0 \begin{Bmatrix} v_r \\ 1 \end{Bmatrix} e^{i\omega_c \psi_0} + \mu \begin{Bmatrix} a_{02} \\ b_{02} \end{Bmatrix} e^{i\psi_0} + \mu^2 A_0^2 \begin{Bmatrix} \alpha_2 \\ \beta_2 \end{Bmatrix} e^{i 2\omega_c \psi_0} + \mu^2 (A_0)^* \begin{Bmatrix} a_{13} \\ b_{13} \end{Bmatrix} e^{i(1-\omega_c)\psi_0}$$

$$+ A_0 \mu^2 \begin{Bmatrix} a_{14} \\ b_{14} \end{Bmatrix} e^{i(1+\omega_c)\psi_0} + \mu^2 \begin{Bmatrix} a_{15} \\ b_{15} \end{Bmatrix} e^{i 2\psi_0} \Bigg) + \tag{5.74}$$

$$\mu^2 A_0 (A_0)^* \begin{Bmatrix} \bar{\alpha}_3 \\ \bar{\beta}_3 \end{Bmatrix} + \mu^2 \begin{Bmatrix} a_{16} \\ b_{16} \end{Bmatrix} + \ldots$$

As can be seen from this equation for the lower order terms (multiplied by μ), only the nonlinearities and the forcing have an effect, while in the higher order terms (multiplied by μ^2), the nonlinearities, the parametric excitation, and the forcing will all have an influence on the blade response.

5.5.3 Case C -- Forward Flight with Dominant Parametric Excitation

For this case, the flutter frequency $\omega_c = 1/2 + \varepsilon\nu$. As shown before in this case, $\mu = \mu_1 \varepsilon$ ($\mu_o = o$) and μ_1 can be taken as $\mu_1 = 1$. Therefore, the perturbation parameter $\varepsilon = \mu$. The condition for suppressing the secular term for this case is given by Eq. 5.50 or Eq. 5.52 which cannot be solved in closed form. Conclusions regarding the behavior of A_o can be reached without actually solving Eq. 5.52 by using a phase plane analysis as described in Refs. 21 and 22. This method was applied to a similar problem by Tong (Ref. 7) and Kevorkian (Ref. 14). Suppose A_o can be written as

$$\bar{A}_o = \xi + i\eta \quad ; \quad (\bar{A}_o)^* = \xi - i\eta \tag{5.75}$$
$$\xi^2 + \eta^2 = \rho^2 = |A_o|^2$$

From the last relations and Eq. 5.52

$$\frac{\partial \xi}{\partial \psi_1} = (\bar{\kappa}_{2R} + \mu_1 \kappa_{5R} + \rho^3 \kappa_{3R})\xi - (\bar{\kappa}_{2I} - \mu_1 \kappa_{5I} + \rho^2 \kappa_{3I})\eta = X(\xi, \eta)$$
$$\frac{\partial \eta}{\partial \psi_1} = (\bar{\kappa}_{2I} + \mu_1 \kappa_{5I} + \rho^2 \kappa_{3I})\xi + (\bar{\kappa}_{2R} - \mu_1 \kappa_{5R} + \rho^2 \kappa_{3R})\eta = Y(\xi, \eta) \tag{5.76}$$

A singular point occurs when both expressions in Eq. 5.76 vanish simultaneously; thus a singular point occurs at $\xi = \eta = 0$, then $\rho = 0$.

According to Minorsky (Ref. 21), the investigation of the behavior of the equations near the origin can be limited to the linear system which can be written as

$$\frac{\partial \xi}{\partial \psi_1} = (\bar{\kappa}_{2R} + \mu_1 \kappa_{5R})\xi - (\bar{\kappa}_{2I} - \mu_1 \kappa_{5I})\eta$$

$$\frac{\partial \eta}{\partial \psi_1} = (\bar{\kappa}_{2I} + \mu_1 \kappa_{5I})\,\xi + (\bar{\kappa}_{2R} - \mu_1 \kappa_{5R})\,\eta \tag{5.77}$$

A proof which justifies the neglection of the higher order terms in Eq. 5.76 can be found in Minorsky (Ref. 21). As shown in Ref. 21, the stability of the system in the vicinity of the singular (or equilibrium point) can be qualitatively determined by using the characteristic equation

$$\begin{vmatrix} \bar{\kappa}_{2R} + \mu_1 \kappa_{5R} - S & -\kappa_{2I} + \mu_1 \kappa_{5I} \\ \kappa_{2I} + \mu_1 \kappa_{5I} & \bar{\kappa}_{2R} - \mu_1 \kappa_{5R} - S \end{vmatrix} = 0 \tag{5.78}$$

The solution of this quadratic equation for S yields

$$S_{1,2} = +\bar{\kappa}_{2R} \pm \sqrt{\bar{\kappa}_{2R}^2 - |\bar{\kappa}_2|^2 + \mu_1 |\kappa_5|^2}$$

which is also equivalent to

$$S_{1,2} = \bar{\kappa}_{2R} \pm \sqrt{\mu_1^2 |\kappa_5|^2 - \bar{\kappa}_{2I}^2} \tag{5.79}$$

According to Ref. 21, for distinct roots of Eq. 5.79, the following cases can occur:

(I) S_1, S_2 real of the same sign. The singular point is a node which is stable if S_1, S_2 are negative and unstable if they are positive.

The roots are real if $\mu_1^2 > \bar{\kappa}_{2I}/|\kappa_5|^2$. They will have the same sign if

$$\bar{\kappa}_{2R} > |\kappa_5| \sqrt{\mu_1^2 - \frac{\bar{\kappa}_{2I}^2}{|\kappa_5|^2}}$$

or $$\mu_1^2 < \frac{\bar{\kappa}_{2R}^2 + \bar{\kappa}_{2I}^2}{|\kappa_5|^2} = \frac{|\bar{\kappa}_2|^2}{|\kappa_5|^2}$$

From the last two relations, the singular point is a node when

$$\frac{\bar{\kappa}_{2I}^2}{|\kappa_5|^2} < \mu_1^2 < \frac{|\bar{\kappa}_2|^2}{|\kappa_5|^2} \tag{5.80}$$

The node is stable when $\bar{\kappa}_{2R} < 0$, and is unstable if $\bar{\kappa}_{2R} > 0$. Recall that

$$\bar{\kappa}_2 = \kappa_2 + i\nu$$

Therefore the node is stable when $\kappa_{2R} < 0$ and is unstable when $\kappa_{2R} > 0$.

(II) S_1, S_2 are of opposite sign. The singular point is a saddle point and the equilibrium is always unstable. This will occur when

$$\bar{\kappa}_{2R} < |\kappa_5| \sqrt{\mu_1^2 - \frac{|\bar{\kappa}_{2I}|^2}{|\kappa_5|^2}}$$

or when

$$\mu_1^2 > \frac{|\bar{\kappa}_2|^2}{|\kappa_5|^2} \tag{5.81}$$

(III) If S_1, S_2 are complex conjugates, the singular point is a focus. For this case, the stability of the singular point is determined by Re(s). If Re(s) < 0, the focus is stable; if Re(s) > 0, it is unstable.

The roots S_1, S_2 are complex conjugates if

$$\mu_1^2 < \frac{\bar{\kappa}_{2I}^2}{|\kappa_5|^2} \tag{5.82}$$

For this case, Eq. 5.79 can be rewritten as

$$S_{1,2} = \bar{\kappa}_{2R} \pm i|\kappa_5| \sqrt{\frac{|\bar{\kappa}_{2I}|^2}{|\kappa_5|^2} - \mu_1^2} \tag{5.83}$$

The stability depends upon the real part of S:

If $\kappa_{2R} < 0$, the focus is stable

If $\kappa_{2R} > 0$, the focus is unstable

It has been shown by Tong (Ref. 7) that additional singular points besides the origin can exist. These will have a relatively minor influence on the considerations which will be given below; therefore, these additional singular points will not be written out in detail.

In the analysis given above, the behavior of Eq. 5.52 has been analyzed in the vicinity of the singular (or equilibrium point). Another item of major importance is the determination of the conditions for the existence of closed trajectory curves (or limit cycles) of Eq. 5.52 in the ξ,η-plane. For this purpose, the Poincaré-Bendixson theory can be used (Ref. 21). In order to apply this theory the following quantity must be defined.

$$\nabla = \frac{\partial X}{\partial \xi} + \frac{\partial Y}{\partial \eta} \tag{5.84}$$

From Eqs. 5.76

$$\frac{\partial X}{\partial \xi} = \bar{\kappa}_{2R} + \mu_1 \kappa_{5R} + \rho^2 \kappa_{3R} + 2\xi^2 \kappa_{3R} - 2\xi\eta\kappa_{3I}$$

$$\frac{\partial Y}{\partial \eta} = \bar{\kappa}_{2R} - \mu_1 \kappa_{5R} + \rho^2 \kappa_{3R} + 2\eta^2 \kappa_{3R} + 2\xi\eta\kappa_{3I} \tag{5.85}$$

and

$$\nabla = 2\left(\bar{\kappa}_{2R} + 2\kappa_{3R}\rho^2\right) \tag{5.86}$$

From Green's theorem

$$\int_D \nabla \, d\xi \, d\eta = \oint (X \, d\eta - Y \, d\xi) \tag{5.87}$$

According to the Negative Criterion of Bendixson, if ∇ does not change sign (or vanish identically) with a region D of the ξ,η-plane, no closed trajectory can exist in D.

Therefore, the following possibilities exist:

(a) If $\bar{\kappa}_{2R}\kappa_{3R} > 0$ (they have the same sign, $\rho^2 > 0$)

This means that ∇ cannot change sign or vanish and the integral (Eq. 5.87) cannot be zero. Therefore no solution of Eq. 5.52 can form a closed trajectory in the ξ,η-plane.

(b) If $\bar{\kappa}_{2R}\kappa_{3R} < 0$ (i.e., they have different signs)

From Eq. 5.86

$$\nabla = 4\kappa_{3R}\left(\frac{\bar{\kappa}_{2R}}{2\kappa_{3R}} + \rho^2\right) \tag{5.88}$$

for $\rho^2 < -(\bar{\kappa}_{2R})/(2\kappa_{3R})$, ∇ will not vanish and Eq. 5.52 can have no solution which forms a closed trajectory in this region. Therefore, if there exists (the negative criterion of Bendixson does not quarantee existence) a solution of Eq. 5.52 which does form a closed trajectory in the ξ,η-plane, its minimum radial distance from the origin, ρ_{min}^2 must satisfy

$$\rho_{min}^2 \geq -\frac{\bar{\kappa}_{2R}}{2\kappa_{3R}} \tag{5.89}$$

The upper bound of ρ_{min} can be estimated when rewritting Eq. 5.52 in polar coordinates.

Let $\bar{A}_0 = \xi + i\eta = \rho e^{i\delta}$

and $\kappa_5 = |\kappa_5| e^{i\phi}$

from these and Eq. 5.52

$$\frac{\partial \rho}{\partial \psi_1} = \left[\bar{\kappa}_{2R} + \mu_1 |\kappa_5| \cos(2\delta - \phi) + \kappa_{3R} \rho^2 \right] \rho$$

$$\frac{\partial \delta}{\partial \psi_1} = \left[\bar{\kappa}_{2I} - \mu_1 |\kappa_5| \sin(2\delta - \phi) + \kappa_{3I} \rho^2 \right] \tag{5.90}$$

The upper bound will be estimated without making use of Bendixson's negative criterion. The quantity ρ is always positive. Therefore, the right-hand side of Eq. 5.90 will be monotonic and will not change sign outside of the range

$$\max\left(0, -\frac{\bar{\kappa}_{2R}}{\kappa_{3R}} - \mu_1 \frac{|\kappa_5|}{|\kappa_{3R}|}\right) \leq \rho^2 \leq -\frac{\bar{\kappa}_{2R}}{\kappa_{3R}} + \mu_1 \frac{|\kappa_5|}{|\kappa_{3R}|} \tag{5.91}$$

From this relation, if Eq. 5.90 has a solution in the form of a closed trajectory in the ξ,η-plane, its radial distance from the origin must be bounded by Eq. 5.91.

The last bounds, Eqs. 5.91 and 5.89, can be combined to give a bound on the limit cycle amplitude, if it exists.

$$\max\left(-\frac{\bar{\kappa}_{2R}}{2\kappa_{3R}}, -\frac{\kappa_{2R}}{\kappa_{3R}} - \mu_1 \frac{|\kappa_5|}{|\kappa_{3R}|}\right) \leq \rho_{min}^2 \leq -\frac{\bar{\kappa}_{2R}}{\kappa_{3R}} + \mu_0 \frac{|\kappa_5|}{|\kappa_{3R}|} \tag{5.92}$$

Note that in both cases considered above, ρ is a monotonic function of ψ_1.

For large amplitudes (i.e., large values of ρ), the behavior of ρ can be approximated by

$$\frac{\partial \rho}{\partial \psi_1} \simeq \kappa_{3R} \rho^3 \tag{5.93}$$

From Eq. 5.93, if $\kappa_{3R} < 0$, ρ will monotonically decrease in the region of large amplitudes; i.e., the solution will converge to a limit cycle if it exists, or to a stable equilibrium point (or singular point). Therefore, this represents a stable situation.

If $\kappa_{3R} > 0$, will monotonically increase in the region of large amplitudes; i.e., the blade is always unstable, if the disturbance is large enough. From Eq. G.71, it is clear that κ_3 depends mainly upon the nonlinear coupling

of the system, so that the nonlinear coupling is the decisive factor at large disturbances. From Eq. G.73, it can be seen that κ_5 depends upon both the parametric excitation and nonlinear coupling with response due to forward flight. Therefore, on the basis of this approximate analysis, it can be concluded that the location of the singular points and the magnitude of the limit cycle oscillation (if it exists) will depend upon the parametric excitation and nonlinear coupling.

In addition to the effects discussed, a change in the forward flight velocity with C_T fixed will affect κ_{2R} by changing θ_1, and λ_1 according to Eq.5.72 discussed in the previous section. Therefore forward flight will considerably influence the stability of the system and it will also affect all of the bounds obtained for the limit cycle amplitude in this section.

The amplitudes of blade response can be obtained from Eqs. 5.1, 5.20, and 5.33.

$$\begin{Bmatrix} \chi_1 \\ \chi_2 \end{Bmatrix} = 2\,\mathrm{Real}\left(\mu^{1/2} A_0 \begin{Bmatrix} \nu_r \\ 1 \end{Bmatrix} e^{i\omega_c \psi_0} + \mu A_0^2 \begin{Bmatrix} \alpha_2 \\ \beta_2 \end{Bmatrix} e^{i2\omega_c \psi_0} + \mu (A_0)^* A_0 \begin{Bmatrix} \alpha_3 \\ \beta_3 \end{Bmatrix} + \mu \begin{Bmatrix} \alpha_1 \\ \beta_1 \end{Bmatrix} e^{i\psi_0} + \cdots \right) \tag{5.94}$$

Due to the convenient form of the solution (Eq. 5.94), it is possible to rewrite Eq. 5.52 in terms of the actual physical quantities associated with the problem in a manner described in detail in Subsection 5.5.4.

Let $$\tilde{\chi}_2 = \epsilon^{1/2} \bar{A}_0 = \epsilon^{1/2} A_0 e^{i\nu\psi_1}$$

Then Eq. 5.52 can be rewritten as

$$\frac{d\bar{\chi}_2}{d\psi_0} = \left[\kappa_{2\theta_1}(\theta - \theta_c) + \kappa_{2\lambda_1}(\lambda_0 - \lambda_{0c}) + i\left(\omega_c - \frac{1}{2}\right) \right] \tilde{\chi}_2 + \mu \kappa_5 (\tilde{\chi}_2)^* + \kappa_3 \tilde{\chi}_2^2 (\tilde{\chi}_2)^* \tag{5.52a}$$

When considering only the linear part of this equation which is equivalent to Eq. 5.77, the last term in Eq. 5.52a can be neglected. Consequently, the characteristic equation (Eq. 5.79) can also be rewritten in terms of the physical quantities as

$$S_{1,2} = (K_{2\theta_1})_R(\theta - \theta_c) + (K_{2\lambda_1})(\lambda_o - \lambda_{oc}) \pm \sqrt{\mu^2 |K_5|^2 - \left[(K_{2\theta_1})_I(\theta - \theta_c) + (K_{2\lambda_1})_I(\lambda_o - \lambda_{oc}) + \left(\omega_c - \frac{1}{2}\right)\right]^2} \tag{5.79a}$$

The solution of the linearized system is the same as the one derived in Appendix H for Eqs. H.2 and H.3, and can be written as

$$\tilde{\chi}_2 = \bar{\bar{D}}_1 e^{S_1 \psi_o} + \bar{\bar{D}}_2 e^{S_2 \psi_o}$$

where $\bar{\bar{D}}_1$ and $\bar{\bar{D}}_2$ are equivalent to D_1, D_2 used in Appendix H when $K_6 = 0$ and $\mu^2 K_9$ is replaced by μK_5 in the appropriate relations. As is shown in Appendix H, A_o for the linearized system can be written as

$$A_o = \frac{\tilde{\chi}_2 e^{-i\nu\mu\psi_o}}{\mu^{1/2}}$$

5.5.4 Case D, Forward Flight with $\omega_c = 1 + \varepsilon\nu$

This is a case in which the flutter frequency is close to the forcing frequency. Since the system is being excited at its resonance frequency, the amplitudes of blade response can be expected to occur at moderate levels only when the excitation is assumed to be small (see Section 5.4.4). The excitation is represented by $\mu F_o(\psi_o, \theta_c); \mu H_o(\psi_o, \theta_c)$ where F_o, H_o are given by Eqs. 5.36 and 5.37. In most cases considered, θ_c cannot be assumed to be too small (see Section 7). Therefore, it will be necessary to assume that the solution derived in this section is valid for small values of the advance ratio μ and small values of C_T.

For this case, a complete phase-plane analysis similar to the one performed in the previous section is possible, but cumbersome; therefore a somewhat different approach will be used. Using Eqs. 5.1, 5.20 and 5.38, the solution for this case can be written as

$$\begin{Bmatrix} \chi_1 \\ \chi_2 \end{Bmatrix} = 2\,\mathrm{Real}\left(\mu A_o \begin{Bmatrix} v_r \\ 1 \end{Bmatrix} e^{i\omega_c \psi_o} + \mu^2 A_o^2 \begin{Bmatrix} \alpha_2 \\ \beta_2 \end{Bmatrix} e^{i\omega_c \psi_o 2} + \right.$$

$$\mu^2 (A_o)^* \begin{Bmatrix} \bar{a}_{13} \\ \bar{b}_{13} \end{Bmatrix} e^{i(1-\omega_c)\psi_o} + \mu^2 A_o \begin{Bmatrix} \bar{a}_{14} \\ \bar{b}_{14} \end{Bmatrix} e^{i(1+\omega_c)\psi_o}$$

$$\left. + \mu^2 \begin{Bmatrix} \bar{a}_{15} \\ \bar{b}_{15} \end{Bmatrix} e^{i2\psi_o} \right) + \mu^2 A_o (A_o)^* \begin{Bmatrix} \bar{\alpha}_3 \\ \bar{\beta}_3 \end{Bmatrix} +$$

$$\mu^2 \begin{Bmatrix} \bar{a}_{16} \\ \bar{b}_{16} \end{Bmatrix} + \ldots\ldots \qquad (5.94)$$

Due to the convenient form of the solution for this case, it is possible to rewrite Eq. 5.58 in terms of the actual physical quantities associated with the problem. For this purpose, it is convenient to define a quantity

$$\bar{\chi}_2 = \varepsilon^{1/2} \tilde{A}_o \tag{5.95}$$

where A_o is given by Eq. 5.57. Thus, the first-order solution for the lag motion, according to Eq. 5.94 is given by

$$\chi_2 = 2\, Real(\bar{\chi}_2) = 2\varepsilon^{1/2}\, Real(\tilde{A}_o) \tag{5.96}$$

Using Eqs. 5.59, 5.72, and 5.73 together with

$$\omega_c = 1 + \varepsilon\hat{\nu}$$

the following relation can be written

$$\tilde{\kappa}_2 = (\kappa_{2\theta_1})\frac{(\theta - \theta_c)}{\varepsilon} + (\kappa_{2\lambda_1})\frac{(\lambda_o - \lambda_{oc})}{\varepsilon} + \frac{i(\omega_c - 1)}{\varepsilon} \tag{5.97}$$

Using Eqs. 5.95 and 5.97, together with $\mu = \mu_o \varepsilon^{1/2}$ and $\psi_1 = \varepsilon\psi_o$, Eq. 5.58 can be rewritten in terms of the physical quantities

$$\frac{d\bar{\chi}_2}{d\psi_o} = \left[\kappa_{2\theta_1}(\theta - \theta_c) + \kappa_{2\lambda_1}(\lambda_o - \lambda_{oc}) + i(\omega_c - 1)\right]\bar{\chi}_2 + \mu^2\left[\bar{\kappa}_6\bar{\chi}_2 + \kappa_9(\bar{\chi}_2)^*\right]$$

$$+ \kappa_3\bar{\chi}_2^2(\chi_2)^* + \mu\left[\kappa_8(\bar{\chi}_2)^* + \kappa_{10}\bar{\chi}_2\right]\bar{\chi}_2 +$$

$$\mu\kappa_4 + \mu^3\kappa_7 \tag{5.98}$$

In the last relation, the term $\kappa_3\chi_2^2(\bar{\chi})^*$ is due to the nonlinear coupling of the flutter mode, while the term $\mu[\kappa_8(\bar{\chi}_2)^* + \kappa_{10}\bar{\chi}_2]\,\bar{\chi}_2$ is due to the nonlinear coupling of the flutter mode and the parametric excitation. The solution of Eq. 5.98 in closed form is required in order to investigate the nonlinear response of the blade. Due to the complex form, Eq. 5.98, this would

be very complicated; therefore, the linearized form of Eq. 5.98 as given by Eq. 5.99 will be treated first.

$$\frac{d\bar{\chi}_2}{d\psi_0} = \left[K_{2\theta_1}(\theta-\theta_c) + K_{2\lambda_1}(\lambda_0-\lambda_{0c}) + \mu^2 \bar{K}_6 \right] \bar{\chi}_2$$

$$+ \mu^2 K_9 (\bar{\chi}_2)^* + \mu K_4 + \mu^3 K_7 \tag{5.99}$$

Let

$$\bar{\chi}_2 = \xi + i\eta \tag{5.100}$$

then the real and imaginary parts of Eq. 5.99 yield a system of two first-order differential equations:

$$\frac{d\xi}{d\psi_0} = \left[(K_{2\theta_1})_R (\theta-\theta_c) + (K_{2\lambda_1})_R + \mu^2 \bar{K}_{6R} \right] \xi - \left[(K_{2\theta_1})_I (\theta-\theta_c) + (K_{2\lambda_1})_I (\lambda_0-\lambda_{0c}) \right.$$

$$\left. + (\omega_c - 1) + \mu^2 \bar{K}_{6I} \right] \eta + \mu^2 \left[K_{9R} \xi + K_{9I} \eta \right]$$

$$+ \mu K_{4R} + \mu^3 K_{7R} \tag{5.101}$$

$$\frac{d\eta}{d\psi_0} = \left[(K_{2\theta_1})_R (\theta-\theta_c) + (K_{2\lambda_1})_R (\lambda_0-\lambda_{0c}) + \mu^2 \bar{K}_{6R} \right] \eta +$$

$$\left[(K_{2\theta_1})_I (\theta-\theta_c) + \mu^2 \bar{K}_{6I} + (K_{2\lambda_1})_I (\lambda_0-\lambda_{0c}) + (\omega_c - 1) \right] \xi +$$

$$+ \mu^2 \left(K_{9I} \xi - K_{9R} \eta \right) + \mu K_{4I} + \mu^3 K_{7I} \tag{5.102}$$

The solution to Eqs. 5.101 and 5.102 can be found in Ref. 22, and it is analogous to the treatment given to Eqs. 5:77 in Subsection 5.5.3. For the sake of completeness, the solution of these equations is given in Appendix H.

The solution of the homogeneous linearized system is given by Eqs. H.6 and its stability depends upon the roots of the characteristic equation:

$$S_{1,2} = (K_{2\theta_1})_R(\theta-\theta_c)+(K_{2\lambda_1})_R(\lambda_o-\lambda_{oc}) \pm \sqrt{\mu^4|K_q|^2 - \left[(K_{2\theta_1})_I(\theta-\theta_c)+(K_{2\lambda_1})_I(\lambda_o-\lambda_{oc})+(\omega_c-1)+\mu^2\bar{K}_{6I}\right]^2} \tag{5.103}$$

The linearized solution is stable if $Re(S_1)$ and $Re(S_2) < 0$, and the stability boundary is given by

$$Re(S_1) = 0 \tag{5.104}$$

The solution to the complete nonhomogeneous equations is given by Eq. H.14. From this relation, an approximate relation for A_o can be written as:

$$A_o = \frac{1}{\mu} e^{-i\nu\mu^2\psi_0}\left[\bar{D}_1 e^{S_1\psi_0} + \bar{D}_2 e^{S_2\psi_0} + \xi_p + i\eta_p\right] \tag{5.105}$$

It is important to note that due to the nonhomogeneous form of Eqs. 5.101 and 5.102, the flutter mode for this case will always be excited. This is also evident from Eq. 5.105.

As mentioned in Subsection 5.5.2, for trimmed forward flight with a fixed value of C_T, the variation of μ will strongly affect the quantity $(\theta - \theta_c)$ and $(\lambda_o - \lambda_{oc})$. Thus, the stability boundary represented by Eq. 5.104 will be strongly dependent upon the advance ratio.

SECTION 6

UNIFORMLY VALID SOLUTIONS

6.1 Uniformly Valid Expansion

From the numerical results obtained, which will be discussed in detail in the following section, it is clear that the cases of practical interest will occur at values of collective pitch $\theta < \theta_c$. Therefore, it is important to extend the validity of the solutions obtained in the previous sections (which are valid near the critical condition) to a region which extends below the critical condition.

This problem is discussed in detail in Ref. 8 where a conventional method (Ref. 6) for matching asymptotic solutions near and below the critical condition is used.

The matching is achieved by using an additional small parameter $\tilde{\varepsilon}$ which has the following properties:

$$1 >> \tilde{\varepsilon} > 0 \qquad \text{and} \qquad \frac{\varepsilon}{\tilde{\varepsilon}} << 1$$

$\tilde{\varepsilon}$ is related to the parameters of the problem by Eq. 6.1:

$$\theta - \theta_c = -\frac{\varepsilon}{\tilde{\varepsilon}} \tag{6.1}$$

The last equation can be also rewritten as

$$\tilde{\varepsilon} = -\frac{\varepsilon}{\theta - \theta_c} = -\frac{1}{\theta_1} \tag{6.2}$$

In the cases with forward flight, the perturbation parameter ε can be associated either with $\varepsilon = \mu^2$ (Cases B and D) or with $\varepsilon = \mu$ (Case C).

From the numerical results presented in Section 7, it is clear that in trimmed forward flight at fixed C_T, the range of variation for $|\theta - \theta_c|$ is

$$0 < |\theta - \theta_c| \leq .12$$

while the range of variation for μ can be taken as

$$0 < \mu \leq .3$$

Then for Cases B and D

$$\tilde{\varepsilon} = -\frac{\mu^2}{\theta - \theta_c} = -\frac{1}{\theta_1} \tag{6.3}$$

and the requirement that $\tilde{\varepsilon} < 1$ may not be satisfied for certain combinations of C_T and μ.

For Case C

$$\tilde{\varepsilon} = -\frac{\mu}{\theta - \theta_c} = -\frac{1}{\theta_1} \tag{6.4}$$

Therefore, for this case, the uniformly valid expansion will be correct for $\mu < 0.15$, approximately.

If the expansion near the critical condition and below the critical condition are denoted by subscripts "n" and "b", respectively, the requirement for matching the solutions is (Ref. 8):

$$\frac{\begin{Bmatrix} \chi_1 \\ \chi_2 \end{Bmatrix}_n - \begin{Bmatrix} \chi_1 \\ \chi_2 \end{Bmatrix}_b}{\varepsilon^{\alpha}} \to 0 \tag{6.5}$$

as $\varepsilon, \tilde{\varepsilon} \to 0$ with ψ_1 fixed, for $\alpha = 1/2, 1, 3/2$ and the uniformly valid expansion can be written as

$$\begin{Bmatrix} \chi_1 \\ \chi_2 \end{Bmatrix} = \begin{Bmatrix} \chi_1 \\ \chi_2 \end{Bmatrix}_n + \begin{Bmatrix} \chi_1 \\ \chi_2 \end{Bmatrix}_b - \begin{Bmatrix} \chi_1 \\ \chi_2 \end{Bmatrix}_{\text{common}} \tag{6.6}$$

where the last term in Eq. 6.6 is the common part in the expansions

$$\begin{Bmatrix} \chi_1 \\ \chi_2 \end{Bmatrix}_n \quad \text{and} \quad \begin{Bmatrix} \chi_1 \\ \chi_2 \end{Bmatrix}_b \; .$$

6.2 Uniformly Valid Solutions for the Various Cases Considered

The uniformly valid solutions for the four cases considered in Section 5 can be easily obtained.

Case A, Hovering Flight ($\mu = 0$)

For this case, the solution below the critical condition is

$\begin{Bmatrix} \chi_1 \\ \chi_2 \end{Bmatrix}_b = 0$ while $\begin{Bmatrix} \chi_1 \\ \chi_2 \end{Bmatrix}_n$ is given by Eqs. 5.65.

According to Eq. 5.72, κ_2 is linearly proportional to θ_1, below the critical condition $\theta_1 = \theta - \theta_c$ and is a negative quantity. For this case, the last term in Eq. 5.47 can be neglected and its solution can be written as

$$A_o = A_i \, e^{\kappa_2 \psi_1} \tag{6.7}$$

where A_i is a constant determined from the initial conditions. The solution will be exponentially decaying below θ_c and Eq. 6.5 is satisfied.

Case B, General Forward Flight Case

As mentioned before, for this case $\mu = \varepsilon^{1/2}$ and the flutter frequency can be arbitrary, except $\omega_c = 1/2 + \varepsilon\nu$ or $\omega_c = 1 + \varepsilon\nu$. According to Subsection 5.5.2 for $\theta < \theta_c$ and $\mu < 0.3$, Eq. 5.46 represents an exponentially decaying function. For this case A_o can be approximately taken as

$$A_o = A_i \, e^{\kappa_2 \psi_1} \tag{6.8}$$

The solution for $\begin{Bmatrix} \chi_1 \\ \chi_2 \end{Bmatrix}_n$ is given by Eq. 5.74. The solution below the critical condition, with Eq. 6.8, will be composed only of the parts of Eq. 5.74 which are independent of A_o. These parts will match and Eq. 6.5 will be satisfied. From Eqs. 6.6 and 5.74, the uniformly valid asymptotic expansion can be written as

$$\begin{Bmatrix} \chi_1 \\ \chi_2 \end{Bmatrix} = 2\,\mathrm{Real}\left(\mu A_0 \begin{Bmatrix} v_r \\ 1 \end{Bmatrix} e^{i\omega_c \psi_0} + \mu \begin{Bmatrix} a_{02} \\ b_{02} \end{Bmatrix} e^{i\psi_0} \right.$$

$$+ \mu^2 A_0^2 \begin{Bmatrix} \alpha_2 \\ \beta_2 \end{Bmatrix} e^{i2\omega_c \psi_0} + \mu^2 (A_0)^* \begin{Bmatrix} a_{13} \\ b_{13} \end{Bmatrix} e^{i(1-\omega_c)\psi_0}$$

$$\left. + \mu^2 A_0 \begin{Bmatrix} a_{14} \\ b_{14} \end{Bmatrix} e^{i(1+\omega_c)\psi_0} + \mu^2 \begin{Bmatrix} a_{15} \\ b_{15} \end{Bmatrix} e^{i2\psi_0} \right)$$

$$+ \mu^2 (A_0)(A_0)^* \begin{Bmatrix} \bar{\alpha}_3 \\ \bar{\beta}_3 \end{Bmatrix} + \mu^2 \begin{Bmatrix} a_{16} \\ b_{16} \end{Bmatrix}$$

(6.9)

Equation 6.9 is similar to Eq. 5.74. The only difference is that for Eq. 6.9, the various quantities a_{o2}, b_{o2}, α_2, β_2, a_{13} ..., X_{Ho}, Y_{Go}, ..., etc., must be evaluated at the actual value of θ and λ_o as determined by the trim calculation, instead of evaluating them at the critical condition.

Case C, Forward Flight with Dominant Parametric Excitation

For this case, the flutter frequency is $\omega_c = 1/2 + \varepsilon\nu$ and $\mu = \varepsilon$. Below the critical condition A_o can be taken as given by the last equation on page 46. The flutter mode is not excited and will be a decaying oscillation. Thus, the solution below the critical condition will be independent of A_o and will match the appropriate part of $\begin{Bmatrix} \chi_1 \\ \chi_2 \end{Bmatrix}_n$, satisfying Eq. 6.5. From Eqs. 5.94 and 6.6, the uniformly valid expansion can be written as

$$\begin{Bmatrix}\chi_1\\ \chi_2\end{Bmatrix} = 2\,\text{Real}\left(\mu^{1/2} A_o \begin{Bmatrix}v_r\\ 1\end{Bmatrix} e^{i\omega_c \psi_o} + \mu A_o^2 \begin{Bmatrix}\alpha_2\\ \beta_2\end{Bmatrix} e^{i2\omega_c \psi_o} + \right.$$

$$\left. + \mu\, A_o (A_o)^* \begin{Bmatrix}\alpha_3\\ \beta_3\end{Bmatrix} + \mu \begin{Bmatrix}\alpha_1\\ \beta_1\end{Bmatrix} e^{i\psi_o} + \cdots \right)$$

(6.10)

As pointed out in Subsection 6.1, Eq. 6.10 is valid for $0 < \mu < 0.15$. In Eq. 6.10, the various quantities α_2, β_2, α_3, β_3, α_1, β_1, ... , etc. must be evaluated at the values of θ and λ_o as determined from the trim calculation.

Case D, Forward Flight with $\omega_c = 1 + \varepsilon\nu$

For this case $\mu = \varepsilon^{1/2}\mu_o$ and $\mu_o = 1$. Below the critical condition A_o can be approximately determined from Eqs. H.14 and H.15 given in Appendix H and the solution for $\begin{Bmatrix}\chi_1\\ \chi_2\end{Bmatrix}_b$ is given by Eq. 5.94. As pointed out previously in Subsection 5.5.4, for this case, due to the nonhomogeneous form of Eqs. 5.101 and 5.102, the flutter mode will always be excited; therefore, the matching procedure is no longer simple. The solution $\begin{Bmatrix}\chi_1\\ \chi_2\end{Bmatrix}_h$ can be obtained only by solving Eq. 5.98 which is difficult to obtain in closed form; therefore $\begin{Bmatrix}\chi_1\\ \chi_2\end{Bmatrix}_{\text{common}}$ cannot be evaluated. It can be concluded, therefore, that a uniformly valid expansion for this case is difficult to obtain analytically. Therefore, this case can be handled most conveniently by direct numerical integration. As mentioned in Subsection 5.5.4, the analytical treatment for this case is correct only for small values of the harmonic forcing which implies low values of μ (i.e., $0 < \mu < 0.20$) Therefore, direct numerical treatment of this case will have the additional advantage of not being limited to small values of μ and C_T.

SECTION 7

RESULTS AND DISCUSSION

7.1 Numerical Quantities Used in the Calculation

In this section, the numerical values of the various quantities used in the computation of the results are given:

(1) Mass distribution was taken as a constant along the blade span

(2) C_{d_o} = 0.010 in all of the calculations

(3) Lift-curve slope, a = 2π

(4) Equivalent flat-plate area was taken as $f/\pi R^2 = 1/100$ unless otherwise stated. This value of f results in C_{Dp} = 0.01. This quantity is typical for modern well-designed helicopters

(5) The mode shape in flap is the same as the mode shape in lag; both were approximated by the first nonrotating mode shape which can be approximately written as

$$\eta_1 = \left(-\frac{1}{3}\right)\left[1 - 4\bar{X}_o - (1-\bar{X}_o)^4\right] \tag{7.1}$$

This relation was taken from Ref. 12.

Equation 7.1 satisfies all of the boundary conditions of the problem. As pointed out by Bramwell (Ref. 20), to get the correct first rotating flapping mode shape of a hingeless blade, as many as six or more expressions of type Eq. 7.2 should be combined:

$$\eta_j = a_j\left[1 - (j+3)\bar{X}_o - (1-\bar{X}_o)^{j+3}\right] \tag{7.2}$$

Approximation (Eq. 7.1) to the mode would have influenced the results to a certain degree if the rotating flap and lag frequencies were calculated by using the $(EI)_y$, $(EI)_z$, and m distributions.

In fact, in all of the calculations, the values of $\bar{\omega}_{Fl}$, $\bar{\omega}_{Ll}$ were selected so as to give a certain ω_c, or θ_c and the mode shape was kept constant during all of the calculations.

(6) The flap and lag coefficients, F^i, L^i defined in Appendix C (and mass quantities defined in Appendix B) were numerically evaluated using a seven-point Gaussian integration. This integration scheme is accurate up to polynomials of degree 13 (Ref. 25). The weights for Gaussian integration were taken from Ref. 26. The numerical values for these coefficients for $\ell/R = 1.0$ and $\bar{A} = 0$, $\bar{B} = 1$ are given in Table 1.

(7) The quantities $\tilde{C}_1$, $\tilde{D}_1$, $\tilde{F}_1$, $\tilde{G}_1$, $\tilde{\eta}_1(1)$ used in the trim calculation described in Appendix F were evaluated using the approximate equations given for them in Ref. 20. The approximations of these relations in Bramwell (Ref. 20) are based upon a concept of an equivalent rotor with an elastic hinge offset and are sufficient for trim calculations. The concept of equivalent hinge offset employed by Bramwell is not similar to Young's more widely used concept of equivalent blade because its value is associated only with the frequency (Ref. 27).

(8) The range of thrust coefficients used in the calculations is $0.005 < C_T < 0.015$. The practical range is $0.005 < C_T < 0.01$. The range 0.005 to 0.015 was selected so as to include cases which could occur during violent maneuvers or gusts.

(9) The range of frequencies for flap was taken between

$$1.05 < \bar{\omega}_{Fl} < 1.6$$

For lag, the range was selected as

$$0.8 < \bar{\omega}_{Ll} < 1.5$$

For most cases devoted to studying the flap-lag-type of instability, the lag frequency was taken as greater than one to avoid the possibility of air or ground resonance (Ref. 28). A limited number of cases with lag frequencies below one were studied in Ref. 9.

(10) The range of Locke numbers was taken as

$5 \leq \gamma \leq 10$

All calculations were performed for either $\gamma = 5$, or $\gamma = 10$. The Locke numbers more representative of a hingeless helicopter blade are $7 < \gamma < 10$ (Ref. 28).

(11) Unless otherwise stated, the solidity ratio in all of the calculations was taken as

$$\sigma = 0.05$$

(12) The range for the structural damping in the calculations was taken as

$$0 < \eta_{SF1}, \eta_{SL1} < 0.02$$

This range is sufficient to clearly illustrate the effect of structural damping. In some modern elastomeric bearings, the value of the structural damping can be as high as 0.05.

7.2 Description of the Methods Used for Obtaining Numerical Results

The results presented in this section were obtained by two distinct methods:

(a) The expressions obtained by solving Eqs. 3.23 and 3.24 by the perturbation method were programmed on a computer, to obtain the analytical solution in numerical form.

(b) For a certain number of cases, the solutions were obtained by direct numerical integration of Eqs. 3.23 and 3.24, using the predictor-corrector method (Ref. 29).

The reason for numerical integration was twofold. First, it served as a convenient way to check the solutions obtained analytically. Second, in some cases, the two methods were complementary to each other; i.e., by knowing the solutions from numerical integration, it was easier to derive them in analytical form.

It should be mentioned that the a priori knowledge of the limit cycle amplitude as obtained from Eq. 5.66 was extremely helpful in obtaining the limit cycle by numerical integration. Specifically, the low damping in lag and the

the time scale $\psi_1 = \varepsilon\psi_o$ in which the amplitude growth is represented, combine so that the time required to reach a limit cycle can be of order $\psi_o = 600$, if the initial conditions are not close to the limit cycle value of the amplitudes. This can be shown analytically, also. This effect would preclude the use of numerical integration for obtaining limit-cycle amplitudes in hover without a priori knowledge of the value of the limit-cycle amplitudes.

Finally, it is of interest to note that the predictor-corrector method is equivalent in accuracy and computing time to the fourth order Runge Kutta method. At first glance, it appears that the predictor-corrector method should be more efficient in terms of computing time because it requires one half the number of points per interval of integration as the Runge Kutta method. As pointed out by Lapidus (Ref. 30), the numerical stability of the predictor-corrector method for linear problems is worse than that of the Runge Kutta method by a factor of two (approximately). Therefore, in order to obtain the same accuracy, twice as many intervals are required in the predictor-corrector method. This effect will cancel the apparent advantage of the predictor-corrector method due to the smaller number of points per interval. For a nonlinear analysis, this situation will be somewhat modified, but numerical experiments performed indicate that the two methods are essentially equivalent in computing time when requiring the same amount of accuracy.

7.3 Results for Hovering Flight

7.3.1 Stability Boundaries in Hover Without Structural Damping

From the solution to the linearized problem, described in Section 4, with no structural damping ($\eta_{SF1} = \eta_{SL1} = 0$), stability boundaries resembling ellipses can be drawn. The value of θ_c specified on the curve is the value of collective pitch above which the linear system becomes unstable in hover. The unstable combinations of $\bar{\omega}_{F1}$ and $\bar{\omega}_{L1}$ are given by the area inside of the curve.

Figures 3 and 4 show the stability boundaries with the inflow evaluated from Eq. 5.5 for hingeless elastic blades with F^i, L^i as given in Table 1. The limit cycle amplitudes which would occur when crossing into the post-critical range $\theta > \theta_c$ were calculated using the equations and the criteria given in

Subsection 5.5.1. The dotted part of the stability boundaries represents combinations of flap and lag frequencies such that unstable limit cycles occur. In order to check upon this prediction of stable and unstable limit cycles, three points along the stability boundary (Fig. 4, $\theta_c = 0.20$), denoted by a, b, c in Fig. 4 were also checked by numerical integration. The results are shown in Figs. 5, 6, and 7. Figures 5 and 6 indicate the stable limit cycles, while Fig. 7 shows an unstable limit cycle.

From Figs. 3 and 4, it is clear that by increasing γ, the unstable areas enclosed are considerably increased.* The inner curve $\theta_c = 0.175$ in Fig. 4 shows approximately the minimum value of θ_c for $\gamma = 10$ below which no instability can occur.

Figures 8 and 10 show the appropriate stability boundaries for the elastic blade where the inflow as represented by Eq. 5.5 is replaced by the inflow calculated from Eq. 7.3.

$$\lambda_o = \frac{a\sigma}{16}\left[\sqrt{1 + \frac{24\theta}{a\sigma}} - 1\right] \tag{7.3}$$

This inflow relation is equivalent to taking the induced velocity at 3/4R of the blade as representative of the constant induced velocity over the whole disc. As pointed out in Appendix D, this assumption gives values of C_T which are not in agreement with those given by momentum theory. The use of Eq. 7.3 in the computation of the stability boundaries decreases the size of the unstable areas enclosed by the stability boundaries. The physical explanation for this effect is clear if the effective angle of attack defined as

$$\bar{\alpha} = \xi_1\theta - \xi_2\lambda_o$$

$$\xi_1 = \left(\frac{\ell}{R}\right)^2 \frac{1}{\bar{M}_{FI}} 4F' \quad ; \quad \xi_2 = \left(\frac{\ell}{R}\right)^2 \frac{1}{\bar{M}_{FI}} 4F^2 \tag{7.4}$$

is considered, as the physically meaningful quantity.

---

*Stability boundaries given for $\gamma = 5$ and $\gamma = 10$ can also be considered to be representative of the lift deficiency function of $C(k) = 0.5$ (with respect to $\gamma = 10$). ($C(k)$ for this case is not frequency dependent (Ref. 31)).

Equation 7.3 yields higher values of λ_o than Eq. 4.6 for the same value of θ; therefore, from Eq. 7.4 it is clear that the use of this inflow relation yields lower values of $\bar{\alpha}$, resulting in a system which is more stable than in reality.

Finally, if Eq. 7.3 is replaced by the assumption that constant induced velocity is that which would be obtained by taking the angle of inflow at 3/4R as representative of the blade, the following relation for λ_o is obtained

$$\lambda_o = \frac{a\sigma}{12}\left[\sqrt{1+\frac{24\theta}{a\sigma}}-1\right] \tag{7.5}$$

Of the various inflow relations (i.e., Eqs. 5.5, 7.3, and 7.5) the highest value of inflow, for a given value of pitch setting, is obtained from Eq. 7.5. A typical stability boundary obtained using Eq. 7.5 is shown in Fig. 9. Comparison of Figs. 4, 8, and 9 shows that this assumption results in a further reduction in the unstable area inside the stability boundary.

Figure 10 shows the comparison of the stability boundaries obtained by considering the elastic blade as modeled in this report and comparing it to the centrally-hinged, spring-restrained blade for which the stability boundaries were obtained by Ormiston and Hodges (Ref. 3). Only the case $\gamma = 5$, $\theta_c = 0.20$ is considered. As seen, the elastic modeling of the blade results in a slight increase in the unstable area inside of the stability boundary, while at the same time the location of the whole ellipse is shifted in the $\bar{\omega}_{Fl}$, $\bar{\omega}_{Ll}$ plane.

Comparison of the two stability boundaries given in Fig. 10 reveals a significant effect of the mode shape in shifting the stability boundaries. This result implies that a hinge offset should be included in the centrally-hinged, spring restrained rigid blade model of the elastic hingeless blade.

7.3.2 The Effect of Structural Damping on the Stability Boundaries

Figures 11 and 12 show the effect of structural damping in lag on the value of θ_c for the following four cases:

(1) $\omega_{F10} = 1.2$ $\omega_{L10} = 1.03861$ $\eta_{SF1} = 0.005$ $\gamma = 10$

$\omega_{F10} = 1.2625$ $\omega_{L10} = 1.1$ $\eta_{SF1} = 0.005$ $\gamma = 10$

$\omega_{F10} = 1.200$ $\omega_{L10} = 1.1375$ $\eta_{SF1} = 0.005$ $\gamma = 10$

$\omega_{F10} = 1.175$ $\omega_{L10} = 1.33319$ $\eta_{SF1} = 0.005$ $\gamma = 10$

As seen from these curves, the structural damping has a very strong effect on the value of θ_c. The increase in θ_c due to the addition of η_{SL1} is very strong for small additions of structural damping and levels off around $\eta_{SL1} \tilde{=} 0.015$. This is mainly due to the low value of C_{d_o}/a.

The effect of the structural damping on the stability boundaries is very important because it raises the values of θ_c beyond practical values of collective pitch, and consequently (see Fig. 4) it raises the minimum value of θ_c below which no instability in the linear sense can occur.

The amount of structural damping in flap has no effect on the value of θ_c, except that it changes the third significant figure in θ_c, within $0 < \eta_{SF1} < 0.02$.

7.3.3 Limit Cycle Amplitudes

For the cases where stable limit cycles exist, see Figs. 3 and 4. The limit-cycle amplitudes can be obtained from Eq. 5.66.

From Eq. 5.65, for values of ϵ, $\epsilon/\theta_c < 1$, the maximum values of χ_1, χ_2 at their limit cycle value can be obtained approximately from

$$|A_o| = \rho_{l.c.}$$

where $\rho_{l.c.}$ is given by Eq. 5.66 and

$$\begin{Bmatrix} \chi_1 \\ \chi_2 \end{Bmatrix}_{l.c} = 2\rho_{l.c.}\,\epsilon^{1/2} \begin{Bmatrix} |v_r| \\ 1 \end{Bmatrix} \tag{7.6}$$

A typical limit-cycle amplitude-response curve as obtained from Eq. 7.6 is given in Fig. 13 and is indicated by the full lines.

In order to check the results obtained from the perturbation method, these results were also obtained by numerical integration. As seen from Fig. 13, the agreement between the results is quite good.

Figure 14 shows the effect of the structural damping on $\rho_{\ell.c.}$ for a typical case. As can be seen, the decrease in $\rho_{\ell.c.}$ starts to level off around $\eta_{SL1} \tilde{=} 0.015$.

To illustrate the effect of the structural damping on the location and steepness of the limit cycle, amplitude-response curves, the points corresponding to $\eta_{SL1} = 0$, $\eta_{SL1} = 0.0025$ and $\eta_{SL1} = 0.00625$ of Fig. 14 are plotted in Fig. 15. These curves were calculated using Eq. 7.6. As seen from Fig. 15, the structural damping changes drastically the location of the limit-cycle response curves. Increasing the value of η_{SL1} tends also to reduce the steepness of the limit-cycle-response curves.

The steepness of the limit-cycle-response curves is an indication of the stabilizing effect of the nonlinearities of the system. It also indicates how far θ_c can be exceeded before the amplitudes of response become too large to be of any practical value. From the results presented in this section, it can be seen that the limit-cycle amplitude response curves are quite steep. This means that the nonlinearities in the system are weak and their stabilizing effect is not strong enough to reduce the amplitudes of limit-cycle response to practical levels once the critical condition is exceeded.

7.4 Results for Forward Flight

7.4.1 Trim Curves

As pointed out previously in this report, the effect of forward flight can be correctly investigated only when considering the behavior of the rotor at a fixed value of C_T while varying μ. This can be accomplished by requiring that the rotor be in a trimmed condition. Using the trim procedure described in Appendix F, a subroutine which calculates the trim conditions has been incorporated in the two computer programs (one using numerical integration and

one using the analytical expressions of the perturbation method).

A typical set of trim curves for $\bar{\omega}_{F1} = 1.20$ and two typical values of C_T are shown in Figs. 16 and 17. It is clearly evident from these figures that an increase in μ is always first accompanied by a decrease in θ and λ_o up to $\sim \mu = 0.2$, after which θ increases quite rapidly.

7.4.2 Effect of Forward Flight from Numerical Integration

Before starting to discuss the results obtained from the use of the perturbation method, it is instructive to look at a typical case in forward flight which has been solved by numerical integration.

The results showing the amplitude response for trimmed flight at $C_T = 0.006$ are given in Fig. 18 for various values of μ. The range applicability of the analysis done in the present report is

$$0 < \mu < .30$$

For the case considered, the $\theta < \theta_c$; therefore, the system is below critical and the amplitude grows with increasing μ. The quantity $(\chi_1)_{av}$ plotted in the amplitude response curves is defined by

$$(\chi_1)_{av} = \frac{\chi_{1max} - \chi_{1min}}{2} \tag{7.7}$$

It is necessary to use Eq. 7.7 because the natural equilibrium condition defined by Eqs. 3.20 and 3.21 is defined for $\mu = 0$. Therefore, the equilibrium position about which the blade will oscillate in reality will be a function of μ. This effect is very small in lag (therefore only the max. value of χ_2 is plotted), but considerable in flap. As seen from Fig. 18, the increase in forward flight speed increases the amplitudes of response. Below the values of μ the appropriate values of θ are given for trimmed flight at fixed C_T. At $\mu = 0.1$, θ is much lower than θ_c and the blade response is moderate, and $(\chi_1)_{av} > \chi_2$.

For $\mu = 0.4$, $\theta = 0.2936$ which is only 5% less than θ_c; therefore, the typical behavior of the lag degree of freedom near the critical condition manifests itself by a sudden growth in χ_2.

7.4.3 Effect of Forward Flight on Case B

This case represents the general forward and flight case with $\mu = \varepsilon^{1/2}$ and $\omega_c \neq 1 + \varepsilon\nu$ or $\omega_c = 1/2 + \varepsilon\nu$. For this case two possibilities exist:

(1) The combination of C_T, μ and the structural damping in lag η_{SL1} result in a flight condition for which the collective pitch is below critical (i.e., $\theta < \theta_c$). The blade response is given by Eqs. 6.8 and 6.9. This case represents essentially the forced response of the system because the flutter mode is a decaying oscillation. The flutter mode is a decaying oscillation because

$$\kappa_{2R} \simeq \left(\kappa_{2\theta_1}\right)_R \frac{\theta-\theta_c}{\mu^2} + \left(\kappa_{2\lambda_1}\right)_R \frac{\lambda_0-\lambda_{0c}}{\mu^2} \tag{7.8}$$

is usually a relatively large negative quantity.

(2) The combination of C_T, μ and low or zero structural damping can result in a flight condition for which $\theta > \theta_c$. In this case, the blade response is determined from Eqs. 5.74 and 5.70. The stability in this case will be determined by κ_{2R}, κ_{3R}, and κ_{6R}. As shown in Subsection 5.5.2, the quantity which determines the stability is

$$\kappa_{2R} + \mu_0^2 \kappa_{6R} = \left(\kappa_{2\theta_1}\right)_R \frac{\theta-\theta_c}{\mu^2} + \mu_0^2 \kappa_{6R} + \left(\kappa_{2\lambda_1}\right)_R \frac{\lambda_0-\lambda_{0c}}{\mu^2} \tag{7.9}$$

Stable limit-cycle oscillations can occur when $\kappa_{2R} + \mu_0^2 \kappa_{6R} > 0$ and $\kappa_{3R} < 0$. The quantity in Eq. 7.9 is strongly dependent upon the trim condition through the variation of $\theta_1 = (\theta - \theta_c)/\mu^2$ with forward flight. The amplitude growth in this case occurs in the time scale $\psi_1 = \varepsilon\psi_0 = \mu^2\psi$. The quantity A_0 governing the postcritical amplitude response can be written in the following functional form as

$$A_0 = A_0\left(\frac{\theta-\theta_c}{\mu^2}, \frac{\lambda_0-\lambda_{0c}}{\mu^2}, \mu^2\psi\right)$$

The two possibilities mentioned above are illustrated by the numerical results given below. A representative case was chosen with the following properties.

$$\omega_{F10} = \bar{\omega}_{F1} = 1.175$$

$$\omega_{L10} = \bar{\omega}_{L1} = 1.33319$$

$$\omega_c = 1.32641 \qquad \theta_c = 0.357523$$

$$\gamma = 10, \quad \sigma = 0.05, \quad C_{d_o} = 0.01, \quad a = 2\pi$$

$$C_{Dp} = 0.012$$

$$\eta_{SF1} = \eta_{SL1} = 0.005$$

$$C_T = 0.01$$

For this case, due to the presence of the structural damping $\theta < \theta_c$, Figure 19 illustrates the blade response at fixed C_T as a function of μ. At four values of $\mu(\mu = 0.1; 0.2; 0.25; 0.32)$ the values of the collective pitch θ as obtained from the trim calculation are also given. The dotted lines in Fig. 19 represent the results obtained by using Eqs. 6.8 and 6.9. The flap and lag amplitudes were taken as the maximum values occuring between $250 < \psi < 350$, the quantity $(\chi_1)_{av}$ is defined by Eq. 7.7. Due to the remarks concerning the validity of the uniformly valid expansion made in Subsection 6.1, the same curves were also calculated by direct numerical integration. The results from the numerical integration are given by the full lines in Fig. 19. The agreement between the two sets of curves is quite reasonable.

In order to show that Eqs. 6.7 and 6.8 represent correctly the time history of the blade response, the time history for the blade response at $\mu = 0.25$ was obtained by numerical integration and is given in Fig. 20. Figure 21 represents the same blade response history as given by Eqs. 6.7 and 6.8. The two sets of curves are quite similar.*

Figure 22 shows the blade response amplitudes as evaluated from Eqs. 6.7 and 6.8 for $C_T = 0.0078$. As can be seen, decreasing C_T reduces the blade response levels.

---

*From a mathematical point of view, the results of the numerical integration should be harmonically analyzed, and the coefficients for a_{02}, b_{02}, a_{13}, b_{13}, ... , etc., should be obtained. These should then be compared to the same coefficients as obtained from the perturbation method.

Considering the same case for which the relevant quantities were given above, with structural damping set equal to zero ($\eta_{SF1} = \eta_{SL1} = 0$), the blade response in the postcritical range ($\theta > \theta_c$) can be considered. Removal of the structural damping results in a new value for the critical value of the collective pitch $\theta_c = 0.20$ (see also Fig. 12). The blade response amplitudes are given in Fig. 23 for $C_T = 0.0078$. The curves given in Fig. 23 were evaluated using Eqs. 5.70 and 5.74. As can be seen, the postcritical region is characterized by large amplitudes in lag. Although this is a stable limit cycle oscillation, the amplitudes in lag are so large that the results do not have any practical significance. By comparing the blade response at $\theta < \theta_c$ with the response at $\theta > \theta_c$ (Figs. 19 and 23), it is interesting to note that below the critical condition the amplitudes in flap are usually larger than in lag. While in the vicinity of θ_c and above it, the lag amplitudes are much larger than the flap amplitudes.

Comparing Fig. 22 to typical blade response in hover, Fig. 13, it is seen that forward flight tends to reduce $(|\chi_2|)/(|\chi_1|)$.

The effect of trim at fixed C_T on the stability of the blade and the amplitudes of the blade response are illustrated by Figs. 24 and 25. Figure 24 shows a plot of the quantity defined by Eq. 7.9. As can be seen, this quantity is considerably affected by μ. Figure 25 shows a plot of $\rho_{\ell.c.}$ as calculated from Eq. 5.71. This quantity which determines the magnitude of the blade response is also considerably affected by the μ through the requirement of trim at fixed C_T.

7.4.4 Effect of Forward Flight on Case C

The flutter frequency for this case is $\omega_c = 1/2 + \varepsilon\nu$ and $\mu = \varepsilon$. In this case, parametric excitation will be the predominant effect.

From the stability boundaries given for $\gamma = 5.0$ and $\gamma = 10$ (Figs. 3 and 4), it is clear that the value of θ_c, even with $\eta_{SF1} = \eta_{SL1} = 0$ for this case will be so high as to have almost no practical value. Adding a small amount of structural damping ($\eta_{SL1} = 0.005$) will increase θ_c even further. Thus it appears that the cases of interest would be $\theta < \theta_c$, which would require the use of the uniformly valid expansion. As mentioned in Subsection 6.1,

the validity of this expansion is good for $\mu < 0.15$. For such low values of forward flight, it is doubtful whether parametric excitation could have a significant effect.

As shown in Subsection 5.5.3, the solution for this case is given by Eq. 5.94. It has been shown that in the vicinity of the origin, the stability is governed by the real part of s_1 where s_1 is given by Eq. 5.79a, page 46. When Real $(s_1) < 0$, the system is stable and for Real $(s_1) > 0$ the system is unstable. Also due to the homogeneous form of the linear part of Eq. 5.52, the flutter mode below the critical condition will not be excited. It is also shown in Subsection 5.5.3, that if a closed trajectory (limit cycle) exists its distance from the origin will be bounded by Eq. 5.92. Also, for stability in the nonlinear range, it is required that $\kappa_{3R} < 0$. It has also been shown, by applying the perturbation method in the neighborhood of the critical condition, that the location of the equilibrium point and the magnitude of the limit-cycle amplitude (if it exists) will depend upon the parametric excitation. The blade response up to the first order can be approximately written as

$$\chi_2 \cong 2\mu^{1/2}\, Real\left[A_0\left(\mu\psi_0, \frac{\theta-\theta_c}{\mu}, \frac{\lambda_0-\lambda_{0c}}{\mu}\right)\right] \tag{7.10}$$

Due to the large values of θ_c for this case, no numerical results are given since they would be impractical.

7.4.5 Effect of Forward Flight on Case D

The flutter frequency for this case is $\omega_c = 1 + \varepsilon\nu$ and $\mu = \varepsilon^{1/2}$. In this case, parametric excitation has an effect, but the forcing will be predominant because the system is excited very close to its resonant frequency.

Near the critical condition, the flutter mode is determined by Eq. 5.58 or Eq. 5.98. The stability of the system near the origin depends upon the sign of $Re(s_1)$, for $Re(s_1) > 0$ the system is unstable and when $Re(s_1) < 0$, the system is stable. The linearized system is nonhomogeneous, Eqs. 5.101 and 5.102.

Therefore the flutter mode is always excited the same is true for Eq. 5.98. The solution for this case is given by Eq. 5.94, and up to the first order, the lag motion can be approximated by

$$\chi_2 = 2\mu \, Real \left[A_0\left(\frac{\theta-\theta_c}{\mu^2}, \frac{\lambda_0-\lambda_{0c}}{\mu^2}, \mu^2\psi\right)\right]$$

It should be noted that the analysis for this case was performed with the assumption that C_T and μ are small.

For numerical calculations, a representative case with the following properties was chosen:

$\omega_{F10} = \bar{\omega}_{F1} = 1.20$

$\omega_{L10} = \bar{\omega}_{L1} = 1.03861$

$\omega_c = 1.04146 \qquad \theta_c = 0.20$

$\gamma = 10, \quad \sigma = 0.05, \quad C_{d_o} = 0.01 \quad a = 2\pi$

$C_{Dp} = 0.012$

$\eta_{SF1} = \eta_{SL1} = 0.0$

$C_T = 0.0080$

For the value of C_T chosen above $\theta > \theta_c$.

Numerical results for this case can be obtained either by integrating numerically Eqs. 5.58 or 5.98, and then making use of Eq. 5.94, or by using the numerical integration program. For convenience, the second method was used. The results showing the blade response amplitudes are given in Fig.26. As can be seen, this case is characterized by large amplitudes of blade response which become very high even for moderate values of forward flight. Therefore, flutter frequencies ω_c close to $\omega_c = 1$ should be avoided in practice.

Numerical integrations done for this case indicate that the special expansion used for Case D, and physically characterized by the beating phenomenon as represented by the term $e^{-i\nu\mu^2}\psi_o$ in Eq. 5.105 (or in Eq. 5.57), is valid up to the advance ratios of $\mu < 0.2$.

SECTION 8

GENERAL EQUATIONS FOR NONLINEAR, COUPLED FLAP-LAG-PITCH MOTION OF HINGELESS HELICOPTER BLADES

8.1 Introduction

Although research in the field of aeroelastic problems of helicopter blades, both hingeless and articulated, has been going on for a considerable amount of time (Ref. 32), a complete set of consistently-derived equations for nonlinear, coupled flap-lag-pitch motion of hingeless (or even articulated) helicopter blades is not available in the literature. The author believes that the lack of these equations has acted as an obstacle in the development of reliable analytical methods for predicting rotor blade stability in the range where the amplitude of the blade motion is large, because most of the work in this field was restricted to solving a special system of equations derived under a particular set of simplifying assumptions. Thus, the basis for a meaningful comparison of the results obtained by various researchers was not available and the comparisons were usually of a qualitative nature.

It is instructive, therefore, to review the various systems of equations available in this field. In this review, both the linear and nonlinear equations of motion will be considered.

The best system of equations is the one derived by Miller and Ellis (Ref. 11). This system of equations, which was derived in order to treat linear blade response problems, identified all of the important physical effects associated with the coupled flap, pitch and lag motion of the blade. Another advantage of this derivation is that it also considered distributed torsional effects and some finite displacement effects, like effects due to large coning angles. Another useful device used in this derivation was the modeling of the blade by a concentrated mass at the blade c.g. offset by a distance x_I from the elastic axis. Finally, the last advantage of this derivation is its clear treatment of the derivation of the aerodynamic loads.

Chronologically, the next system of equations was derived by Houbolt

and Brooks (Ref. 10). The purpose of the authors in Ref. 10 was to derive a linear system of equations for coupled flap-lag-pitch motion; as such, their derivation was quite successful. They succeeded in deriving an engineering beam-type theory for treating the elastic deformation in flap-lag and torsion of thin elastic rotating beams in a consistent manner. The linear inertia loads were also consistently and systematically derived. However, the Coriolis inertia load, due to the elastic shortening effect, was not included in their derivation. An additional point in favor of the Houbolt and Brooks (Ref. 10) derivation is that it contains some of the elements required for extending the derivation into the nonlinear range. Their treatment includes finite, spanwise varying, built-in twist and offset between the blade elastic axis and the line of cross-sectional centers of gravity. However, in these equations no provision was made for treating built-in coning and the aerodynamic forces were not treated. The system of equations derived in Ref. 10 has been used in a number of papers dealing with blade flutter.

The equations of motion derived in Ref. 10 have been extended by Lemnios in Ref. 33 to include the Coriolis force in the chordwise direction due to flapwise bending (elastic shortening effect, see Eq. 3.9). In addition, the aerodynamic terms of the equations of motion were treated in detail in Ref. 33. The only nonlinear effect taken into account by Lemnios is the elastic shortening effect, while many other second-order effects associated with the inertia-loading terms have not been considered; thus, his equations are not consistent. In Ref. 33, only the offset between the elastic axis and the blade center of gravity was considered. Built-in twist and distributed torsion were both treated.

A further improvement of the equations of motion derived by Houbolt and Brooks (Ref. 10) was made by Pizialli (Ref. 34). This system of equations, although still limited to the linear range, had the following improvements:

1. Built-in twist as in Ref. 10
2. Noncoincident and nonstraight cross section; e.g., centroid and elastic axes which do not pass through the rotor axis of rotation.

3. Details of articulation such as to include:
   (a) Root elastic boundary conditions
   (b) Radial and chordwise hinge offsets
   (c) Hinge inclinations
   (d) Pitch axis offset and inclination

Another system of equations of motion has been derived by Bielawa (Ref. 35). These were derived for the purpose of investigating the higher-order effects due to both elastic root torsion and distributed elastic torsion in the spanwise direction. In order to simplify matters, the location of the blade elastic axis, the blade center of gravity, and the blade aerodynamic center were assumed to be coincident in each cross section of the blade; thus a large number of second-order effects vanish. Large elastic displacements in flap and lag were assumed. On the other hand, the Coriolis loads due to the blade shortening effect were neglected. The effect of large displacements on the aerodynamic loads was not carefully treated. Thus, no clear picture of the various approximations involved could be obtained from Ref. 35. The main contribution of Ref. 35 is a careful and detailed treatment of the various torsional effects. Thus, this work, too, suffers from a certain amount of lack of consistency.

Finally, another detailed linearized version of the coupled flap-lag-pitch equations of motion has been derived by Arcidiacono (Ref. 36). The equations of motion were derived for linearly twisted rotor blades. The motions include flapping and lagging for the articulated blade, as well as flatwise, edgewise, and torsional deformations for the articulated and non-articulated blade. Fully-coupled aerodynamic forcing functions were also derived based on quasi-steady aerodynamic theory. These differential equations of motion were also expanded in terms of the uncoupled vibratory nodes of the blade.

In this section, an attempt will be made to derive, consistently and systematically, a system of equations of motion for coupled nonlinear flap-lag-pitch motion of hingeless helicopter blades.

The equations will be carefully derived so that the various approximations involved in obtaining the elastic, inertia and aerodynamic loads will

be made clear.

It is of importance to note that for a hingeless blade, the equations of motion are more complicated than for an articulated one. The reason is that for a hingeless blade, the only physically meaningful reference plane is the hub plane. In this reference plane, the angle of pitch setting cannot be taken as a fixed quantity in time, but will be a time-dependent quantity due to the presence of the cyclic pitch. Due to this effect, additional inertia terms will appear in the equations of motion.

For the particular case of an articulated blade, where for convenience, blade stability analyses are usually performed in the no feathering plane, the general equations derived in this section will still be applicable by setting $\theta^{*}=\theta^{**}=0$ and replacing the elastic hingeless mode shapes by appropriate mode shapes for an articulated blade.

In the equations which will be derived, only elastic root torsion will be treated and no provision for built-in twist will be made. Small angles of built-in coning will be included in the analysis. The arguments for neglecting higher order nonlinear effects will be stated and consistently applied to obtain the final form of the equations of motion in a general form.

8.2 Basic Assumptions

The assumption used in the derivation of the equations of motion will be given below. For convenience, they are divided into three groups:

A. Geometrical Assumptions

These are assumptions regarding the geometry of the blade and its attachment to the hub.

(1) The elastic blade is attached to the hub at some offset distance e_1 from the axis of rotation (see Fig. 27)

(2) At its root, the blade can have a built-in coning angle β_p. In addition, the feathering axis can have an inclination β (measured in a vertical plane) with respect to the hub plane. It is assumed that these angles are sufficiently small so that the assumptions $\sin\beta=\beta$, $\cos\beta=1$ (and the same for β_p) are valid, unless otherwise stated.

(3) The feathering hinge is inboard of the "virtual" flap and lag hinge (see Figs. 27a and 27b)

(4) The blade is initially straight. There is no angle of built-in twist.

(5) The cross sections of the blade are assumed to be symmetrical about the major principal axis (see Fig. 28).

(6) The equations will be derived in such a manner as to enable the following choice in the location of the elastic axis (E.A.), aerodynamic center (A.C.), axis of twist [(A.T.) or feathering axis] and blade cross section C.G. (C.G.):

(a) E.A., A.C., A.T., coincident with C.G. offset.

(b) E.A. and A.T. coincident, both offset with respect to A.C. and C.G. which are coincident.

B. Elastic Assumptions

These are assumptions regarding the elastic properties of the blade and its deformations.

(7) During the deformations, cross sections are assumed to remain plane and normal to the elastic axis.

(8) Shear is neglected.

(9) The Blade is a thin flexible blade attached to the hub.

(10) The blade can bend in two directions normal to the elastic axis.

(11) The blade is torsionally rigid, except at the hub. The twisting of the blade is represented by a root torsion denoted by Φ.

(12) The deflections of the blade are moderately small so that terms of $O(\varepsilon_D^2)$ can be neglected when compared to 1. (ε_D being the order of magnitude of the deflection.) With this assumption, it is sufficient to retain only the linear and the second-order nonlinear terms in the equations of motion. All third order terms can be neglected.

(13) Only a linear treatment of the elastic restoring forces will be considered; i.e., large deflections will have only a small effect on the tension due to elastic effects in the blade since one of its ends is free. This assumption is consistent with neglecting terms of $O(\epsilon_D^3)$.

C. Aerodynamic Assumptions

These are the assumptions made in calculating the airloads acting on the blade.

(14) Two-dimensional quasi-steady aerodynamic loads are used.

(15) Apparent mass effects in the aerodynamic loads are neglected.

(16) Stall, compressibility and reversed flow effects are neglected; thus, the aerodynamic loads are valid for $\mu \leq 0.3$.

8.3 Displacements, Coordinate Systems, and Coordinate Transformations

8.3.1 Sample Displacement Fields

In the present analysis, the feathering axis of the blade will be assumed to have an orientation given by an angle β with respect to the hub plane (see Fig. 27a). Therefore, it is important to define sample displacement fields which can be used latter with the general equations of motion, carefully and in detail.

A. First Displacement Field

Consider first the case where there is no elastic root torsion. The geometry for this case is shown in Fig. 27a. The required quantities are the displacements of a point A (A' in deformed state) located on the elastic axis of the blade. For this purpose, only the hub plane coordinate system, attached to the blade and rotating with angular velocity Ω is required. According to assumption (4) Subsection 8.2, the initial position of point A on the elastic

axis coincides with the x-axis. Also note that in its undeformed state, the blade cross section at A has a collective pitch setting of θ. From the geometry of Fig. 27a*

$$\hat{W} = x_o \sin\beta + w_e \cos\beta \tag{8.1}$$

$$\hat{v} = v_e \tag{8.2}$$

$$\hat{U} = -w_e \sin\beta - x_o(1-\cos\beta) - \frac{1}{2}\int_0^{x_o}\left[\left(\frac{\partial v_e}{\partial x_1}\right)^2 + \left(\frac{\partial w_e}{\partial x_1}\right)^2\right] dx_1 \tag{8.3}$$

Now assumption (2), Subseciton 8.2, will be used. Thus

$$\hat{W} = x_o\beta + w_e \tag{8.1a}$$

$$\hat{v} = v_e \tag{8.2a}$$

$$\hat{U} = -w_e\beta - x_o\frac{\beta^2}{2} - \frac{1}{2}\int_0^{x_o}\left[\left(\frac{\partial v_e}{\partial x_1}\right)^2 + \left(\frac{\partial w_e}{\partial x_1}\right)^2\right] dx_1 \tag{8.3a}$$

In Eq. 8.3, all quantities are small second-order quantities, therefore the approximation cos β = 1 is not permissible. The last term in Eq. 8.3 is the elastic shortening effect, also given in Eq. 3.9. The quantity w_e is measured perpendicular to the real position of the undeformed blade (see Fig. 27a).

Finally, the displacements due to the root torsion will be taken into account. The assumption will be made that the torsional displacement occurs after the elastic flap and lag displacements (i.e., w_e, v_e) have occurred. If the torsional displacement around the feathering axis is Φ (see Fig. 27a), then the displacements due to torsion are (Φ is a small angle)

$$\left.\begin{aligned} w_T &= v_e\,\Phi \\ v_T &= -w_e\,\Phi \end{aligned}\right\} \tag{8.4}$$

*Note that the inextensibility assumption is used in Eq. 8.3. In general, this is not absolutely necessary.

Thus, the total displacements of a point on the elastic axis of the blade can be written as

$$w = \hat{w} + w_T = x_o\beta + w_e + v_e\Phi$$

$$v = \hat{v} + v_T = v_e - w_e\Phi \tag{8.5}$$

$$U = -w_e\beta - x_o\frac{\beta^2}{2} - \frac{1}{2}\int_o^{x_o}\left[\left(\frac{\partial v_e}{\partial x_1}\right)^2 + \left(\frac{\partial w_e}{\partial x_1}\right)^2\right] dx_1$$

It is important to realize that if the elastic flapping and lagging displacements are not assumed to occur before the root torsional elastic displacement, then the additional displacements due to the coupling between the steady-state elastic flap and lag with Φ will have a different form.

B. Second Displacement Field

Another possible displacement field is one in which the feathering axis has an orientation determined by the angle β with respect to the hub plane, while in addition, the blade has a built-in preconing angle given by β_p with respect to the feathering axis. This displacement field is schematically shown in Fig. 27b.

From considerations identical to those applied in the previous sample displacement field

$$\hat{U} = -w_e(\beta + \beta_p) - \frac{x_o}{2}(\beta + \beta_p)^2$$

$$- \frac{1}{2}\int_o^{x_o}\left[\left(\frac{\partial v_e}{\partial x_1}\right)^2 + \left(\frac{\partial w_e}{\partial x_1}\right)^2\right] dx_1$$

$$\hat{v} = v_e - x_o \beta_p \sin\theta$$

$$\hat{w} = x_o(\beta + \beta_p) + w_e \tag{8.6}$$

Again, the displacements due to torsion are given by

$$v_T = -x_o \beta_p \Phi \cos\theta - w_e \Phi$$

$$w_T = v_e \Phi \tag{8.7}$$

Thus, the total displacements of a point on the elastic axis of the blade is given by

$$\left.\begin{aligned} U = \hat{U} &= -w_e(\beta + \beta_p) - \frac{x_o}{2}(\beta + \beta_p)^2 \\ &\quad - \frac{1}{2}\int_0^{x_o}\left[\left(\frac{\partial v_e}{\partial x_1}\right)^2 + \left(\frac{\partial w_e}{\partial x_1}\right)^2\right] dx_1 \\ v = \hat{v} + v_T &= v_e - w_e\Phi - x_o\beta_p(\sin\theta + \Phi\cos\theta) \\ W &= x_o(\beta + \beta_p) + w_e + v_e\Phi = \hat{w} + w_T \end{aligned}\right\} \tag{8.8}$$

In Eqs. 8.7 and 8.8, the relation

$$\sin(\theta + \Phi) = \sin\theta + \Phi\cos\theta$$

has been used. For the particular case of $\beta_p = 0$, Eqs. 8.8 reduce to Eqs. 8.5.

8.3.2 Coordinate Systems and Coordinate Transformations

In order to handle, in a convenient manner, the various inertia and aerodynamic loads derived in this section, the vector method will be used. As will be seen below, six different coordinate systems are required to describe the various quantities. These are:

1. The hub plane coordinate system, shown in Fig. 27a rotating at constant angular velocity with the blade. The z-axis coincides with the axis of rotation; the x-axis coincides with the assumed initial position of the elastic axis and the y-axis is perpendicular to the x-z plane. The unit vectors of this coordinate system are denoted by $\underset{\sim}{i}$, $\underset{\sim}{j}$, $\underset{\sim}{k}$.
2. A second coordinate system shown in Fig. 29a. Its unit vectors are denoted by $\underset{\sim}{i}_1$, $\underset{\sim}{j}_1$, $\underset{\sim}{k}_1$. The $\underset{\sim}{i}_1$ unit vector coincides with the orientation of the feathering axis, the $\underset{\sim}{j}$, $\underset{\sim}{j}_1$ axes are parallel and $\underset{\sim}{k}_1$ is perpendicular to $\underset{\sim}{i}_1$ and $\underset{\sim}{j}_1$.
3. A third coordinate system with unit vectors $\underset{\sim}{i}_2$, $\underset{\sim}{j}_2$, $\underset{\sim}{k}_2$ is shown in Fig. 29b. It is obtained by rotating the $\underset{\sim}{i}_1$, $\underset{\sim}{j}_1$, $\underset{\sim}{k}_1$ system by an angle $\theta + \Phi$ around the $\underset{\sim}{i}_1$ axis.
4. A fourth coordinate system with unit vectors $\underset{\sim}{I}_1$, $\underset{\sim}{J}_1$, $\underset{\sim}{K}_1$ is defined in Subsection I.1, Appendix I.
5. A fifth coordinate system will be attached to the cross section of the blade at its elastic axis. It moves with the cross section as the blade deflects. The unit vectors for this system are: $\underset{\sim}{I}_2$, tangential to the deformed elastic axis of the blade; $\underset{\sim}{J}_2$, normal to the deformed elastic axis and parallel to the hub plane, and $\underset{\sim}{K}_2$ normal to $\underset{\sim}{I}_2$ and $\underset{\sim}{J}_2$.

The projections of these unit vectors, at a point P on the elastic axis, are schematically shown in Fig. 27.

6. A sixth coordinate system similar to the previous one and rotated about the $\underset{\sim}{I}_2$ axis by an angle $\theta+\Phi$. The unit vectors are $\underset{\sim}{I}_3$ coincident with $\underset{\sim}{I}_2$; $\underset{\sim}{J}_3$ coincident with the blade chord, and $\underset{\sim}{K}_3$ normal to $\underset{\sim}{I}_3$ and $\underset{\sim}{J}_3$. These unit vectors are schematically shown in Figs. 27 and 28.

   According to the proof of equivalence of rotations given in Appendix I, within the approximations inherent in the various coordinate transformations, the unit vector $\underset{\sim}{J}_3$ can be considered a good approximation to the blade-chord orientation in space after the deformations have occurred.

The relations between the various coordinate systems are given in detail in Appendix I.

8.4 Derivation of the Inertia Loads and Moments

8.4.1 Derivation of the Inertia Loads in the x,y,z Directions

The inertial loads will be derived using the blade model shown in Fig. 28. The blade is assumed to be represented by its mass-per-unit span m, concentrated at the blade cross section C.G., and offset by a distance x_I from the elastic axis. This model, used first by Miller (Ref. 11), is much more convenient than the distributed mass used by Houbolt (Ref. 10). On the other hand, care must be taken to correct the propeller moment and the rotational inertial term in q_x, by the missing cross-sectional polar moment of inertia.

Let x, y, and z denote the undeformed position of the cross-sectional blade C.G., while its position in the deformed state will be given by x_1, y_1, and z_1. Then the following relations can be written:

$$\left.\begin{aligned} x &= x_o + e_1 \\ y &= x_I \cos\theta \\ z &= x_I \sin\theta \end{aligned}\right\} \tag{8.9}$$

$$x_1 = x_o + e_1 + U - \frac{\partial v}{\partial x}(y_1 - v) - \frac{\partial w}{\partial x_o}(z_1 - w) \tag{8.10}$$

$$y_1 = v + x_I \cos(\theta + \Phi) = v + (x_I \cos\theta - x_I \Phi \sin\theta) \tag{8.11}$$

$$z_1 = w + x_I \sin(\theta + \Phi) = w + x_I (\sin\theta + \Phi \cos\theta) \tag{8.12}$$

Note that the blade cross section is not in the y-z plane, but is normal to the elastic axis. Only the E.A. point is in the y-z plane. This is the reason for the last two terms of Eq. 8.10. In addition, it will always be assumed that Φ is small, so that

$$\begin{aligned} \cos(\theta + \Phi) &= \cos\theta - \Phi \sin\theta \\ \sin(\theta + \Phi) &= \sin\theta + \Phi \cos\theta \end{aligned} \tag{8.13}$$

From Eqs. 8.10 through 8.12, the position vector, the blade center of gravity in the deformed position is given by

$$\underset{\sim}{r}_R = \underset{\sim}{i} x_1 + \underset{\sim}{j} y_1 + \underset{\sim}{k} z_1 \tag{8.14}$$

From elementary mechanics (Ref. 37), the acceleration in inertial space can be written as

$$\underset{\sim}{a} = \ddot{\underset{\sim}{r}}_R + 2\,\underset{\sim}{\omega} \times \dot{\underset{\sim}{r}}_R + \dot{\underset{\sim}{\omega}} \times \underset{\sim}{r}_R + \underset{\sim}{\omega} \times (\underset{\sim}{\omega} \times \underset{\sim}{r}_R) \tag{8.15}$$

Due to steady rotation, the third term of Eq. 8.15 is zero. From the geometry $\partial/\partial x = \partial/\partial x_o$, using Eqs. 8.14 and 8.15,

$$\underset{\sim}{a} = \underset{\sim}{i}\left(\ddot{x}_1 - x_1\Omega^2 + 2\dot{y}_1\Omega\right) + \underset{\sim}{j}\left(\ddot{y}_1 - y_1\Omega^2 + 2\dot{x}_1\Omega\right) + \underset{\sim}{k}\,\ddot{z}_1 \qquad (8.15a)$$

From Eqs. 8.15 and 8.10 through Eq. 8.12:

$$\underset{\sim}{a} = \underset{\sim}{i}\left\{ \ddot{v} - \frac{\partial^3 v}{\partial x_o \partial t^2} x_I \cos(\theta+\Phi) + 2\frac{\partial^2 v}{\partial x_o \partial t} x_I \sin(\theta+\Phi)(\dot{\theta}+\dot{\Phi}) \right.$$

$$+ \frac{\partial v}{\partial x_o} x_I \cos(\theta+\Phi)(\dot{\theta}+\dot{\Phi})^2 + \frac{\partial v}{\partial x_o} x_I \sin(\theta+\Phi)(\ddot{\theta}+\ddot{\Phi})$$

$$- \frac{\partial^3 w}{\partial x_o \partial t^2} x_I \sin(\theta+\Phi) - 2\frac{\partial^2 w}{\partial x_o \partial t} x_I \cos(\theta+\Phi)(\dot{\theta}+\dot{\Phi})$$

$$+ \frac{\partial w}{\partial x_o} x_I \sin(\theta+\Phi)(\dot{\theta}+\dot{\Phi})^2 - \frac{\partial w}{\partial x_o} x_I \cos(\theta+\Phi)(\ddot{\theta}+\ddot{\Phi})$$

$$- \Omega^2\left[x_o + e_1 + u - \frac{\partial v}{\partial x_o} x_I \cos(\theta+\Phi) - \frac{\partial w}{\partial x_o} x_I \sin(\theta+\Phi) \right]$$

$$\left. - 2\Omega\left[\dot{v} - x_I \sin(\theta+\Phi)(\dot{\theta}+\dot{\Phi}) \right] \right\}$$

$$+ \underset{\sim}{j}\left\{ \ddot{v} - x_I \cos(\theta+\Phi)(\dot{\theta}+\dot{\Phi})^2 - x_I \sin(\theta+\Phi)(\ddot{\theta}+\ddot{\Phi}) \right.$$

$$- \Omega^2\left[v + x_I \cos(\theta+\Phi) \right] + 2\Omega\left[\dot{u} - \frac{\partial^2 v}{\partial x_o \partial t} x_I \cos(\theta+\Phi) \right.$$

$$+ \frac{\partial v}{\partial x_o} x_I \sin(\theta+\Phi)(\dot{\theta}+\dot{\Phi}) - \frac{\partial^2 w}{\partial x \partial t} x_I \sin(\theta+\Phi)$$

$$- \frac{\partial w}{\partial x_o} x_I \cos(\theta+\Phi)(\dot{\theta}+\dot{\Phi}) \Big\}$$

$$+ \underset{\sim}{k}\Big\{ \ddot{w} - x_I \sin(\theta+\Phi)(\dot{\theta}+\dot{\Phi})^2 + x_I \cos(\theta+\Phi)(\ddot{\theta}+\ddot{\Phi}) \Big\} \qquad (8.16)$$

The components of the acceleration in the x,y,z directions, respectively, can be obtained from Eq. 8.16.After substituting Eqs. 8.13, the complete expressions for a_x, a_y, a_z are given in Eqs. J.1 through J.3 of Appendix J.

From the form of these expressions, it is clear that a considerable number of terms are negligible. The considerations for neglecting terms are given below.

Denoting the order of magnitude of the displacements by $0(\varepsilon_D)$:

1. v,w and their derivatives are of $0(\varepsilon_D)$
2. u from Eq. 8.6 is usually a second-order quantity; thus, $u \sim 0(\varepsilon_D^2)$
3. Φ is usually a small quantity ($0 < \Phi < 3°$); thus is usually $\Phi < \partial v/\partial x_o$, $\partial w/\partial x_o$
   Therefore $0(\varepsilon_D^3) < \Phi^2 < 0(\varepsilon_D^2)$. Thus, $\dot{\Phi}\ddot{\Phi}, \Phi^2, \dot{\Phi}\dot{\Phi}$ can be considered negligible when compared to other second-order quantities
4. It is reasonable to assume that the order of magnitude of $\sin\theta \tilde{=} 0(\varepsilon_D)$. Thus

$$0(\varepsilon_D)\,\Phi \sin\theta \cong 0(\varepsilon_D^3)$$

$$0(\varepsilon_D)\,\theta\Phi \cong 0(\varepsilon_D^3)$$

5. From the first part of this report it was found that the cyclic pitch is usually bounded by $\theta \leq 0.5\ \theta_o$, where θ_o, is the constant collective pitch setting. Thus, it is reasonable to say that the order of magnitude of $\theta^2(\partial w/\partial x)$, $\theta^2 w$ is given by:

$$\dot{\theta}^2\, O(\varepsilon_D) \cong O(\varepsilon_D^3)$$

6. From the first part of this report, it was found that in the vicinity of the critical region ($\theta_o \geq \theta_c$), the lag displacements were 3 to 5 times larger than the flap displacements. Therefore, when neglecting terms in the following equations, it will be usually assumed that

$$v \sin\theta \cong w \cos\theta$$

and

$$v \cos\theta > w \sin\theta$$

All quantities, which according to considerations 1 through 6 above are of $O(\varepsilon_D^3)$, will be neglected, unless otherwise stated.

Neglecting almost all $O(\varepsilon_D^3)$ in Eq. J.1, the inertia load in the x-direction will be given by

$$P_{XI} = -m a_x = P_x \tag{8.17}$$

[Because L_x (see Eq. 8.56) is assumed to be zero]

From Eqs. J.1 and 8.17, using the nondimensional time derivative, Eq. 8.18 is obtained

$$P_{XI} = -m\Omega^2 \left[\overset{**}{U} - (X_o + e_1 + U) - 2\overset{*}{v} \right] - \Omega^2 m X_I \left\{ -\frac{\partial^2 v}{\partial X_o \partial \Psi^2} \cos\theta \right.$$

$$\left. - \frac{\partial^3 w}{\partial X_o \partial \Psi^2} \sin\theta + \left(\frac{\partial v}{\partial X_o} \cos\theta + \frac{\partial w}{\partial X_o} \sin\theta \right) + 2\overset{*}{\Phi} \sin\theta \right\}$$

$$- m\Omega^2 X_I \left\{ \Phi \left[\frac{\partial^3 v}{\partial X_o \partial \Psi^2} \sin\theta - \frac{\partial^3 w}{\partial X_o \partial \Psi^2} \cos\theta + \left(\frac{\partial w}{\partial X_o} \cos\theta - \frac{\partial v}{\partial X_o} \sin\theta \right) \right] \right.$$

$$+ 2\overset{*}{\Phi}\left(\frac{\partial^2 v}{\partial x_0 \partial \psi}\sin\theta - \frac{\partial^2 w}{\partial x_0 \partial \psi}\cos\theta\right) + \overset{**}{\Phi}\left(\frac{\partial v}{\partial x_0}\sin\theta - \frac{\partial w}{\partial x_0}\cos\theta\right)$$

$$- 2\Omega^2 x_I \left\{ 2\left(\frac{\partial^2 v}{\partial x_0 \partial \psi}\sin\theta - \frac{\partial^2 w}{\partial x_0 \partial \psi}\cos\theta\right)\overset{*}{\theta} + \overset{**}{\theta}\left(\frac{\partial v}{\partial x_0}\sin\theta\right.\right.$$

$$\left.\left. - \frac{\partial w}{\partial x_0}\cos\theta\right) + 2\overset{*}{\theta}\left(\sin\theta + \Phi\cos\theta\right)\right\}$$

(8.18)

In the last expression, the first two brackets [ ] and { } represent the linear inertia load which was also obtained by Houbolt (Ref. 10). The second { } bracket represents the nonlinear terms, while the last { }bracket represents the additional inertia load due to the presence of cyclic pitch. It should be emphasized that a considerable number of terms in Eq. 8.18 are still negligible. These are retained for the sake of generality.

In a similar manner, neglecting the $0(\epsilon_D^3)$ terms of Eq. J.2, the inertia load in the y-direction will be given by

$$P_{yI} = -m a_y \tag{8.19}$$

From Eqs. 8.19 and J.2:

$$P_{yI} = -m\Omega^2\left(\overset{**}{v} + 2U - v\right) - m x_I \Omega^2 \left\{ -\left[\ddot{\Phi}\sin\theta\right.\right.$$

$$\left.\left. - \left(\cos\theta - \Phi\sin\theta\right) - 2\left(\frac{\partial^2 v}{\partial x_0 \partial \psi}\cos\theta - \frac{\partial^2 w}{\partial x_0 \partial \psi}\sin\theta\right)\right]\right.$$

$$+\left[2\Phi\left(\frac{\partial^2 v}{\partial x_0 \partial \psi}\sin\theta-\frac{\partial^2 w}{\partial x_0 \partial \psi}\cos\theta\right)+2\dot{\Phi}\left(\frac{\partial v}{\partial x_0}\sin\theta-\frac{\partial w}{\partial x_0}\cos\theta\right)\right]$$

$$+\left[-\left(\dot{\theta}^2+2\dot{\theta}\dot{\Phi}\right)\cos\theta-\ddot{\theta}\left(\sin\theta+\Phi\cos\theta\right)+2\left(\frac{\partial v}{\partial x_0}\sin\theta\right.\right.$$

$$\left.\left.-\frac{\partial w}{\partial x_0}\cos\theta\right)\dot{\theta}+2\Phi\dot{\theta}\frac{\partial v}{\partial x_0}\cos\theta\right]\Bigg\} \tag{8.20}$$

Again, the first group of terms in Eq. 8.20 are the linear terms identical to Houbolt's (Ref. 10). The other two groups are the nonlinear terms and those due to cyclic pitch.

The total load per unit span in the y-direction is given by

$$P_y = L_{y_T} + P_{y_I} \tag{8.21}$$

Similarly, using Eq. J.3 and

$$P_z = -m a_z \tag{8.22}$$

the inertia load in the z-direction is obtained

$$P_{z_I} = -m\Omega^2\left(\ddot{w}+x_I\ddot{\Phi}\cos\theta\right)-m x_I \Omega^2\ddot{\theta}\left(\cos\theta-\Phi\sin\theta\right) \tag{8.23}$$

The total load per unit length in the z-direction is given by

$$P_z = L_{z_T} + P_{z_I} \tag{8.24}$$

It should be emphasized that the total loads are always assumed to be acting at the elastic axis of the blade cross section. In reality, the

inertia loads act at the blade cross section center of gravity. Therefore, at the elastic axis, these loads will also generate a system of inertia moments.

8.4.2 Derivation of the Feathering Moment at the Blade Root

In deriving the feathering moment due to the complete system of loads acting on the blade, the various moment arms must be carefully considered. According to assumption (3), Subsection 8.2, the pitch bearing (or the feathering hinge) is inboard of the "virtual" flap or lag hinges. Geometrically, its location will be taken at $x = e_1$ (or $x_o = 0$).

In writting the moments, the $\underset{\sim}{i}_1$, $\underset{\sim}{j}_1$, $\underset{\sim}{k}_1$ coordinate system defined in Subsection 8.3 is useful. From Eq. I.1, assuming that β is small

$$\begin{aligned} \underset{\sim}{i} &= \underset{\sim}{i}_1 - \underset{\sim}{k}_1 \beta \\ \underset{\sim}{j} &= \underset{\sim}{j}_1 \\ \underset{\sim}{k} &= \underset{\sim}{i}_1 \beta + \underset{\sim}{k}_1 \end{aligned} \tag{8.25}$$

The moment vector about the elastic axis in the hub plane coordinate system is

$$\underset{\sim}{q} = q_x \underset{\sim}{i} + q_y \underset{\sim}{j} + q_z \underset{\sim}{k} \tag{8.26}$$

From Eqs. 8.25 and 8.26

$$\underset{\sim}{q} = (q_x + \beta q_z) \underset{\sim}{i}_1 + q_y \underset{\sim}{j}_1 + (q_z - q_x \beta) \underset{\sim}{k}_1 \tag{8.27}$$

The total loading per unit length at the elastic axis can be written as

$$\underset{\sim}{p} = p_x \underset{\sim}{i} + p_y \underset{\sim}{j} + p_z \underset{\sim}{k} \tag{8.28}$$

or

$$\underset{\sim}{p} = (p_x + \beta p_z) \underset{\sim}{i}_1 + p_y \underset{\sim}{j}_1 + (p_z - p_x \beta) \underset{\sim}{k}_1 \tag{8.29}$$

The position vector of a point on the elastic axis of the deformed blade, with respect to the pitch bearing, can be written as (see Fig. 27a)

$$\underset{\sim}{r}_E = \underset{\sim}{i}(x_o + u) + \underset{\sim}{j} v + \underset{\sim}{k} w \tag{8.30}$$

Or using Eqs. 8.25

$$\underset{\sim}{r}_E = \underset{\sim}{i}_1 \left[(x_o + u) + \beta w\right] + \underset{\sim}{j}_1 v + \underset{\sim}{k}_1 \left[w - (x_o + u)\beta\right] \tag{8.31}$$

The moment of the loads given by Eq. 8.29 about the point represented by the pitch bearing is given by

$$\underset{\sim}{M}_P = \underset{\sim}{r}_E \times \underset{\sim}{P} = \underset{\sim}{i}_1 \left\{ v(P_z - \beta P_x) - P_y \left[w - \beta(x_o + u)\right] \right\} + \underset{\sim}{j}_1 (\cdots) + \cdots \tag{8.32}$$

The required moment about the feathering axis at the blade root is given by the $\underset{\sim}{i}_1$ component of Eq. 8.32

$$M_{P_{i1}} = v(P_z - \beta P_x) - P_y \left[w - \beta(x_o + u)\right] \tag{8.33}$$

The total feathering moment will be given by

$$M_{T.F.A} = \int_0^R M_{P_{i1}}\, dx + \int_0^R q_{i1}\, dx \tag{8.34}$$

where

$$q_{i1} = q_x + \beta q_z \tag{8.35}$$

In order to evaluate the feathering moment, the quantities M_{Pil}, q_{il} are required. The derivation of these quantities, together with the various approximations involved, is given in Appendix K.

From Eqs. K.6, K.10, K.14, 8.35 and 8.34, $M_{T.F.A.}$ can be written in its final form. Note that between $0 < x < e_1$, L_{z_T}, L_{y_T}, u, v, w, k_m, x_I, and m are all zero. Thus

$$M_{T.F.A} = \int_0^{\ell} \Big\{ v L_z - L_y (w - \beta x_0) + Ma - m\Omega^2 \Big(v \overset{**}{w} + x_I \Phi v \cos\theta \Big)$$

$$+ m\Omega^2 \Big[\Big(\overset{**}{v} - v \Big) w - \overset{**}{v} x_0 \beta \Big] - m\Omega^2 e_1 \beta v + m\Omega^2 2 \overset{*}{v} (w - \beta x_0) + m x_I \Omega^2 \Big[- \cos\theta (w - \beta x_0)$$

$$+ \Phi \sin\theta (w - \beta x_0) - \overset{**}{\Phi} \sin\theta (w - \beta x_0) - 2 (w - \beta x_0) \Big(\frac{\partial^2 v}{\partial \psi \partial x_0} \cos\theta$$

$$- \frac{\partial^2 w}{\partial x_0 \partial \psi} \sin\theta \Big) \Big] \Big\} dx_0 - \Omega^2 I_f \overset{**}{\Phi} - \Omega^2 I_f \left(\sin\theta \cos\theta + \Phi \cos 2\theta \right)$$

$$+ \int_0^{\ell} \Big\{ - m x_I \Omega^2 \left(\sin\theta + \Phi \cos\theta \right) v + m x_I \Omega^2 \Big[\overset{**}{v} \left(\sin\theta + \Phi \cos\theta \right)$$

$$- \overset{**}{w} \cos\theta + 2 \overset{*}{v} \left(\sin\theta + \Phi \cos\theta \right) - x_0 \beta \cos\theta - 2 \overset{*}{v} \beta \cos\theta \Big]$$

$$- m x_I^2 \Omega^2 \Big[2 \Big(\frac{\partial^2 v}{\partial x_0 \partial \psi} \sin\theta \cos\theta + \frac{\partial^2 w}{\partial x_0 \partial \psi} \sin^2\theta - 2 \Phi \frac{\partial^2 v}{\partial x_0 \partial \psi} \cos 2\theta \Big]$$

$$+ m x_I^2 \Omega \Big[\Big(\frac{\partial v}{\partial x_0} \cos^2\theta + \frac{\partial w}{\partial x_0} \sin\theta \cos\theta \Big) \beta - \frac{\partial^2 v}{\partial x_0 \partial \psi^2} \cos^2\theta \beta$$

$$- 2 \frac{\partial^2 w}{\partial x_0 \partial \psi^2} \sin\theta \cos\theta \beta \Big] \Big\} dx_0 - I_f \Omega^2 \overset{**}{\theta} - \left(I_f - I_0 \right) \overset{*}{\theta}^2 \Omega^2 \sin\theta \cos\theta$$

$$+ \int_0^{\ell} \Big\{ - m\Omega^2 x_I \overset{**}{\theta} v \cos\theta - m x_I^2 \Omega^2 \Big[- 2 \Big(\frac{\partial v}{\partial x_0} \sin\theta$$

$$- \frac{\partial w}{\partial x_0} \cos\theta \Big) \overset{*}{\theta} \sin\theta \Big] \Big\} dx_0 \qquad (8.36)$$

where I_f is the feathering moment of inertia of the blade

$$I_f = \int_0^\ell \left(k_o^2 + x_I^2 \right) m \, dx_o \tag{8.37}$$

and

$$I_o = \int_0^\ell m k_o^2 \, dx_o \tag{8.38}$$

Thus,

$$\int_0^\ell x_I^2 \, m \, dx_o = I_f - I_o \tag{8.39}$$

8.5 Derivation of the Aerodynamic Loads

8.5.1 Approximations Made in Deriving the Airloads

The purpose of this subsection is to show the various approximations involved in evaluating the aerodynamic loads acting on a section of the blade. In calculating these loads, assumptions (13) through (15) of Subsection 8.2 will be used.

Consider the deformed position of the blade in the hub plane coordinate system (x, y, z system, see Figs. 27 and 28). The position of the elastic axis is given by the position vector

$$\underset{\sim}{\pi}_E = \left(x_o + e_1 + u \right) \underset{\sim}{i} + v \underset{\sim}{j} + w \underset{\sim}{k} \tag{8.40}$$

For air-load calculation, the displacement u in the axial direction (which is a second-order quantity, anyway) is unimportant and will be neglected in this treatment. Thus

$$\underset{\sim}{\pi}_E = \left(x_o + e_1 \right) \underset{\sim}{i} + \underset{\sim}{j} v + w \underset{\sim}{k} \tag{8.41}$$

The velocity of this point (the elastic axis), can be written as

$$\underset{\sim}{v}_{EA} = \dot{\underset{\sim}{\pi}}_E + \underset{\sim}{\omega} \times \underset{\sim}{\pi}_E \tag{8.42}$$

Or, using Eq. 8.41

$$\underset{\sim}{v}_{EA} = -v\Omega \underset{\sim}{i} + \left[\Omega(x_o + e_1) + \dot{v}\right] \underset{\sim}{j} + \dot{w} \underset{\sim}{k} \tag{8.43}$$

From the geometry shown in Fig. 2, the velocity of the air in the hub plane coordinate system is given by

$$\underset{\sim}{V} = \mu\Omega R \cos\Psi \underset{\sim}{i} - \mu\Omega R \sin\Psi \underset{\sim}{j} - \Omega R\lambda \underset{\sim}{k} \tag{8.44}$$

(Note that in this report the induced velocity is positive down.)

From Eqs. 8.43 and 8.44, the flow relative to the blade at the elastic axis is given by

$$\begin{aligned} \underset{\sim}{U} = \underset{\sim}{V}_a - \underset{\sim}{v}_{EA} = \underset{\sim}{i}\left[\mu\Omega R\cos\Psi + v\Omega\right] - \underset{\sim}{j}\left[\mu\Omega R \sin\Psi \right. \\ \left. + \dot{v} + \Omega(x_o + e_1)\right] + \underset{\sim}{k}\left[-\Omega R\lambda - \dot{w}\right] \end{aligned} \tag{8.45}$$

In order to transform the flow relative to the blade, as given by Eq. 8.45, into a physically meaningful form, it is convenient to use the $\underset{\sim}{I}_2$, $\underset{\sim}{J}_2$, $\underset{\sim}{K}_2$ attached to the elastic axis of the blade and defined previously in Subsection 8.3.2.

Note that it is important to use this coordinate system because according to assumption (7), Subsection 8.2, the cross section of the blade is normal to the elastic axis. In this plane, the instantaneous geometric angle of pitch is given by the angle between the vectors $\underset{\sim}{J}_2$ and $\underset{\sim}{J}_3$ or $(\theta+\Phi)$.

From the relation between the various unit vectors, Eqs. I.5, the following relation can be written.

$$\underset{\sim}{i} = \underset{\sim}{I}_2 - \frac{\partial v}{\partial x}\underset{\sim}{J}_2 - \frac{\partial w}{\partial x}\underset{\sim}{K}_2$$

$$\underset{\sim}{j} = \frac{\partial v}{\partial x}\underset{\sim}{I}_2 + \underset{\sim}{J}_2$$

$$\underset{\sim}{k} = \frac{\partial w}{\partial x}\underset{\sim}{I}_2 + \underset{\sim}{K}_2 \tag{8.46}$$

From Eqs. 8.45 and 8.46, the flow relative to the blade can be expressed in terms of the $\underset{\sim}{I}_2$, $\underset{\sim}{J}_2$, $\underset{\sim}{K}_2$ system. Thus

$$\begin{aligned}\underset{\sim}{U} = {} & \underset{\sim}{I}_2\left[\mu\Omega R\cos\Psi + v\Omega - \frac{\partial v}{\partial x}\mu\Omega R\sin\Psi - \dot{v}\frac{\partial v}{\partial x} - \frac{\partial v}{\partial x}\Omega\left(x_0+e_1\right)\right] \\ & + \underset{\sim}{J}_2\left[-\frac{\partial v}{\partial x}\mu\Omega R\cos\Psi - \frac{\partial v}{\partial x}v\Omega - \mu\Omega R\sin\Psi - \dot{v} - \Omega\left(x_0+e_1\right)\right] \\ & + \underset{\sim}{K}_2\left[-\frac{\partial w}{\partial x}\mu\Omega R\cos\Psi - v\Omega\frac{\partial w}{\partial x} - \dot{w} - \Omega R\lambda\right]\end{aligned} \tag{8.47}$$

or

$$\underset{\sim}{U} = U_{x_2}\underset{\sim}{I}_2 + U_{y_2}\underset{\sim}{J}_2 + U_{z_2}\underset{\sim}{K}_2 \tag{8.48}$$

For convenience, a picture of the blade and flow geometry resulting from these considerations is given in Fig. 30.

The total load on the blade can be written symbolically as

$$\underset{\sim}{L}_A = L_{z_2}\underset{\sim}{K}_2 + L_{y_2}\underset{\sim}{J}_2 \tag{8.49}$$

From two-dimensional quasi-steady aerodynamics, it is well known (Ref. 11) that the quasi-steady lift at the aerodynamic center (c/4 point) is due to the angle of attack at the rear neutral point (3/4 c). At the rear neutral point the induced velocity can be written as

$$-U_{z_2} + \left(\frac{c}{2} - x_A\right)\left(\dot{\theta} + \dot{\phi}\right)$$

Thus

$$L_{Z_2} \cong \rho_A U_{Y_2}^2 a b R \left[(\theta + \Phi) - \frac{U_{Z_2}}{U_{Y_2}} + \frac{\left(\frac{c}{2} - X_A\right)(\dot{\theta} + \dot{\Phi})}{U_{Y_2}} \right] \quad (8.50)$$

$$L_{Y_2} \cong -\rho_A L_{Z_2} \frac{U_{Z_2}}{U_{Y_2}} - \rho_A U_{Y_2}^2 b R C_{do} \quad (8.51)$$

Where the following approximations were made in writting Eqs. 8.50 and 8.51

$$tan^{-1}\left(\frac{U_{Z_2}}{U_{Y_2}}\right) \cong \frac{U_{Z_2}}{U_{Y_2}}$$

i.e., the angle of inflow is small and

$$\frac{1}{2}\rho_A\left(U_{Y_2}^2 + U_{Z}^2\right) = \frac{1}{2}\rho_A U_{Y_2}^2\left[1 + \left(\frac{U_{Z_2}}{U_{Y_2}}\right)^2\right] \cong \frac{1}{2}\rho_A U_{Y_2}^2$$

both of which are reasonable approximations. Also, the u_{X2} component of the velocity parallel to the blade deformed elastic axis will have no effect on the aerodynamic loads.

From Eqs. 8.49 and I.5, L_A can be rewritten in the $\underset{\sim}{i}_1$, $\underset{\sim}{j}$, $\underset{\sim}{k}$ coordinate system. Thus

$$\underset{\sim}{L}_A = -\underset{\sim}{i}\left[L_{Z_2}\frac{\partial W}{\partial X} + L_{Y_2}\frac{\partial V}{\partial X}\right] + \underset{\sim}{j} L_{Y_2} + \underset{\sim}{k} L_{Z_2} \quad (8.52)$$

According to the symbol convention of this report, L_A can also be written as

$$\underset{\sim}{L}_A = \underset{\sim}{i} L_{X_T} + \underset{\sim}{j} L_{Y_T} + \underset{\sim}{k} L_{Z_T} \quad (8.53)$$

Comparing the last two equations, it is clear that

$$L_{yT} = L_{Y_2} \tag{8.54}$$

$$L_{zT} = L_{z_2} \tag{8.55}$$

$$L_{xT} = -L_{z_2}\frac{\partial w}{\partial x} - L_{Y_2}\frac{\partial v}{\partial x} \tag{8.56}$$

It should be noted that Eqs. 8.54 through 8.56 are a direct result of the approximations inherent in the coordinate transformation, Eq. I.7.

In the present report, the quantity L_{xT} will be neglected in the calculation of p_x because it is a small quantity when compared with the centrifugal force acting in the opposite direction. This is a nonconservative assumption because the L_{xT} load per unit length tends to reduce the stabilizing effect of the centrifugal force.

Finally, the aerodynamic moment along the $\underset{\sim}{I}_2$ direction can be symbolically written as

$$\underset{\sim}{M}_A \cong M_{x_2}\underset{\sim}{I}_2 \tag{8.57}$$

From Eqs. 8.57 and 8.46

$$\underset{\sim}{M}_A = M_{x_2}\underset{\sim}{i} - M_{x_2}\frac{\partial v}{\partial x}\underset{\sim}{j} - M_{x_2}\frac{\partial w}{\partial x}\underset{\sim}{k} \tag{8.58}$$

These two moments in the $\underset{\sim}{j}$, $\underset{\sim}{k}$ direction will introduce additional small bending moments in the flapwise and chordwise directions. These will also be neglected in the present report. Thus, the aerodynamic moment can be written as

$$\underset{\sim}{M}_A \cong M_{x_2}\underset{\sim}{i} = M_a\underset{\sim}{i} \tag{8.59}$$

Finally, approximate expressions for the velocity components, as given by Eq. 8.47, are required. Consider Eq. 8.47: u_{x2} is not required in this analysis and will be left unchanged. For low values of μ [assumption (16)

of Subsection 8.2], the first two terms in the expression for u_{Y2} can be considered small when compared with the other terms. Thus

$$v \frac{\partial v}{\partial x} \Omega << \Omega \left(x_0 + e_1 \right)$$

and

$$\mu \frac{\partial v}{\partial x} << \Omega \left(x_0 + e_1 \right)$$

so that

$$U_{Y_2} \cong -\mu \Omega R \sin\Psi - \dot{v} - \Omega \left(x_0 + e_1 \right) \tag{8.60}$$

Similarly, in the expression for u_{Z2}, $v(\partial w/\partial x)\Omega < \overset{*}{w}\Omega$ and will be neglected so that

$$U_{Z_2} \cong -\frac{\partial W}{\partial X} \mu \Omega R \cos\Psi - \dot{W} - \Omega R \lambda \tag{8.61}$$

Comparing Eqs. 8.60 and 8.61 with Eqs. 3.14 and 3.15, it can be seen that they are identical. Thus

$$\begin{aligned} U_P &= -U_{Z_2} \\ U_T &= -U_{Y_2} \end{aligned} \tag{8.62}$$

8.5.2 Derivation of the Aerodynamic Loads and Moments per Unit Span

Originally, it was intended to derive the air-laods per unit span in a general form and use the quasi-steady assumption (assumption (14), Subsection 8.2) C(k) = 1 only in the actual numerical calculation. Unfortunately, the presence of the cyclic pitch, constant pitch, and time dependent motion at flutter frequency would require a formal splitting of the aerodynamic loading into these three distinct groups. Thus, in order to remove this unncessary complication, it was decided to invoke the quasi-steady assumption right at the beginning.

In order to clarify the various assumptions associated with the quasi-steady approximation and neglecting the apparent mass effects, the

results of two-dimensional unsteady aerodynamics will be given below. For the case of a two-dimensional airfoil, in unsteady motion, determined by a time-dependent angle of attack α and a downward displacement of the elastic axis h, (see Fig. 8.1), the unsteady load and moment per unit span can be written as (Ref. 12)

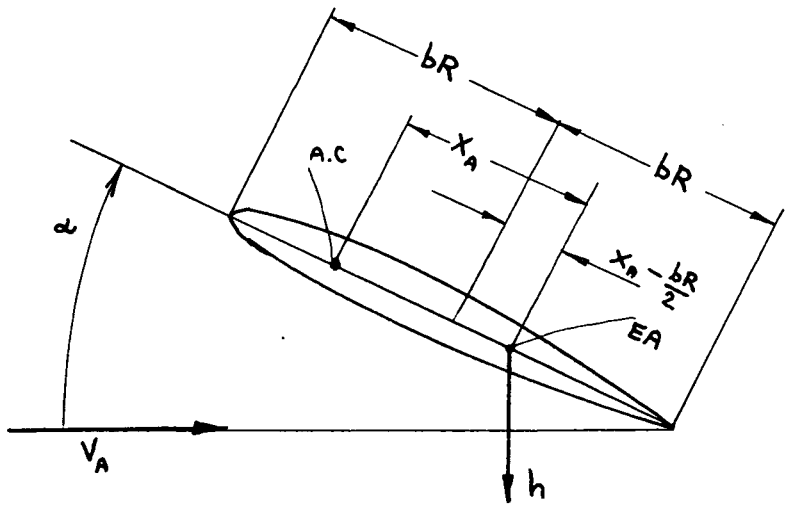

FIG. 8.1

$$L = L_Q C(k) + \frac{a}{2} \rho_A (bR)^2 \left[\ddot{h} + V_A \dot{\alpha} - \left(x_A - \frac{bR}{2} \right) \ddot{\alpha} \right] \tag{8.63}$$

where L_Q is the quasi-steady lift given by

$$L_Q = a \rho_A V_A \, bR \left[V_A \alpha + \dot{h} + (bR - x_A) \dot{\alpha} \right] \tag{8.64}$$

and

$$M = C(k) L_Q x_A + \rho_{\frac{A}{2}} a (bR)^3 (x_A - .5bR)\left[\ddot{h} - (x_A - .5bR)\ddot{\alpha}\right]$$

$$-\rho_A \frac{a}{2} V_A \dot{\alpha}\left[bR - x_A\right](bR)^2 - \rho_A \frac{a}{16}(bR)^4 \ddot{\alpha}$$

(8.65)

Here the assumption has been made that the aerodynamic center is at C/4. Setting C(k) = 1, as justified in Ref. 11, and neglecting the apparent mass terms associated with h and α yields

$$L = a\rho_A V_A bR\left[V_A \alpha + \dot{h} + \left(\frac{3}{2} - \bar{x}_A\right) bR\dot{\alpha}\right] \tag{8.66}$$

$$M = a\rho_A V_A (bR)^2 x_A\left[V_A \alpha + \dot{h}\right] + a\rho_A V_A (bR)^2 (1 - \bar{x}_A) bR\dot{\alpha}(\bar{x}_A - .5)$$

(8.67)

where $\bar{x}_A = x_A/bR$.

Replacing $\dot{h} = -U_P$, $V_A = U_T$, $\alpha = \theta + \Phi$ and $\dot{\alpha} = \dot{\theta} + \dot{\Phi} = \Omega(\overset{*}{\theta} + \overset{*}{\Phi})$ Eqs. 8.66 and 8.67 become (for small angles of inflow)

$$L_{z_T} = a\rho_A U_T bR\left[U_T(\theta + \Phi) - U_P + \left(\frac{3}{2} - \bar{x}_A\right) bR\Omega\left(\overset{*}{\theta} + \overset{*}{\Phi}\right)\right] \tag{8.68}$$

$$M_a = a\rho U_T (bR)^2\left\{\bar{x}_A\left[U_T(\theta + \Phi) - U_P\right] + (1 - \bar{x}_A)(x_A - .5) bR\Omega\left(\overset{*}{\theta} + \overset{*}{\Phi}\right)\right\} \tag{8.69}$$

Finally, the loading in the y-direction can be obtained from Fig. 2

$$L_{y_T} = -\frac{U_P}{U_T} L_z - \rho_A bR C_{d_o} U_T^2 \tag{8.70}$$

In Eq. 8.70 it is implied that

$$\tan^{-1}\frac{U_p}{U_T} \simeq \frac{U_p}{U_T}$$

and

$$\cos\left[\tan^{-1}\left(\frac{U_p}{U_T}\right)\right] = 1$$

From Eqs. 8.68 and 8.70

$$L_y = -\rho_A a b R\left\{U_p\left[U_T\left(\theta+\Phi\right)-U_p\right]+\left(\frac{3}{2}-\bar{X}_A\right)U_p b R\Omega\left(\dot{\theta}^*+\dot{\Phi}^*\right)\right.$$

$$\left.+\frac{C_{do}}{a}U_T^2\right\} \qquad (8.71)$$

8.6 The Equations of Motion

8.6.1 The Elastic Restoring Forces

According to assumption (13) Subsection 8.2, a linear treatment of the elastic restoring forces will be considered sufficient. Such a treatment has been derived by Houbolt and Brooks (Ref. 10). In writing the equations of equilibrium for the beam element, another convenient assumption will be made, following Ref. 10. It will be assumed that the element is cut by slices perpendicular to the hub plane. This assumption is one of convenience (in calculating the loads and moments, it was always assumed that the cross section is normal to the elastic axis), and will have a negligible effect on the results. Finally, in the beam equilibrium equations in the y and z-directions, the terms $\partial q_y/\partial x_o$, $\partial q_z/\partial x_o$ will be neglected. Thus the equations of equilibrium can be written as

$$\frac{\partial^2}{\partial x_o^2}\left\{\left[(EI)_y\cos^2\theta+(EI)_z\sin^2\theta\right]\frac{\partial^2 w_e}{\partial x_o^2}+\left[(EI)_z-(EI)_y\right]\sin\theta\cos\theta\frac{\partial^2 v_e}{\partial x_o^2}\right.$$

$$\left.-T_{eA}\sin\theta\right\}-\frac{\partial}{\partial x_o}\left[T(x_o)\frac{\partial w}{\partial x_o}\right] = P_z$$

$$\frac{\partial^2}{\partial x_o^2}\left\{\left[(EI)_z-(EI)_y\right]\sin\theta\cos\theta\,\frac{\partial^2 w_e}{\partial x_o^2}+\left[(EI)_y\sin^2\theta+(EI)_z\cos^2\theta\right]\frac{\partial^2 v_e}{\partial x_o^2}\right.$$

$$\left.-T_{eA}\cos\theta\right\}-\frac{\partial}{\partial x_o}\left[T(x_o)\frac{\partial v}{\partial x_o}\right]=p_y \qquad (8.72)$$

Note, that only the elastic deformation contributes to the elastic energy of the system. Therefore v_e, w_e defined in Fig. 27 are used in Eqs. 8.72.

The elastic restoring moment about the feathering axis can be assumed to be represented by a spring constant $K_\Phi = I_f\,\omega_o^2$.

8.6.2 Blade Equations of Motion

The equation of motion in the z-direction is obtained by combining Eqs. 8.72, 8.23, and 8.68.

The equation of motion in the y-direction is obtained by combining Eqs. 8.72, 8.20 and 8.71.

The feathering equation of motion can be symbolically written as

$$M_{T.F.A} = I_f\,\omega_o^2\,\Phi \qquad (8.73)$$

where $M_{T.F.A.}$ is given by Eqs. 8.36, 8.68, 8.69, and 8.71.

SECTION 9

NONLINEAR AND LINEARIZED EQUATIONS FOR THE COUPLED FLAP-LAG-PITCH MOTION OF HINGELESS BLADES IN HOVERING FLIGHT

9.1 Introduction

In this section, the general equations of motion derived in the previous section will be specialized to the case of coupled flap-lag-pitch motion in hovering flight. Using Galerkin's method for the spatial variable, the partial differential equations will be reduced to a system of nonlinear ordinary differential equations. In this process, no attempt will be made to include an arbitrary number of elastic modes (as was done previously for the case of flap lag); thus only one elastic mode for each elastic degree of freedom (i.e., flap and lag) will be used. Due to the considerable amount of algebraic manipulations involved, this process of reduction is given in a most concise form possible. Where details are required, they are given in the various appendices.

Based on physical reasoning, it is shown that the nonlinear effects in the feathering equation must be treated in a different manner than those associated with the flap and lag equations. Therefore, the treatment of the flap and lag equations is separated from the treatment of the feathering equation .

The resulting system of coupled ordinary differential equations is linearized about a natural equilibrium position, which is taken to be the equivalent linear steady-state position. In this process, various nonlinear effects are transformed into coupling effects. Thus the linearized equations contain many new terms when compared with those which would have been obtained from a purely linear treatment.

Next, the linearized equations of motion are transformed into a system which can be conveniently solved by defining various flutter derivatives (Refs. 11 and 39).

Finally, by adding the nonlinear terms to the linearized equations of motion, the complete coupled nonlinear equations of motion are written in a

form suitable for numerical integration.

9.2 Assumptions Made in Reducing the General Equations

In order to reduce the number of terms in the general equations, some assumptions must be made. These assumptions, given below, are only a matter of convenience, and will have little effect on the mechanism of instability.

(a) In order to simplify the inertia loads, it is assumed that the offset between the elastic axis and the blade cross-sectional center of gravity is zero, i.e., $x_I = 0$.

(b) The distance e_A between the area centroid of the tensile member and the blade elastic axis is also taken as $e_A = 0$.

(c) In order to describe the displacements of the blade, displacement field B, given by Eqs. 8.8 and shown in Fig. 27b, will be used.

(d) It is assumed that the flap and lag motions of the blade can be represented with a sufficient degree of accuracy by using one elastic mode in each of these degrees of freedom; thus

$$w_e = \ell \eta_1(\bar{x}_o)\, g_1(t)$$
$$v_e = -\ell \gamma_1(\bar{x}_o)\, h_1(t) \qquad (9.1)$$

(See Figs. 27a or 27b for the definition of w_e, v_e.)

The mode shapes used in Eqs. 9.1 represent the appropriate mode shapes of a rotating beam without the effect of elastic coupling, i.e., at $\theta = 0$.

(e) The boundary conditions for v_e, w_e are taken as the usual ones for a hingeless blade, i.e., Eqs. 3.6 are assumed to apply to v_e, w_e replacing v and w.

(f) The angle of preconing β_p and the built-in coning angle of the feathering axis β are assumed to be small.

9.3 The Equations of Motion in Flap and Lag

From Eqs. 8.8 and 9.1, the displacement field can be written as

$$u = -l\eta_1 g_1 (\beta+\beta_p) - \frac{\bar{x}_o l}{2}(\beta+\beta_p)^2 - \frac{1}{2} l \int_0^{\bar{x}_o} \left[(\eta_1')^2 g_1^2 + (\gamma_1')^2 h_1^2 \right] d\bar{x}_1 \tag{9.2}$$

$$v = -l h_1 \gamma_1 - l\eta_1 g_1 \Phi - x_o l \beta_p (\sin\theta + \Phi\cos\theta) \tag{9.3}$$

$$w = l\bar{x}_o(\beta+\beta_p) + \eta_1 g_1 l - l h_1 \gamma_1 \Phi \tag{9.4}$$

From Eqs. 8.17, 8.18, 8.20, 8.21, 8.23, and 8.24, assuming that $x_I = 0$, the loads can be written as

$$P_x = -\frac{\partial T}{\partial x_o} = -m\Omega^2 \left[\overset{**}{u} - (x_o + e_1 + u) - 2\overset{*}{v} \right] \tag{9.5}$$

$$P_y = L_{yT} - m\Omega^2 \left(\overset{**}{v} + 2\overset{*}{u} - v \right) - g_{SL}\Omega \overset{*}{v}_e \tag{9.6}$$

$$P_z = L_{zT} - m\Omega^2 \overset{**}{w} - g_{SP}\Omega \overset{*}{w}_e \tag{9.7}$$

where the effect of a viscous type of structural damping has been included in the last two relations. Note that only the elastic part of the displacement will dissipate energy through structural damping.

Denoting the elastic coupling effect by Ec_1 and Ec_2 as defined in Appendix L by Eqs. L.3 and L.4, and using the assumption that $e_A = 0$, Eqs. 8.72 can be rewritten as

$$\frac{\partial}{\partial x_o^2}\left\{ \left[(EI)_y + E_{c1} \right] \frac{\partial^2 w_e}{\partial x_o^2} - E_{c2} \frac{\partial^2 v_e}{\partial x_o^2} \right\} = P_z + \frac{\partial}{\partial x_o}\left(T \frac{\partial w}{\partial x_o} \right) \tag{9.8}$$

$$\frac{\partial}{\partial x_o^2}\left\{E_{c2}\frac{\partial^2 w_e}{\partial x_o^2}+\left[-E_{c1}+(EI)_z\right]\frac{\partial^2 v_e}{\partial x_o^2}\right\}=p_y+\frac{\partial}{\partial x_o}\left(T\frac{\partial v}{\partial x_o}\right) \tag{9.9}$$

Substituting Eqs. 9.2 through 9.7 into Eqs. 9.8 and 9.9 yields a system of equations on which Galerkin's method is applied. The application of Galerkin's method consists of the following steps:

(a) The $\overset{**}{u}$, u terms occurring in Eq. 9.5 are neglected.

(b) The flap equation is multiplied by $\eta_1 \ell^2 d\bar{x}_o$ and the terms associated with the inertia and elastic forces are integrated between $\bar{x}_o = 0$ and $\bar{x}_o = \ell$, while the aerodynamic loading terms are integrated between $\bar{x}_o = \bar{A}$ and $\bar{x}_o = \bar{B}$, where $\bar{A}$ and $\bar{B}$ are the tip loss factors.

(c) The resulting equation is nondimensionalized by dividing by $I_b \Omega^2$.

(d) The lag equation is multiplied by $\gamma_1 \ell^2 d\bar{x}_o$, then steps (b) and (c), described above, are repeated.

The algebraic process detailed above is straightforward and elementary; therefore, the details of the algebraic manipulation will not be given. The equations of motion obtained from this process for the flap and lag degrees of freedom are given in Eqs. 9.10 and 9.11, respectively.

$$\bar{M}_{F1}\overset{**}{q}_1+2\bar{M}_{F1}\bar{\omega}_{F1}\eta_{SF1}\overset{*}{q}_1+\left(\bar{M}_{F1}\bar{\omega}_{F1}^2+\bar{E}_{c1}\right)q_1=$$

$$\bar{B}^7\left(\overset{**}{h_1\Phi}\right)-\bar{B}^1(\beta+\beta_p)+\bar{B}^2 h_1\Phi+2\bar{P}_{111}\overset{*}{h_1}q_1 \tag{9.10}$$

$$+2\bar{B}^3\overset{*}{h_1}(\beta+\beta_p)+\bar{E}_{c2}h_1+A_{FIT}$$

$$\bar{M}_{L1}\ddot{h}_1 + 2\bar{M}_{L1}\bar{\omega}_{L1}\eta_{SL1}\dot{h}_1 + \left(\bar{M}_{L1}\bar{\omega}_{L1}^2 - \bar{E}_{c1}\right)h_1 =$$

$$g_1 E_{c2} - \bar{B}^7\left[\left(\ddot{g_1\Phi}\right) - g_1\Phi\right] - 2\bar{B}^7\dot{g}_1(\beta+\beta_p)$$

(9.11)

$$-\bar{B}^{11}\beta_p\left[\cos\theta\left(\ddot{\Phi} - \Phi\right) - \sin\theta\right] + 2\left[\bar{S}_{111} - \left(\bar{M}_\gamma\right)_{111}\right]h_1\dot{h}_1 - 2\left(\bar{M}_\eta\right)_{111}g_1\dot{g}_1$$

$$-\bar{B}^2 g_1\Phi - \bar{B}^{10}\beta_p\left(\sin\theta + \Phi\cos\theta\right) + 2\bar{B}^8\beta_p\sin\theta\,\dot{h}_1 + A_{L1T}$$

In the derivation of Eqs. 9.10 and 9.11, the orthogonality conditions for rotating beams, Eqs. A.2 and A.4 have been used. It should be mentioned that Eq. A.4 should be modified to account for the effect of the total coning angle $(\beta + \beta_p)$. As shown in Ref. 23, this effect will increase the rotating lag frequency $\bar{\omega}_{L1}^2$ by an amount $1/2(\beta + \beta_p)^2$. In the present treatment this small correction term will be neglected.

The quantities $\bar{E}_{c1}$, $\bar{E}_{c2}$ appearing in Eqs. 9.10 and 9.11 are the elastic coupling effects. These quantities are defined in Eqs. L.16 and L.17 (or L.5 and L.6). The quantities $\bar{B}^i$ appearing in Eqs. 9.10 and 9.11 are generalized mass terms defined in Appendix M.

The quantities A_{F1T} and A_{L1T} are generalized aerodynamic forces in flap and lag, respectively, defined by

$$A_{F1T} = \frac{l^2}{\Omega^2 I_b}\int_{\bar{A}}^{\bar{B}} L_{zT}\eta_1\, d\bar{x}_0 \qquad (9.12)$$

$$A_{L1T} = \frac{\ell^2}{\Omega^2 I_b} \int_{\bar{A}}^{B} L_{yT}\, \gamma_1\, d\bar{x}_o \tag{9.13}$$

Next, the aerodynamic loading terms A_{F1T} and A_{L1T} will be evaluated. The aerodynamic loads L_{zT} and L_{yT} are given by Eqs. 8.68 and 8.71, while the relations for U_p and U_T are given by Eqs. 8.60, 8.61, and 8.62. For hover, $\mu = 0$, and

$$U_p = \overset{*}{w}\Omega + \Omega R\lambda \tag{9.14}$$

$$U_T = \overset{*}{v}\Omega + \Omega\left(x_o + e_1\right) \tag{9.15}$$

Substituting Eqs. 9.2 through 9.4 into Eqs. 9.14, 9.15, 8.68, 8.71, 9.12, and 9.13 and performing the required integrations yields:

$$\begin{aligned} A_{F1T} = \frac{\gamma}{2}\left(\frac{\ell}{R}\right)^2 \Bigg\{ & F'\left(\theta + \Phi\right) - \lambda_o F^2 - \frac{\ell}{R}\overset{*}{g}_1 F^8 \\ & - \frac{\ell}{R}\left[2F^{10}\left(\theta+\Phi\right) - \lambda_o F''\right] h_1^* \\ & + \left[\left(\frac{\ell}{R}\right)^2 \theta\, h_1^{*2} F^{13} + \left(\frac{\ell}{R}\right)^2 h_1^* \overset{*}{g}_1 F^{15}\right. \\ & \left. + \frac{\ell}{R} L^7\left(\overset{*}{h_1\Phi}\right)\right] - 2\frac{\ell}{R} F' \beta_p \overset{*}{\Phi}\theta\cos\theta \\ & + \left(\frac{3}{2} - \bar{x}_A\right) b F^2 \overset{*}{\Phi} \Bigg\} \end{aligned} \tag{9.16}$$

and

$$A_{LIT} = \frac{\gamma}{2}\left(\frac{\ell}{R}\right)^2 \left\{ \lambda_0 \left[L^1(\theta+\Phi) - L^2\lambda_0 \right] + \frac{C_{d_0}}{a} L^4 \right.$$

$$+ \overset{*}{g}_1 \frac{\ell}{R}\left[L^7(\theta+\Phi) - 2L^9\lambda_0 \right] - \frac{\ell}{R}\overset{*}{h}_1 \left[\lambda_0(\theta+\Phi)L^{13} + 2\frac{C_{d_0}}{a} L^{14} \right]$$

$$\left. + \left[-\frac{\ell}{R} L^{14}\theta\left(\overset{*}{\widehat{h_1\Phi}}\right) - \left(\frac{\ell}{R}\right)^2 L^{19}\overset{*}{h}_1\overset{*}{g}_1\theta - \left(\frac{\ell}{R}\right)^2 L^{18}\overset{*2}{g}_1 \right] \right\} \tag{9.17}$$

The quantities L^i, F^i used in Eqs. 9.16 and 9.17 are defined in Eqs. C.1 and C.2.

In all of the equations associated with the flap and lag degrees of freedom, most third-order terms have been neglected. Also, some small terms multiplied by C_{d_o}/a have been neglected.

9.4 The Feathering Equation of Motion

9.4.1 The Higher Order Terms in the Feathering Equation

In treating the feathering equation, it is important to realize that the third-order inertia terms in this equation can be of importance and are non-negligible. The reason for this is clear when the general form of the feathering equation is considered. From Eqs. 8.36 and 8.73, where $x_I = 0$, the feathering equation can be simply written as

$$\Omega^2 I_f \overset{**}{\Phi} + \Omega^2 I_f\left(\sin\theta\cos\theta + \Phi\cos 2\theta\right) + I_f \omega_o^2 \Phi =$$

$$\int_0^\ell \left\{ v L_{zT} - L_{yT}(w-\beta x_o) + M_a - m\Omega^2 v\overset{**}{w} + m\Omega^2\left[w\left(\overset{**}{v}-v\right) \right.\right.$$

$$\left.\left. - \overset{**}{v}\beta x_o \right] - m\Omega^2 e_1 \beta v + 2m\Omega^2 \overset{*}{U}(w-\beta x_o) \right\} d\bar{x}_o$$

(9.18)

The left-hand side of this equation is multiplied by the feathering moment of inertia of the blade which for the case of $x_I = 0$ is a small quantity. It can be easily shown that after the integrations, all of the quantities on the right-hand side of Eq. 9.18 are multiplied by the flapping (or lagging) moment of inertia of the blade I_b, or by similar generalized mass quantities which are of the same order of magnitude. The ratio of $I_b/I_f \cong 1000$ for most hingeless blades. Thus, the small nonlinear inertia and aerodynamic terms on the right-hand side of Eq. 9.19 are multiplied by a large quantity and their influence on the stability of the torsional degree of freedom could be considerable. This has also been found in Ref. 11. Great care is, therefore, taken in treating these terms in this derivation and none of the potentially important terms are neglected. On the other hand, all fourth-order terms or terms of equivalent magnitude will be neglected.

9.4.2 Final Form of the Feathering Equation

The final form of the feathering equation can be obtained by substituting Eqs. 9.2 through 9.4, 8.68, 8.69, 8.71, 9.14, and 9.5 into Eq. 9.19. After performing the required integrations, which are straightforward, and dividing the result by $I_b\Omega^2$, the following final result is obtained. [Also, using $\sin\theta \cong \theta$, $\cos\theta \cong 1$]

$$
\begin{aligned}
&I\ddot{\Phi} + I\left[\theta + \Phi + \bar{\omega}_\phi^2 \Phi\right] = \left[\bar{B}^7 h_1 \ddot{g}_1 + \overline{M_{F1}}\, \ddot{g}_1 g_1 \Phi + \bar{B}^{12}\beta_p \ddot{g}_1 (\theta + \Phi)\right. \\
&\left. - \overline{M_{L1}}\, h_1 \widehat{(h_1 \Phi)}\right] + \left\{\bar{B}^{11}(h_1 - \ddot{h}_1)(\beta + \beta_p) + \bar{B}^7 (h_1 - \ddot{h}_1) g_1 + \bar{B}^{12}\left[g_1 \Phi\right.\right. \\
&\left.\left. - \widehat{(g_1 \Phi)}\right](\beta + \beta_p) + \overline{M_{F1}}\, g_1 \left[g_1 \Phi - \widehat{(g_1 \Phi)}\right] + \beta_p(\beta + \beta_p)(\Phi + \theta - \ddot{\Phi})\right. \\
&\left. + \bar{B}^{12} g_1 \beta_p (\theta + \Phi - \ddot{\Phi}) - \overline{M_{L1}}\, h_1 \Phi (h_1 - \ddot{h}_1)\right\} - 2\left\{\bar{B}^{12}\dot{g}_1 \beta_p (\beta + \beta_p)\right. \\
&\left. + \bar{B}^{15}\beta_p g_1 \dot{g}_1 + \bar{B}^{16}\beta_p h_1 \dot{h}_1 + \overline{M_{F1}}\, g_1 \dot{g}_1 (\beta + \beta_p) + \bar{B}^{17} g_1^2 \dot{g}_1 + \bar{B}^{18} g_1 h_1 \dot{h}_1\right\} \\
&+ \beta\left[\bar{B}^{11}\ddot{h}_1 + \bar{B}^{12}\widehat{(g_1 \Phi)} + \beta_p \ddot{\Phi}\right] + \bar{e}_1 \bar{C}_1 \beta h_1 + A_{T1}
\end{aligned}
\tag{9.19}
$$

where A_{T1} is given by

$$
\begin{aligned}
A_{T1} = \frac{\gamma}{2}\frac{\ell}{R} b \Big\langle \bar{x}_A \Big\{ & T'(\theta+\Phi) - T^2\lambda_o - \frac{\ell}{R}F^2 g_1^* - \frac{\ell}{R}\left[2L'(\theta+\Phi) - L^2\lambda_o\right] h_1^* + \left[\theta h_1^{*2}\left(\frac{\ell}{R}\right)^2 L^{13}\right. \\
& \left. + \left(\frac{\ell}{R}\right)^2 F'' h_1^* g_1^* + \frac{\ell}{R} L'(\widehat{h_1^*\Phi})\right] - 2\frac{\ell}{R}T'\beta_p \Phi^*\theta \Big\} + b(1-\bar{x}_A)(\bar{x}_A - .5)\left(T^2\Phi^* - \frac{\ell}{R}h_1^*\Phi^* L^2\right) \Big\rangle \\
- \frac{\gamma}{2}\left(\frac{\ell}{R}\right)^2 \Big\langle \Big\{ & L^4(\theta+\Phi)h_1 - L'\lambda_o h_1 - \frac{\ell}{R}g_1^* h_1 F^{10} - \frac{\ell}{R}\left[2(\theta+\Phi)L^{14} - \lambda_o L^{13}\right] h_1 h_1^* \\
& - \frac{\ell}{R}\beta_p \theta g_1^* F' + T^3\beta_p\theta(\theta+2\Phi)\Big\} + \Big\{\left(\frac{3}{2}-\bar{x}_A\right) b\Phi^* L' h_1 + \left(F'\theta - \lambda_o F^2\right) g_1\Phi \\
& - T'\lambda_o\beta_p\theta + L^{14}(\widehat{h_1^*\Phi}) h_1 L^{14} - \frac{\ell}{R}\beta_p \Phi g_1^* F' \Big\} + \Big\{ -\frac{\ell}{R} g_1^* g_1 \Phi F^8 - \lambda_o\beta_p\Phi T' \\
& + \frac{\ell}{R} h_1^* g_1^* h_1 L^{19} + \left(\frac{3}{2}-\bar{x}_A\right) b\Phi^*\left[F^2 g_1\Phi + T'\beta_p\theta - \frac{\ell}{R}h_1 h_1^* L^{13} - \frac{\ell}{R}\beta_p\theta h_1^* L'\right]\Big\} \Big\rangle \\
+ \frac{\gamma}{2}\left(\frac{\ell}{R}\right)^2 \Big\langle \Big\{ & \lambda_o\beta_p\left[T'(\theta+\Phi) - \lambda_o T^2\right] + \frac{\ell}{R} g_1^*\beta_p\left[F'(\theta+\Phi) - 2\lambda_o F^2\right] \\
& - \frac{\ell}{R}\beta_p h_1^*\left[\lambda_o L'(\theta+\Phi) + 2\frac{C_{do}}{a}L^4\right] + g_1\lambda_o\left[F^2(\theta+\Phi) - \lambda_o F^3\right] \\
& + \frac{C_{do}}{a}\left[T^3\beta_p + g_1 F'\right]\Big\} + \Big\{ \frac{\ell}{R} g_1 g_1^*\left[F^8(\theta+\Phi) - 2\lambda_o F^9\right] \\
& - \frac{\ell}{R}\left[\lambda_o F^{11}(\theta+\Phi) + 2\frac{C_{do}}{a}F^{10}\right] h_1^* g_1 \Big\} + \Big\{ \left(\frac{3}{2}-\bar{x}_A\right) b\Phi^*\lambda_o\left[T^2\beta_p + F^3 g_1\right] \\
& + \left(\frac{3}{2}-\bar{x}_A\right) b\Phi^*\frac{\ell}{R}g_1^*\left[\beta_p F^2 + g_1^* F^9\right] - \frac{\ell}{R}\theta h_1^* g_1^*\left[\beta_p F^{10} + g_1 L^{18}\right]\Big\} \Big\rangle
\end{aligned}
\tag{9.20}
$$

In writting the last equation, the assumption $\sin\theta \cong \theta$, $\cos\theta \cong 1.0$ has been used. The quantities T^1, T^2, T^3 used in Eq. 9.20 are defined by Eqs. M.19 through M.21.

9.5 Linearization of the Equations for Coupled Flap-Lag-Pitch Motion

9.5.1 Determination of the Static Equilibrium Condition

The complicated system of nonlinear differential equations obtained in the previous sections will be linearized about the static, linear equilibrium condition. Denoting the static equilibrium position in flap, lag, and torsion by g_1^o , $h_{1'}^o$ and Φ_o , respectively, the dependent variables can be written as

$$
\begin{aligned}
g_1 &= g_1^\circ + \chi_1 \\
h_1 &= h_1^\circ + \chi_2 \\
\Phi &= \Phi_\circ + \varphi
\end{aligned}
\tag{9.21}
$$

It is important to note that the quantities g_1°, h_1°, although similar in nature to those given by Eqs. 3.22,will have different values and will be given by different algebraic relations due to the presence of the torsional degree of freedom.

Setting all the dynamic terms equal to zero in Eqs. 9.10, 9.11, 9.16, 9.17, 9.19, and 9.20, and substituting Eqs. 9.21 in the resulting equations gives (after some algebraic manipulation) the following system of equations, which for convenience is written in matrix form

$$
\begin{bmatrix} S_{11} & S_{12} & S_{13} \\ S_{21} & S_{22} & S_{23} \\ S_{31} & S_{32} & S_{33} \end{bmatrix} \begin{Bmatrix} g_1^\circ \\ h_1^\circ \\ \Phi_\circ \end{Bmatrix} = \begin{Bmatrix} F_{SN} \\ L_{SN} \\ T_{SN} \end{Bmatrix} + \begin{Bmatrix} C_1 \\ C_2 \\ C_3 \end{Bmatrix} \tag{9.22}
$$

where the quantities S_{ij}, F_{SN}, L_{SW}, T_{SN}, and C_{ij} are given in Eqs. N.1 through N.15.

The quantities F_{SN}, L_{SN}, T_{SN} represent the static nonlinear quantities in the flap, lag, and feathering equations. The linear static equilibrium condition about which the equations of motion are linearized will be defined as that obtained from solving Eq. 9.22 with the nonlinear terms set equal to zero, i.e.,

$$
\begin{Bmatrix} g_1^\circ \\ h_1^\circ \\ \Phi_\circ \end{Bmatrix} = \left[S_{ij} \right]^{-1} \left\{ C_i \right\} \tag{9.23}
$$

9.5.2 The Linearized Equations

Using the static linear equilibrium conditions, determined in the previous section, the linearized equations can be obtained by substituting Eqs. 9.21 into Eqs. 9.10, 9.11, 9.16, 9.17, 9.19 and 9.20. In this process only the linear terms in χ_1, χ_2, and ϕ will be retained. The linear steady state part of the equations will vanish due to Eqs. 9.23, and the nonlinear part of the steady values will be tacked onto the nonlinear equations, which will be treated in the following section. After dividing the flap equation by $\bar{M}_{F1}$, and the lag equations by $\bar{M}_{L1}$ the linearized flap and lag equations can be written in the following convenient manner.

$$\ddot{\chi}_1 + \bar{g}_{D1}\dot{\chi}_1 + \left(\bar{\omega}_{F1}^2 + F_{\chi_1}\right)\chi_1 = F_{\ddot{\chi}_2}\ddot{\chi}_2 + F_{\dot{\chi}_2}\dot{\chi}_2$$

$$+ F_{\chi_2}\chi_2 + F_{\ddot{\phi}}\ddot{\phi} + F_{\dot{\phi}}\dot{\phi} + F_{\phi}\phi \qquad (9.24)$$

$$\ddot{\chi}_2 + \bar{g}_{D2}\dot{\chi}_2 + \left(\bar{\omega}_{L1}^2 - L_{\chi_2}\right)\chi_2 = L_{\ddot{\chi}_1}\ddot{\chi}_1 + L_{\dot{\chi}_1}\dot{\chi}_1$$

$$+ L_{\chi_1}\chi_1 + L_{\ddot{\phi}}\ddot{\phi} + L_{\dot{\phi}}\dot{\phi} + L_{\phi}\phi \qquad (9.25)$$

The quantities $F^{**}_{\chi_2}$, $F^{*}_{\chi_2}$, F_{χ_2}, F^{**}_{ϕ}, F^{*}_{ϕ}, F_{ϕ} and $L^{**}_{\chi_1}$, $L^{*}_{\chi_1}$, L_{χ_1}, L^{**}_{ϕ}, L^{*}_{ϕ}, L_{ϕ} are flutter derivatives associated with the flap and lag equations, respectively. These quantities are defined in Eqs. N.16 and N.17. The quantities g_{D1}, g_{D2} represent equivalent damping terms in the flap and lag equations given in Eqs. N.16 and N.17 (the last equation in each group). These are partially due to structural damping and partially due to aerodynamic damping. Finally, it should be mentioned that in this process of linearization, while the quantity Φ has been replaced everywhere by $\Phi_o+\phi$, the inflow ratio λ_o has

been left unchanged and is calculated from Eqs. 4.6 and 4.7. Physically, this approximation means that the linearization has been performed in such a manner as to allow small variations in the thrust coefficient.

Next, the feathering equation is linearized. In this case, due to the algebraic form of the equation obtained, it is convenient to divide the equation by the quantity I_E (see Eqs. N.18 and N.19)

$$I_E = I - T_{\varphi}^{**} \tag{9.26}$$

Physically, I_E represents the increased moment of feathering inertia of the blade due to the blade elastic axis displacement from the feathering axis. Thus the feathering equation can be written in a convenient form by

$$\ddot{\varphi} + \bar{g}_{D3}\dot{\varphi} + \bar{K}_E\varphi = T_{\chi_1}^{**}\ddot{\chi}_1 + T_{\chi_1}^{*}\dot{\chi}_1 + T_{\chi_1}\chi_1 + T_{\chi_2}^{**}\ddot{\chi}_2 + T_{\chi_2}^{*}\dot{\chi}_2 + T_{\chi_2}\chi_2 \tag{9.27}$$

where the quantities $T_{\chi_1}^{**}$, $T_{\chi_1}^{*}$, T_{χ_1}, $T_{\chi_2}^{**}$, $T_{\chi_2}^{*}$, T_{χ_2} represent the flutter derivatives for the feathering equation. While $\bar{g}_{D3}$ is the equivalent damping in feathering, it is of aerodynamic origin only, and $\bar{K}_E$ is the equivalent spring in the feathering degree of freedom. These quantities are defined by Eqs. N.24 and N.41.

9.6 Nonlinear Equations for Coupled Flap-Lag-Pitch Motion

The nonlinear equations for coupled flap-lag-pitch motion can be easily obtained by using the linearized equations of motion obtained in the previous section. The nonlinear parts of Eqs. 9.10, 9.11, 9.16, 9.17, 9.19, and 9.20 are extracted, the nonlinear steady-state parts from Eq. 9.22 added, and the resulting relations added to the linear system, Eqs. 9.24 through 9.27, obtained in the previous section. The final form of these equations is given below.

$$\ddot{\chi}_1 - \left(F_{\dot{\chi}_2} + \frac{\bar{B}^T \varphi}{\bar{M}_{F1}} \right) \ddot{\chi}_2 - \left(F_{\dot{\varphi}} + \frac{\bar{B}^T \chi_2}{\bar{M}_{F1}} \right) \ddot{\varphi} =$$

$$- \bar{g}_{D1} \dot{\chi}_1 - \left(\bar{\omega}_{F1}^2 + F_{\chi_1} \right) \chi_1 + F_{\dot{\chi}_2} \dot{\chi}_2 + F_{\chi_2} \chi_2 + F_{\dot{\varphi}} \dot{\varphi}$$

$$+ F_{\varphi} \varphi + F_{NL} \left(\dot{\chi}_1, \dot{\chi}_2, \chi_2, \dot{\varphi}, \varphi \right) \tag{9.28}$$

$$- \left(L_{\dot{\chi}_1} - \frac{\bar{B}^T \varphi}{\bar{M}_{L1}} \right) \ddot{\chi}_1 + \ddot{\chi}_2 - \left(L_{\dot{\varphi}} - \frac{\bar{B}^T \chi_1}{\bar{M}_{L1}} \right) \ddot{\varphi} =$$

$$- \bar{g}_{D2} \dot{\chi}_2 - \left(\bar{\omega}_{L1}^2 - L_{\chi_2} \right) \chi_2 + L_{\dot{\chi}_1} \dot{\chi}_1 + L_{\chi_1} \chi_1 + L_{\dot{\varphi}} \dot{\varphi}$$

$$+ L_{\varphi} \varphi + L_{NL} \left(\chi_1, \dot{\chi}_1, \chi_2, \dot{\chi}_2, \varphi, \dot{\varphi} \right) \tag{9.29}$$

$$- \left(T_{N\ddot{\chi}_1} + T_{\dot{\chi}_1} \right) \ddot{\chi}_1 - \left(T_{N\ddot{\chi}_2} + T_{\dot{\chi}_2} \right) \ddot{\chi}_2 + \left(1 - T_{N\ddot{\varphi}} \right) \ddot{\varphi} =$$

$$- \bar{g}_{D3} \dot{\varphi} - \bar{K}_E \varphi + T_{\dot{\chi}_1} \dot{\chi}_1 + T_{\chi_1} \chi_1 + T_{\dot{\chi}_2} \dot{\chi}_2 + T_{\chi_2} \chi_2$$

$$+ T_{NL} \left(\chi_1, \dot{\chi}_1, \chi_2, \dot{\chi}_2, \varphi, \dot{\varphi} \right) \tag{9.30}$$

where the quantities F_{NL}, L_{NL}, T_{NL}, $T^{**}_{N\chi_1}$, $T^{**}_{N\chi_2}$, $T^{**}_{N\phi}$ are defined in Eqs. 0.1 through 0.6.

Note that all second derivatives are written on the left-hand side of Eqs. 9.27 through 9.29. This form is necessary for the numerical integration of these equations.

SECTION 10

STABILITY OF FLAP-LAG-PITCH MOTION IN HOVER

10.1 Introduction

10.1.1 Brief Review of Past Work

In this section, the stability of flap-lag-pitch motion will be investigated using the equations obtained in the previous section. Both static stability or divergence and dynamic stability, or flutter will be considered. When searching in the available literature for previous investigations in this area, one finds that the complete three degree-of-freedom problem has not been investigated before.

The most extensively investigated case has been the case of flap-pitch motion which is similar to the classical flutter problem associated with fixed wing aircraft. For this case, both flutter and divergence in hover have been investigated by Miller and Ellis in Ref. 11. They concluded that the important parameter of the problem is the offset between the blade cross-sectional center of gravity and the aerodynamic center. Both flutter and divergence boundaries were plotted as a function of this parameter. The important effect of preconing on both flutter and divergence has also been pointed out in Ref. 11.

The flutter boundaries in flap pitch for hovering flight were also obtained by Daughaday, DuWald and Gates in Ref. 42. Their results were in general agreement with those of Ref. 11. Divergence boundaries were not presented in Ref. 42. The flutter boundaries obtained support, the claim made in Ref. 11, that quasi-steady aerodynamics yields conservative flutter boundaries. The experimental results obtained in Ref. 42 seemed to indicate better agreement with quasi-steady aerodynamics. Furthermore, it was found in this work that flutter could occur when the mass and aerodynamic centers were coincident with the elastic axis; this was found to be due to gyroscopic coupling between torsion and flapping.

It is interesting to note, therefore, that no investigation of the

static or dynamic stability of the complete flap-lag-pitch motion in hover has been undertaken up to the present. In particular, the various effects of feathering axis orientation with respect to the hub plane, preconing, collective pitch setting combined with elastic coupling, and inplane stiffness of the rotor on the divergence boundaries has not been investigated.

Finally, it is worthwhile to mention briefly a few other papers which have a connection with the coupled flap-lag-pitch problem. The pitch-lag problem in hovering of an articulated blade has been excellently treated by Chou in Ref. 43. Chou identified the mechanism of instability as due to pitch changes caused by lag motion; the coupling between these degrees of freedom was due to rotor head geometry. Stability criteria for hovering rotors were obtained.

The aeroelastic stability of helicopter rotors in hovering flight was studied by Zvara in Ref. 44, both theoretically and experimentally. The main purpose of this work was to determine the relative merits of the various aerodynamic theories as applied to different rotor configurations. Cantilevered, articulated, and teetering blades were evaluated. Only the flap-pitch degrees of freedom were considered.

Perisho (Ref. 45) treated the flap-pitch motion in forward flight, including the effect of reversed flow. Blade response curves were obtained using numerical integration. Stability boundaries and divergence boundaries were not explicitly obtained, although some of these boundaries are indicated on his curves. Bielawa (Ref. 35) treated the complete flap-lag-pitch problem, considering mainly second-order effects due to distributed torsion, together with the effect of time-dependent coefficients. Stability in hovering flight and divergence boundaries were not considered by Bielawa.

Recent flutter analyses seem to be devoted to considering some effects while neglecting other effects, usually of equal importance. Representative examples of this trend are found in a recent paper by Stammers (Ref. 46), where the effect of the periodicity of the coefficients was investigated using a regular perturbation method. The Coriolis effects in the flap-pitch equations of motion were neglected, reversed flow effects were also neglected,

and inertia terms associated with the feathering equation did not include all of the important effects. In this paper divergence boundaries were obtained as a function of the blade center-of-gravity elastic axis offset, and flutter boundaries were also obtained. Another example of this trend is in Ref. 47 where the effect of the wake in forward flight on the blade stability is treated by extending Loewy's aerodynamic theory (Ref. 48) to forward flight while neglecting the effect of periodic coefficients and reversed flow at advance ratios of $0.3 < \mu \leq 0.8$. The inertia characteristics of the blade in Ref. 47 were represented by taking the tip cross section of the blade as a typical cross section of the problem. In this case, stability boundaries for forward flight were obtained. Again, only the flap-pitch degrees of freedom were considered.

10.1.2 Objectives of the Present Study

In the present study, using the linearized equations of motion, the divergence of the coupled flap-lag-pitch motion will be investigated first. The effect of preconning, elastic coupling, feathering-axis orientation with respect to the hub plane, and inplane stiffness of the rotor on the divergence boundaries will be shown.

Next, the flutter, or dynamic stability of the linearized system of equations (Eqs. 9.24, 9.25 and 9.27) will be considered and stability boundaries similar to those obtained in Section 7 will be given.

10.2 Divergence Boundaries

10.2.1 The Linearized or Approximate Divergence Boundary

A linearized approximate divergence boundary can be immediately obtained from Eq. 9.23 by requiring that $\det |S_{ij}| = 0$. The divergence boundaries obtained from this requirement are similar to those of Ref. 11. They are characterized by the property that the divergence boundary is independent of the values of the quantities g_1^o, h_1^o, and Φ_o which represent the linear static equilibrium condition of the blade.

From Eqs. N.1 through N.9, it is easy to see that the only element of the $[S_{ij}]$ matrix which contains $\bar{\omega}_o$ explicitly is S_{33}. Therefore from the

requirement that det $|S_{ij}| = 0$, the following relation can be written

$$\bar{\omega}_o^2 = \frac{1}{I}\left\{ \beta_p(\beta+\beta_p) + \frac{\gamma}{2}\frac{\ell}{R} b \bar{x}_A T' - \frac{\gamma}{2}\left(\frac{\ell}{R}\right)^2 \beta_p \left[T^3\theta - T'\lambda_o\right]2 \right.$$

$$\left. - i_1 - i_2 \right\} - 1 \tag{10.1}$$

where

$$i_1 = \frac{S_{12}S_{23}S_{31} - S_{11}S_{23}S_{32}}{S_{22}S_{11} - S_{12}S_{21}} \tag{10.2}$$

$$i_2 = \frac{S_{13}\left[S_{21}S_{32} - S_{22}S_{31}\right]}{S_{22}S_{11} - S_{12}S_{21}} \tag{10.3}$$

where S_{ij} is given by Eqs. N.1 through N.9. From Eqs. 10.1 through 10.3, the approximate or linearized divergence boundary can be easily calculated.

10.2.2 The Exact Divergence Boundary

The exact divergence boundaries are obtained by including the effect of the static equilibrium condition of the blade (i.e., q_1^o, h_1^o, and Φ_o). Mathematically, the exact condition for the divergence can be shown to be given by the following relation:

$$\begin{vmatrix} \left(S_{11} - \frac{\partial F_{SN}}{\partial q_1^o}\right) & \left(S_{12} - \frac{\partial F_{SN}}{\partial h_1^o}\right) & \left(S_{13} - \frac{\partial F_{SN}}{\partial \Phi_o}\right) \\ \left(S_{21} - \frac{\partial L_{SN}}{\partial q_1^o}\right) & \left(S_{22} - \frac{\partial L_{SN}}{\partial h_1^o}\right) & \left(S_{23} - \frac{\partial L_{SN}}{\partial \Phi_o}\right) \\ \left(S_{31} - \frac{\partial T_{SN}}{\partial q_1^o}\right) & \left(S_{32} - \frac{\partial T_{SN}}{\partial h_1^o}\right) & \left(S_{33} - \frac{\partial T_{SN}}{\partial \Phi_o}\right) \end{vmatrix} = 0 \tag{10.4}$$

This requirement is identical to setting $\nu_o = 0$ (where ν_o is derived in the next section).

10.3 The Flutter Boundaries for the Linearized System

The flutter boundaries can be obtained from the solution of the linearized system as represented by Eqs. 9.24, 9.25, and 9.27. The solution to this system of equations is given by

$$\begin{aligned} \chi_1 &= A_1 e^{p\psi} \\ \chi_2 &= A_2 e^{p\psi} \\ \varphi &= A_3 e^{p\psi} \end{aligned} \tag{10.5}$$

Substitution of these relations into the linearized equations of motion yields the characteristic equation, Eq. 10.6, given on the next page. This equation can be expanded to give a sixth order equation which can be written as

$$\nu_6 p^6 + \nu_5 p^5 + \nu_4 p^4 + \nu_3 p^3 + \nu_2 p^2 + \nu_1 p + \nu_o = 0 \tag{10.7}$$

where the coefficients $\nu_6, \ldots, \nu_o$ are given in Appendix P, Eqs. P.1 through P.7.

At the flutter condition

$$p = i\omega_c \tag{10.8}$$

Substituting Eq. 10.8 into Eq. 10.7 gives two equations, one for the real and one for the imaginary part of Eq. 10.7.

From the real part

$$\begin{vmatrix} p^2 + \bar{g}_{D1} p + (\bar{\omega}_{F1}^2 + F_{\chi_1}) & -[p^2 F_{\ddot{\chi}_2} + p F_{\dot{\chi}_2} + F_{\chi_2}] & -[p^2 F_{\ddot{\varphi}} + p F_{\dot{\varphi}} + F_{\varphi}] \\ -[p^2 L_{\ddot{\chi}_1} + p L_{\dot{\chi}_1} + L_{\chi_1}] & p^2 + \bar{g}_{D2} p + (\bar{\omega}_{L1}^2 - L_{\chi_2}) & -[L_{\ddot{\varphi}} p^2 + p L_{\dot{\varphi}} + L_{\varphi}] \\ -[p^2 T_{\ddot{\chi}_1} + p T_{\dot{\chi}_1} + T_{\chi_1}] & -[p^2 T_{\ddot{\chi}_2} + p T_{\dot{\chi}_2} + T_{\chi_2}] & (p^2 + \bar{g}_{D3} p + \bar{K}_E) \end{vmatrix} = 0 \tag{10.6}$$

$$-\vartheta_6 \omega_c^6 + \vartheta_4 \omega_c^4 - \vartheta_2 \omega_c^2 + \vartheta_0 = 0 \tag{10.9}$$

From the imaginary part

$$\vartheta_5 \omega_c^5 - \omega_c^3 \vartheta_3 + \omega_c \vartheta_1 = 0$$

or

$$\vartheta_5 \omega_c^4 - \vartheta_3 \omega_c^2 + \vartheta_1 = 0 \tag{10.10}$$

The last equation is a quadratic in ω_c^2 which can be easily solved; thus

$$\left(\omega_c^2\right)_{1,2} = \frac{\vartheta_3 \pm \sqrt{\vartheta_3^2 - 4\vartheta_1\vartheta_5}}{2\vartheta_5} \tag{10.11}$$

From Eqs. 10.11 and 10.9 the flutter boundaries can be obtained.

10.4 Flap-Pitch Stability Boundary

In the presentation of the results, it will be useful to have stability boundaries for flap-pitch motion similar to those obtained previously for coupled flap-lag in Section 4. Therefore, the stability boundary for flap-pitch motion will be derived below. From Eq. 10.6

$$\begin{vmatrix} p^2 + g_{D1}\, p + \left(\bar{\omega}_{F1}^2 + F_{x_1}\right) & -\left[p^2 F_{\varphi\varphi}^* + p F_{\varphi}^* + F_{\varphi}\right] \\ -\left[p^2 T_{x_1 x_1}^* + p T_{x_1}^* + T_{x_1}\right] & p^2 + p\,\bar{g}_{D3} + \bar{K}_E \end{vmatrix} = 0 \tag{10.12}$$

In analogy to Section 4, at the flutter condition $p = i\omega_c$ and the imaginary part of the characteristic equation (Eq. 10.12) yields the appropriate relation for the flutter frequency

$$\omega_c^2 = \frac{\bar{g}_{D1}\bar{K}_E + \bar{g}_{D3}\left(\bar{\omega}_{F1} + F_{x_1}\right) - F_{\varphi} T_{x_1}^* - T_{x_1} F_{\varphi}^*}{\bar{g}_{D1} + \bar{g}_{D3} - F_{\varphi}^* T_{x_1 x_1}^*} \tag{10.13}$$

The real part of Eq. 10.12 yields

$$\left[-\omega_c^2 + \left(\bar{\omega}_{F_1}^2 + F_{\chi_1}\right)\right]\left(-\omega_c^2 + \bar{K}_E\right) - \omega_c^2 \bar{g}_{D_1} \bar{g}_{D_3}$$

$$-\left(-\omega_c^2 T_{\chi_1}^* + T_{\chi_1}\right) F_\varphi + \omega_c^2 F_\varphi^* \bar{T}_{\chi_1}^* = 0 \qquad (10.14)$$

The simultaneous solution of Eqs. 10.13 and 10.14, with an appropriate relation for the inflow ratio, yields the critical value of the pitch setting θ_c at which pitch-flap flutter occurs for a given torsional stiffness $\bar{\omega}_o$.

SECTION 11

RESULTS AND DISCUSSION

11.1 Numerical Quantities Used in the Calculation

Most numerical quantities used in the calculations are identical to those given in Section 7.1 unless otherwise stated. For all flap-lag-pitch calculations $x_I = 0$.

In the calculation of the divergence boundaries, the following geometrical blade properties were used:

$$\gamma = 8; \quad \sigma = 0.08; \quad b = 0.0313; \quad I = 0.0013$$

These properties are close to those of the Boelkow M105 4-bladed hingeless rotor.

In the calculation of the effect of the torsional degree of freedom on the flap-lag-type of instability, the previous values for γ and σ, used in the flap-lag calculations had to be used again. Thus, for this case

$$\gamma = 10; \quad \sigma = 0.05; \quad b = 0.025; \quad I = 0.001$$

In the calculation of the effect of lag on the flap-pitch instability, the same values of γ, σ, b and I were used as for the divergence boundary calculations.

For convenience, the inflow for all cases calculated was taken from Eq. 7.3.*

11.2 Static Stability Boundaries

11.2.1 Approximate Divergence Boundaries

For convenience in numerical calculations, only the linearized or approximate divergence boundaries, defined in Subsection 10.2.1, Eq. 10.1, were evaluated. Conceptually, these approximate stability boundaries are similar to those evaluated by Miller (Ref. 11). Equation 10.11 includes up to the first order, the destabilizing feathering moment due to the drag

*In all coupled flap-lag-pitch calculations the structural damping in the flap and lag degress of freedom $\eta_{SF} = \eta_{SL} = 0$. The sructural damping in the feathering degree of freedom was always assumed to be zero.

acting through the initial deflection (static) in flap together with the stabilizing feathering moment due to the lift acting through the initial deflection (static) in lag.

Figure 31 is a typical divergence boundary of this type. The blade cross sectional center of gravity and the elastic axis are taken to be coincident.

Thus, $\bar{x}_A$ represents the aerodynamic center-blade cross sectional center-of-gravity offset. As can be seen from Fig. 31, the rotating-lag frequency (or chordwise stiffness of the blade) has a considerable effect on the divergence boundary because it changes the effective moment arm through which the lift produces a stabilizing feathering moment. As can be seen, changes in $\bar{\omega}_{L1}$ between 1 and 2 have the greatest effect. It is clear from Fig. 31 that the soft inplane hingeless blade has superior divergence characteristics.

Figure 32 shows the effect of collective pitch setting θ on the approximate divergence boundaries. These plots indicate that at lower collective pitch setting the blade is statically more unstable. Physically, it expresses the fact that the stabilizing moment due to lift is approximately proportional to θ^2, while the destabilizing moment due to drag is proportional to a power of θ somewhere between 1.5 and 1.2. Calculations made for pitch flap with the exact divergence boundary (nonlinear) show that increasing θ could be destabilizing.

Figure 33 shows the destabilizing effect of the preconing, which has also been indicated in Ref. 11. From this plot it is clear that preconing has a strongly destabilizing effect on static stability.

Figure 34 shows the effect of feathering axis orientation β with respect to the hub plane, measured in a plane perpendicular to the hub plane. Again, this is a destabilizing effect, similar to β_p, but not as strong.

The effect of elastic coupling is stabilizing. Figure 33 was recalculated, including elastic coupling; it was found to be stabilizing, but only to a minor degree. The effect of elastic coupling is dependent upon the combination of flap and lag frequencies. Therefore, for some other combination of

these quantities, the effect could be stronger.

11.2.2 The Exact Divergence Boundary for Flap Pitch

In order to illustrate the considerable difference between the approximate and exact divergence boundary, these two are given in Fig. 35. The exact divergence boundary for flap pitch is treated in Appendix R, and the appropriate curve was calculated using Eq. R.5.

As can be seen from Fig. 35, the exact divergence boundary is approximately 33% higher than the approximate linear divergence boundary. Additional cases for different values of collective pitch setting θ were also computed and the same difference between approximate and exact boundaries was observed.

It is of interest to compare the initial static values of g_1^o, Φ_o evaluated at the exact divergence boundary and compare them with the values resulting from Eq. 9.23.

For the $\bar{\bar{x}}_A = 0.04$ point of Fig. 35

$(\Phi_o)_{exact} = 0.04919$ $\qquad$ $(g_1^o)_{exact} = 0.1011$

$(\Phi_o)_{linear} = 0.0623$ $\qquad$ $(g_1^o)_{linear} = 0.1117$

The flutter calculations are dependent upon the initial values g_1^o, Φ_o; thus, the exact calculation of these quantities, can have an effect on the result of the flutter calculation.

11.3 Flutter Boundaries

11.3.1 General

The purpose of this section is twofold. First, it will show the effect of the addition of the torsional degree of freedom on the flap-lag-type of instability treated in the first part of this work. Second, it will show the effect of the addition of the lag degree of freedom on the flap-pitch type of instability as evaluated from Eqs. 10.13 and 10.14.

The coupled flap-lag-pitch stability boundaries are evaluated from Eqs. 10.9 and 10.11 using a computer program which searches and iterates for the flutter points occurring between $0 < \theta < 0.5$ for a given combination of

flap, lag,and torsional frequencies. This program also continuously checks the value of ν_o, evaluated using the linear static equilibrium condition, for the occurrence of divergence.

The coupled flap-pitch stability boundary is evaluated using Eqs. 10.13 and 10.14 by a separate program which searches and iterates for the value of $\bar{\omega}_o$ at which flutter occurs at a given collective pitch setting θ. This program evaluates only the upper branch of the stability boundary.

11.3.2 Effect of Torsional Degree of Freedom on the Flap-Lag-Type of Instability

In order to illustrate this effect, the following cases* are considered:

Case 1	(a)	$\bar{\omega}_{Fl} = 1.175;$	$\bar{\omega}_{Ll} = 1.075764$
	(b)	$\bar{\omega}_{Fl} = 1.175;$	$\bar{\omega}_{Ll} = 1.28303$
Case 2	(a)	$\bar{\omega}_{Fl} = 1.25;$	$\bar{\omega}_{Ll} = 1.11966$
	(b)	$\bar{\omega}_{Fl} = 1.25;$	$\bar{\omega}_{Ll} = 1.39403$

Note that all cases plotted are calculated without the effect of elastic coupling.

Cases 1 and 2 correspond to the appropriate points on the stability boundary given in Fig. 8 for $\theta_c = .20$. Point (a) is on the lower branch while (b) is always on the upper branch.

Figure 36 shows the effect of torsion on Case 1(a). At a high value of $\bar{\omega}_o$ ($\bar{\omega}_o = 100$), this simulates a torsionally rigid blade; for this case, $\theta_c = 0.2068$ which compares well with the value $\theta_c = 0.20$ obtained from the flap-lag calculation. As the torsional stiffness is gradually decreased, the value of θ_c is slowly increasing. In the vicinity of $\bar{\omega}_o \tilde{=} 32$, θ_c increases sharply. At some very high value of θ divergence occurs. Thus, the effect of addition of the torsional degree of freedom is stabilizing for the lower branch of the flap-lag stability boundary shown in Fig. 8.

When the same process is repeated for the upper branch of the flap-lag stability boundary, Case 1(b), it is seen from Fig. 37 that the value of θ_c

*A limited number of additional cases will be considered in Ref. 9.

is continuously decreasing and at $\bar{\omega}_o = 5$, it reaches a value of $\theta_c = 0.047$. Thus, the addition of the torsional degree of freedom is strongly destabilizing for the upper branch of the flap-lag stability boundary.

During this process, the flutter frequency remains fixed for both the upper and the lower branch of the stability boundary, and is approximately equal to the lag frequency.

For the sake of completeness, two additional points on the flap-lag stability boundary were considered. These are Case 2(a) and Case 2(b); the results are shown in Figs. 38 and 39. Again, the torsional degree of freedom is destabilizing for the upper branch and stabilizing for the lower branch.

11.3.3 Effect of Lag Degree of Freedom on the Flap-Pitch-Type of Instability

In order to evaluate this effect, a pitch-flap stability boundary is required; this boundary is shown in Fig. 40. As can be seen, the pitch setting is strongly destabilizing.

In Fig. 41, the flutter frequencies associated with the stability boundary shown in Fig. 40 are given. It is of interest to note that the flutter frequencies in pitch-flap are usually lower than $\bar{\omega}_o$.

A representative point on the flutter boundary (Fig. 40) with

$$\theta_c = 0.20 \qquad \bar{\omega}_o = 7.8125 \qquad \bar{\omega}_{F1} = 1.2$$

will be used to investigate the effect of adding the lag degree of freedom.

The results of adding the lag degree of freedom are shown in Fig. 42. For $\bar{\omega}_{L1} = 20$, which represents a blade with the lag degree of freedom effectively suppressed, $\theta_c = 0.197$, which is quite close to $\theta_c = 0.20$. Decreasing the lag stiffness of the blade gradually reduces the value of θ_c. The flutter frequency during this process is shown in Fig. 43. It is interesting to note that during this gradual decrease, the flutter frequency is essentially the flap-pitch flutter frequency.

In the vicinity of $\bar{\omega}_{L1} = 5.0$, where the rapid dip in the value of θ_c occurs, the nature of the instability changes; it becomes a flap-lag-type of

instability and the flutter frequency is very close to the lag frequency. At $\bar{\omega}_{L1} \tilde{=} 2.25$, θ_c attains a minimal value of $\theta_c = 0.04$. This region is obviously identical to the region of low θ_c's shown in Figs. 37 and 39. In the vicinity of $\bar{\omega}_{L1} \tilde{=} 1.1$, a rapid growth in the value of θ_c occurs, and no flutter occurs below $\bar{\omega}_{L1} \leq 1.0$. This seems to indicate that the soft inplane hingeless blade seems to have the best coupled flap-lag-pitch flutter characteristics. This apparent advantage of the soft inplane hingeless blade should be considered within the limitation of the analysis performed in the present study. The various other instabilities associated with this type of blade such as ground resonance, air resonance,and instabilities due to positive preconing, were not considered and could be major design problems in the construction of a stable hingeless rotor system.

For a few cases, the effect of elastic coupling on these stability boundaries was investigated. It seems that the elastic coupling is sufficient to eliminate most of the unstable regions, except the unstable region in the vicinity of $\bar{\omega}_{L1} = 2.5$ shown in Fig. 42.

SECTION 12

SUMMARY OF RESULTS AND CONCLUSIONS

12.1 Conclusions for Coupled Flap-Lag Motion

Conclusions for Hovering Flight

1. In the vicinity of the critical condition ($\theta \geq \theta_c$), when flutter occurs, the amplitude of flap motion is much smaller than that for lag. This is due to the fact that the lag mode is the potentially unstable mode, due to its low damping. In this region the ratio of lag over flap amplitudes can be between 5 to 10.

2. The structural damping in flap has no effect on the stability of the system. On the other hand, a small amount of structural damping in lag (η_{SL1} = .5% of critical damping) is sufficient to stabilize the potentially unstable lag mode by raising the values of the critical collective pitch setting θ_c above values which could occur in practice. According to Ref. 3, the elastic coupling effect is also sufficient to eliminate most unstable areas inside the flap-lag stability boundary. In an actual hingeless rotor, these two effects will always coexist, indicating that the flap-lag stability problem may be readily avoided in an actual rotor design.

3. The limit-cycle-amplitude-response curves in lag are steep and the limit-cycle amplitudes are large. This means that the nonlinearities in the system are weak and they cannot stabilize (in a practical sense) the response once the linear-stability boundary is exceeded.

4. Combinations of flap and lag frequencies, corresponding to the region of unstable limit cycles in the stability boundaries (Figs. 3 and 4), should be avoided in the design of hingeless helicopter blades, because for this case a blade stable from a linear point of view can become unstable, if it encounters a disturbance which is large enough.

5. The structural damping in lag tends to reduce the limit-cycle amplitudes in lag and it also reduces the slope ($\partial\chi_2/\partial\theta$) of the limit-cycle-amplitude-response curves in lag (see Figs. 14 and 15).

6. In the neighborhood of the critical condition ($\theta > \theta_c$), the value of κ_{3R}, defined in Eq. G.71, determines the behavior of the blade motion in the large amplitude range because the sign of $\partial|A_o|/\partial\psi_1$ is the same as for κ_{3R} when $|A_o|$ is sufficiently large. Therefore, a large positive κ_{3R} represents a strongly destabilizing nonlinear effect. It is undesirable to have a blade with a positive κ_{3R} because in this case instability can always be excited, if the disturbance is sufficiently large. In violent maneuvers or in strong gusts, such large disturbances may occur in practice. The value of κ_{3R} is independent of the advance ratio and is a complicated function of ω_c, ω_{F1O}, ω_{L1O}, v_r, etc.

7. In hovering, for $\theta > \theta_c$ and $\kappa_{3R} < 0$, the limit-cycle amplitude for lag motion is approximately given by

$$2\left[-\frac{\kappa_{2R}}{\kappa_{3R}}\right]^{1/2}$$

while the limit-cycle amplitude in flap is given by

$$2|v_r|\left[-\frac{\kappa_{2R}}{\kappa_{3R}}\right]^{1/2}$$

8. Figure 10 shows that the effect of using the approximate centrally-hinged, spring-restrained rigid blade mode of the elastic hingeless blade is to significantly shift the region of flap-lag instability to lower values of blade frequency. This indicates that the use of the exact rotating mode shape could be of importance in the calculation of flap-lag stability boundaries.

9. The flutter frequency of flap-lag oscillations is very close to the lag frequency $\bar{\omega}_{L1}$. Therefore, for practical purposes, the lag frequency can be taken as equivalent to the flutter frequency.

Conclusions for the Forward-Flight Cases

10. When the rotating lag frequency of the blade is not in the vicinity of the 1/2 or 1, the time dependent coefficients (or forward flight, μ) in the equations of motion has only a forcing function type of effect. Thus, the time dependent coefficients will not have any influence on the stability of the system for this case and for the range of advance ratios considered in this study ($0 < \mu < .3$).

11. Below the critical condition ($\theta < \theta_c$) for all cases, the flap amplitude χ_1, in forward flight, is larger than the lag amplitude χ_2. At approximately $0.1\theta_c$ below critical the lag amplitude starts to grow, and for $\theta > \theta_c$, the lag amplitudes are much larger than the flap amplitudes. In order to eliminate large oscillations in lag, it is reasonable to design the blades in such a manner that no angle of collective pitch inside the flight envelope should ever exceed $0.7\theta_c$.

12. Due to the large amplitudes of vibrations in lag which can occur in both hover and forward flight, the fatigue life of the blade for inplane vibration could possibly be an important criterion for hingeless blade design.

13. For the general forward flight case, Case B ($\mu = \epsilon^{1/2}$, $\mu_o = 1$, $\omega_c \neq 1/2 + \epsilon\nu$ or $\omega_c \neq 1 + \epsilon\nu$), the blade response and stability in the neighborhood of θ_c is determined by $\mu_o^2\kappa_{6R} + \kappa_{2R}[(\theta - \theta_c)/\mu^2, (\lambda_o - \lambda_{oc})/\mu^2]$ and κ_{3R}. When the first of these quantities is positive and $\kappa_{3R} < 0$, stable limit-cycle oscillations occur. The flutter mode in this case has the functional form of

$$A_o = A_o\left(\frac{\theta-\theta_c}{\mu^2}, \frac{\lambda_o-\lambda_{oc}}{\mu^2}, \mu^2\psi\right)$$

14. Case C ($\mu = \varepsilon$, $\mu_1 = 1$, $\mu_o = 0$, $\omega_c = 1/2 + \varepsilon\nu$). In this case, the parametric excitation is predominant. Up to the first order, the amplitude of the lag motion, near the critical condition, can be approximated by

$$\chi_2 = 2\mu^{1/2}\, Real\left[A_o\left(\frac{\theta-\theta_c}{\mu}, \frac{\lambda_o-\lambda_{oc}}{\mu}, \mu\psi\right)\right]$$

Near the origin ($A_o \tilde{=} 0$), the stability is determined by $Re(s_1)$ (s_1 is given by Eq. 5.79a on page 46). For $Re(s_1) > 0$, the system is unstable and for $Re(s_1) < 0$, the system is stable provided $\kappa_{3R} < 0$.

15. Case D ($\mu = \varepsilon^{1/2}$, $\mu_o = 1$, $\mu_1 = 0$, $\omega_c = 1 + \varepsilon\nu$). The parametric excitation has an effect but forcing is predominant because the system is excited very close to its resonant frequency. Up to the first order terms, the lag motion can be approximated by

$$\chi_2 = 2\mu\, Real\left[A_o\left(\frac{\theta-\theta_c}{\mu^2}, \frac{\lambda_o-\lambda_{oc}}{\mu^2}, \mu^2\psi\right)\right]$$

The stability near the origin ($A_o \tilde{=} 0$) depends upon the sign of $Re(s_1)$. Where s_1 is given by Eq. 5.104, the system is stable for $Re(s_1) < 0$ and is unstable when $Re(s_1) > 0$. For $\mu > 0.25$, this case is usually characterized by large amplitudes of blade response. Therefore, the lag frequency range of $0.88 < \bar{\omega}_{L1} < 1.12$ should be avoided in the design of hingeless helicopter blades.

16. The important nonlinear terms in Eqs. 3.23 and 3.24 have been identified. The strong destabilizing term in Eq. 3.23 is $C_1(\ell/R)\theta F^{13*2}\chi_2$. When neglecting this term, the regions of unstable limit cycles in Figs. 3, 4, and 8 vanish completely. The term $-C_7(\ell/R)L^{18*2}\chi_1$ in Eq. 3.24 is stabilizing. When neglecting this term the regions of unstable limit cycle grow and cover approximately 60% of the stability boundary. Thus, it is dangerous to neglect nonlinear terms when investigating the nonlinear blade stability problem.

17. For all forward-flight cases, the stability and the amplitudes of blade response are considerably affected by the requirement of trimmed flight at fixed C_T. Flutter and blade response calculations, which neglect this effect when evaluating the effect of forward flight, have a doubtful validity.

12.2 Conclusions for Coupled Flap-Lag-Pitch Motion

1. From the numerical calculations performed it was found that the results associated with the stability of the coupled flap-lag-pitch system are quite sensitive to the numerical values of the coefficients in the feathering equation. The various quantities $\bar{F}^i, \bar{L}^i, \bar{B}^i, \bar{P}_{ikm}, (\bar{M}_\eta)_{III}$, etc. are dependent on the assumed mode shape, consequently the use of the exact mode shape of the blade (corresponding to the actual load distribution) may be important for certain flight conditions. Similarly the use of the exact, spanwise varying, inflow could also effect the results. These effects, can also combine to modify the static equilibrium position of the blade, thus affecting both the divergence and flutter boundaries. Use of an additional elastic mode in the flap degree of freedom could also be important. Therefore, the results and conclusions, presented below, should be considered as subject to certain limitations due to the fact that the various effects mentioned above have not been included in the analysis.

2. From the approximate static stability boundaries given, it is clear that the aerodynamic center-blade elastic axis (c.g. in reality) offset is a destabilizing effect. Similarly the effect of preconing (β_p) and blade feathering axis orientation with respect to the hub plane (β) are also destabilizing. The strongest destabilizing effect seems to be the preconing.

3. The lag degree of freedom has an important effect on static stability because the deflections in lag generate an effective moment arm through which the lift produces a stabilizing feathering moment. Thus, a soft inplane hingeless blade has much better divergence characteristics than a blade which is stiff in the chordwise direction.

4. Conceptually, the approximate linear divergence boundary is not the correct divergence boundary of the system. For the small number of cases considered, the approximate divergence boundary seems to be nonconservative.

5. The addition of the torsional degree of freedom has a stabilizing effect on the lower branch of the flap-lag stability boundaries (Figs. 3,4, and 8), while it is destabilizing for the upper branch. Thus, the upper branch of the flap-lag stability boundary should be avoided in the actual design of rotor blades.

6. **The addition of the lag degree of freedom with $\bar{\omega}_{L1} > 1.2$ is destabilizing for the coupled flap-pitch motion.**

8. With rotating lag frequencies of $\bar{\omega}_{L1} < 1.1$, the coupled flap-lag-pitch motion is quite stable. Thus, the soft inplane rotor with a rotating lag frequency in the vicinity of $\bar{\omega}_{L1} = 0.75$ (midway between .5 and 1.0) seems to be the best from both the divergence and flutter point of view. This apparent advantage of the soft inplane hingeless blade should be considered within the limitation of the analysis performed in the present study. The various other instabilities typical of this configuration were not considered (see page 159).

9. Due to the strong effect of the initial deflections g_1^o, h_1^o, Φ_o on both the static and dynamic stability boundaries of the blade, flutter-divergence interactions could easily occur.

10. When including the third order inertia terms in the feathering equation it has been found that it is also necessary to include a considerable number of third order terms, associated with the aerodynamic loads (because they are of the same order of magnitude). This is required in order to represent correctly the behaviour of the blade. It should be pointed out, that this conclusion may be modified by the considerations given in the first conclusion of this section.

11. Based upon this work, a parametric investigation aimed at determining the optimum configuration for a hingeless blade seems feasible.

REFERENCES

1. Young, M.I., "A Theory of Rotor Blade Motion Stability in Powered Flight". J. Am. Hel. Soc., Vol. 9, No. 3, pp. 12-15, 1964.

2. Hohenemser, K.H., and Heaton, P.W., "Aeroelastic Instability of Torionsally Rigid Helicopter Blades". J. Am. Hel. Soc., Vol. 12, No. 2, pp. 1-13, 1967.

3. Ormiston, R.A., and Hodges, D.H., "Flap-Lag Dynamics of Hingeless Helicopter Rotor Blades". U.S. Army Air Mobility & Development Lab., Ames Research Center, 1971. Subsequently published as "Linear Flap-Lag Dynamics of Hingeless Helicopter Rotor Blades in Hover". J.A.H.S. , Vol 17 No. 2, 1972.

4. Hall, E.W., "Application of Floquet Theory to the Analysis of Rotor-Wing VTOL Stability". Stanford University Center for Systems Research, SUDAAR No. 400, 1971.

5. Elman, H.L., Niebanck, C.F., and Bain, L.J., "Prediction of Rotor Instability at High Forward Speeds". Vol. V "Flapping and Flap-Lag Instability", USAAVLABS Tech. Rep 68-18E, Feb. 1969.

6. Cole, J.D., Perturbation Methods in Applied Mathematics. Blaisdell Publishing Company, 1968.

7. Tong, P., "Nonlinear Instability of Rotor Blades". M.I.T., ASRL TR 166-1, 1972

8. Tong, P., "The Nonlinear Instability in Flap-Lag of Rotor Blades in Forward Flight". M.I.T., ASRL TR 166-2, 1972.

9. Friedmann, P., "Investigation of Some Parameters Affecting Hingeless Blade Stability in Hover". (to be published as ASRL TR 166-4, 1972)

10. Houbolt, J.C., and Brooks, G.W., "Differential Equations of Motion for Combined Flapwise Bending, Chordwise Bending, and Torsion of Twisted Nonuniform Rotor Blades". NACA Tech. Rep. 1346, 1956.

11. Miller, R.H., and Ellis, C.W., "Helicopter Blade Vibration and Flutter". J. Am. Hel. Soc., Vol. 1, No. 3, pp. 19-38, 1956.

12. Bispinghoff, R.L., Ashley, H., Halfman, R.L., Aeroelasticity. Addison-Wesley Pub. Co., 1955.

13. Cole, T., and Kevorkian, J., "Uniformly Valid Asymptotic Approximations for Certain Nonlinear Differential Equations", Nonlinear Differential Equations and Nonlinear Mechanics, Academic Press, New York, 1963.

14. Kevorkian, J., "The Two Variable Expansion Procedure for the Approximate Solution of Certain Nonlinear Differential Equations" from Space Mathematics, Part 3, J.B. Rosser, Ed., American Math. Society, 1966, pp. 206-275.

15. Nayfeh, A.H., "A Perturbation Method for Treating Nonlinear Oscillation Problems". J. of Math. and Phy., Vol. 44, pp. 368-374, 1965.

16. Morino, L., "A Perturbation Method for Treating Nonlinear Panel Flutter Problems." AIAA Journal, Vol. 7, No. 3, pp. 405-411, 1969.

17. Morino, L., Kuo, C.C., and Dugundji, J., "Perturbation and Harmonic Balance Methods for Nonlinear Panel Flutter". Massachusetts Institute of Technology, Aeroelastic and Structures Research Laboratory, ASRL TR 164-1, March 1971.

18. Morino, L., and Kuo, C.C., "Detailed Extensions of Perturbation Methods for Nonlinear Panel Flutter". Massachusetts Institute of Technology, Aeroelastic and Structures Research Laboratory, ASRL TR 164-2, March 1971.

19. Gesow, A., and Myers, G.C., Aerodynamics of the Helicopter, Frederick Ungar Publishing Co., New York, 1952.

20. Bramwell, A.R.S., "A Method for Calculating the Stability and Control Derivatives of Helicopters with Hingeless Rotors." City University London, Research Memorandum Aero 69/4, 1969.

21. Minorsky, N., Nonlinear Oscillations. D. Van Nostrand Co., Princeton, 1962.

22. Butenin, N.V., Elements of the Theory of Nonlinear Oscillations. Blaisdell Publishing Co., 1965.

23. Hsu, L., and Renbarger, J.L., "Bending Vibrations of a Rotating Beam". Proc. First U.S. Nat. Cong. of App. Mech. (ASME 1952), pp. 75-79.

24. Ham, N.D., and Zvara, J., "Experimental and Theoretical Analysis of Helicopter Rotor Hub Vibratory Forces". WADC Tech. Rep. 59-522, Oct. 1959.

25. Hildebrand, F.B., Introduction to Numerical Analysis. McGraw-Hill Book Co., Inc., 1956.

26. Abramovitz, M., and Stegun, I.A., Handbook of Mathematical Functions. Dover Publications, Inc., 1965.

27. Young, M.I., "A Simplified Theory of Hingeless Rotors with Application to Tandem Helicopters". Eighteenth National Forum American Helicopter Soc., 1962.

28. Lytwyn, R.T., Miao, W., and Woitsch, W., "Airborne and Ground Resonance of Hingeless Helicopters". J.A.H.S., April 1971, pp. 1-9.

29. Ralston, A., and Wilf, H.S., Mathematical Methods for Digital Computers, Vol. I, John Wiley and Sons Co. 1967.

30. Lapidus, L., and Seinfeld, J., Numerical Solution of Ordinary Differential Equations. Academic Press, 1971.

31. Miller, R.H. "Rotor Blade Harmonic Air Loading". AIAA Journal, Vol. 2, No. 7, 1964, pp. 1254-1269.

32. Loewy, R.G., "Review of Rotary Wing V/STOL Dynamic and Aeroelastic Problems". J. Am. Hel. Soc., Vol. 14, No. 3, pp. 3-23, July 1969.

33. Lemnios, A.Z., "A Nonlinear Aeroelastic Loads Analysis of Rotary Wings". AIAA Symposium on Structural Dynamics and Aeroelasticity, Aug. 30 - Sept. 1, 1965, pp. 108-123.

34. Pizialli, R.A., "An Investigation of the Structural Dynamics of Helicopter Rotors". USAAVLABS Tech. Rep. 70-24, April 1970.

35. Bielawa, R.L., "A Second Order Non-Linear Theory of the Aeroelastic Properties of Helicopter Rotor Blades in Forward Flight". Ph.D. Thesis, Massachusetts Institute of Technology, June 1965.

36. Arcidiacono, P.J., "Prediction of Rotor Instability at High Foward Speeds, Vol. I, Steady Flight Differential Equations of Motion for a Flexible Helicopter Blade with Chordwise Mass Unbalance". USAAVLABS Technical Report 68-18A, February 1969.

37. Meirovitch, L., Methods of Analytical Dynamics. McGraw-Hill Book Co., Inc. 1970, p. 111.

38. Jenkins, J.L., "A Numerical Method for Studying the Transient Blade Motions of a Rotor with Flapping and Lead-Lag Degrees of Freedom". NASA TN D-4195, April 1967.

39. Ham, N.D., AGARD Manual on Aeroelasticity, Vol. III, Ch. 10, Addition Sept. 1967.

40. Yntema, R.T., "Simplified Procedures and Charts for the Rapid Estimation of Bending Frequencies of Rotating Beams", NACA TN 3459, Feb. 1955.

41. Friedmann, P., and Tong, P., "Nonlinear Flap Lag Stability of Hingeless Helicopter Blades", Israel J. of Technology, Vol. 10, No. 1-2, pp. 133-43, Proc. XIV Isr. Ann. Conf. Aviation and Astronautics, March 1972.

42. Daughaday, H., Duwaldt, F., and Gates, C., "Investigation of Helicopter Blade Flutter and Load Amplification Problems", J.A.H.S., July 1957, p. 27-45.

43. Chou, P.C., "Pitch-Lag Instability of Helicopter Rotors", J. of Am. Hel. Soc., July 1961, p. 30-39.

44. Zvara, J., "The Aeroelastic Stability of Helicopter Rotors in Hovering Flight", Massachusetts Institute of Technology, ASRL TR 61-1, September 1956.

45. Perisho, C.H., "Analysis of the Stability of a Flexible Rotor Blade at High Advance Ratio", J. Am. Hel. Soc., April 1959, p. 4-18.

46. Stammers, C.W., "The Flutter of a Helicopter Rotor Blade in Forward Flight", The Aeronautical Quarterly, Feb. 1970, p. 18-48.

47. Shipman, K.W., and Wood, E.R., "A Two Dimensional Theory for Rotor Blade Flutter in Forward Flight", J. of Aircraft, Dec. 1971, pp. 1008-1015.

48. Loewy, R.G., "A Two Dimensional Approximation to the Unsteady Aerodynamics of Rotary Wings", J. Ae. Sci., Feb. 1957, pp. 81.

TABLE 1

Numerical Values of F^i, L^i Coefficients Defined in Appendix C

Flap Coefficient	Numerical Value (Nondimensional)	Lag Coefficient	Numerical Value (Nondimensional)
F^1	0.2253962	L^1	0.2888881
F^2	0.2888881	L^2	0.3999991
F^3	0.3999991	L^3	0.0
F^4	0.0	L^4	0.2253962
F^5	0.0	L^5	0.0
F^6	0.3716033	L^6	0.0
F^7	0.4999981	L^7	0.2059954
F^8	0.2059954	L^8	0.2567891
F^9	0.2567891	L^9	0.0
F^{10}	0.2059954	L^{10}	0.3716033
F^{11}	0.2567891	L^{11}	0.4999981
F^{12}	0.0	L^{12}	0.0
F^{13}	0.1901494	L^{13}	0.2567891
F^{14}	0.3333313	L^{14}	0.2059954
F^{15}	0.1901494	F^{15}	0.0
F^{16}	1.0000000	F^{16}	0.3333315
F^{17}	0.5000000	F^{17}	0.3333313
F^{18}	0.3333333	F^{18}	0.1901494
F^{19}	0.4222209	F^{19}	0.1901494
F^{20}	0.7428541		

Values for the Pertinent Generalized Mass Quantities Defined in App. B

$\bar{P}_{111} = .8148114$ $\qquad$ $\bar{M}_{F1} = .7703672$

$\bar{S}_{111} = .8148114$ $\qquad$ $\bar{M}_{L1} = .7703672$

$(\bar{M}_\gamma)_{111} = .8148102$ $\qquad$ $\bar{C}_1 = 1.199996$

$(\bar{M}_\eta)_{111} = .8148102$

TABLE 2

NUMERICAL VALUES OF $\bar{B}^i$, T^i COEFFICIENTS DEFINED IN APPENDIX M

Coefficient	Numerical Value
$\bar{B}^1$	.8666655
$\bar{B}^2$	.9037014
$\bar{B}^3$	.7703676
$\bar{B}^4$	.7703676
$\bar{B}^5$	.8666654
$\bar{B}^6$	.9037012
$\bar{B}^7$	.7703671
$\bar{B}^8$	.7703676
$\bar{B}^9$	.9037012
$\bar{B}^{10}$	.8666654
$\bar{B}^{11}$	.8666642
$\bar{B}^{12}$	.8666642
$\bar{B}^{13}$	1.1999960
$\bar{B}^{14}$	1.5000000
$\bar{B}^{15}$	.9037001
$\bar{B}^{16}$	.9037001
$\bar{B}^{17}$	.8148102
$\bar{B}^{18}$	.8148102
T^1	.333333
T^2	.500000
T^3	.250000

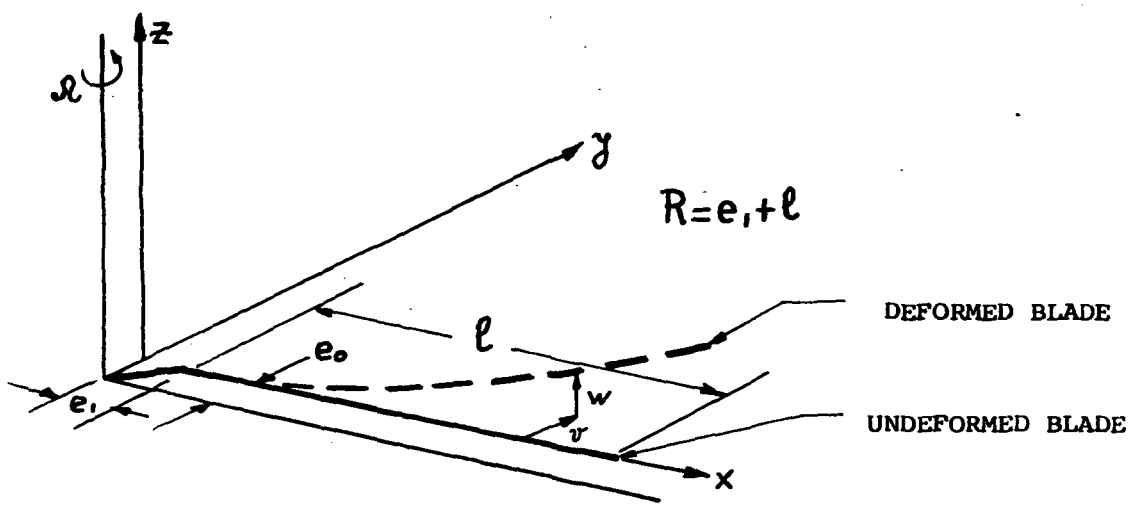

FIG. 1 GEOMETRY OF UNDEFORMED BLADE AND DEFORMED BLADE

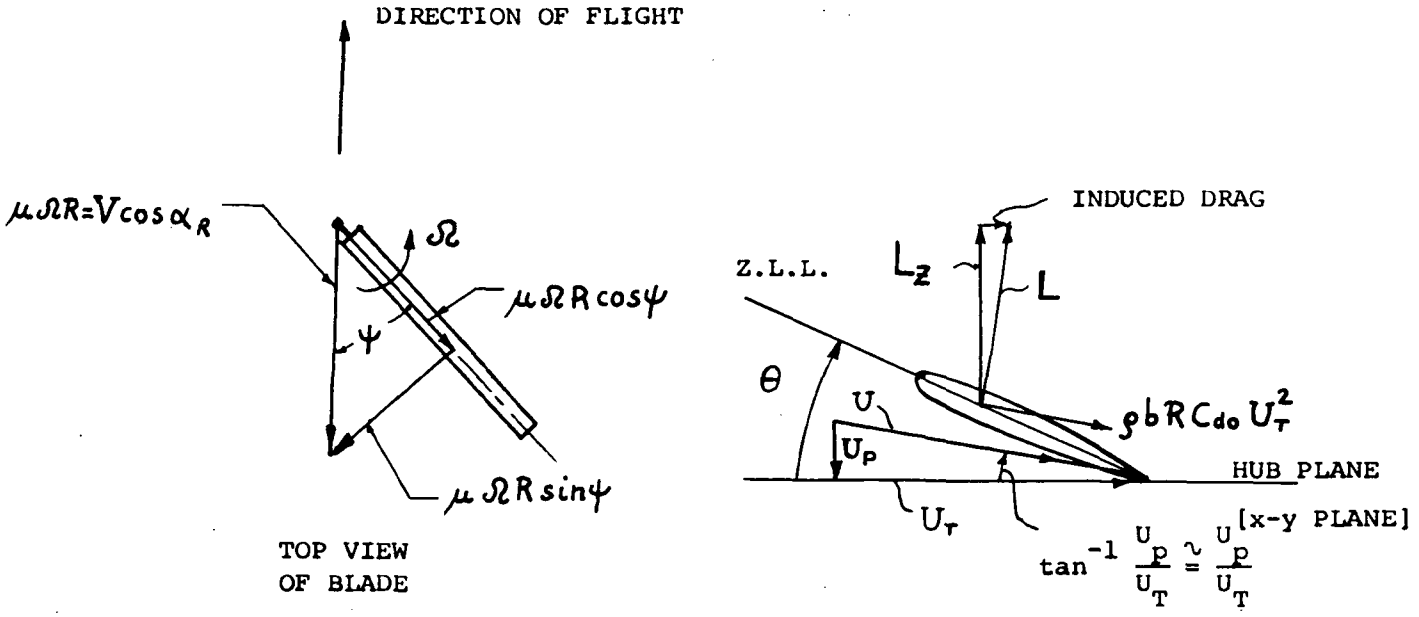

FIG. 2 VELOCITIES IN PLANE OF THE BLADE AND GEOMETRY FOR EVALUATION OF L_y

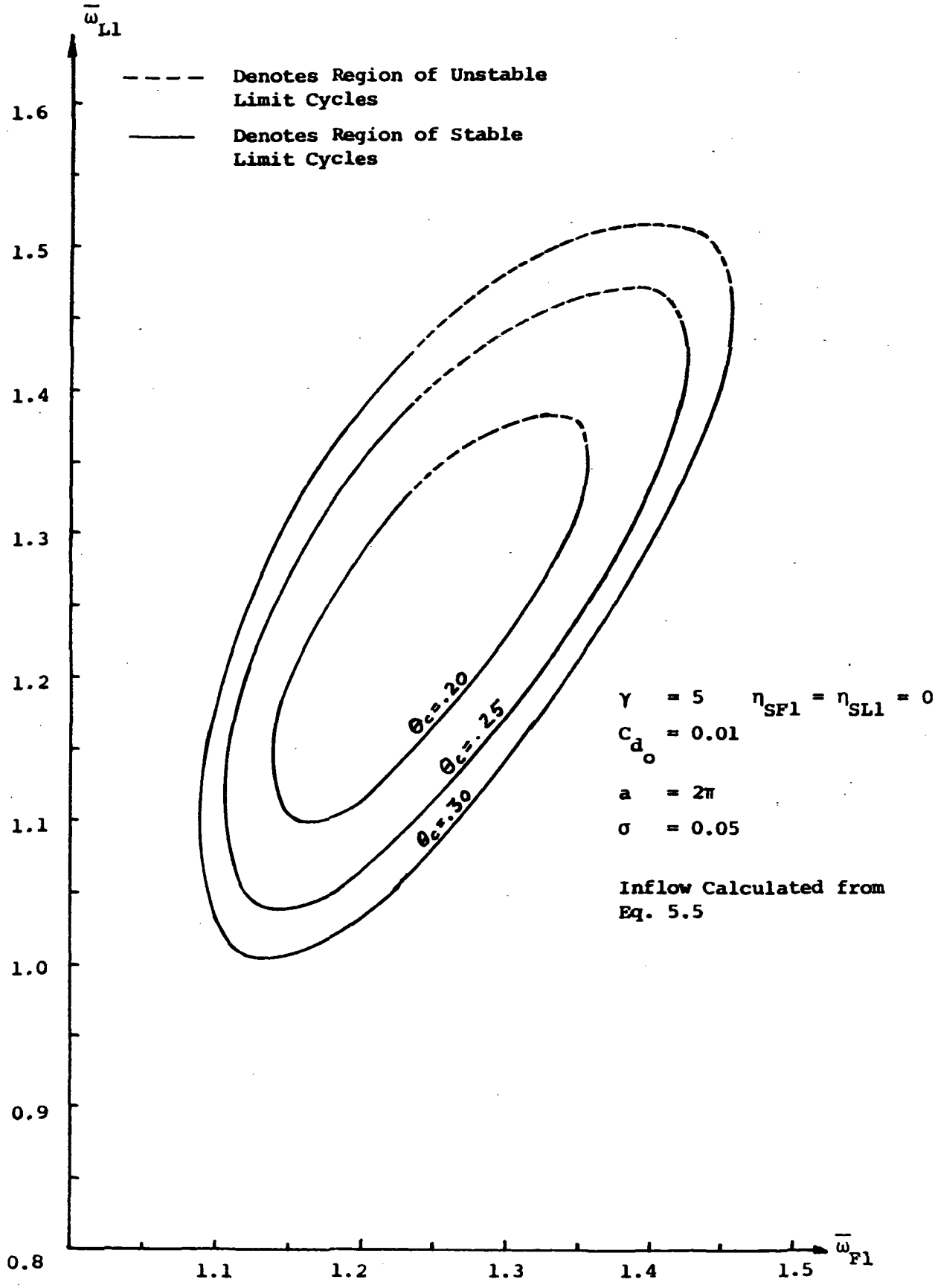

FIG. 3 STABILITY BOUNDARIES FOR VARIOUS VALUES OF θ_c $\gamma = 5$

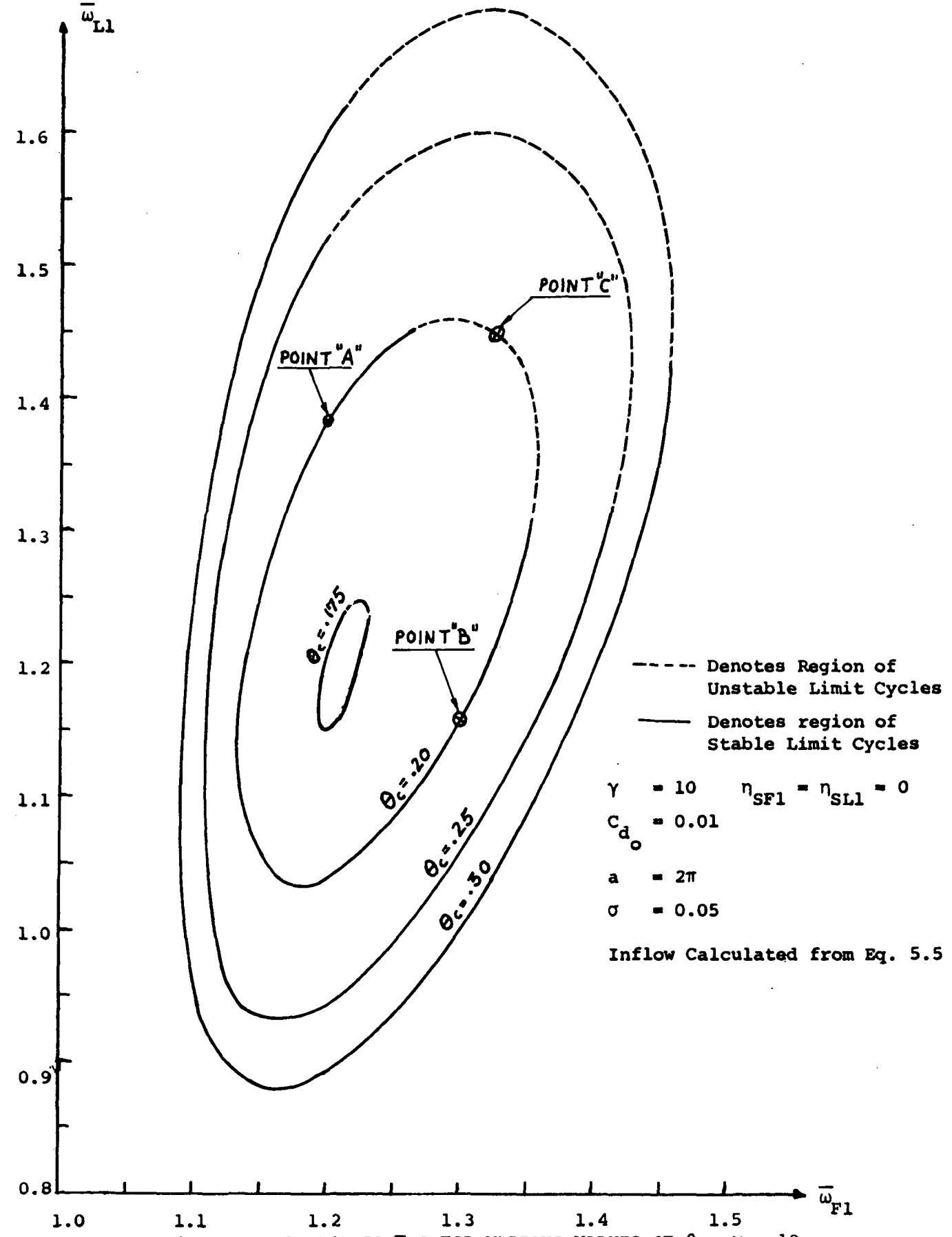

FIG. 4 STABILITY BOUNDARIES FOR VARIOUS VALUES OF θ_c γ = 10

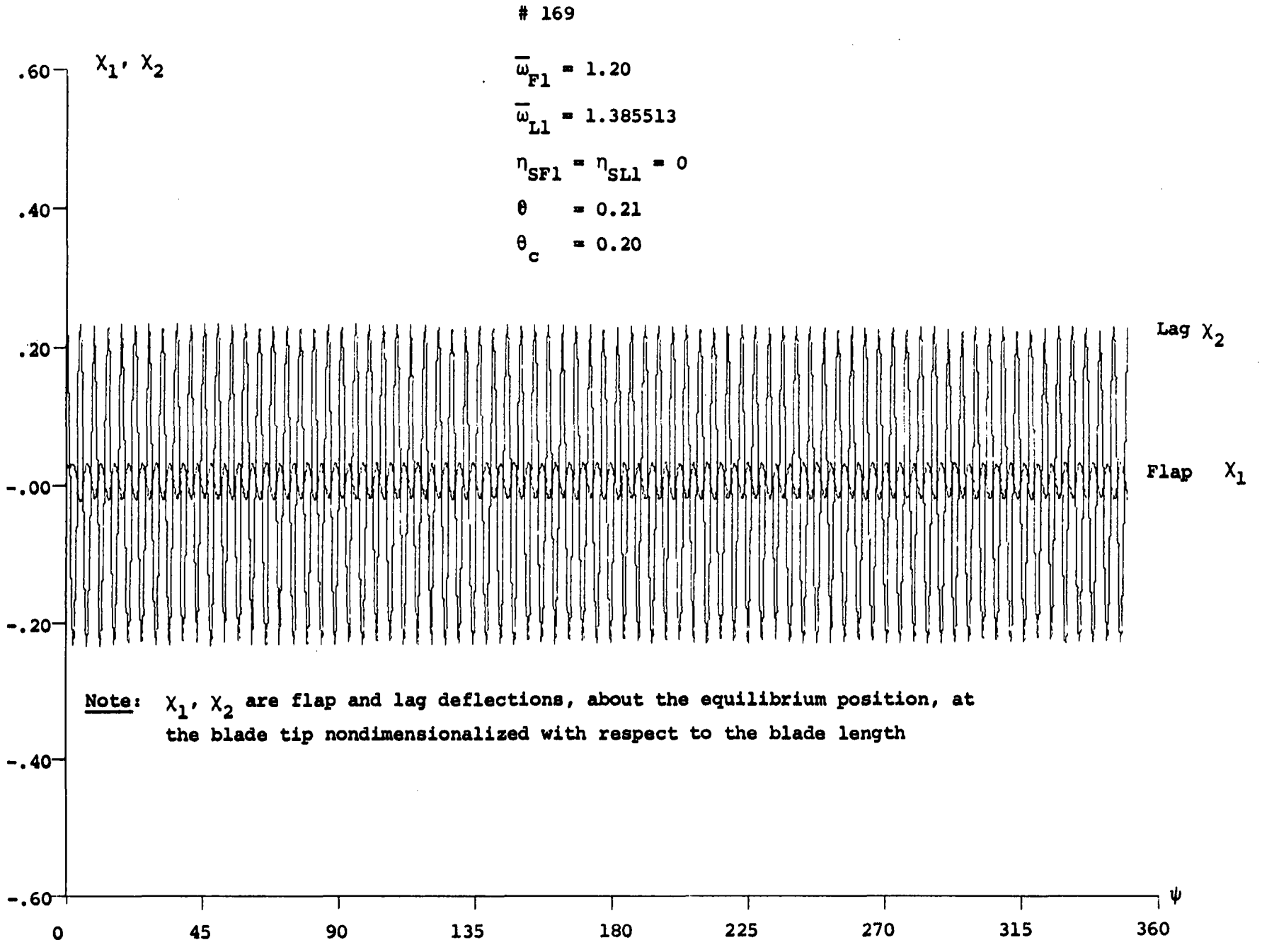

FIG. 5 STABLE LIMIT CYCLE OBTAINED BY NUMERICAL INTEGRATION FOR POINT (A) FIG. 4

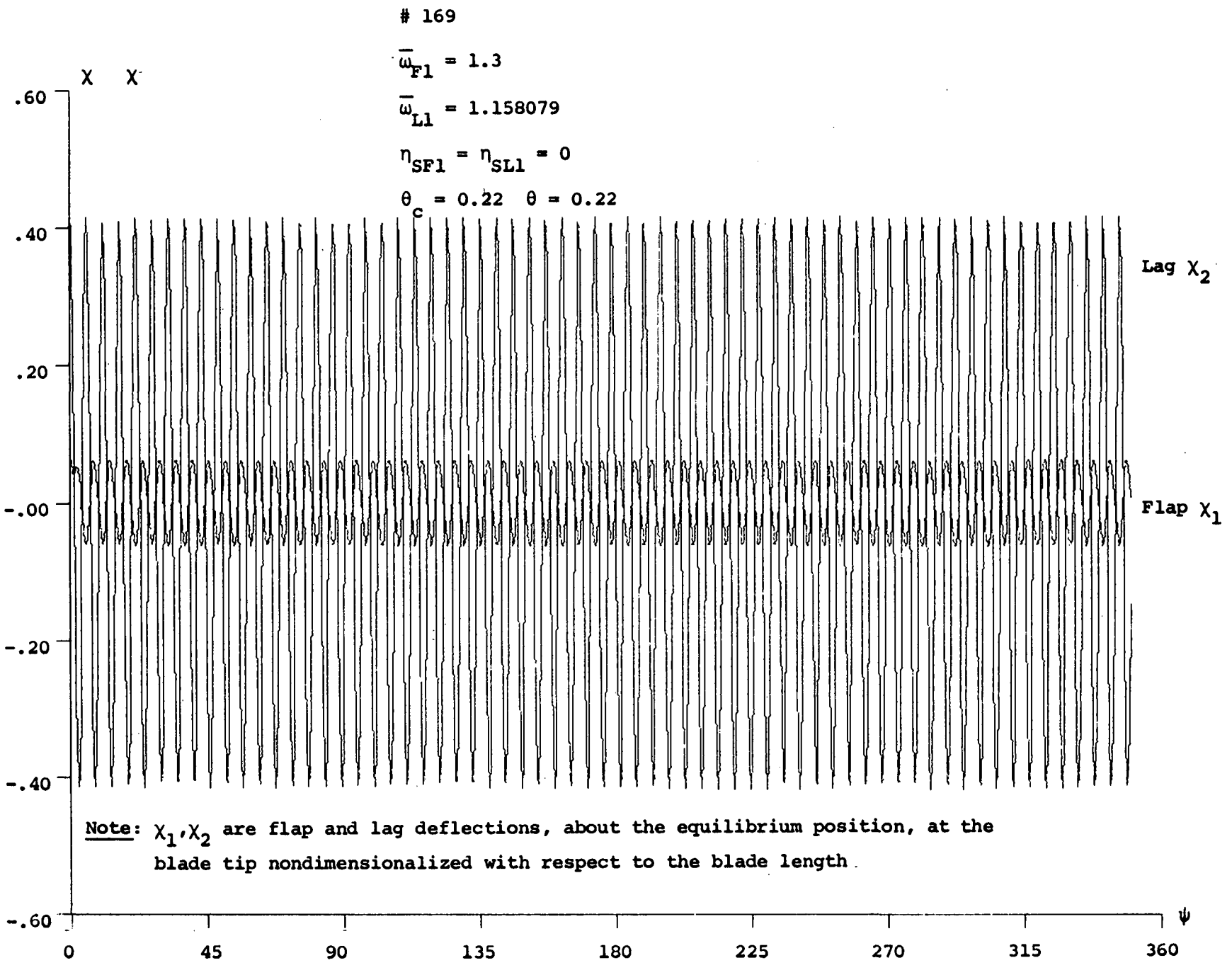

FIG. 6 STABLE LIMIT CYCLE OBTAINED BY NUMERICAL INTEGRATION FOR POINT (B) FIG. 4

Note: χ_1, χ_2 are flap and lag deflections, about the equilibrium position, at blade tip nondimensionalized with respect to the blade length

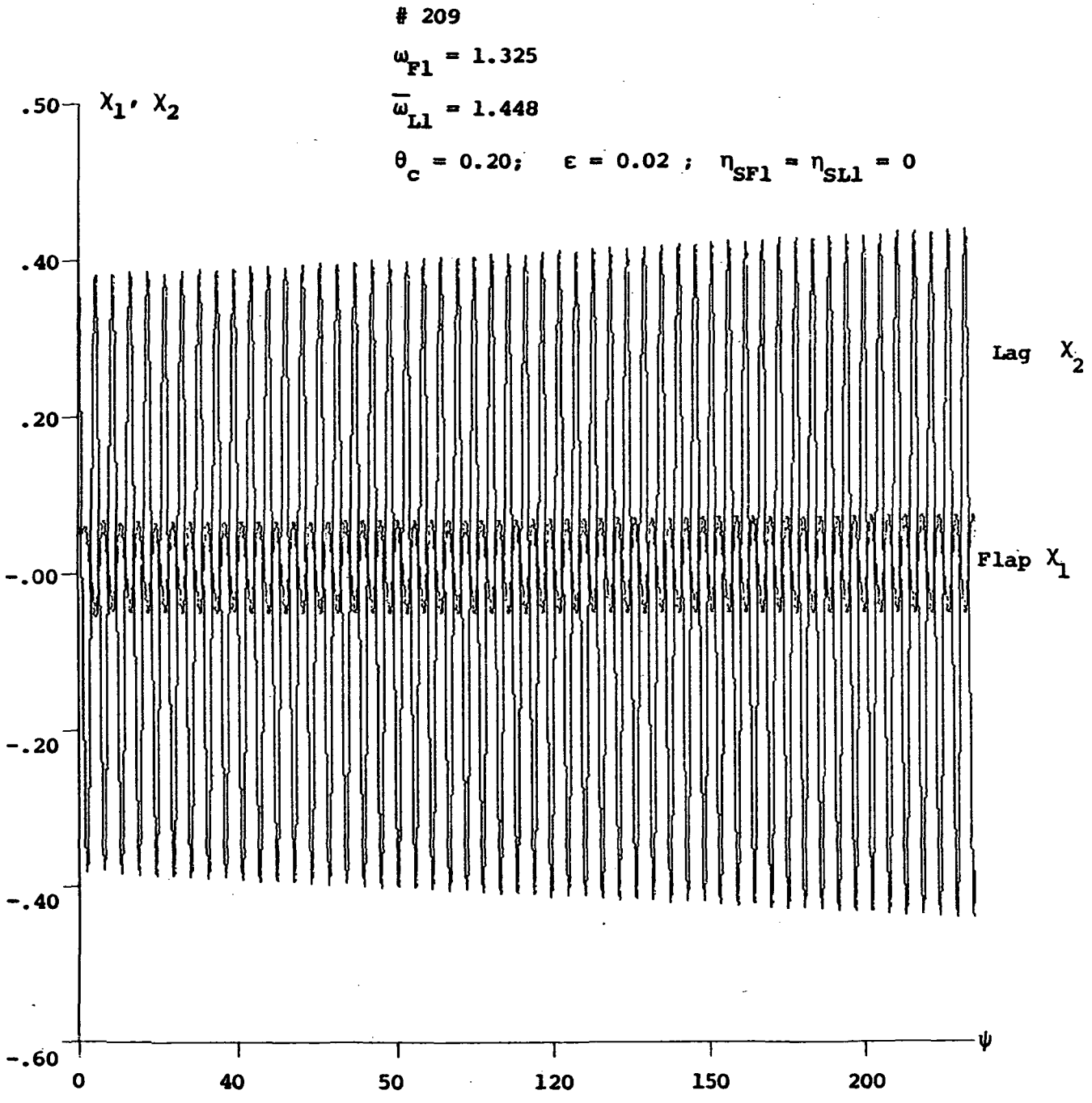

FIG. 7 UNSTABLE LIMIT CYCLE OBTAINED BY NUMERICAL INTEGRATION FOR POINT (C) FIG. 4

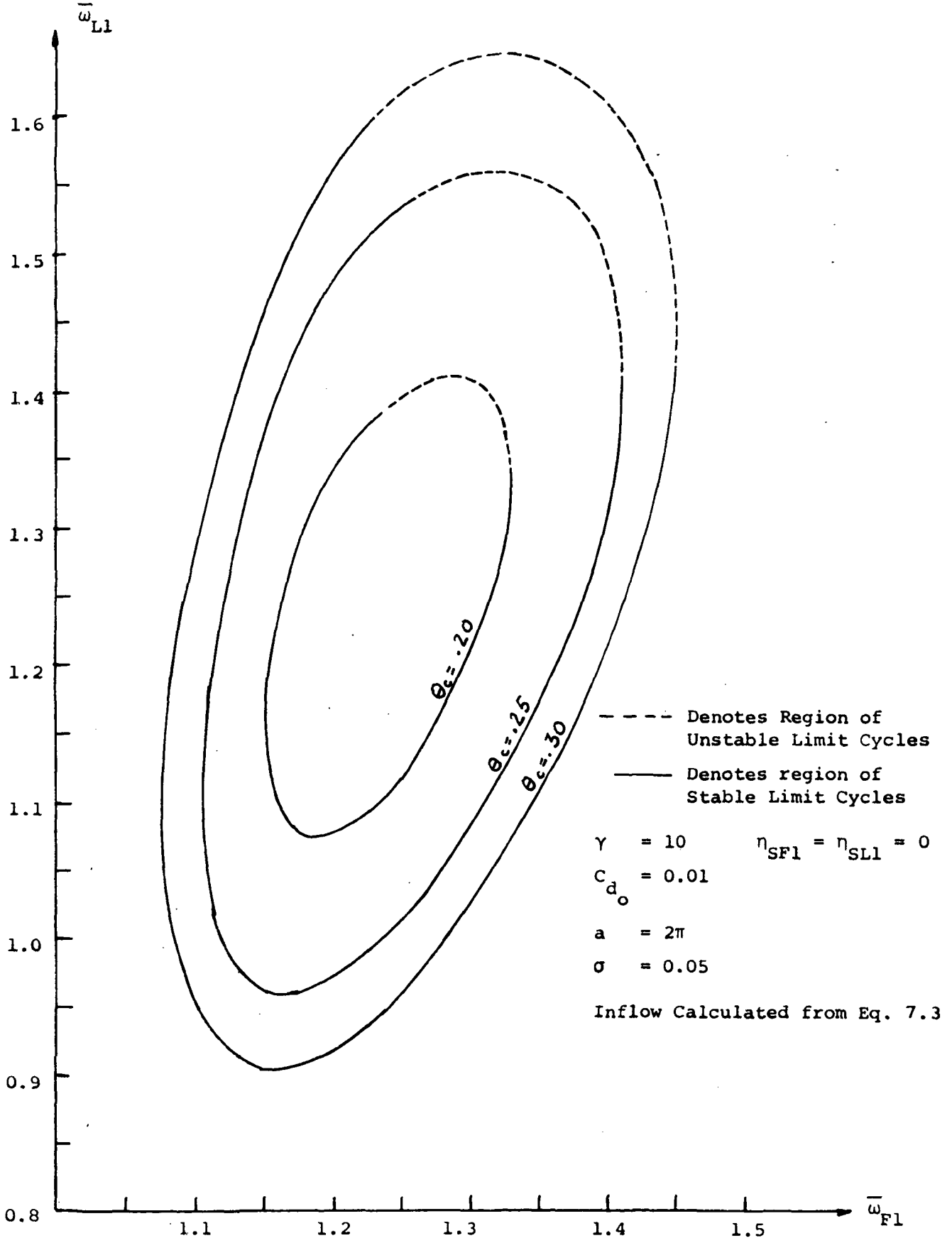

FIG. 8 STABILITY BOUNDARIES FOR VARIOUS VALUE OF θ_c WITH INFLOW RELATION CALCULATED FROM EQ. 7.3

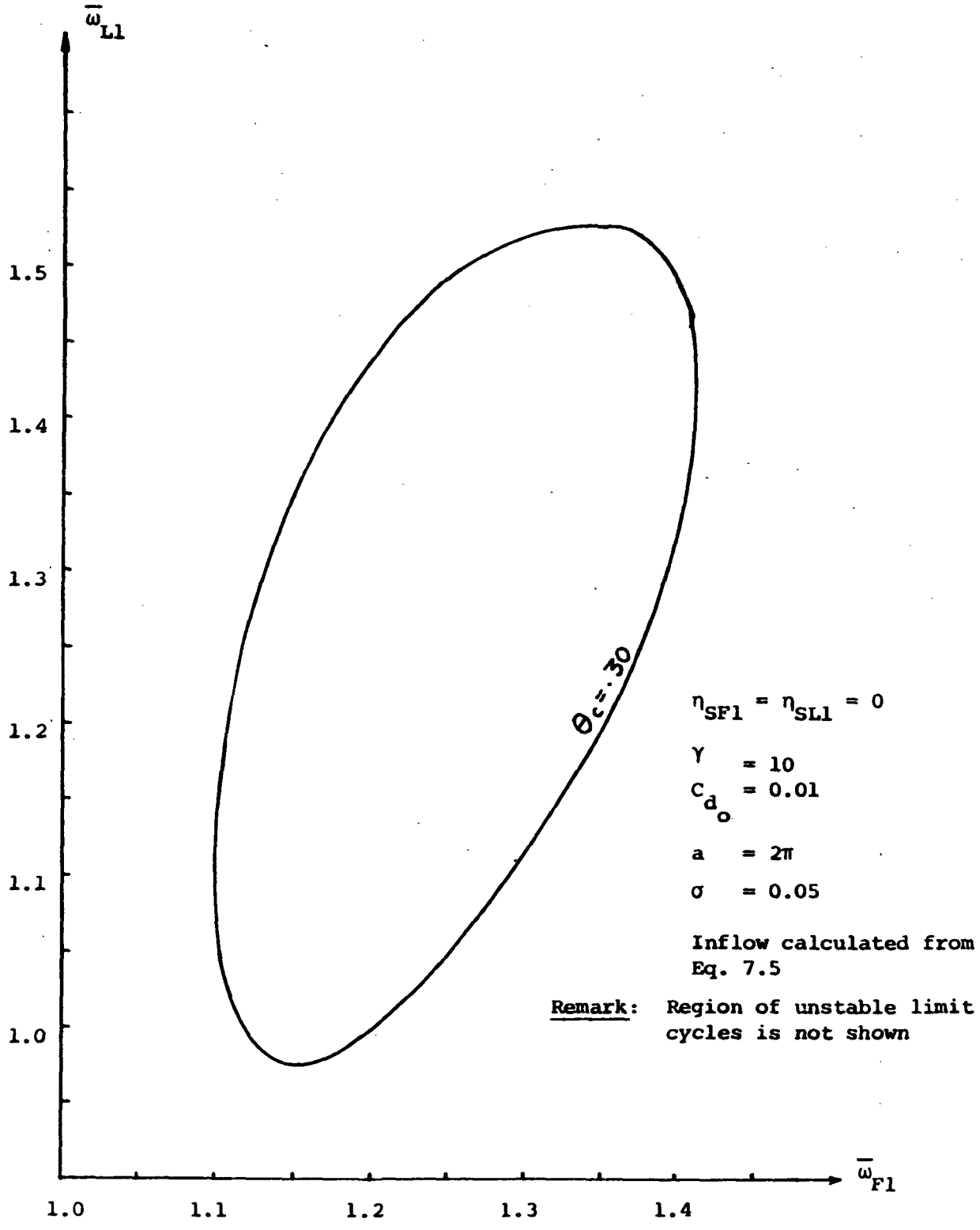

FIG. 9 TYPICAL STABILITY BOUNDARY WITH INFLOW RELATION CALCULATED FROM EQ. 7.5

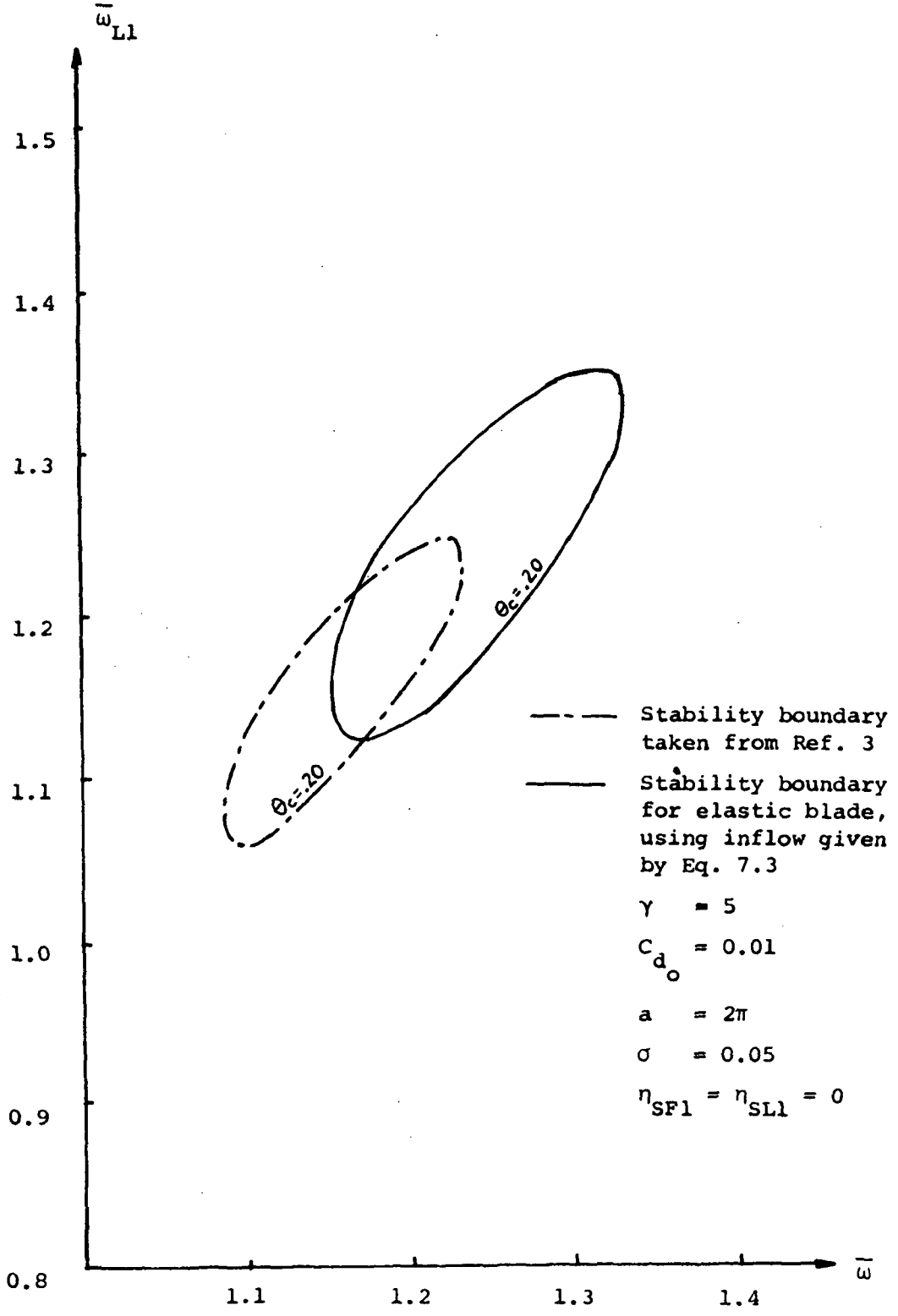

FIG. 10 COMPARISON OF A TYPICAL STABILITY BOUNDARY FOR CENTRALLY HINGED SPRING RESTRAINED BLADE MODEL WITH THAT FOR HINGELESS ELASTIC MODEL

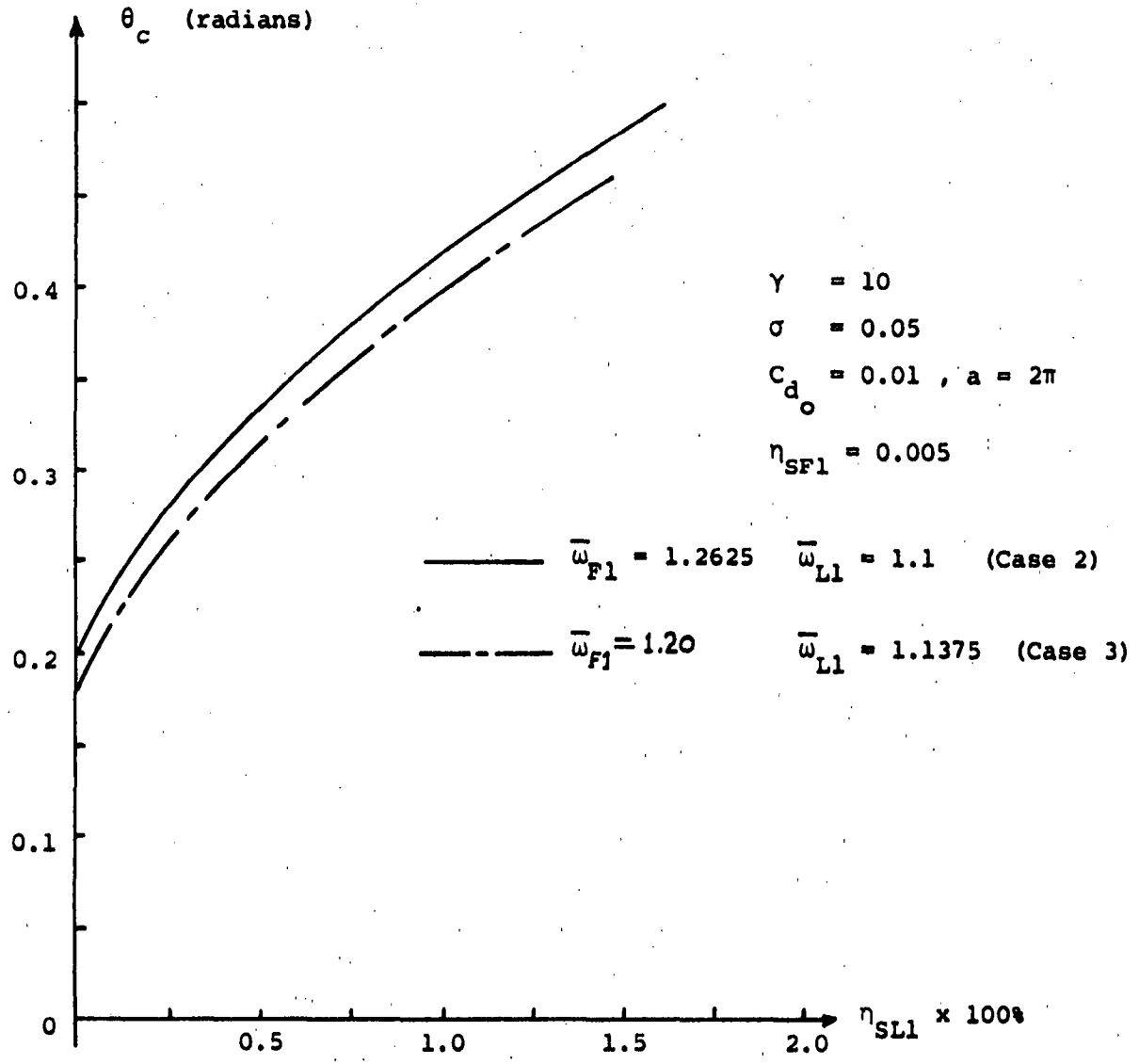

FIG. 11 EFFECT OF VISCOUS STRUCTURAL DAMPING ON ANGLE OF COLLECTIVE PITCH AT CRITICAL CONDITION

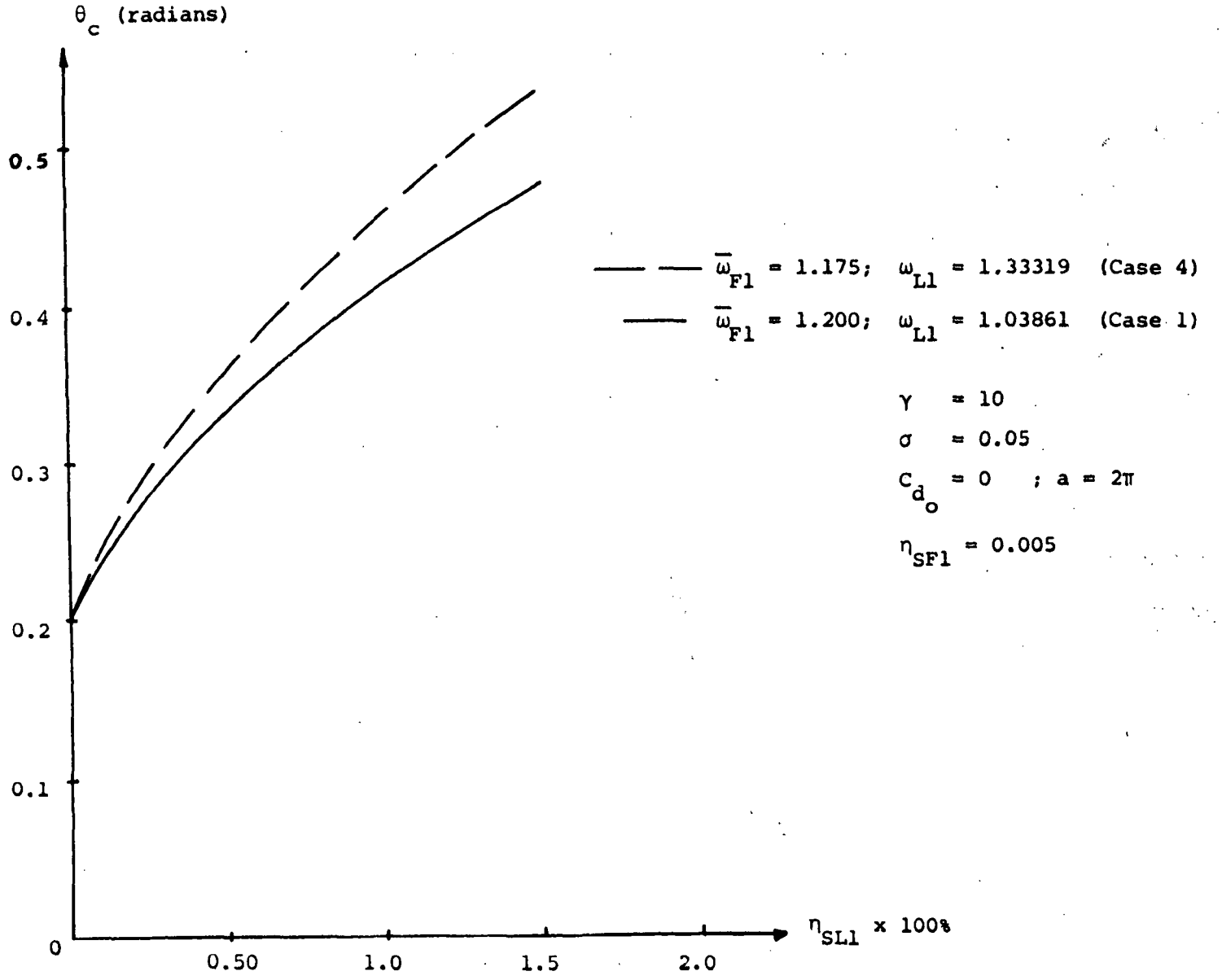

FIG. 12 EFFECT OF VISCOUS STRUCTURAL DAMPING ON ANGLE OF COLLECTIVE PITCH AT CRITICAL CONDITION

Note: χ_1, χ_2 are flap and lag deflections, about the equilibrium position, at the blade tip nondimensionalized with respect to the blade length

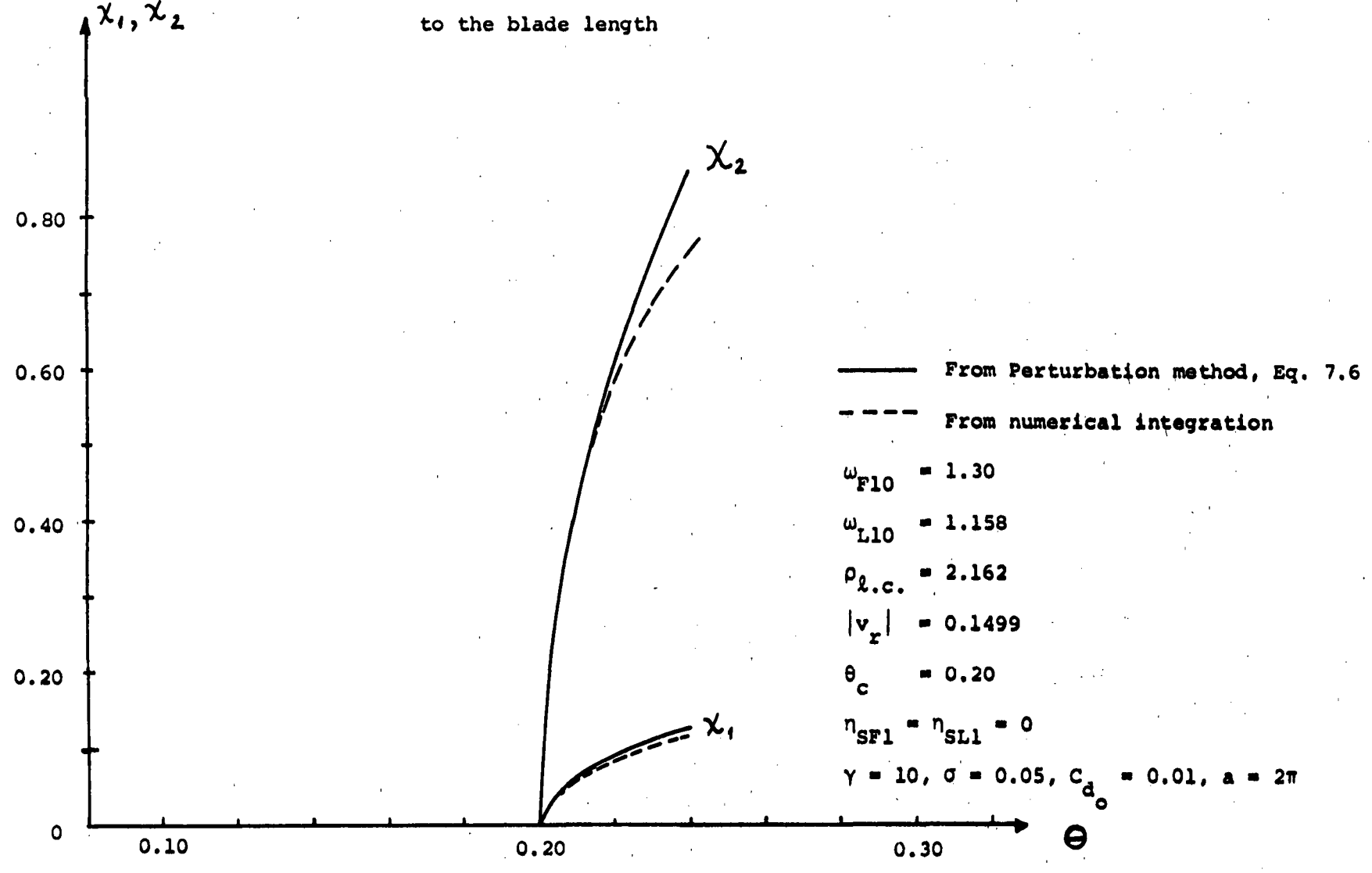

FIG. 13 COMPARISON OF LIMIT CYCLE AMPLITUDE RESPONSE CURVES

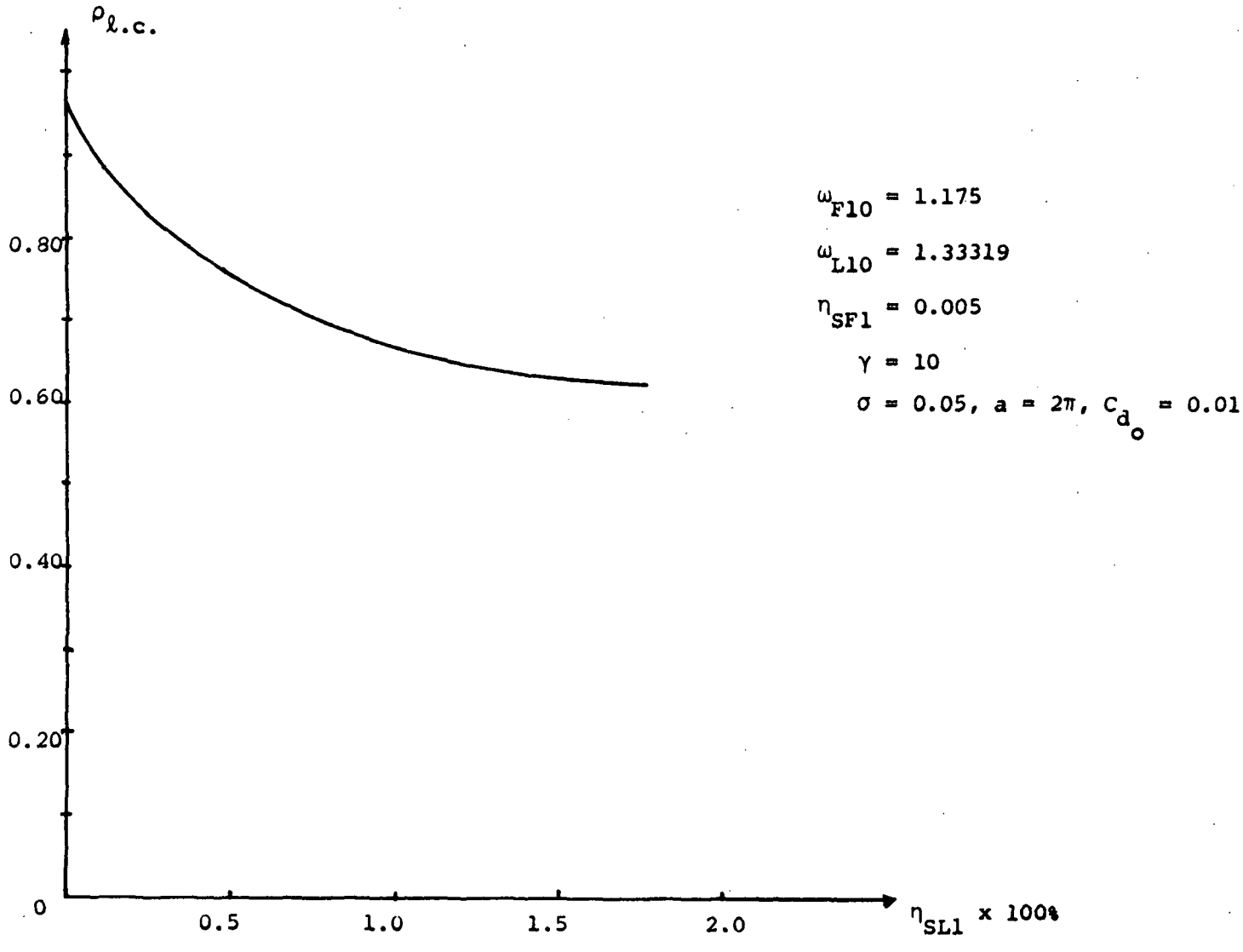

FIG. 14 EFFECT OF VISCOUS STRUCTURAL DAMPING ON LIMIT-CYCLE AMPLITUDE

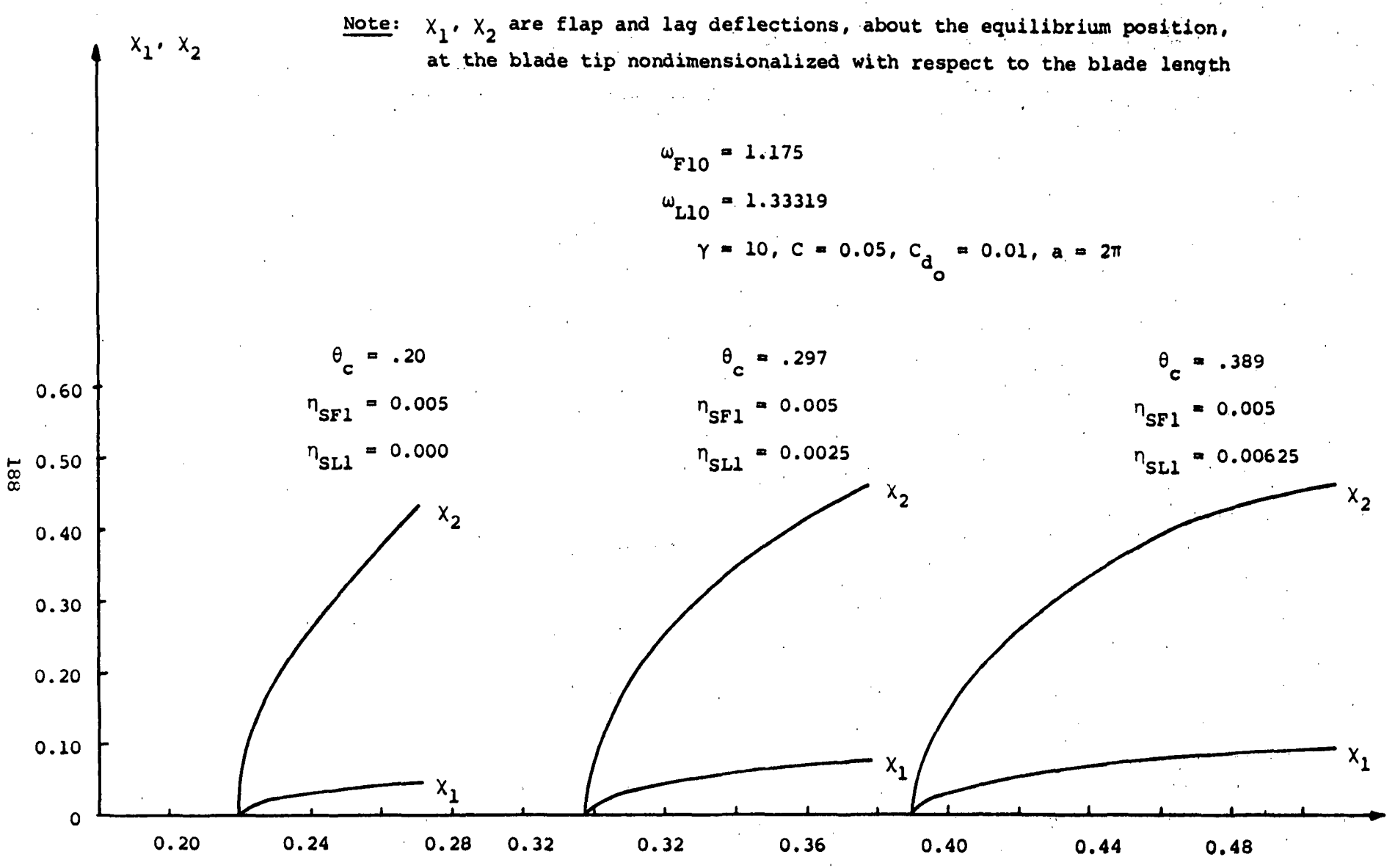

FIG. 15 EFFECT OF VISCOUS STRUCTURAL DAMPING ON THE LOCATION AND STEEPNESS OF THE LIMIT CYCLE RESPONSE CURVES

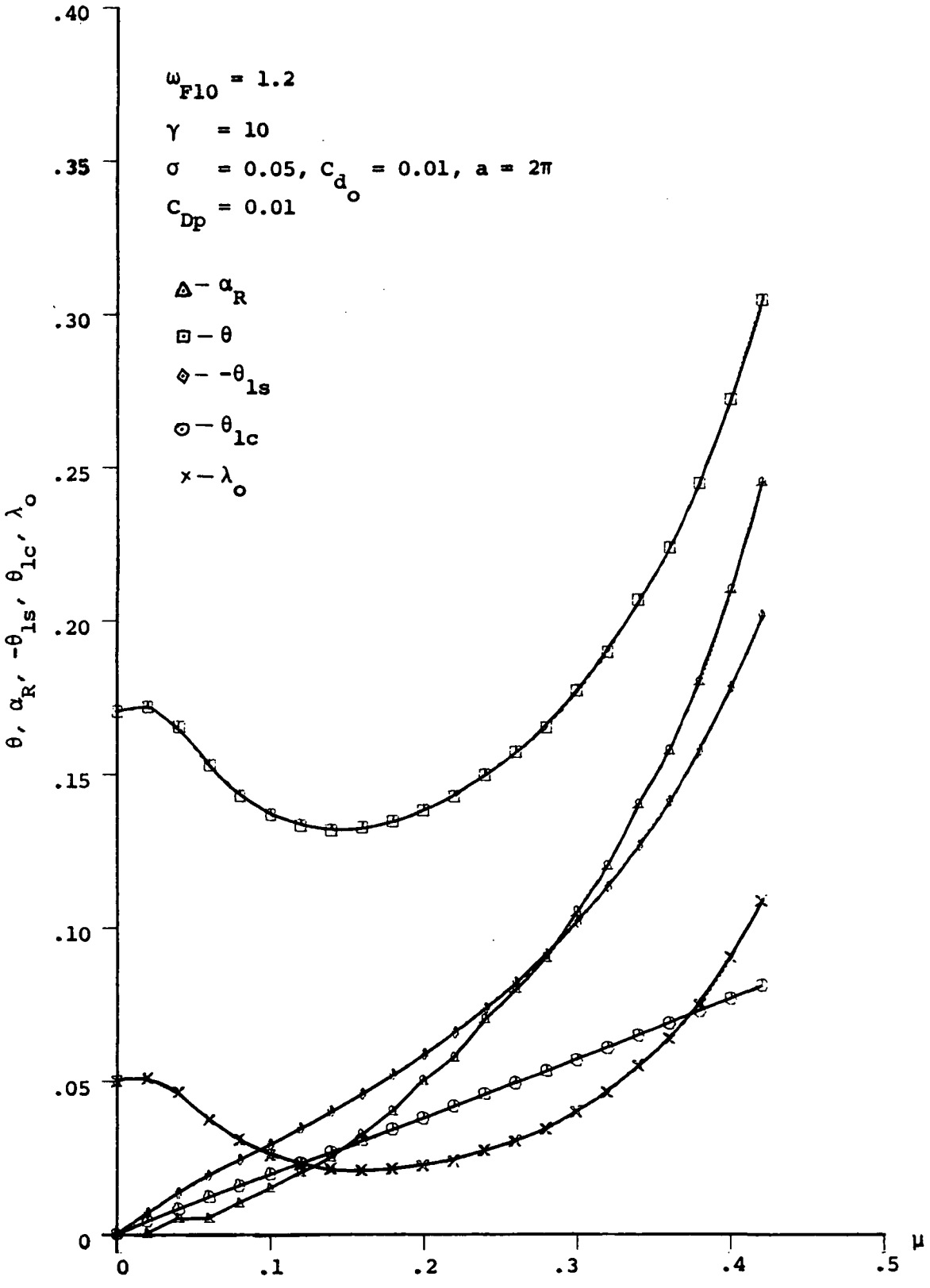

FIG. 16 TYPICAL TRIM CURVES FOR C_T = 0.005

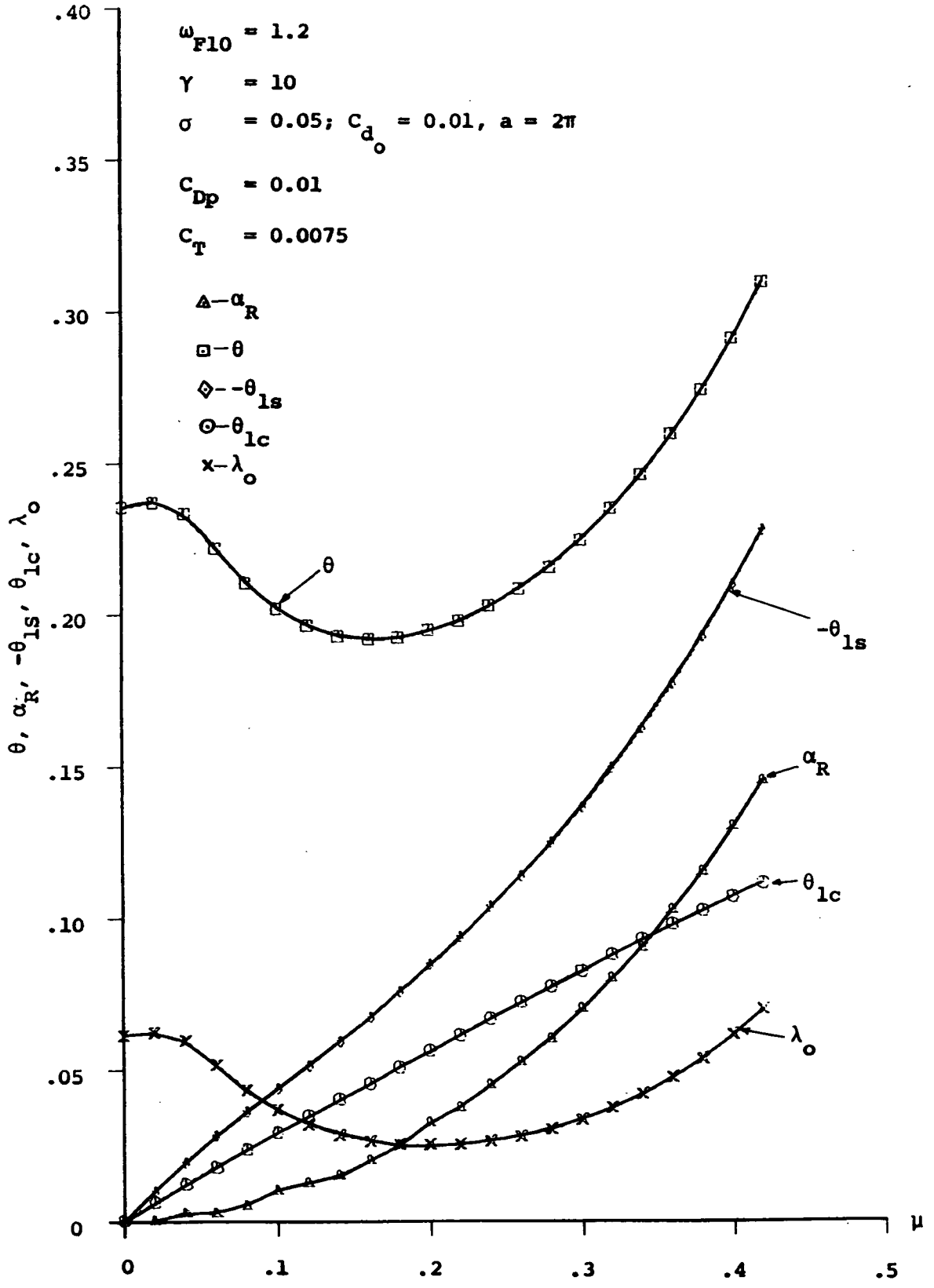

FIG. 17 TYPICAL TRIM CURVES FOR C_T = 0.0075

Note: χ_1, χ_2 are flap and lag deflections, about the equilibrium position, at the blade tip nondimensionalized with respect to the blade length

$\omega_{F10} = 1.20$

$\omega_{L10} = 1.1375$

$\omega_c = 1.139939$; $\theta_c = 0.315614$

$C_T = 0.006$

$\eta_{SF1} = \eta_{SL1} = 0.005$

Note: $\chi_1 = (\chi_1)_{av}$ Eq. 7.

$C_{Dp} = 0.012$, $\gamma = 10$, $\sigma = 0.05$, $C_{d_o} = 0.01$, $a = 2\pi$

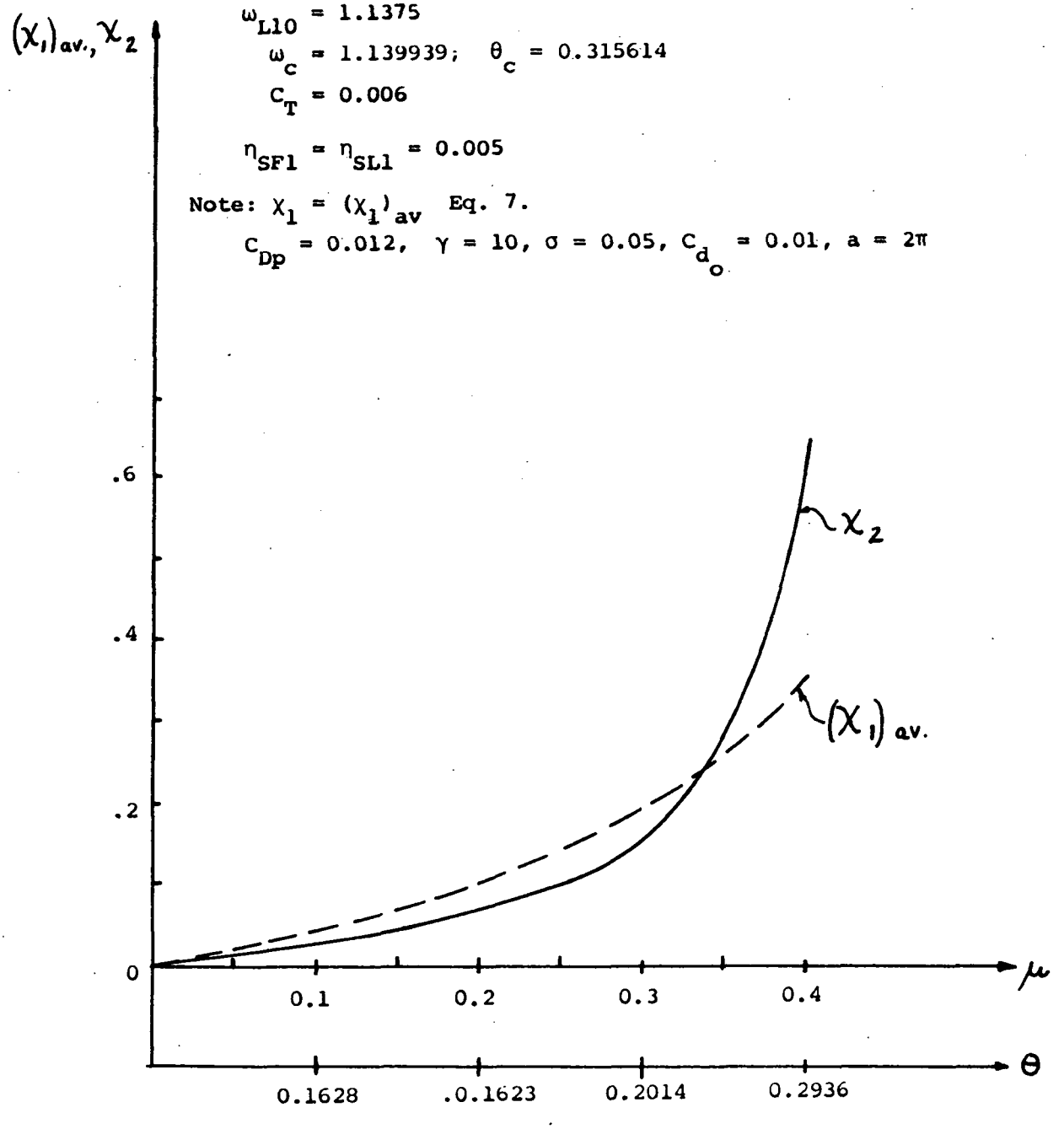

FIG. 18 AMPLITUDE RESPONSE IN FORWARD FLIGHT

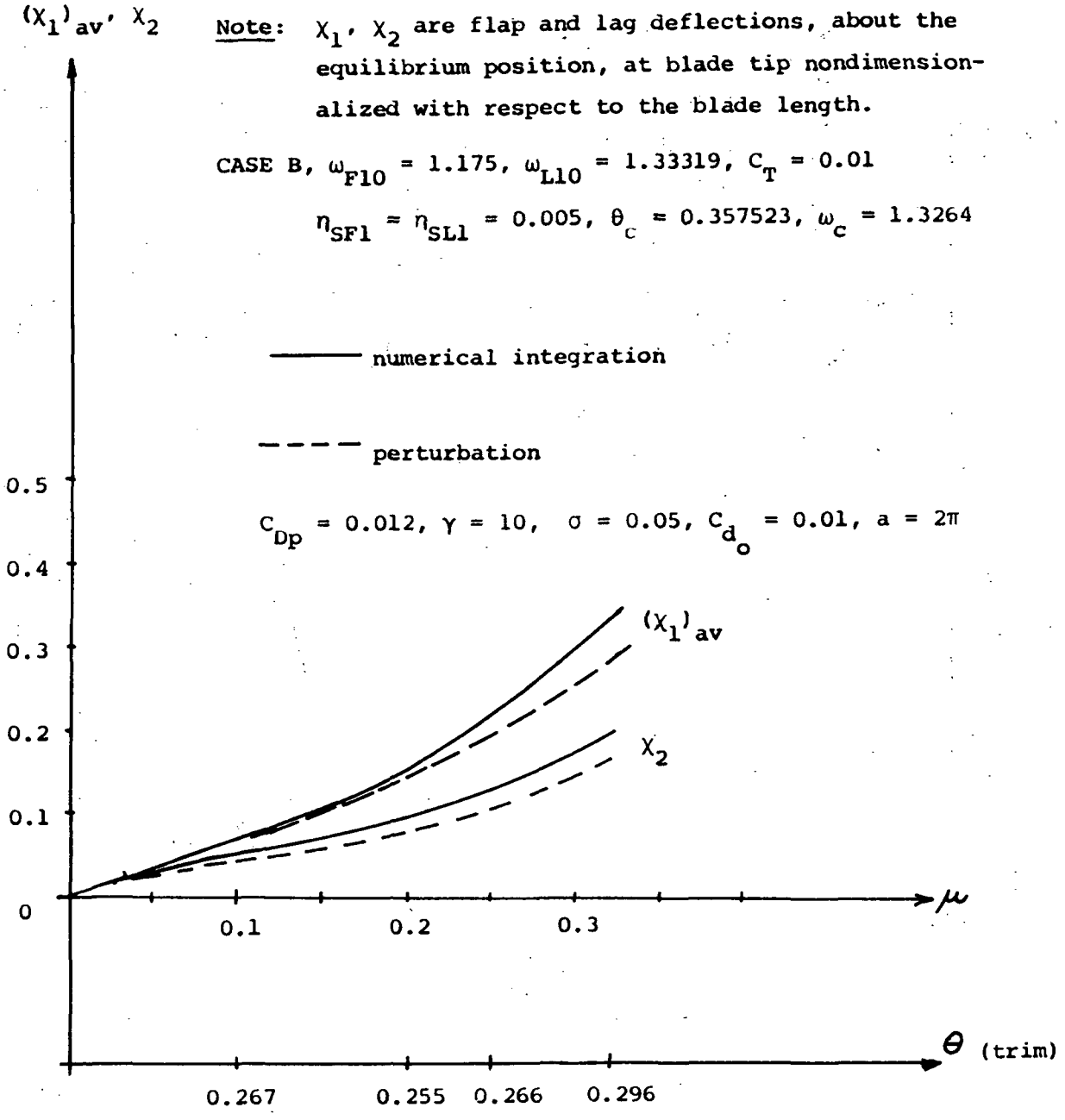

FIG. 19 AMPLITUDE RESPONSE CURVES IN FORWARD FLIGHT, COMPARISON OF RESULTS FROM PERTURBATION AND NUMERICAL INTEGRATION AT SUBCRITICAL CONDITIONS.

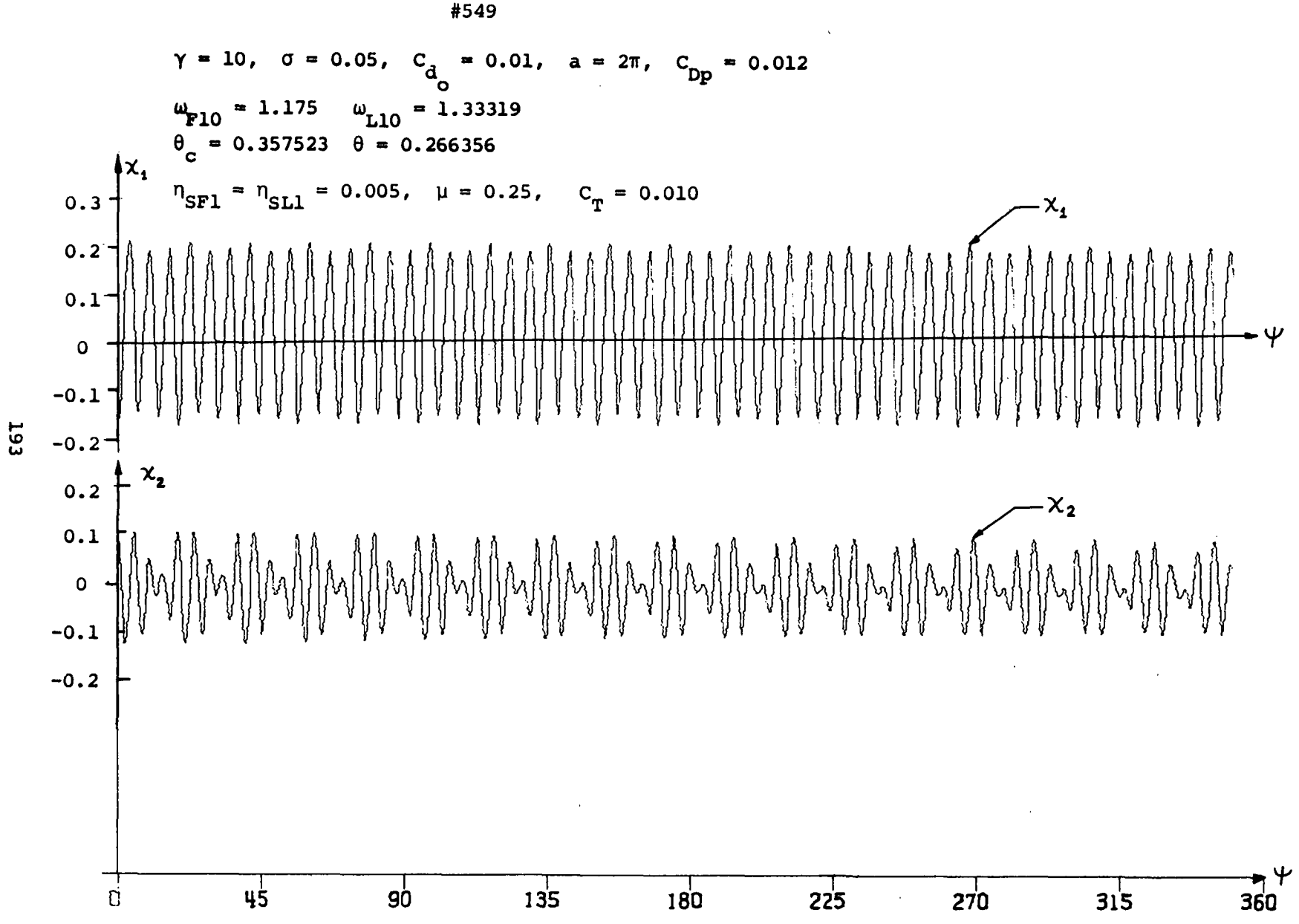

FIG. 20 TIME HISTORY OF BLADE RESPONSE CALCULATED FROM EQS. 6.8 AND 6.9

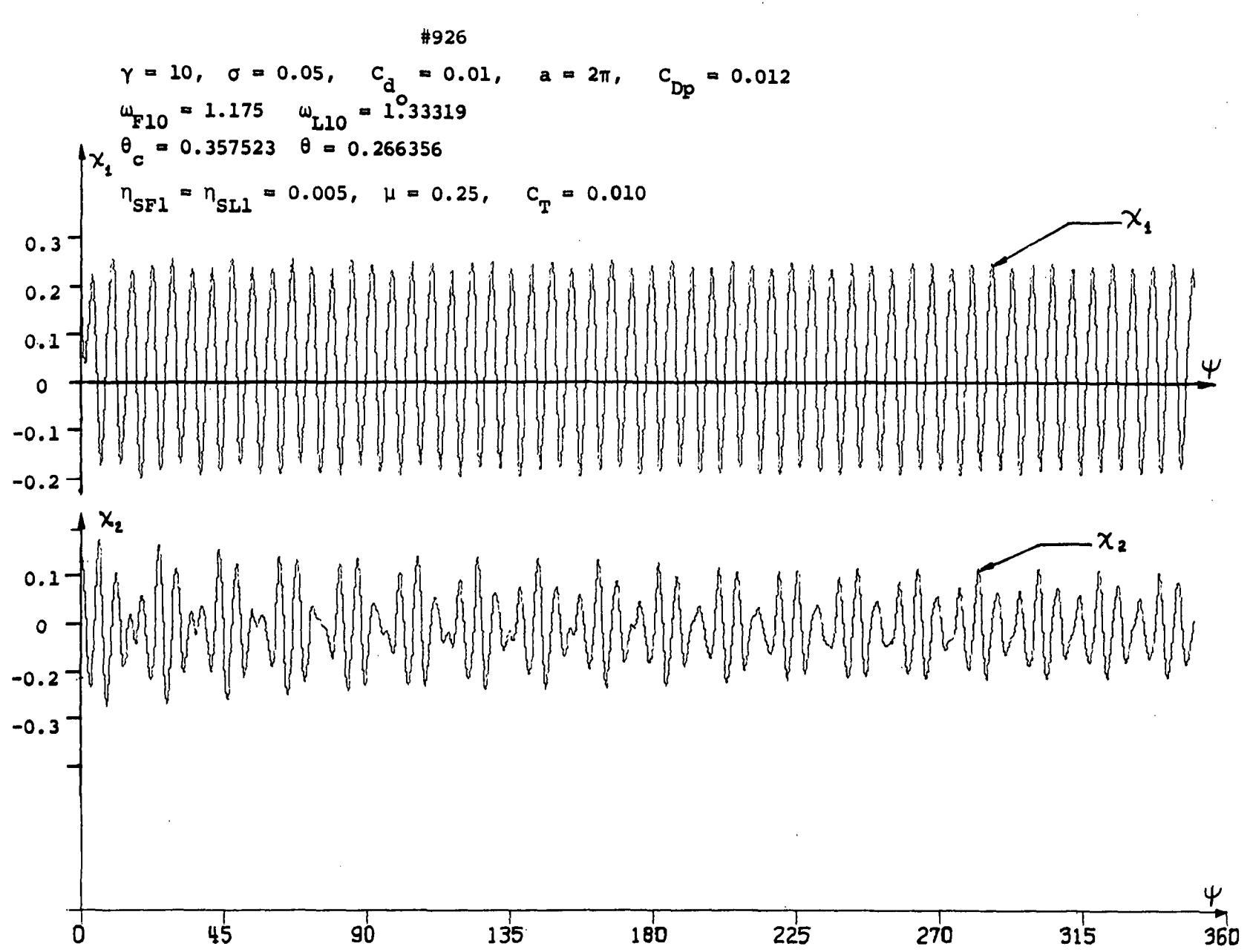

FIG. 21 TIME HISTORY OF BLADE RESPONSE OBTAINED BY NUMERICAL INTEGRATION

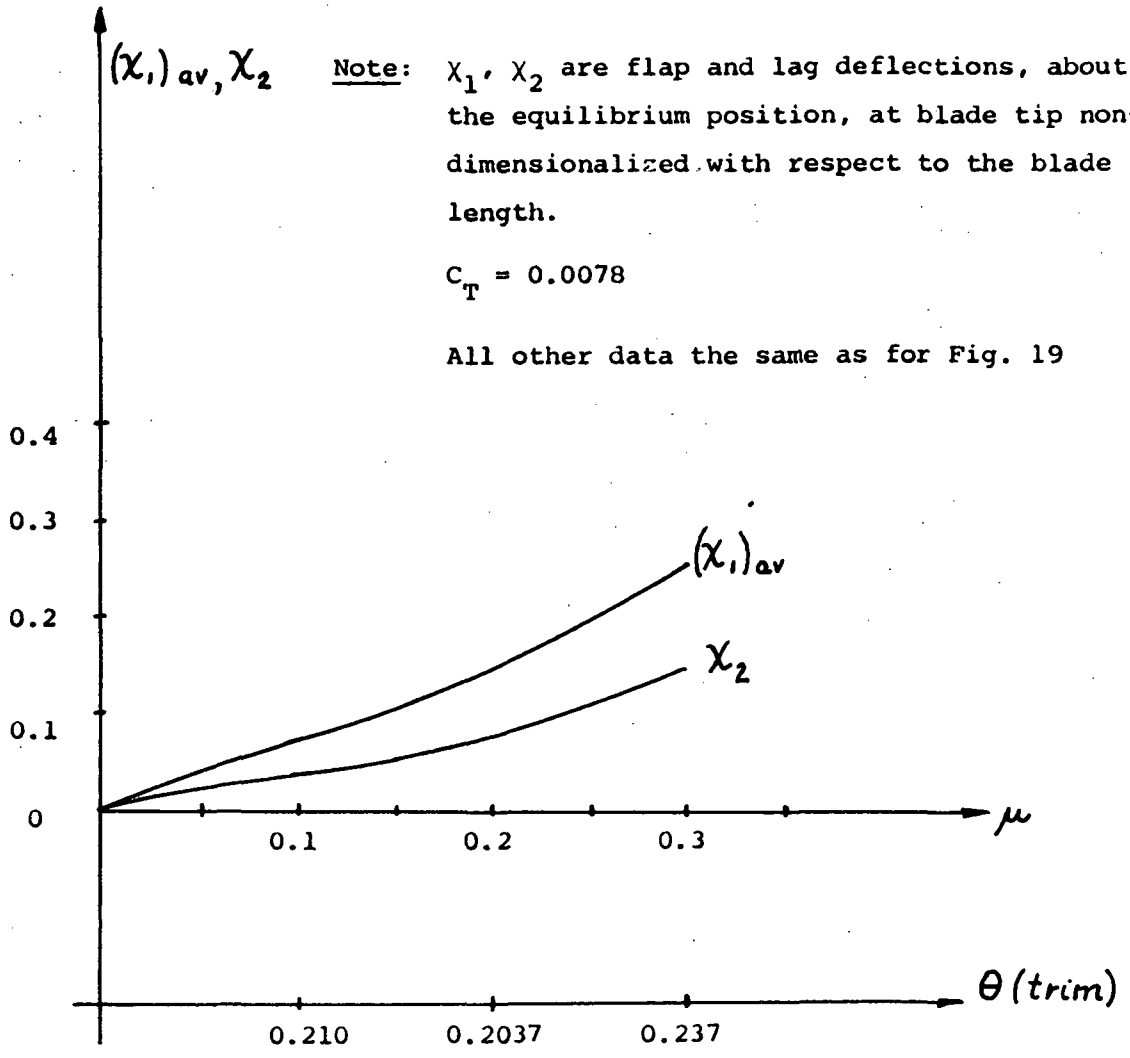

FIG. 22 EFFECT OF C_T ON AMPLITUDE RESPONSE IN FORWARD FLIGHT

Note: χ_1, χ_2 are flap and lag deflections, about the equilibrium position, at blade tip nondimensionalized with respect to the blade length.

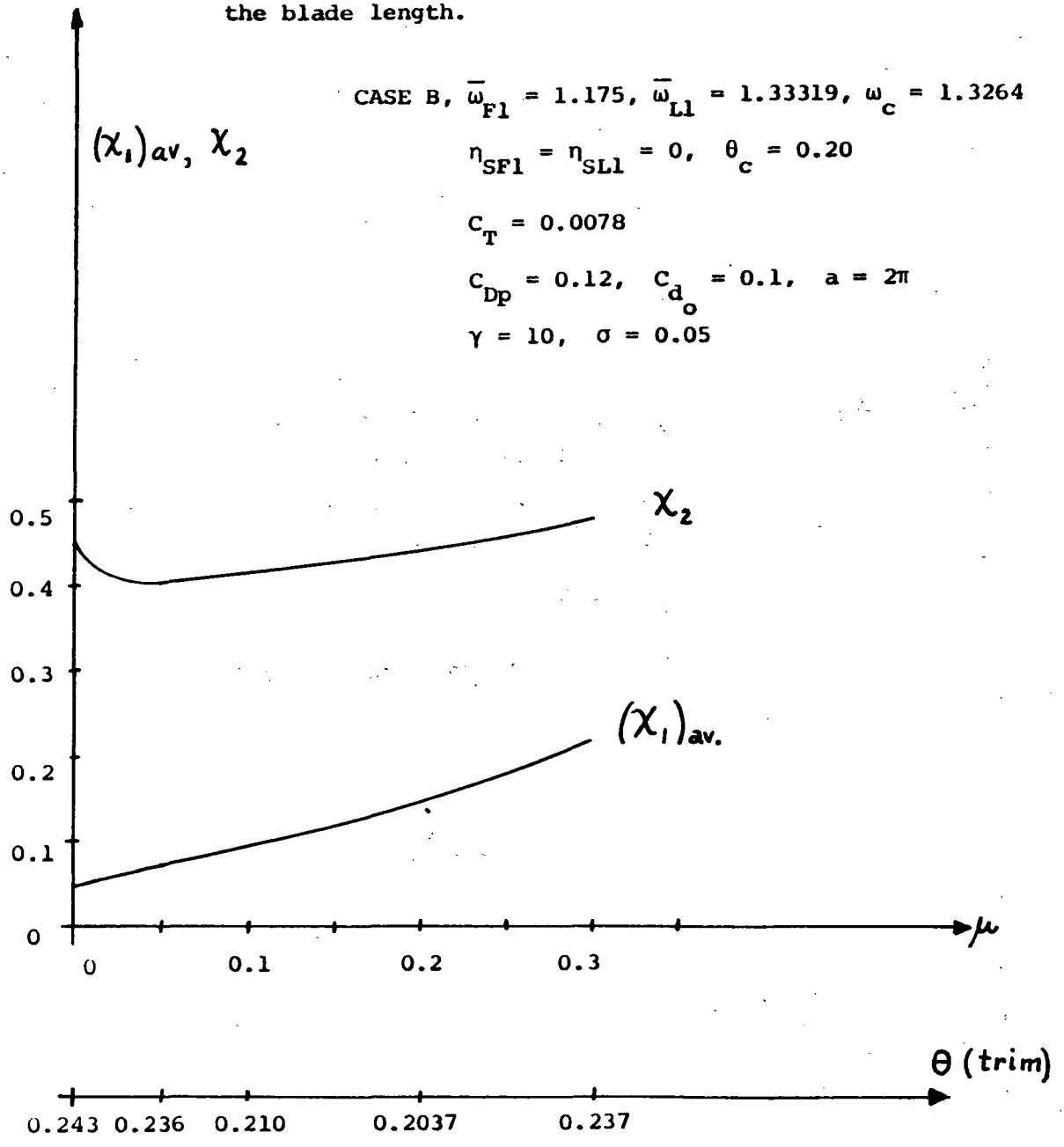

FIG. 23 AMPLITUDE RESPONSE CURVES IN FORWARD FLIGHT, POSTCRITICAL REGION (FROM PERTURBATION METHOD)

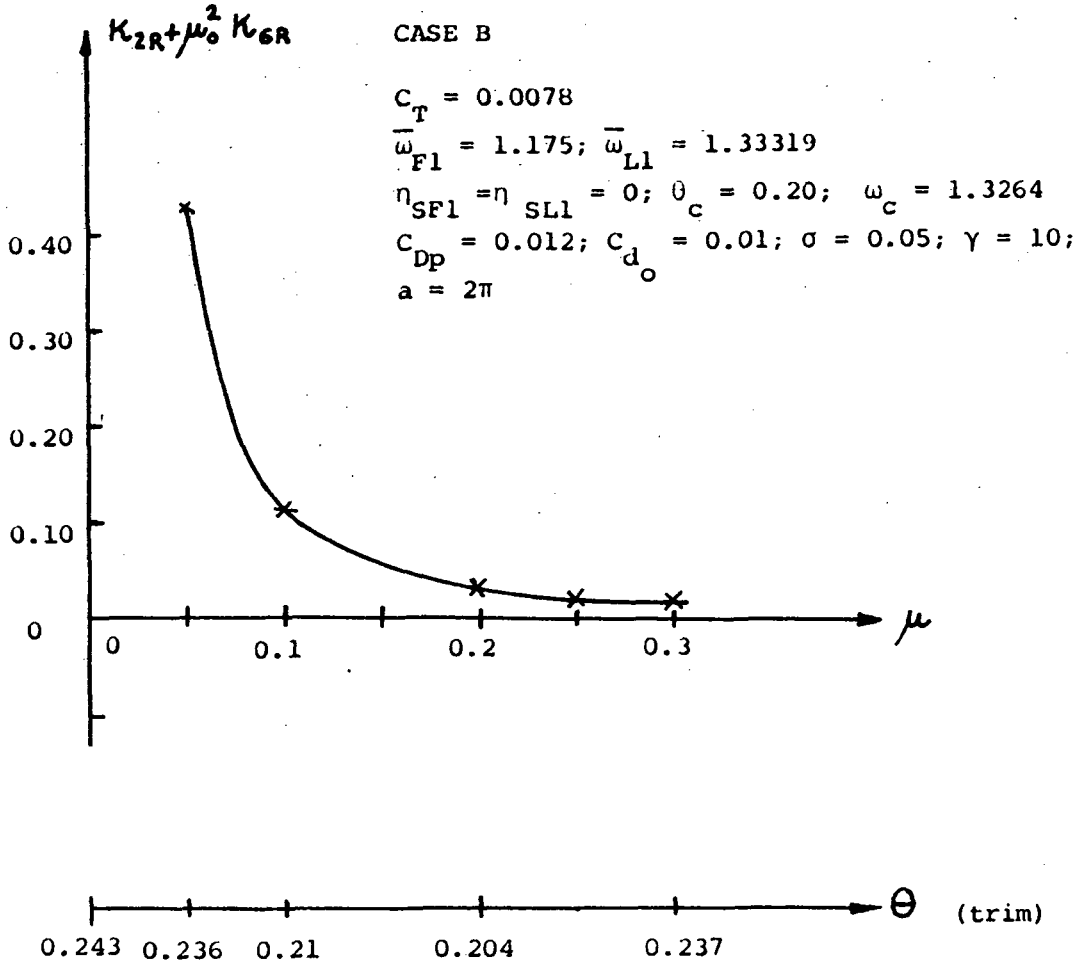

FIG. 24 EFFECT OF FORWARD FLIGHT, WITH TRIM AT FIXED C_T, ON THE QUANTITY $K_{2R} + \mu_o^2 K_{6R}$

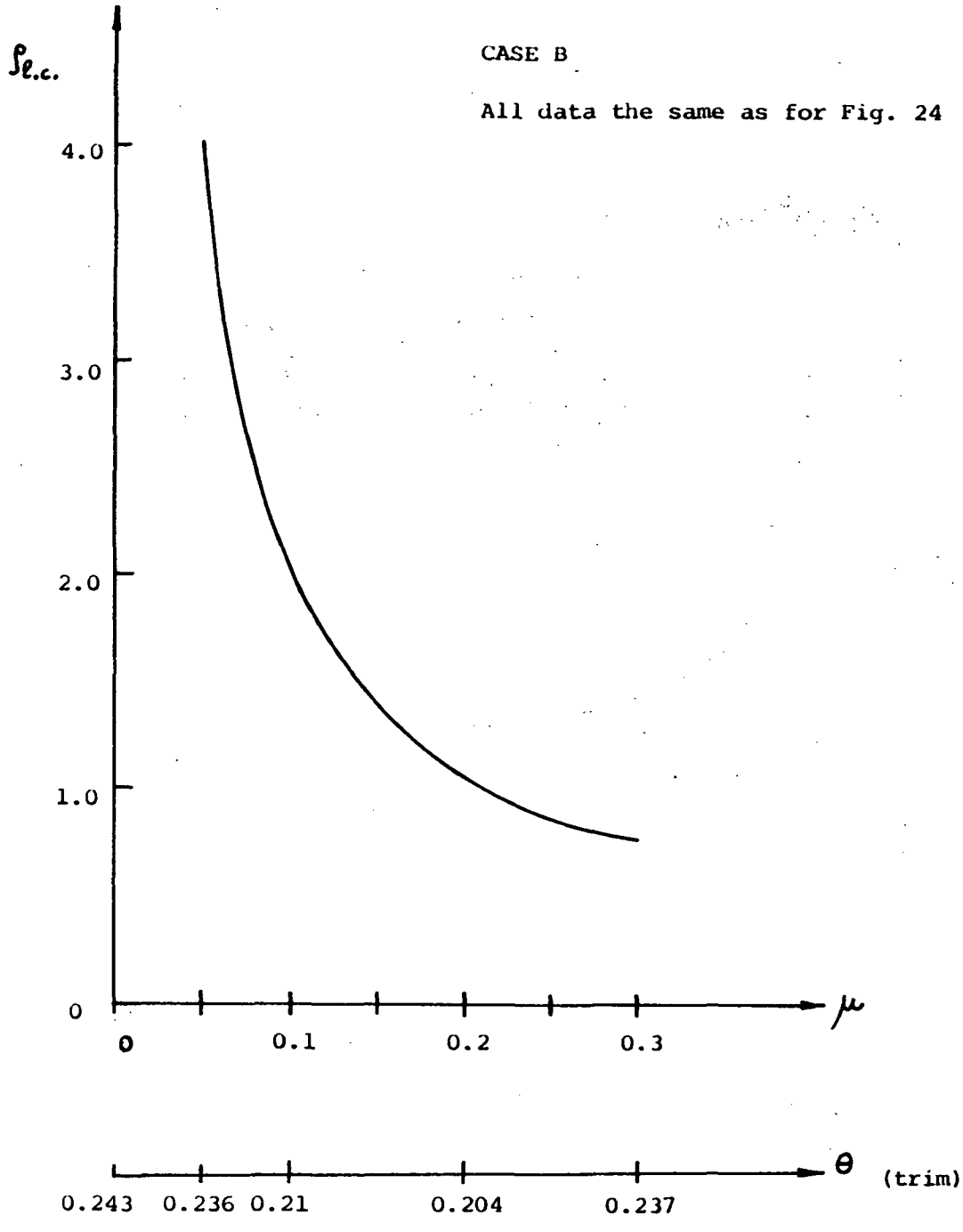

FIG. 25 EFFECT OF FORWARD FLIGHT, WITH TRIM AT FIXED C_T, ON $\rho_{l.c.}$ (CALCULATED FROM EQ. 5.71)

Note: χ_1, χ_2 are flap and lag deflections, about the equilibrium position, at blade tip nondimensionalized with respect to the blade length.

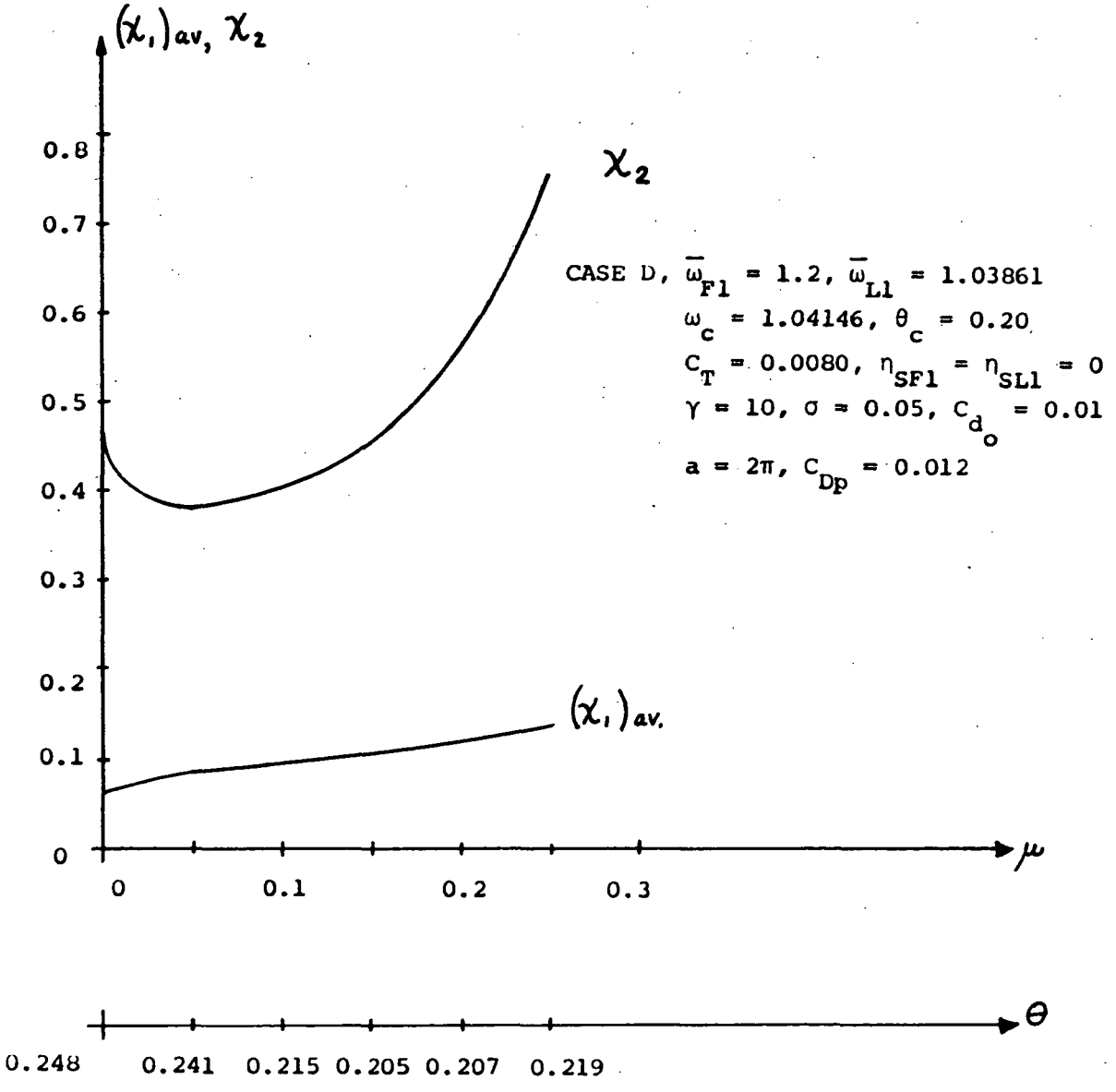

FIG. 26 AMPLITUDE RESPONSE CURVES, IN FORWARD FLIGHT, FOR CASE D, IN POSTCRITICAL REGION (FROM NUMERICAL INTEGRATION)

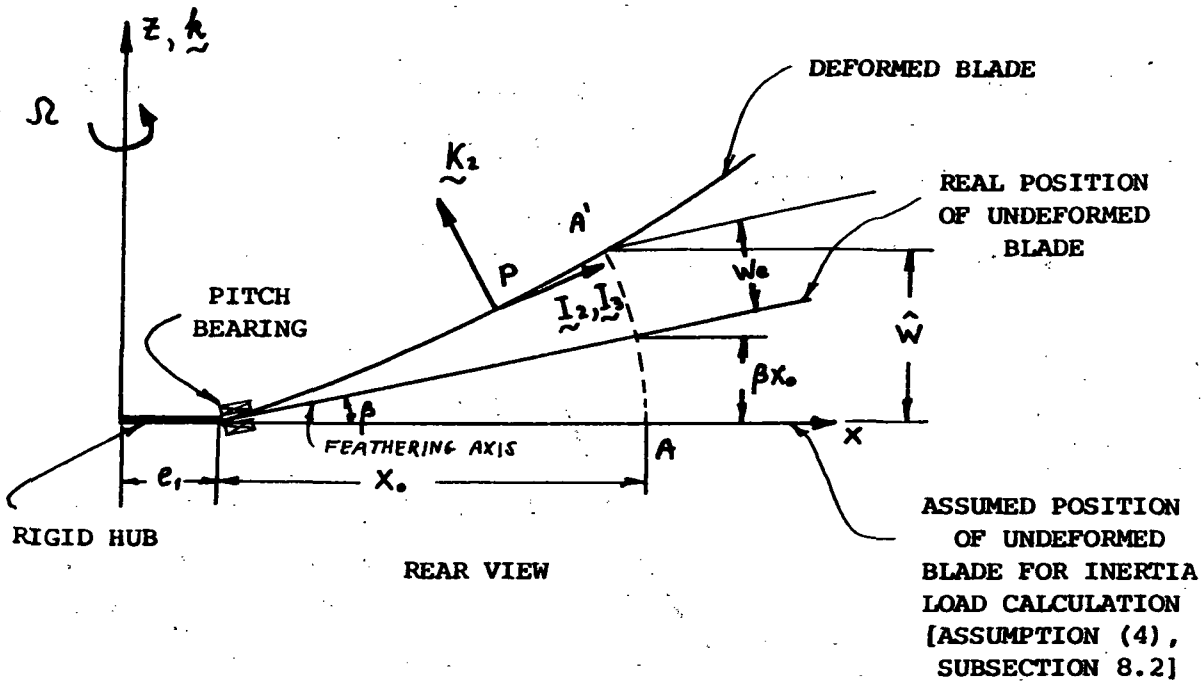

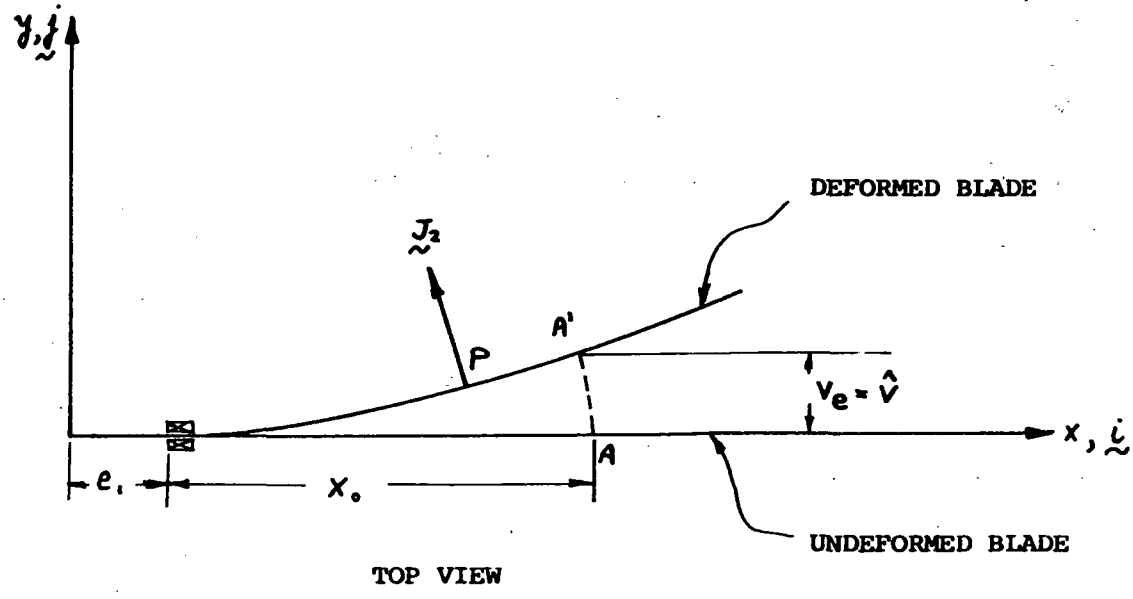

FIG.27a DISPLACEMENT FIELD WITHOUT ROOT TORSION AND WITHOUT PRECONING (β_p=0)

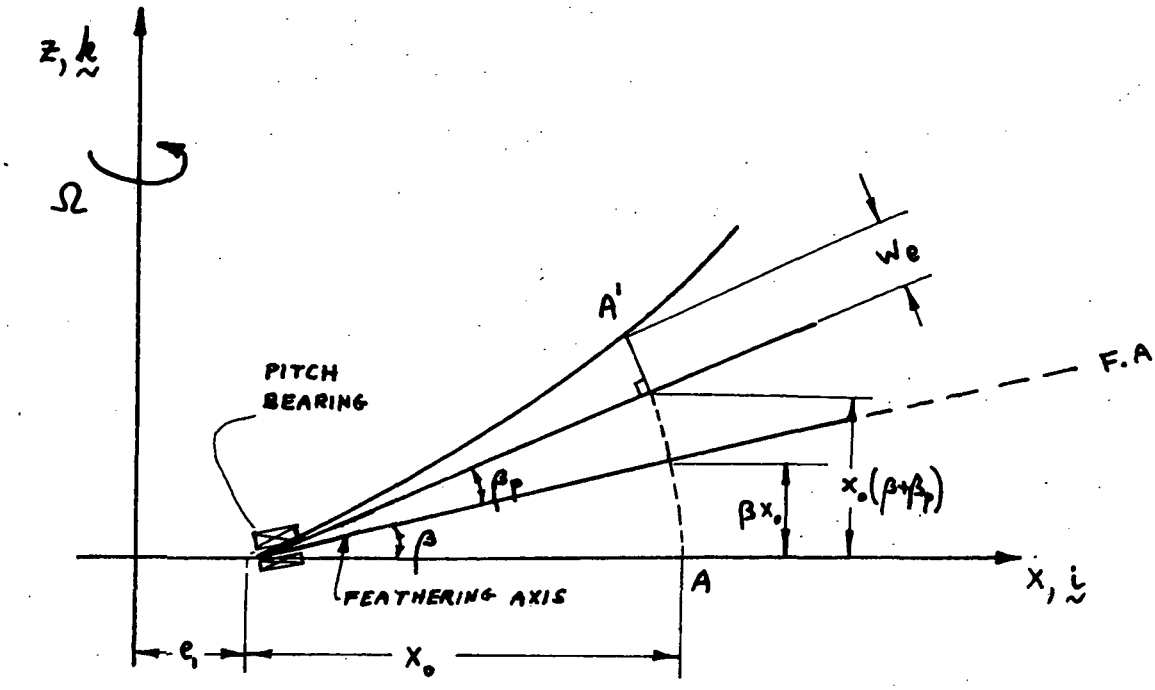

REAR VIEW

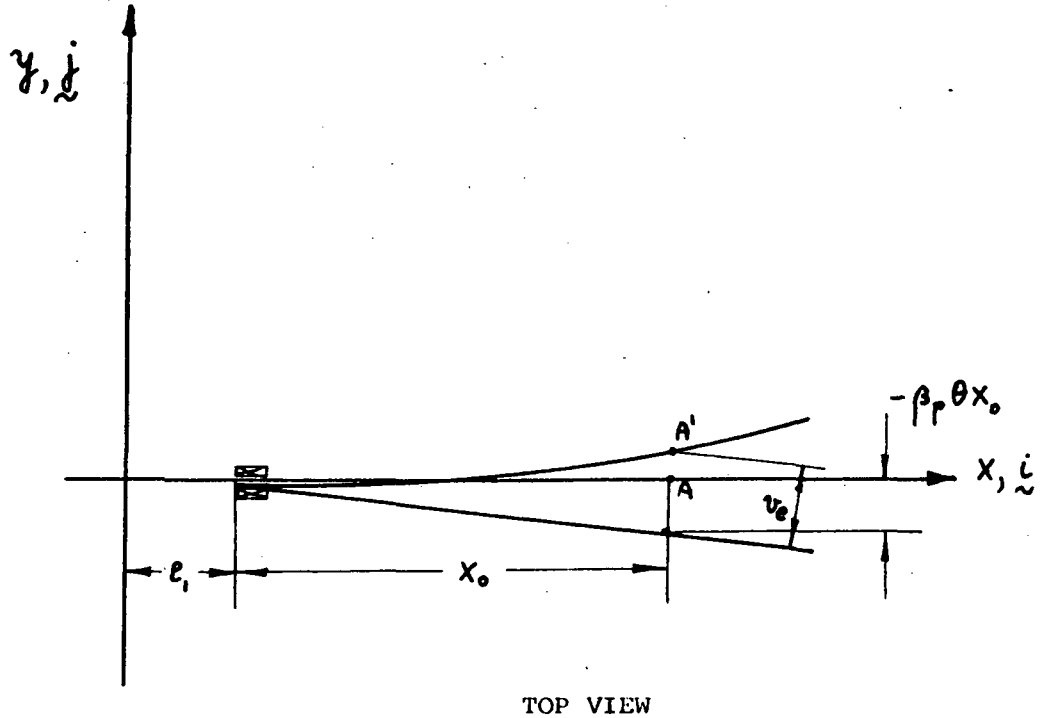

TOP VIEW

FIG. 27b. DISPLACEMENT FIELD WITH PRECONING; b_p AND WITHOUT ROOT TORSION

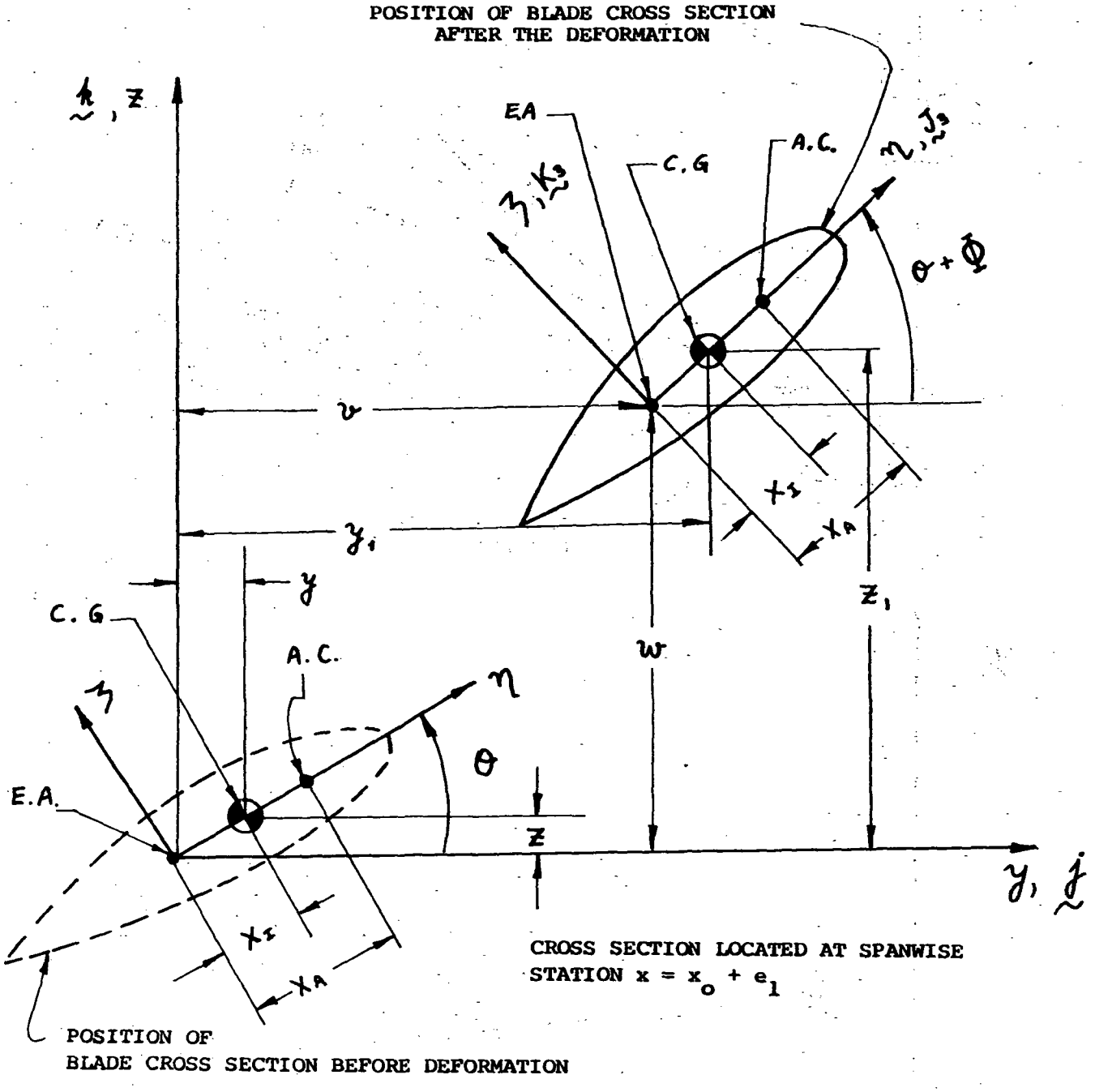

FIG. 28 BLADE MODEL AND POSITIONS OF THE CROSS SECTION BEFORE AND AFTER THE DEFORMATION

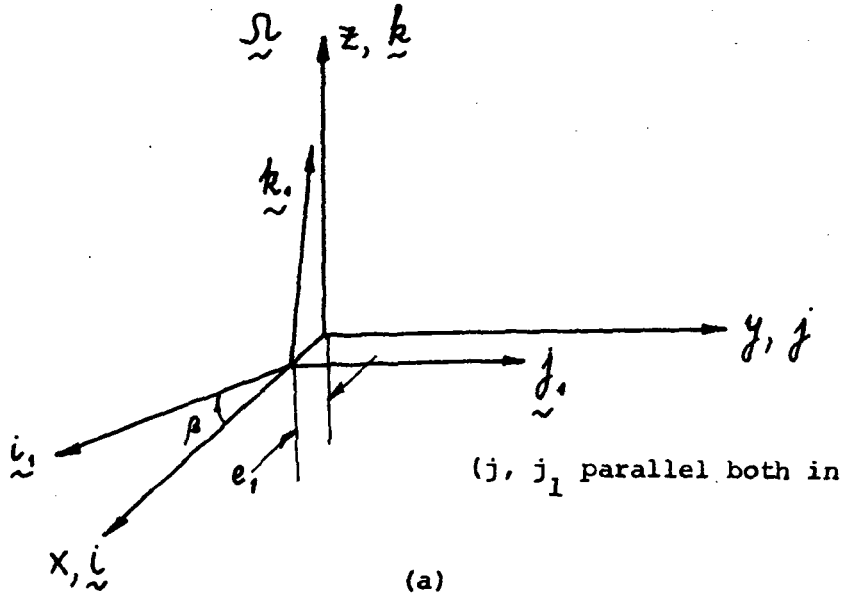

(a)

(a)

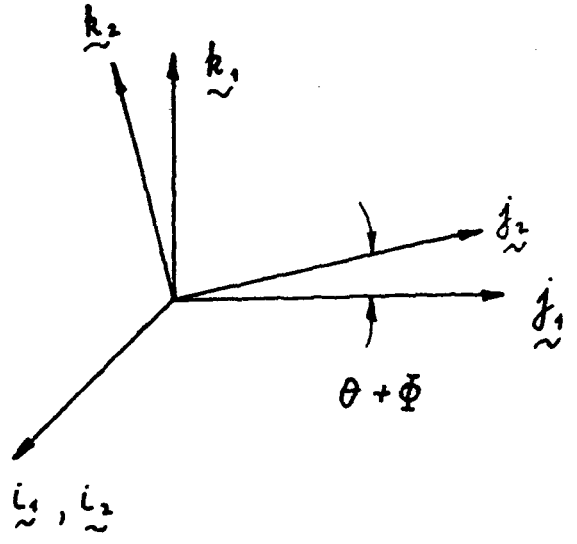

(b)

FIG. 29 GEOMETRY OF COORDINATE SYSTEMS

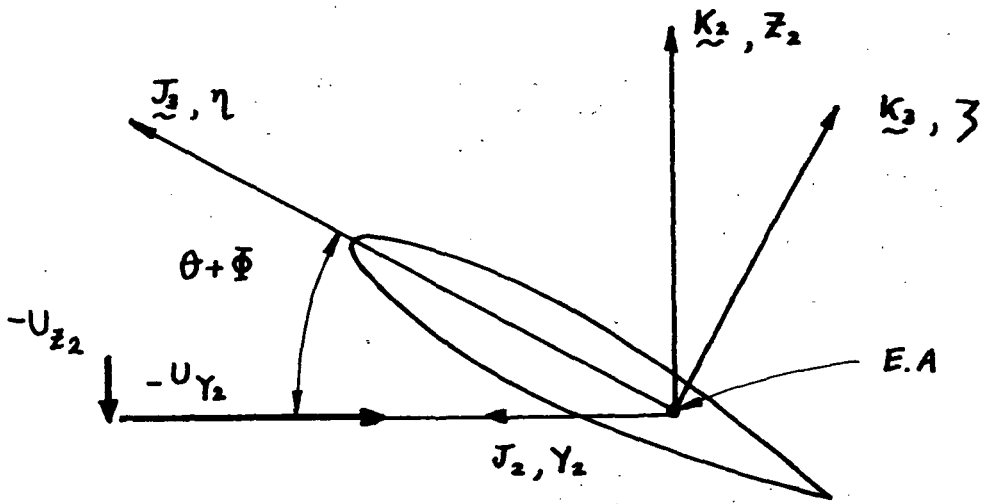

FIG. 30 BLADE GEOMETRY FOR AIR-LOAD CALCULATION

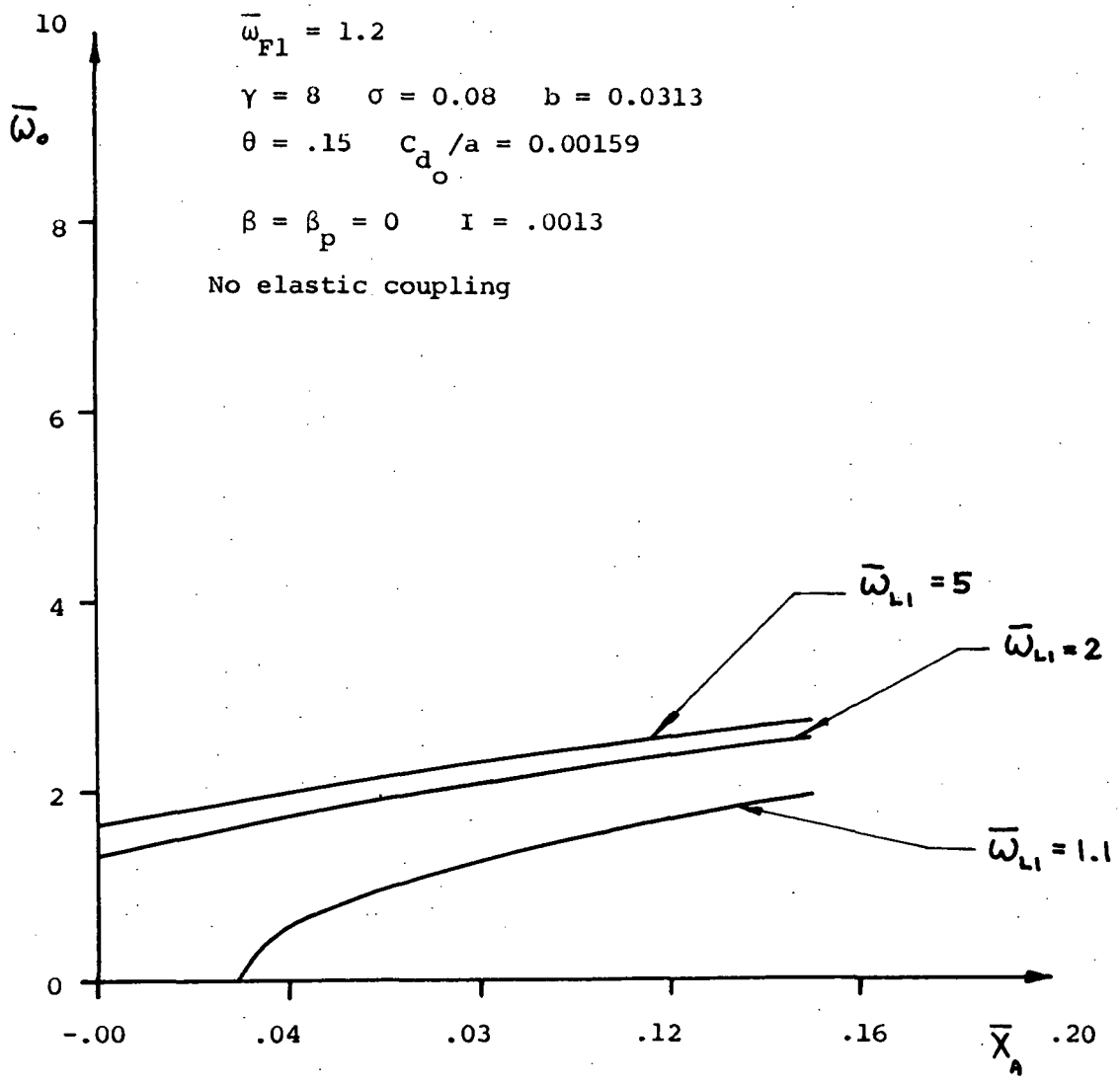

FIG. 31 EFFECT OF AERODYNAMIC CENTER ELASTIC AXIS OFFSET AND LAGWISE BLADE STIFFNESS ON THE APPROXIMATE DIVERGENCE BOUNDARIES

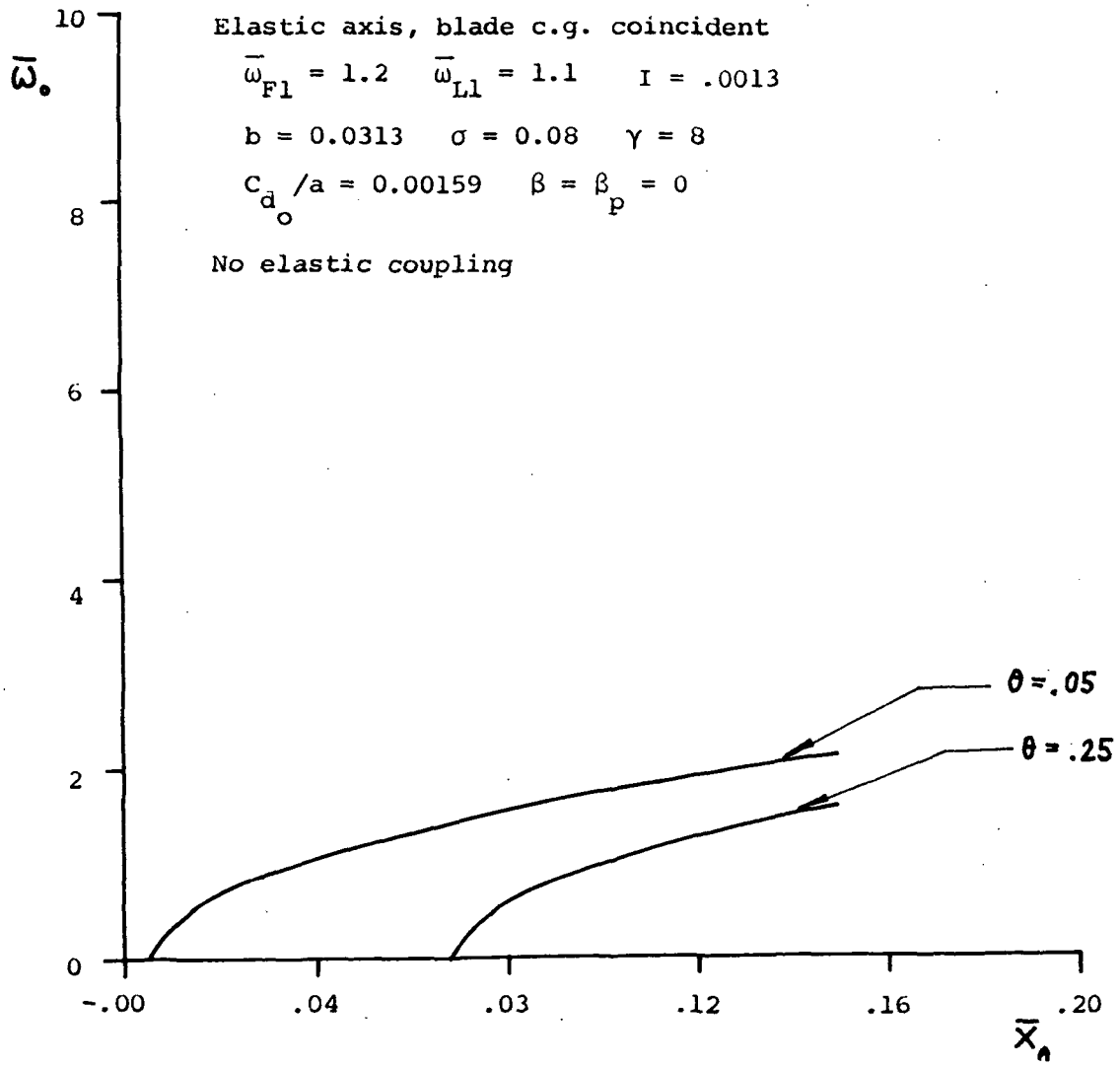

FIG. 32 EFFECT OF AERODYNAMIC CENTER ELASTIC AXIS OFFSET AND COLLECTIVE PITCH ON THE APPROXIMATE DIVERGENCE BOUNDARIES

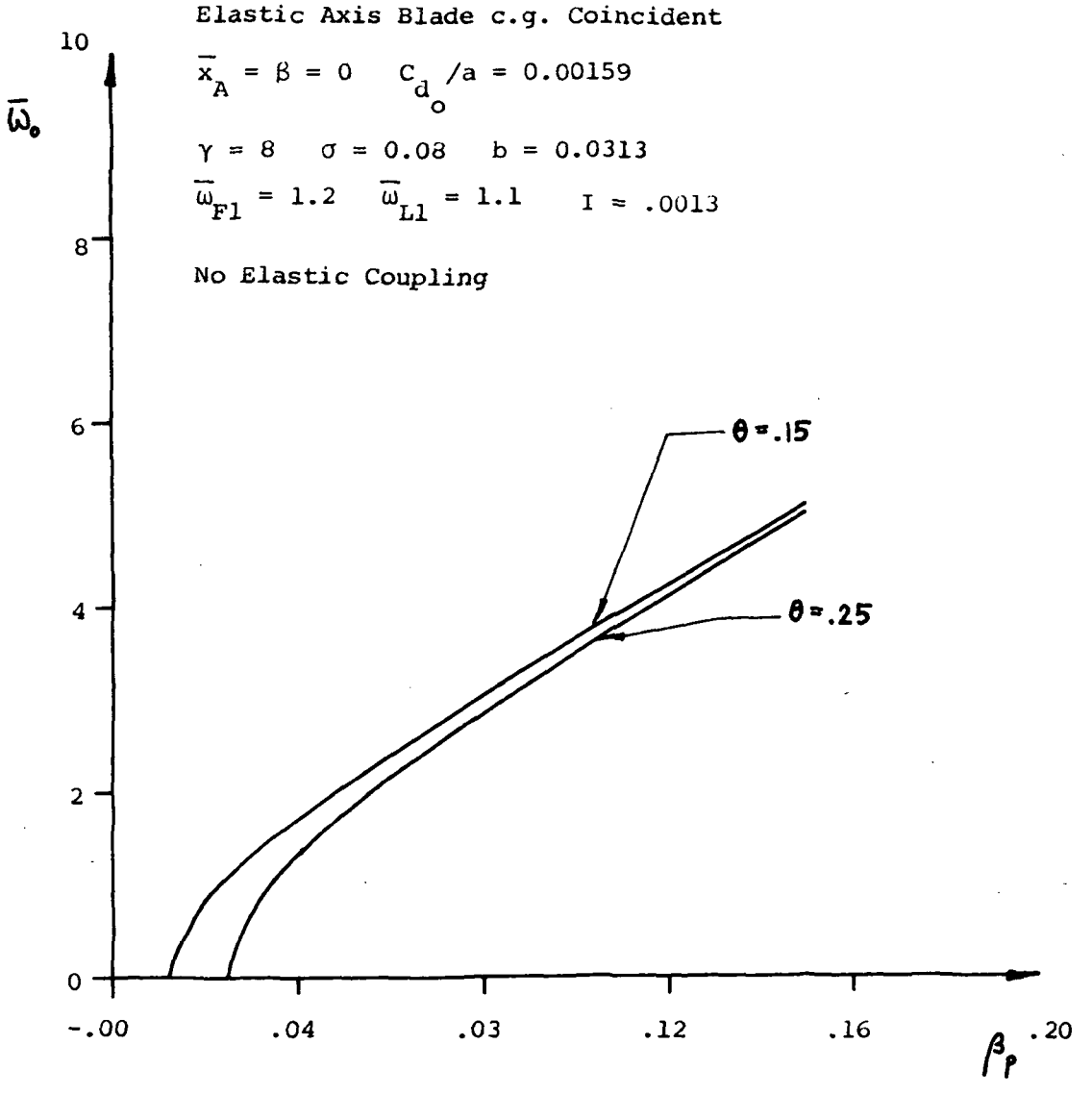

FIG. 33 EFFECT OF PRECONING β_p AND PITCH SETTING θ ON THE APPROXIMATE DIVERGENCE BOUNDARIES

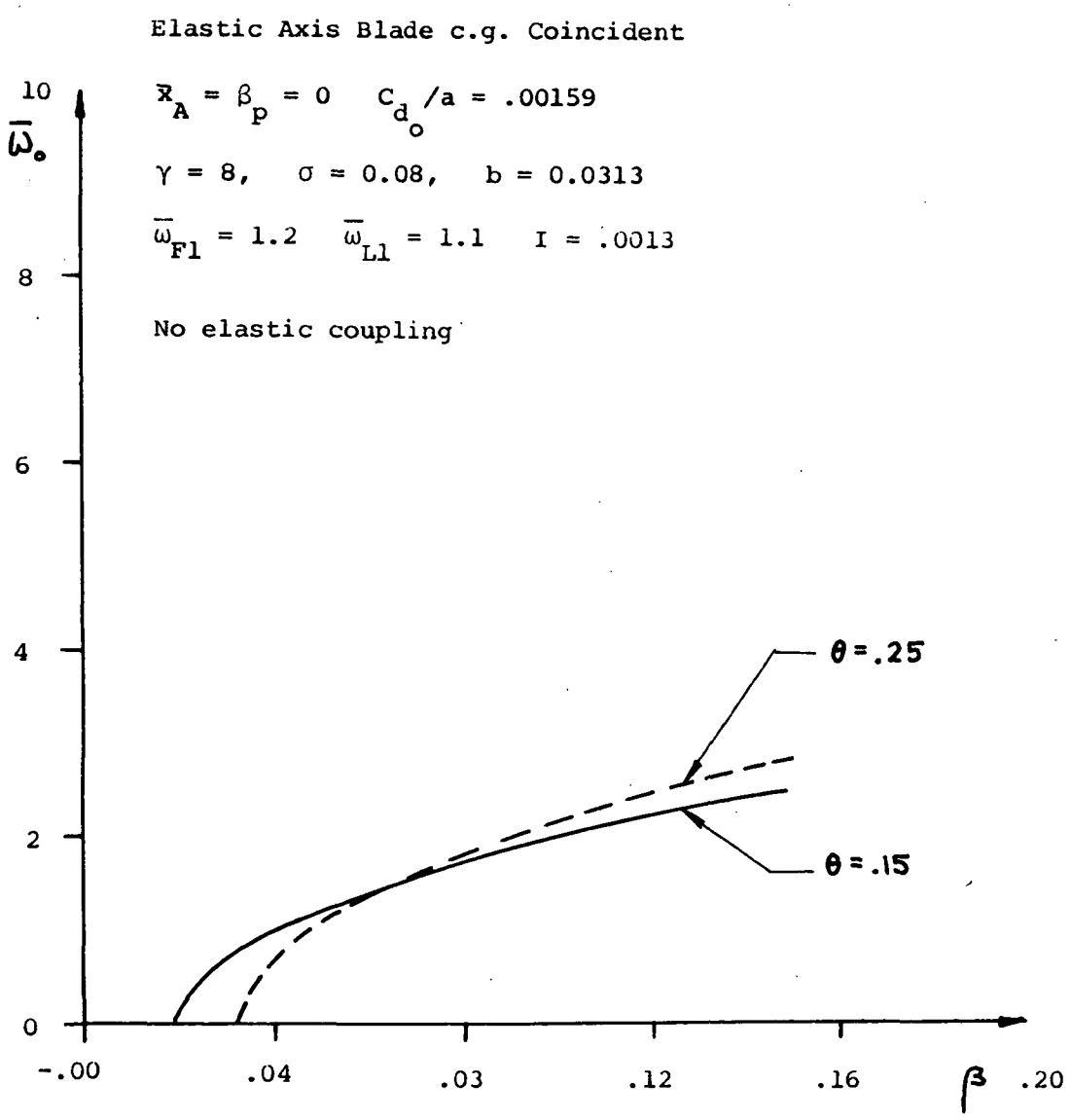

FIG. 34 EFFECT OF FEATHERING AXIS ORIENTATION WITH RESPECT TO HUB PLANE β AND PITCH SETTING θ ON THE APPROXIMATE DIVERGENCE BOUNDARIES

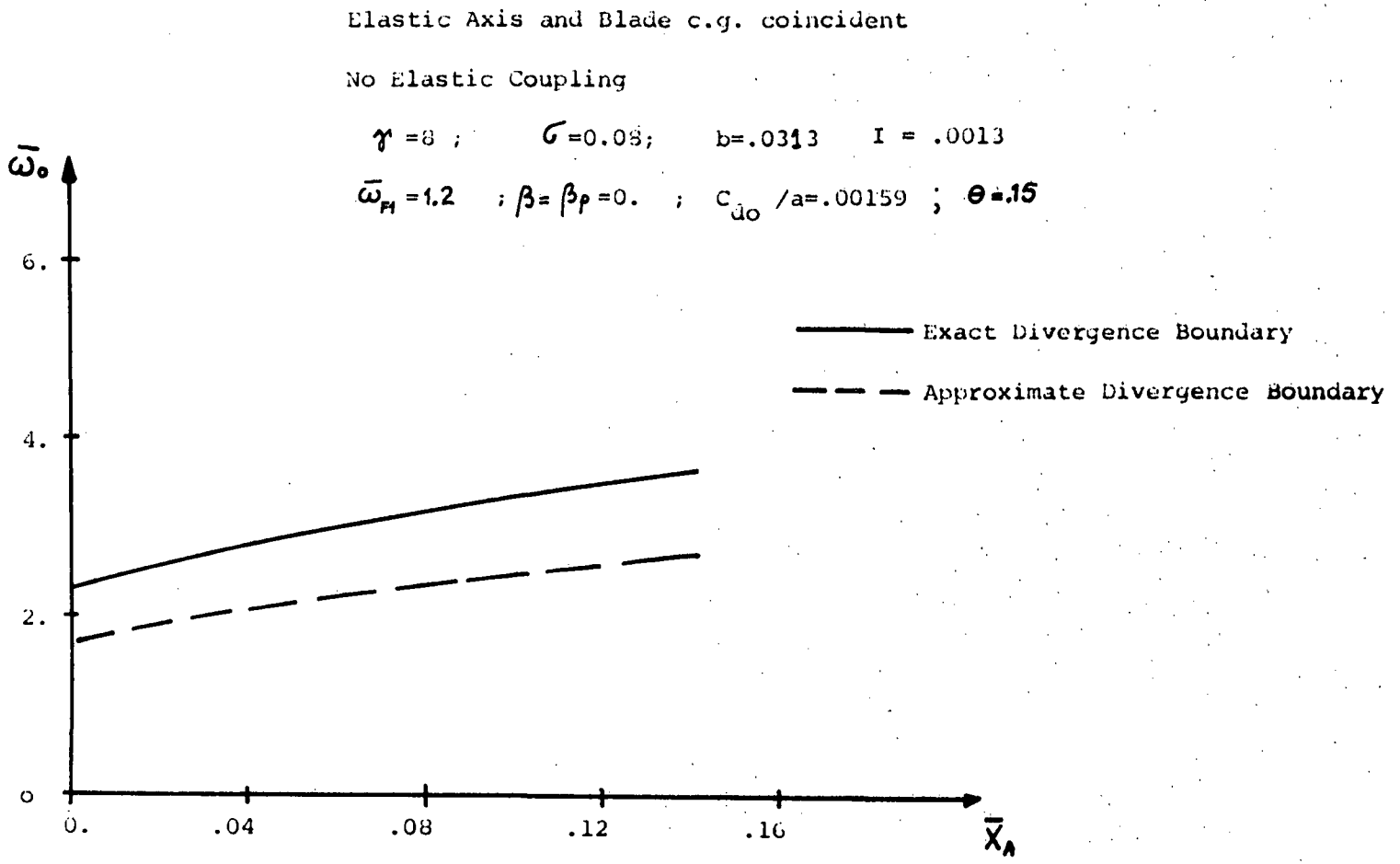

FIG. 35 COMPARISON OF APPROXIMATE AND EXACT DIVERGENCE BOUNDARIES FOR FLAP PITCH

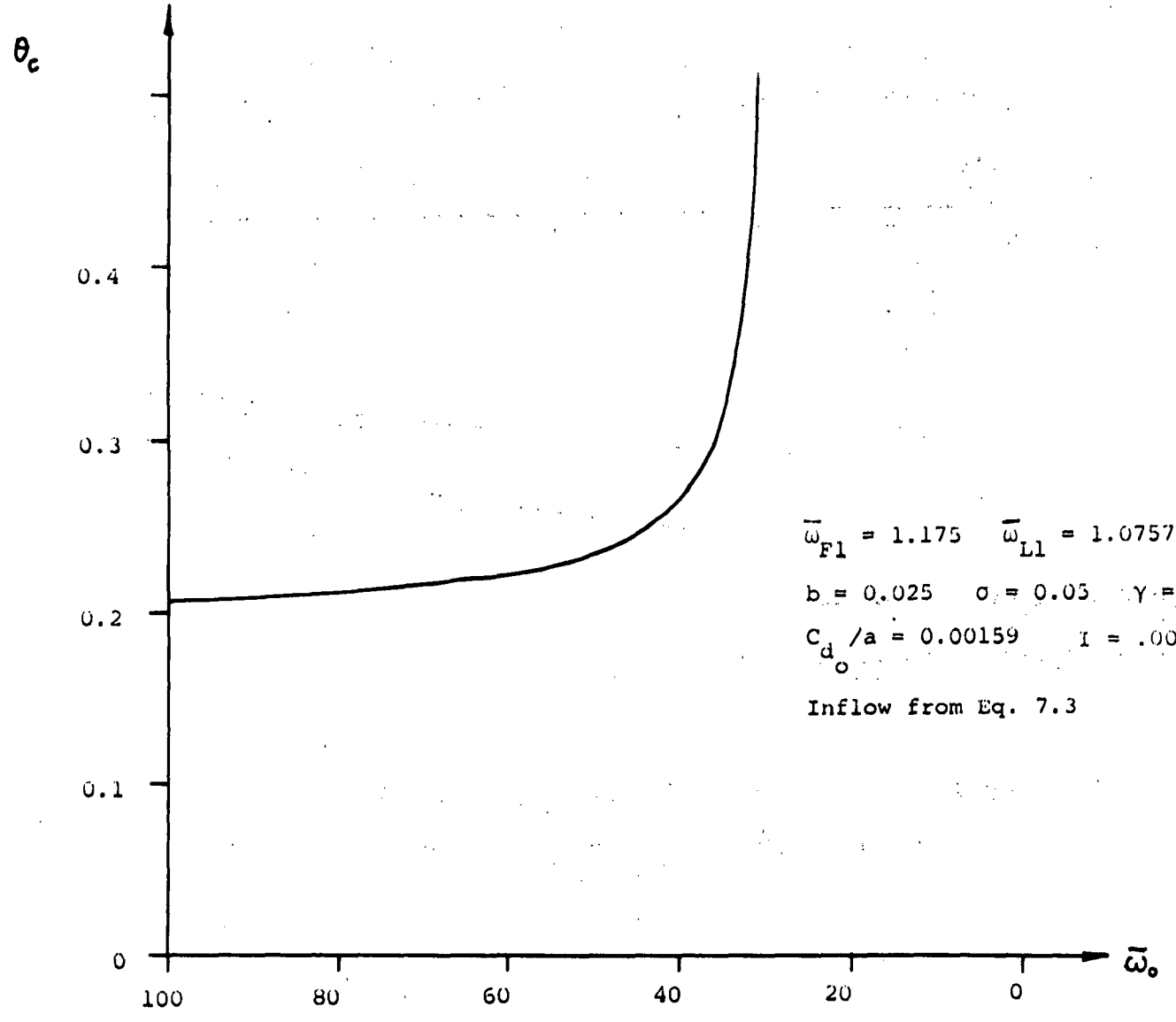

FIG. 36 EFFECT OF TORSIONAL DEGREE OF FREEDOM ON FLAP-LAG-TYPE OF INSTABILITY

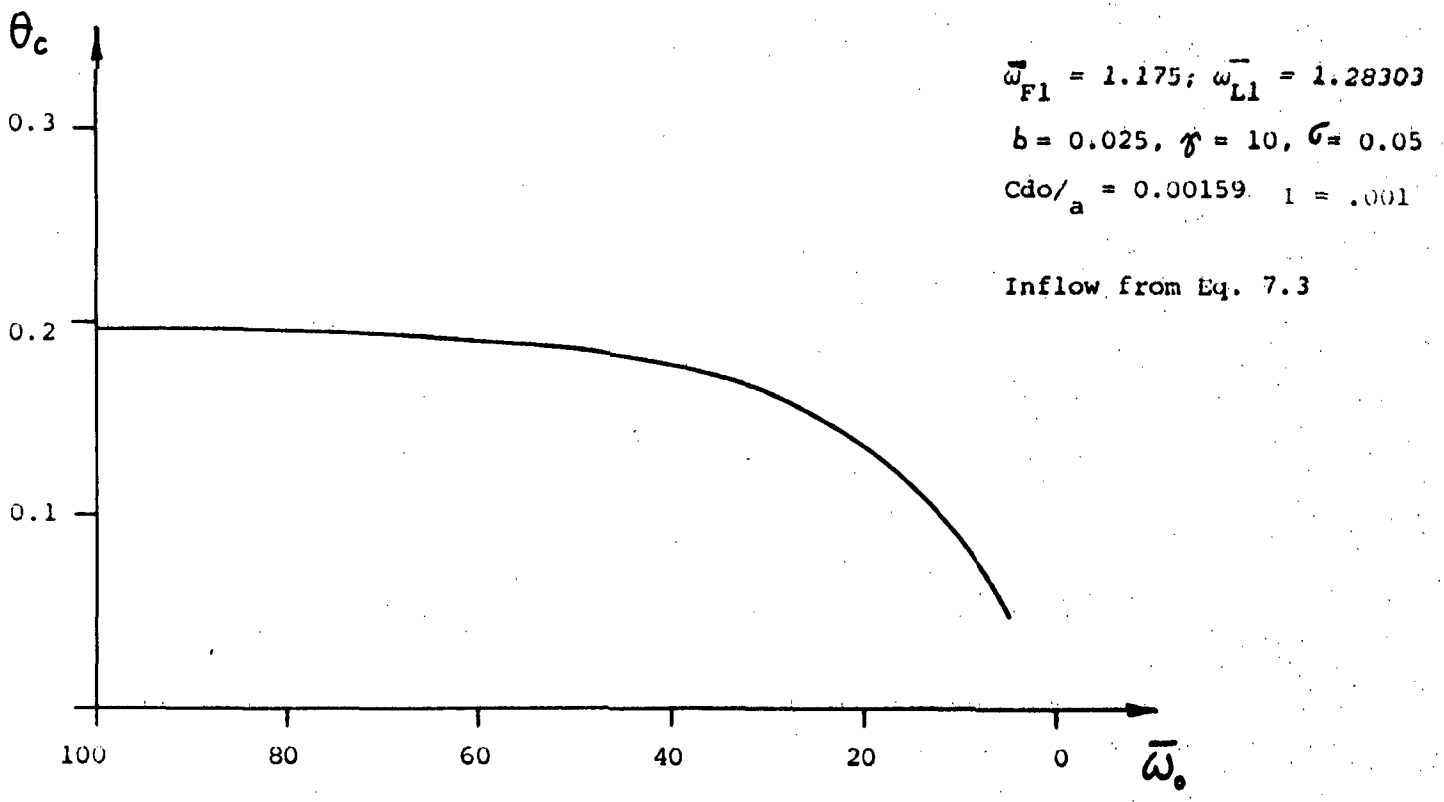

FIG. 37 EFFECT OF TORSIONAL DEGREE OF FREEDOM ON FLAP-LAG TYPE OF INSTABILITY

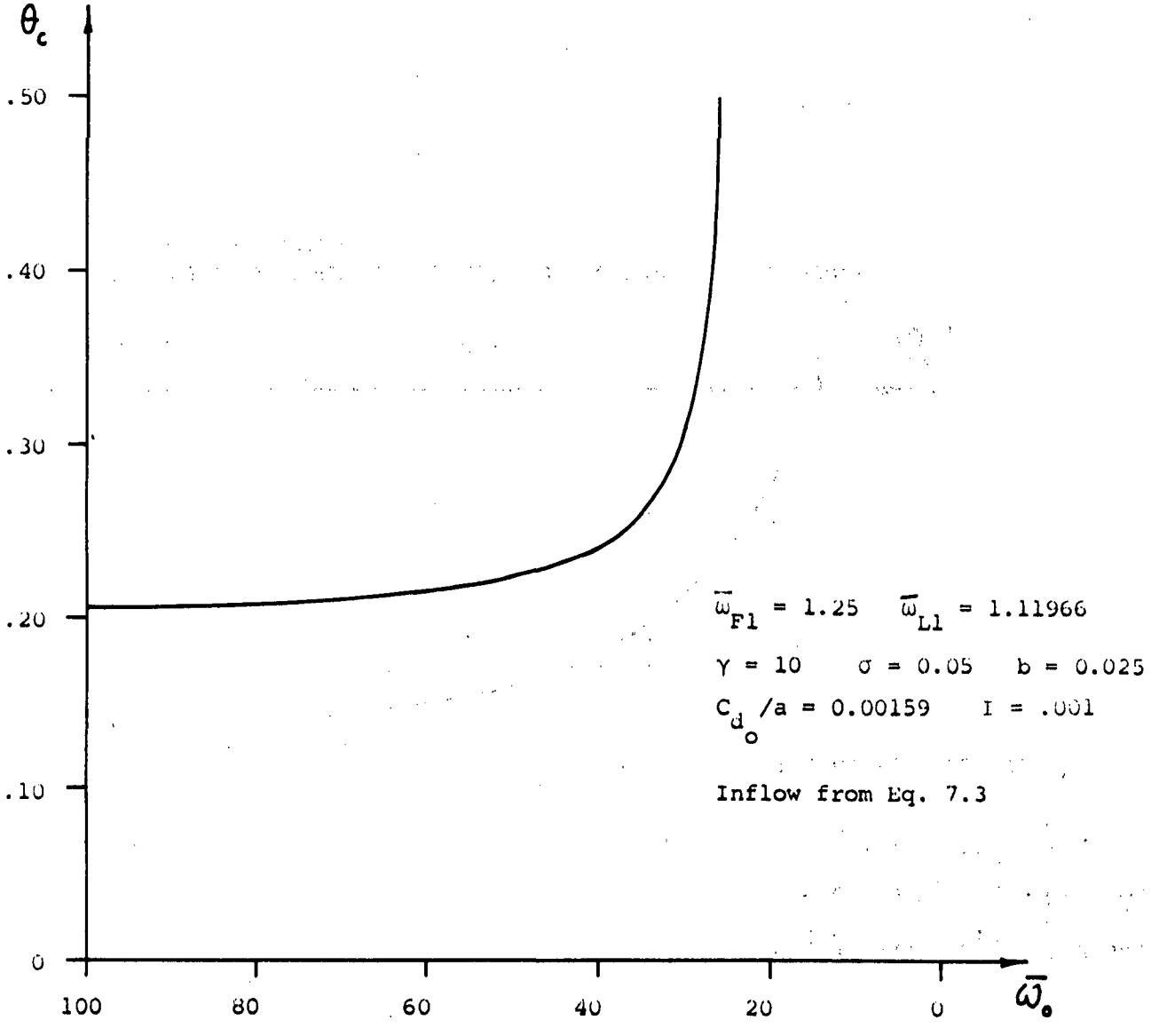

FIG. 38 EFFECT OF TORSIONAL DEGREE OF FREEDOM ON FLAP-LAG-TYPE OF INSTABILITY

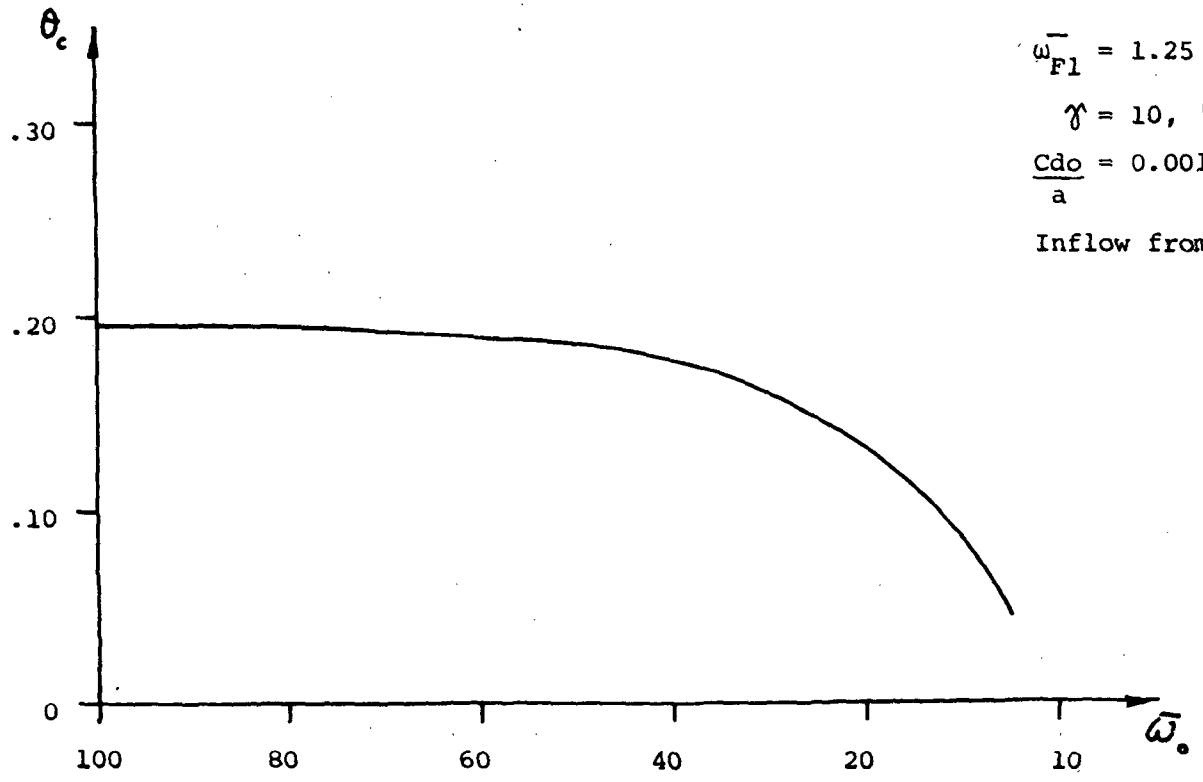

FIG. 39 EFFECT OF TORSIONAL DEGREE OF FREEDOM ON FLAP-LAG TYPE OF INSTABILITY

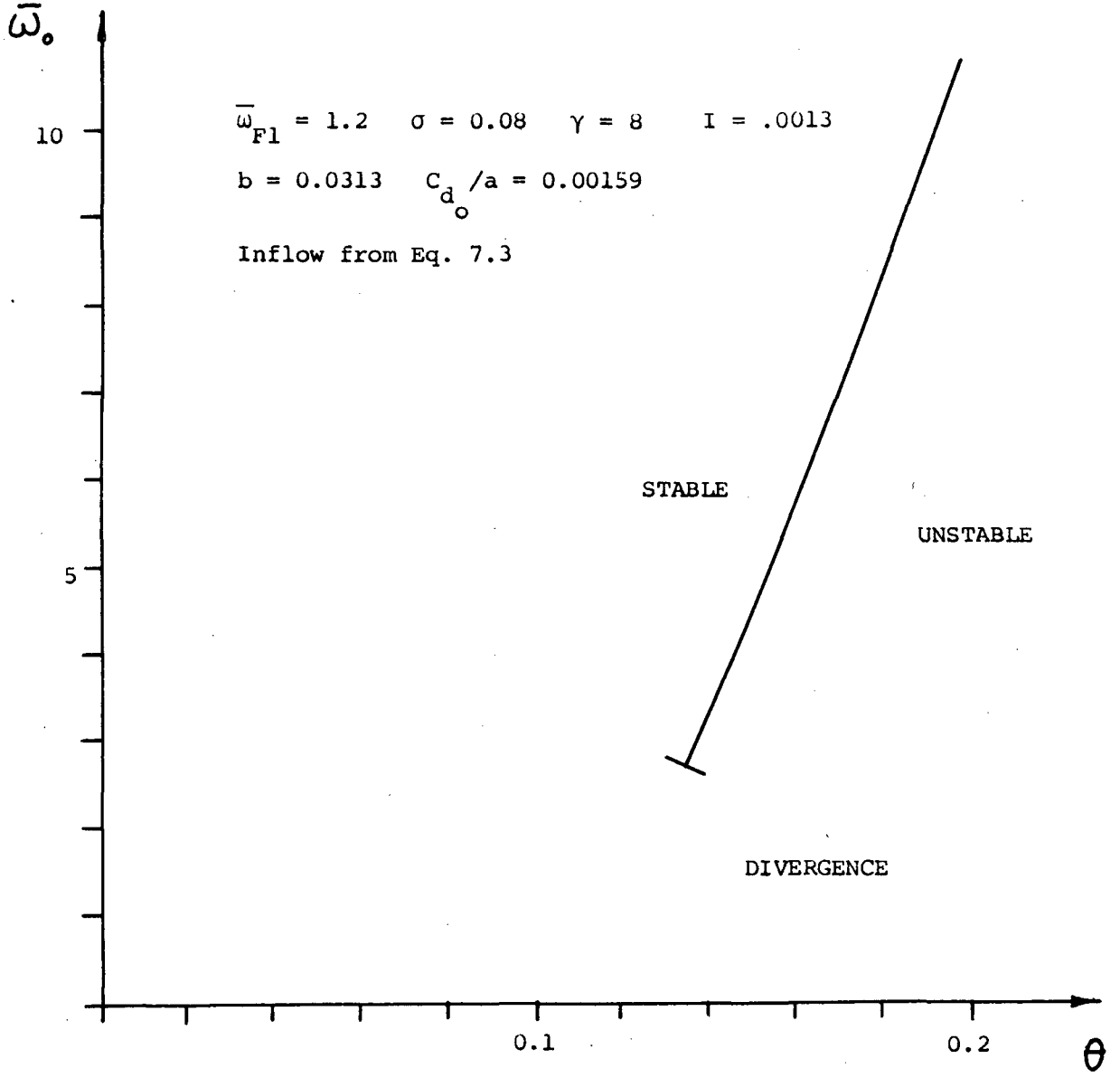

FIG. 40 FLAP-PITCH STABILITY BOUNDARY

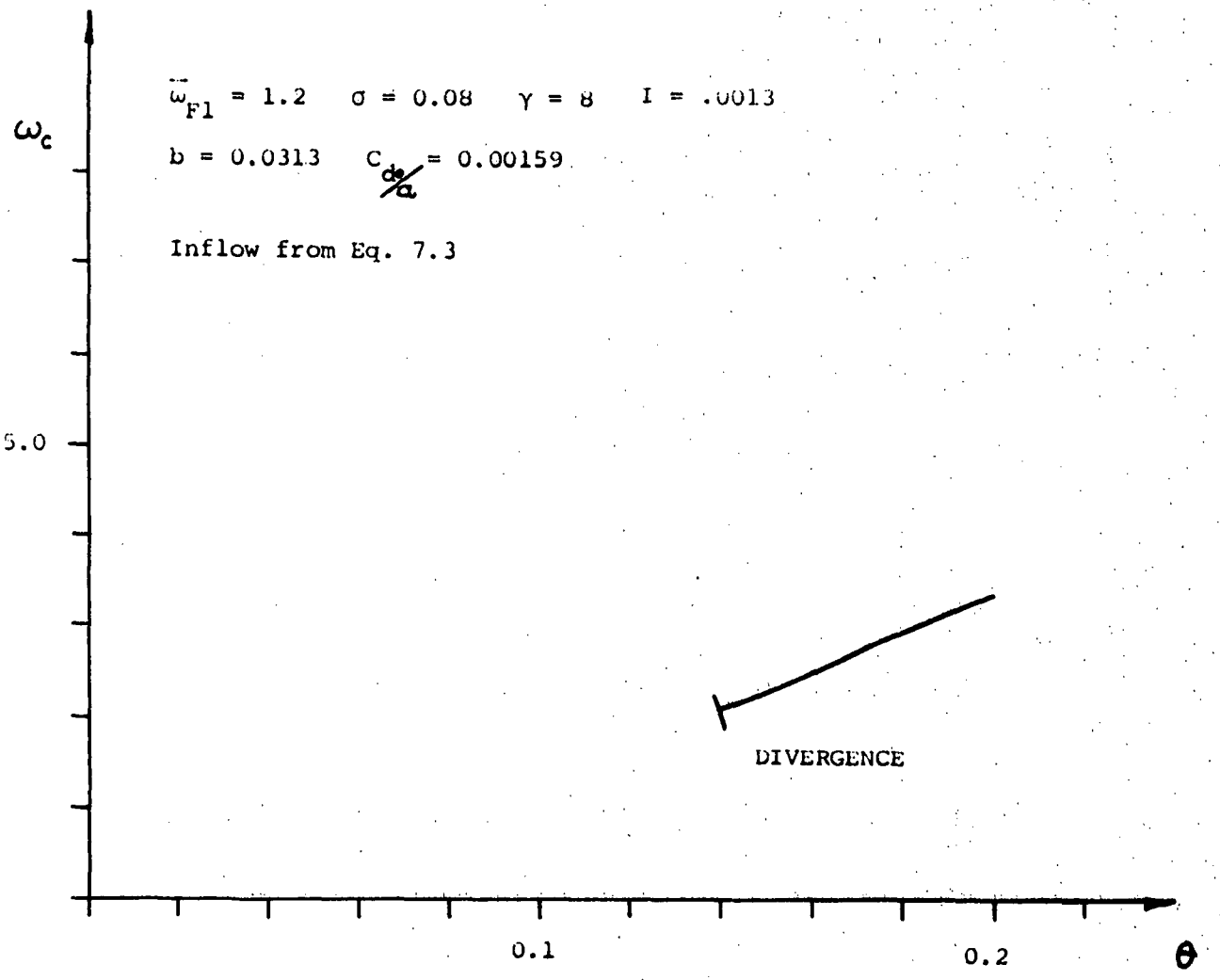

FIG. 41 FLUTTER FREQUENCY AS A FUNCTION OF PITCH SETTING

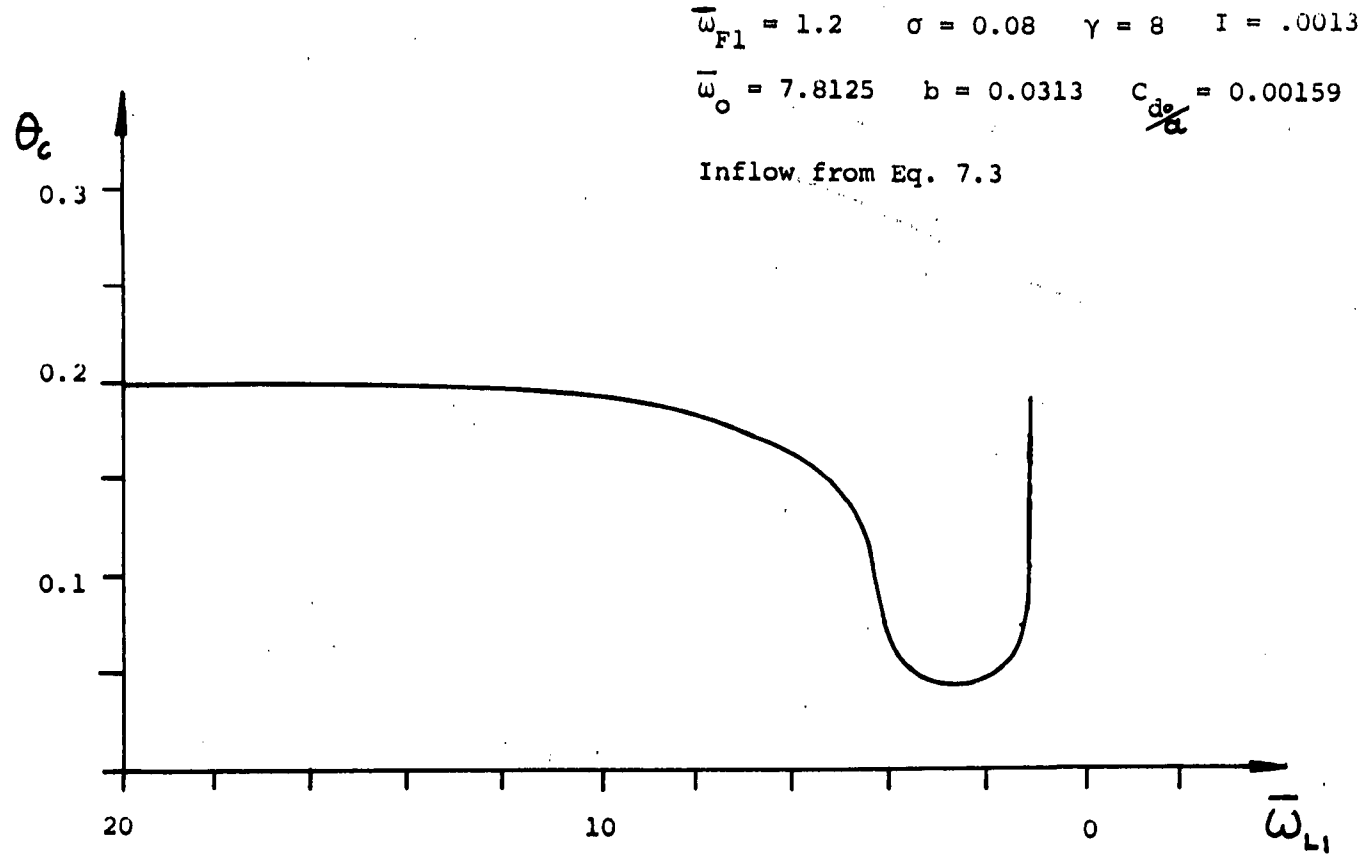

FIG. 42 EFFECT OF LAG DEGREE OF FREEDOM ON FLAP-PITCH-TYPE OF INSTABILITY

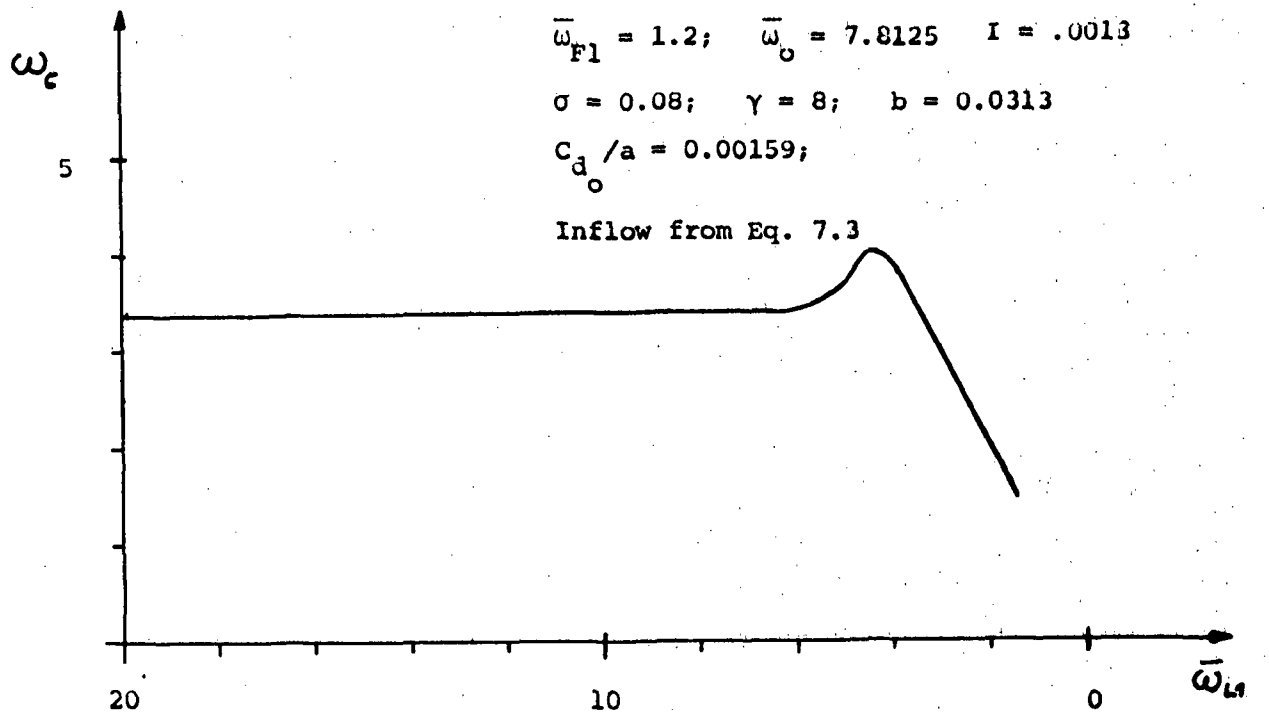

FIG. 43 EFFECT OF LAG DEGREE OF FREEDOM ON FLAP-PITCH-TYPE OF INSTABILITY (CONTINUED), VARIATION OF FLUTTER FREQUENCY

APPENDIX A

ORTHOGONALITY CONDITIONS

The orthogonality condition for a rotating beam vibrating out of the plane of rotation can be obtained following Bisplinghoff (Ref. 12)

$$\frac{1}{\Omega^2 \ell}\int_0^1 (EI)_y \eta_k'' \eta_i \, d\bar{x}_0 + \int_0^1 \eta_i' \eta_k' \left(\ell^3 \int_{\bar{x}_0}^1 m \bar{x}_1 \, d\bar{x}_1\right) d\bar{x}_0 = 0 \tag{A.1}$$

when $i \neq k$ and

$$\frac{1}{\Omega^2 \ell}\int_0^1 (EI)_y (\eta_i'')^2 \, d\bar{x}_0 + \int_0^1 \ell^3 (\eta_i')^2 \left(\int_{\bar{x}_0}^1 m \bar{x}_1 \, d\bar{x}_1\right) d\bar{x}_0 = \frac{\omega_{Fi}^2}{\Omega^2}\int_0^1 m \eta_i^2 \, d\bar{x}_0 \, \ell^3 \tag{A.2}$$

when $i = k$.

For a beam vibrating in its plane of rotation, the orthogonality conditions are (Ref. 23)

$$\frac{1}{\Omega^2 \ell}\int_0^1 (EI)_z \gamma_m'' \gamma_n'' \, d\bar{x}_0 + \ell^3 \int_0^1 \left(\int_{\bar{x}_0}^1 m \bar{x}_1 \, d\bar{x}_1\right) \gamma_m' \gamma_n' \, d\bar{x}_0 - \ell^3 \int_0^1 m \gamma_m \gamma_n \, d\bar{x}_0 = 0 \tag{A.3}$$

when $m \neq n$ and

$$\frac{1}{\Omega^2 \ell}\int_0^1 (EI)_z (\gamma_i'')^2 \, d\bar{x}_0 + \ell^3 \int_0^1 \left(\int_{\bar{x}_0}^1 m \bar{x}_1 \, d\bar{x}_1\right) (\gamma_i')^2 \, d\bar{x}_0 - \ell^3 \int_0^1 m \gamma_i^2 \, d\bar{x}_0 = \left(\frac{\omega_{Li}}{\Omega}\right)^2 \ell^3 \int_0^1 m \gamma_i^2 \, d\bar{x}_0 \tag{A.4}$$

when $m = n = i$

These relations also determine ω_{Fi} and ω_{Li}.

APPENDIX B

COEFFICIENTS ASSOCIATED WITH GENERALIZED MASSES AND DAMPING

$$I_b = \ell^3 \int_0^1 m \bar{x}_0^2 \, d\bar{x}_0$$

$$\bar{P}_{ikm} = \ell^3 \int_0^1 \eta_i' \eta_k' \left(\int_{\bar{x}_0}^1 m \gamma_m(\bar{x}_1) \, d\bar{x}_1 \right) d\bar{x}_0 / I_b$$

$$\bar{M}_{Fi} = \ell^3 \int_0^1 m \eta_i^2 \, d\bar{x}_0 / I_b$$

$$\bar{M}_{Li} = \ell^3 \int_0^1 m \gamma_i^2 \, d\bar{x}_0 / I_b$$

$$\bar{C}_i = \ell^3 \int_0^1 m \gamma_i \, d\bar{x}_0 / I_b$$

$$\bar{S}_{imr} = \ell^3 \int_0^1 \gamma_i' \gamma_r' \left(\int_{\bar{x}_0}^1 m \gamma_m \, d\bar{x}_1 \right) d\bar{x}_0 / I_b$$

$$(\bar{M}_\eta)_{ikl} = \ell^3 \left[\int_0^1 m \left(\int_0^{\bar{x}_0} \eta_k' \eta_l' \, d\bar{x}_1 \right) \gamma_i \, d\bar{x}_0 \right] / I_b$$

$$(\bar{M}_\gamma)_{imr} = \ell^3 \left[\int_0^1 m \left(\int_0^{\bar{x}_0} \gamma_m' \gamma_r' \, d\bar{x}_1 \right) \gamma_i \, d\bar{x}_0 \right] / I_b$$

The nondimensionalized viscous-type structural damping coefficients are

$$g_{SFi} = \frac{\int_0^1 \eta_i^2 \, d\bar{x}_0 \; g_{SF}}{\Omega \int_0^1 m \bar{x}_0^2 \, d\bar{x}_0} = 2 \bar{\omega}_{Fi} \bar{M}_{Fi} \eta_{SFi}$$

$$g_{SLi} = \frac{\int_0^1 \gamma_i^2 \, d\bar{x}_0 \; g_{SL}}{\Omega \int_0^1 m \bar{x}_0^2 \, dx_0} = 2 \bar{\omega}_{Li} \bar{M}_{Li} \eta_{SLi}$$

where η_{SFi} and η_{SLi} represent the fraction of critical damping associated with the ith mode in flap or lag.

APPENDIX C

EXPRESSIONS ASSOCIATED WITH AERODYNAMIC LOADS IN FLAP AND LAG

Note that all integrals are performed between the lower limit $\bar{A}$ and the upper limit $\bar{B}$. $\bar{A}$ and $\bar{B}$ represent the tip loss factors.

$$F_i^1 = \int \bar{x}^2 \eta_i \, d\bar{x}_0$$

$$F_i^2 = \int \bar{x} \, \eta_i \, d\bar{x}_0$$

$$F_i^3 = \int \eta_i \, d\bar{x}_0$$

$$F_i^4 = \int \bar{x} \, g(\bar{x}_0) \, \eta_i \, d\bar{x}_0$$

$$F_i^5 = \int g(\bar{x}_0) \, \eta_i \, d\bar{x}_0$$

$$F_{ik}^6 = \int \bar{x} \, \eta_i \, \eta_k' \, d\bar{x}_0$$

$$F_{ik}^7 = \int \eta_i \, \eta_k' \, d\bar{x}_0$$

$$F_{ik}^8 = \int \bar{x} \, \eta_i \, \eta_k \, d\bar{x}_0$$

$$F_{ik}^9 = \int \eta_i \, \eta_k \, d\bar{x}_0$$

$$F_{im}^{10} = \int \bar{x} \, \eta_i \, \gamma_m \, d\bar{x}_0$$

$$F_{im}^{11} = \int \eta_i \, \gamma_m \, d\bar{x}_0$$

(C.1)

$$L_i^1 = \int \bar{x} \, \gamma_i \, d\bar{x}_0$$

$$L_i^2 = \int \gamma_i \, d\bar{x}_0$$

$$L_i^3 = \int g(\bar{x}_0) \, \gamma_i \, d\bar{x}_0$$

$$L_i^4 = \int \bar{x}^2 \gamma_i \, d\bar{x}_0$$

$$L_i^5 = \int \bar{x} \, g(\bar{x}_0) \, \gamma_i \, d\bar{x}_0$$

$$L_i^6 = \int [g(x_0)]^2 \gamma_i \, d\bar{x}_0$$

$$L_{ik}^7 = \int \bar{x} \, \eta_k \, \gamma_i \, d\bar{x}_0$$

$$L_{ik}^8 = \int \eta_k \, \gamma_i \, d\bar{x}_0$$

$$L_{ik}^9 = \int g(\bar{x}_0) \, \gamma_i \, \eta_k \, d\bar{x}_0$$

$$L_{ik}^{10} = \int \bar{x} \, \eta_k' \, \gamma_i \, d\bar{x}_0$$

$$L_{ik}^{11} = \int \gamma_i \, \eta_k' \, d\bar{x}_0$$

(C.2)

$$F_{im}^{12} = \int g(x_0)\eta_i \gamma_m \, d\bar{x}_0 \qquad L_{ik}^{12} = \int g(\bar{x}_0)\eta_k' \gamma_i \, d\bar{x}_0$$

$$F_{imr}^{13} = \int \eta_i \gamma_m \gamma_r \, d\bar{x}_0 \qquad L_{ik}^{13} = \int \gamma_i \gamma_m \, d\bar{x}_0$$

$$F_{ikm}^{14} = \int \eta_i \eta_k' \gamma_m \, d\bar{x}_0 \qquad L_{ik}^{14} = \int \gamma_i \gamma_m \bar{x} \, d\bar{x}_0$$

$$F_{ikm}^{15} = \int \eta_i \eta_k \gamma_m \, d\bar{x}_0 \qquad L_{ik}^{15} = \int g(\bar{x}_0)\gamma_i \gamma_m \, d\bar{x}_0$$

$$F^{16} = \int d\bar{x}_0 \qquad L_{ikm}^{16} = \int \gamma_i \gamma_m \eta_k' \, d\bar{x}_0$$

$$F^{17} = \int \bar{x} \, d\bar{x}_0 \qquad L_{ike}^{17} = \int \gamma_i \eta_k' \eta_e \, d\bar{x}_0$$

$$F^{18} = \int \bar{x}^2 \, d\bar{x}_0 \qquad L_{ike}^{18} = \int \gamma_i \eta_k \eta_e \, d\bar{x}_0$$

$$F^{19} = \int_0^1 \bar{x}^2 \eta_1' \, d\bar{x}_0 \qquad L_{ikm}^{19} = \int \gamma_i \eta_k \gamma_m \, d\bar{x}_0$$

$$F^{20} = \int_0^1 \bar{x} (\eta_1')^2 \, d\bar{x}_0$$

The quantities A_{Fi}, A_{Li} are defined by the following relations:

$$A_{Fi} = \frac{\gamma}{2}\left(\frac{\ell}{R}\right)^2 \Big\{ \Big[F_i^1 \theta - F_i^2 \lambda_0 + F_i^3 \theta \frac{\mu^2}{2} - \bar{\lambda}_{1c} F_i^4 \cos\psi + \mu \big(2\theta F_i^2 - \lambda_0 F_i^3 \big) \sin\psi - \frac{\mu^2}{2} F_i^3 \theta \cos 2\psi - \bar{\lambda}_{1c} \frac{\mu}{2} F_i^5 \sin 2\psi \Big] - \mu \big(F_{ik}^6 \cos\psi + \frac{\mu}{2} F_{ik}^7 \sin 2\psi \big) g_k - \frac{\ell}{R} \big(F_{ik}^8 + \mu F_{ik}^9 \sin\psi \big) g_k^* -$$

$$- \frac{\ell}{R}\left[\left(2F_{im}^{10}\theta - F_{im}^{11}\lambda_o\right) - \bar{\lambda}_{ic}F_{im}^{12}\cos\psi + 2\mu\theta F_{im}^{11}\sin\psi\right]h_m^*$$

$$+\left[\left(\frac{\ell}{R}\right)^2\theta F_{imr}^{13}h_m^*h_r + \left(\frac{\ell}{R}\right)\mu F_{ikm}^{14}\cos\psi\, g_k h_m^* + \left(\frac{\ell}{R}\right)^2 F_{ikm}^{15} g_k^* h_m^*\right]\Bigg\}$$

(C.3)

$$A_{Li} = \frac{\gamma}{2}\left(\frac{\ell}{R}\right)^2\Bigg\{\Bigg[\lambda_o\left(L_i^1\theta - L_i^2\lambda_o\right) - \frac{1}{2}L_i^6\bar{\lambda}_{ic}^{-2} + \frac{C_{do}}{a}\left(L_i^4 + \frac{\mu^2}{2}\right) +$$

$$\left(L_i^5\theta\bar{\lambda}_{ic} - 2\lambda_o\bar{\lambda}_{ic}L_i^3\right)\cos\psi + \left(\mu\lambda_o\theta L_i^2 + 2\frac{C_{do}}{a}\mu L_i^1\right)\sin\psi$$

$$-\frac{1}{2}\left(\bar{\lambda}_{ic}L_i^6 + \frac{C_{do}}{a}\mu^2 L_i^2\right)\cos 2\psi + \frac{\mu}{2}\theta\bar{\lambda}_{ic}L_i^3\sin 2\psi\Bigg]$$

$$+ g_k^*\left(\frac{\ell}{R}\right)\Big[\left(L_{ik}^7\theta - L_{ik}^8 2\lambda_o\right) - 2\bar{\lambda}_{ic}L_{ik}^9\cos\psi + \mu L_{ik}^8\theta\sin\psi\Big]$$

$$+ g_k\Big[\mu\left(\theta L_{ik}^{10} - 2L_{ik}^{11}\lambda_o\right)\cos\psi - \mu\bar{\lambda}_{ic}L_{ik}^{12}(1+\cos 2\psi) +$$

$$+\theta\frac{\mu^2}{2}L_{ik}^{11}\sin 2\psi\Big] - h_m^*\left(\frac{\ell}{R}\right)\Big[\left(L_{ik}^{13}\lambda_o\theta + 2\frac{C_{do}}{a}L_{ik}^{14}\right) +$$

$$\bar{\lambda}_{ic}\theta L_{ik}^{15}\cos\psi + 2\frac{C_{do}}{a}\mu L_{ik}^{13}\sin\psi\Big] - \Big[\mu\left(\frac{\ell}{R}\right)\left(\theta h_m^* g_k L_{ikm}^{16}\right.$$

$$\left.+ 2L_{ikl}^{17}g_k^* g_l\right)\cos\psi + \left(\frac{\ell}{R}\right)^2\left(L_{ikl}^{18}g_k^* g_l^* + \theta L_{ikm}^{19}g_k^* h_m^*\right)\Big]\Bigg\}$$

(C.4)

APPENDIX D

INFLOW RELATIONS

D.1 Inflow Relation in Hovering Flight

Extended blade element theory (Ref. 19) gives the following relation for the induced velocity

$$\frac{v_i}{\Omega R} = \frac{\sigma a}{16}\left[\sqrt{1 + \frac{32\theta\bar{x}}{a\sigma}} - 1\right] \tag{D.1}$$

Thus, constant induced velocity over the whole rotor area is compatible, with a twist variation inversely proportional to $\bar{x}$. In the present report only constant values of collective pitch will be considered. Therefore, an expression for the constant inflow will be derived in such a manner that it represents a weighted integral of the varying inflow, resulting in the correct value for the thrust coefficient.

From blade element theory with constant induced velocity

$$C_T = \frac{\sigma a}{2}\left(\frac{\theta}{3} - \frac{\lambda_0}{2}\right) \tag{D.2}$$

Also, from blade element theory

$$dT = \frac{1}{2}\rho_a (2bR)\Omega^2 R^3 \bar{x}^2 \left(\theta - \frac{v_i}{\Omega R \bar{x}}\right) d\bar{x} \tag{D.3}$$

From Eqs. D.1 and D.3

$$C_T = \frac{\sigma a}{2}\left\{\frac{\theta}{3} - \int_0^1 \frac{\sigma a}{16}\left[\sqrt{1 + \frac{32\theta\bar{x}}{\sigma a}} - 1\right]\bar{x}\, d\bar{x}\right. \tag{D.4}$$

Evaluating the integral in Eq. D.4 yields:

$$C_T = \frac{\sigma a}{2}\left\{\frac{\theta}{3} - \frac{\sigma a}{16}\left[\frac{2}{15 b_\theta^2}\left\langle (1+b_\theta)^{3/2}(3b_\theta - 2) + 2\right\rangle - \frac{1}{2}\right]\right\} \tag{D.5}$$

From Eqs. D.2 and D.5

$$\lambda_o = \frac{\sigma a}{16}\left\{\frac{4}{15 b_\theta^2}\left[(1+b_\theta)^{3/2}(3b_\theta - 2) + 2\right] - 1\right\} \tag{D.6}$$

where

$$b_\theta = \frac{32\theta}{\sigma a}$$

The advantage of relation D.6 when compared to (D.7)

$$\lambda_o = \frac{a\sigma}{16}\left[\sqrt{1 + \frac{24\theta}{a\sigma}} - 1\right] \tag{D.7}$$

is due to the fact that, for a given C_T, Eq. D.6 agrees to within $\sim$ 4% with $\lambda_o = \sqrt{C_T/2}$, while Eq. D.7 gives a discrepancy of $\sim$ 20%.

D.2 Inflow Relation in Forward Flight

In forward flight, the constant part of the inflow can be obtained from the well-known relation given in Ref. 19

$$\lambda_o = \mu \tan \alpha_R + \frac{C_T}{2\sqrt{\mu^2 + \lambda_o^2}} \tag{D.8}$$

For a given value of C_T and μ, λ_o can be obtained from Eq. D.8 by solving a quartic equation. This has been done by using a simple iterative process on a digital computer.

In practice it has been found that it is possible to replace Eq. D.8 by a simplex relation which provides a reasonable approximation for λ_o in the range of advance ratios ($0 < \mu < 0.3$) and thrust coefficients ($0.005 < C_T < 0.015$, for flutter) considered.

For low values of μ, $\mu \tilde{\sim} 0$, $\lambda_o = \lambda_H = \sqrt{C_T/2}$. For the value of $\mu \tilde{\sim} 0.3$, it has been shown in Ref. 24 that

$$\lambda_o \cong \mu \tan \alpha_R + \frac{C_T}{2\mu}$$

Therefore, an approximate relation which would be good at the endpoints can be written as

$$\lambda_{ap} = \mu \tan \alpha_R + \frac{C_T}{2\left[\mu \tan \alpha_R + \frac{C_T}{2(\lambda_H + \mu)} + \mu\right]} \qquad \text{(D.9)}$$

Using this expression, λ_o can be approximated by

$$\lambda_o = \mu \tan \alpha_R + \frac{C_T}{2\left[\lambda_{ap}^2 + \mu^2\right]^{1/2}} \qquad \text{(D.10)}$$

Expression D.10 can be considered to be an approximate solution to the quartic (D.8). The maximum error due to the approximation occurs at $\mu = 0.05$ and is 7%, at $\mu = 0.1$ the error is 2.5%, at $\mu = 0.15$ the error is less than 0.8% and afterward (D.10) is equal to(D.8) up to 3 significant digits.

Therefore, Eq. 8.10 was used instead of solving Eq. D.8 by iteration for every case considered.

Note that λ_H in Eq. D.9 is calculated from $\lambda_H = \sqrt{C_T/2}$.

APPENDIX E

THRUST COEFFICIENT FOR A HINGELESS BLADE IN FORWARD FLIGHT

In this appendix, the thrust coefficient of a hingeless rotor will be derived. All quantities are referred to the hub plane. According to Bramwell (Ref. 20), the motion of the blade as represented by one elastic mode is sufficient for the derivation of the thrust coefficient. The contributions due to lagging velocity in U_P and U_T will be neglected.

With these assumptions and Eqs. 3.7, 3.8, 3.14, and 3.15, the velocity components U_P and U_T can be written as

$$U_P = \left[\lambda_0 + \mu \eta_1' \beta_1 \cos\psi + \frac{e}{R} \eta_1 \dot{\beta}_1^* \right] \Omega R \tag{E.1}$$

$$U_T = \Omega R \left(\mu \sin\psi + \bar{x} \right) \tag{E.2}$$

From Eq. 3.12

$$T \simeq \frac{nb}{2\pi} \int_0^{2\pi} \int_{\bar{A}}^{\bar{B}} L_2 \, e \, d\bar{x} \, d\psi = \frac{nb}{2\pi} (bR) a \rho_a e \int_0^{2\pi} \int_{\bar{A}}^{\bar{B}} U_T^2 \left(\theta - \frac{U_P}{U_T} \right) d\bar{x} \, d\psi \tag{E.3}$$

Assuming a cyclic pitch variation given by

$$\theta = \theta_0 + \theta_{1S} \sin\psi + \theta_{1C} \cos\psi \tag{E.4}$$

the corresponding flapping motion can be represented by

$$\beta_1 = \beta_1^\circ + \beta_{1S} \sin\psi + \beta_{1C} \cos\psi \tag{E.5}$$

The substitution of relations E.1, E.2, E.4, E.5 into E.3 yields, after a considerable amount of algebraic manipulation,

$$C_T = \frac{\sigma a}{2}\left(\frac{\ell}{R}\right)\left\{\frac{\theta_o}{3}\left(3F^{18} + \frac{3}{2}\mu^2 F^{16}\right) - F^{17}\lambda_o + \mu F^{17}\theta_{1s}\right.$$

$$\left. - \frac{g_{1c}}{2}\left(\int_{\bar{A}}^{\bar{B}} \bar{x}\eta_1' d\bar{x} - \frac{\ell}{R}F^3\right)\mu\right\}$$

(E.6)

For $\bar{A} \tilde{=} 0$, $\bar{B} \tilde{=} 1.0$, by integration by parts

$$\int_{\bar{A}}^{\bar{B}} \bar{x}\eta_1' d\bar{x} = 1 - F^3$$

From its definition $F^3 \tilde{\sim} 0.5$, therefore, the last term of Eq. E.6 is negligible, and the thrust coefficient is given by

$$C_T = \frac{\sigma a}{2}\left(\frac{\ell}{R}\right)\left\{\frac{\theta_o}{3}\left(3F^{18} + \frac{3}{2}\mu^2 F^{16}\right) - F^{17}\lambda_o + \mu F^{17}\theta_{1s}\right\} \qquad \text{(E.7)}$$

where the quantities F^{16}, F^{17}, F^{18} are defined in Appendix C.

Equation E.7 agrees with the corresponding equation given in Ref. 20.

APPENDIX F

APPROXIMATE TRIM EQUATIONS FOR A HINGELESS ROTOR

F.1 Assumptions and Basic Equations

In this appendix, an approximate method for calculating the value of collective pitch θ_o and the appropriate values of α_R, θ_{1c}, θ_{1s} for a given flight condition will be described. The flight condition is determined from the values of C_T and μ which are assumed to be known.

The method of calculation is based upon the following assumptions:

(1) The helicopter is in steady level flight.

(2) Pitching and rolling moments on the rotor are equal to zero.

(3) The rotor hub and the helicopter center of gravity coincide, i.e., the whole aircraft is represented by a point mass coinciding with the hub.

(4) The cyclic pitch variation is assumed to be given by Eq. E.4 and the corresponding flapping motion is given by Eq. E.5.

(5) The angle α_R is small. Then $\sin \alpha_R \tilde{=} \alpha_R$, $\cos \alpha_R = 1$.

The geometry of the problem is given in Fig. F.1.

The equations of equilibrium, tangential and normal to the flight path, can be written as

$$m_T \dot{V} = m_T g \sin \gamma_F - D_{TOT} \tag{F.1}$$

$$m_T V \dot{\gamma}_F = -L + m_T g \cos \gamma_F \tag{F.2}$$

From assumption (2), the moment equilibrium in pitch and roll yields

$$M_{mr} = 0 \tag{F.3}$$

$$M_{\ell r} = 0 \tag{F.4}$$

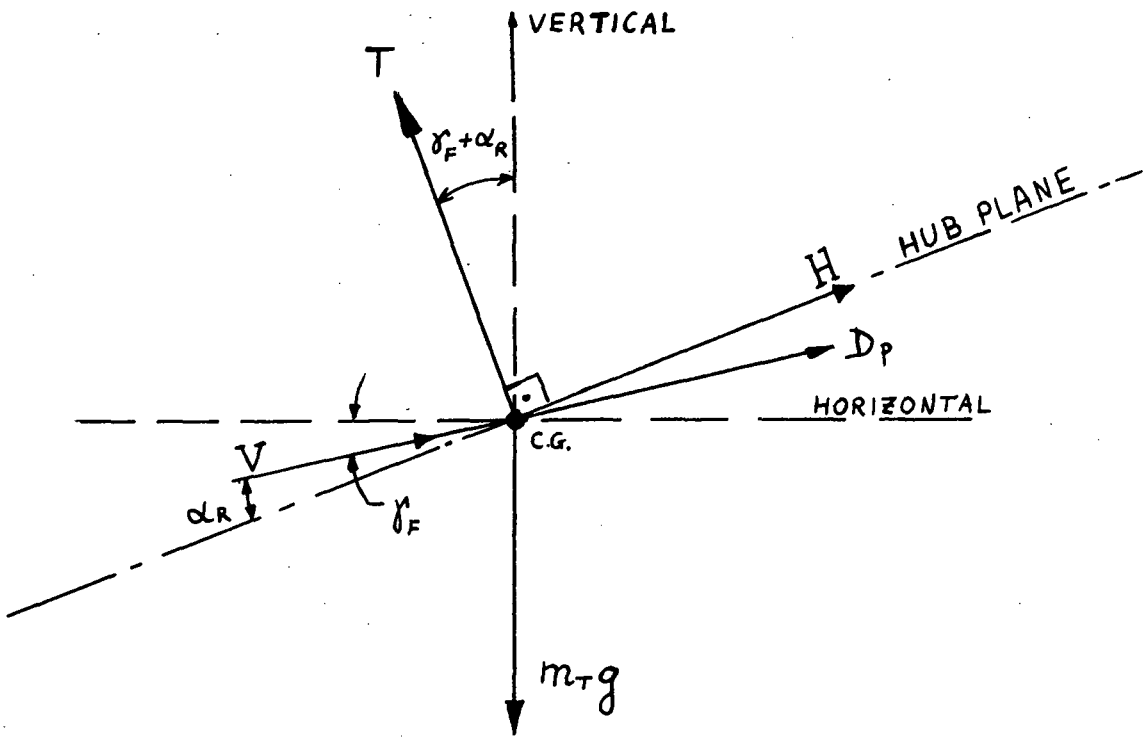

FIG. F.1 GEOMETRY FOR TRIM CALCULATION

These four equations are sufficient to determine the four unknowns θ_o, α_R, θ_{1c}, and θ_{1s}.

From assumption (1), $\gamma = \dot{\gamma} = 0$ $\dot{V} = 0$, and Eqs. F.1 and F.2 reduce to

$$D_{TOT} = 0 \tag{F.5}$$

$$L = m_T g \tag{F.6}$$

From Fig. F.1

$$D_{TOT} = -T\sin\alpha_R + H\cos\alpha_R + D_p \tag{F.7}$$

$$L \cong T\cos\alpha_R \tag{F.8}$$

The drag of the helicopter can be represented by using the equivalent flat-plate area

$$D_p = \frac{1}{2}\rho V^2 f \tag{F.9}$$

With these relations and assumption (5), Eq. F.5 can be rewritten in coefficient form

$$-C_T\alpha_R + C_H + \frac{1}{2}\left(\frac{f}{\pi R^2}\right)\mu^2 = 0 \tag{F.10}$$

In order to solve the problem, the quantities C_H, M_{mr}, $M_{\ell r}$ must be evaluated.

F.2 The Pitching and Rolling Moments

Neglecting the Coriolis forces, Eqs. 3.1 and 3.3 yield

$$\frac{\partial^2}{\partial x_o^2}\left[(EI)_y \frac{\partial^2 w}{\partial x_o^2}\right] - \frac{\partial}{\partial x_o}\left(T\frac{\partial w}{\partial x_o}\right) + m\frac{\partial^2 w}{\partial t^2} = L_z \tag{F.11}$$

By integration, the moment at the blade root due to aerodynamic, centrifugal and inertia forces can be written as (for $\ell = R$, $x_o = x$, and $e_1 = 0$)

$$M_R(0,\psi) = \int_0^{\ell} \left[L_z - m\Omega^2 \frac{\partial^2 w}{\partial \psi^2} - m\Omega^2 w \right] x_o \, dx_o \tag{F.12}$$

Using one elastic mode given by Eq. 3.7, Eqs. F.11 and F.12 yield

$$M_R(0,\psi) = \ell \int_0^{\ell} \left\{ \frac{d^2}{dx_o^2} \left[(EI)_y \frac{d^2\eta_1}{dx_o^2} \right] - \frac{d}{dx_o}\left(T \frac{d\eta_1}{dx_o} \right) - m\Omega^2 \eta_1 \right\} g_1 x_o \, dx_o \tag{F.13}$$

From the free vibration problem equation (A.2)

$$\frac{d^2}{dx_o^2} \left[(EI)_y \frac{d^2\eta_1}{dx_o^2} \right] - \frac{d}{dx_o}\left(T \frac{d\eta_1}{dx_o} \right) = m\bar{\omega}_{F1}^2 \Omega^2 \eta_1 \tag{F.14}$$

From Eqs. F.13, F.14, and D.15

$$M_R(0,\psi) = \ell^3 \Omega^2 (\bar{\omega}_{F1}^2 - 1)(g_1^0 + g_{1c}\cos\psi + g_{1s}\sin\psi) \int_0^1 m \bar{x}_o \eta_1 \, d\bar{x}_o \tag{F.15}$$

According to Fig. F.2 below, the pitching and rolling moments are obtained from M_R by a simple vector decomposition.

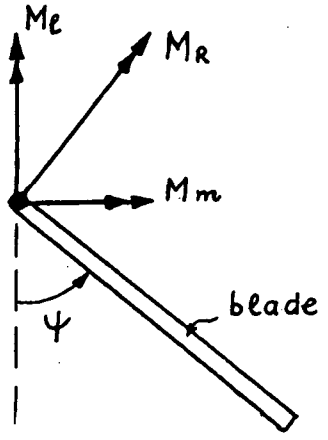

FIG. F.2 BLADE ROOT MOMENT DECOMPOSITION

$$M_m = M_R(0,\psi)\cos\psi$$
$$M_\ell = M_R(0,\psi)\sin\psi \qquad \text{(F.16)}$$

For trim purposes, the average values of these quantities, per revolution, are required.

$$M_{ma} = \frac{1}{2\pi}\int_0^{2\pi} M_R(0,\psi)\cos\psi\, d\psi \qquad \text{(F.17)}$$
$$M_{\ell a} = \frac{1}{2\pi}\int_0^{2\pi} M_R(0,\psi)\sin\psi\, d\psi$$

From Eqs. F.17 and F.15

$$M_{ma} = \frac{1}{2}(\bar{\omega}_{F1}^2 - 1)\ell^3\Omega^2 g_{1C}\int_0^1 m\bar{x}_0\eta_1\, d\bar{x}_0 \qquad \text{(F.18)}$$
$$M_{\ell a} = \frac{1}{2}(\bar{\omega}_{F1}^2 - 1)\ell^3\Omega^2 g_{1S}\int_0^1 m\bar{x}_0\eta_1\, d\bar{x}_0$$

Equation F.18 represents pitching and rolling moments due to one blade, for n_b blades

$$M_{mr} = M_{ma}\, n_b \qquad \text{(F.19)}$$
$$M_{\ell r} = M_{\ell a}\, n_b$$

Thus, Eqs. F.3 and F.4 are equivalent to the requirement that

$$g_{1C} = g_{1S} = 0 \qquad \text{(F.20)}$$

F.3 Flapping Coefficients

The so-called "flapping coefficients" are obtained from the steady-state solution of the flap equation when the Coriolis forces, damping and displacements or velocities, due to lag motion, are neglected. In the analogy to previous derivations, only one elastic mode is used. From Eq. 3.18

$$\bar{M}_{F1}\,\ddot{g}_1^{**} + \bar{M}_{F1}\,\bar{\omega}_{F1}^{-2} g_1 = \quad A_{F1} \tag{F.21}$$

With $\bar{\lambda}_{1c} = 0$, from Eq. C.3

$$A_{F1} = \frac{\gamma}{2}\left(\frac{\ell}{R}\right)^2 \Big\{ \Big[F^1\theta - F^2\lambda_0 + F^3\theta\frac{\mu^2}{2} + \mu\left(2\theta F^2 - \lambda_0 F^3\right)\sin\psi$$

$$- \frac{\mu^2}{2} F^3\theta\cos 2\psi - \mu\Big(F^6\cos\psi +$$

$$\frac{\mu}{2} F^7 \sin 2\psi\Big) g_1 - \frac{\ell}{R}\left(F^8 + \mu F^9\sin\psi\right)\ddot{g}_1^{*} \Big\} \tag{F.22}$$

Substituting Eqs. E.14 and E.15 into Eqs. F.21 and F.22, together with the requirement that the coefficients of the constant term, cos ψ-term and sin ψ-term should be equal to zero, yields the following equations:

$$\bar{\omega}_{F1}^2 g_1^0 - \frac{\gamma}{2}\left(\frac{\ell}{R}\right)\frac{1}{\bar{M}_{F1}}\Big[\theta_0\left(F^1 + \frac{1}{2}F^3\mu^2\right) - F^2\lambda_0 + \mu F^2\theta_{1S}$$

$$- \frac{\gamma}{2}\left(\frac{\ell}{R}\right)^2\frac{1}{\bar{M}_{F1}}\Big[-\frac{F^6}{2} + \left(\frac{\ell}{R}\right)\frac{F^9}{2}\Big]\mu g_{1c} = 0 \tag{F.23}$$

From the cos ψ-term:

$$g_{1c}\left(\bar{\omega}_{F1}^2 - 1\right) - \frac{\gamma}{2}\left(\frac{\ell}{R}\right)^2\frac{1}{\bar{M}_{F1}}\Big[\Big(F^1 + F^3\frac{\mu^2}{4}\Big)\theta_{1c} - \mu g_1^0 F^6$$

$$- g_{1S}\Big(\frac{\ell}{R}F^8 + F^7\frac{\mu^2}{4}\Big)\Big] = 0 \tag{F.24}$$

From the sin ψ-term:

$$g_{1S}\left(\bar{\omega}_{F1}^{-2}-1\right)-\frac{\gamma}{2}\left(\frac{\ell}{R}\right)^2\frac{1}{M_{F1}}\left[\left(F'+3F^3\frac{\mu^2}{4}\right)\theta_{1S}+\right.$$

$$\left.+2\mu\theta_0F^2-\mu\lambda_0F^3+g_{1C}\left(\frac{\ell}{R}F^8-\frac{\mu^2}{4}F^7\right)\right]=0 \qquad \text{(F.25)}$$

Using Eq. F.20, taking $(\ell/R) = 1$, $\bar{A} = 0$, $\bar{B} = 1$, m = const., Eqs. F.23 through F. 25 can be rewritten so as to be similar to the equations given in Bramwell (Ref. 20)

$$\bar{\omega}_{F1}^{-2}\tilde{g}_1^{\circ}-\frac{\gamma}{6}\left[\theta_0\left(\tilde{C}_1+\frac{1}{2}\mu\tilde{G}_1\right)-\tilde{F}_1\lambda_0+\mu\tilde{F}_1\theta_{1S}\right]=0 \qquad \text{(F.26)}$$

$$\left[\left(\tilde{C}_1+G_1\frac{3}{4}\mu^2\right)\theta_{1S}+2\mu\theta_0\tilde{F}_1-\mu\lambda_0\tilde{G}_1\right]=0 \qquad \text{(F.27)}$$

$$-\frac{\gamma}{2}\mu\left[\tilde{\eta}(1)^2-\tilde{D}_1\right]\tilde{g}_1^{\circ}-\frac{\gamma}{6}\left[-\left(\tilde{C}_1+\tilde{G}_1\frac{\mu^2}{4}\right)\theta_{1C}\right]=0 \qquad \text{(F.28)}$$

where

$$\tilde{C}_1\cong F'/F^9 \qquad \tilde{G}_1\cong F^3/F^9$$
$$\tilde{F}_1\cong F^2/F^9 \qquad \tilde{D}_1=1 \qquad \text{(F.29)}$$
$$\tilde{\eta}_1(1)\cong\eta_1(1)/F^9$$

and

$$F^6\cong\frac{1}{2}-\frac{1}{2}F^9$$

From Eqs. F.26 through F. 28

$$\theta_{1S} = \frac{\mu\lambda_0 \tilde{G}_1 - 2\mu\theta_0 \tilde{F}_1}{\tilde{C}_1 + \tilde{G}_1 \frac{3}{4}\mu^2} \tag{F.30}$$

$$\tilde{q}_1^{\,o} = \frac{\gamma}{2}\omega_{F1}^{-2}\left[\theta_0\left(\tilde{C}_1 + \frac{1}{2}\mu^2\tilde{G}_1 - \frac{2\mu^2\tilde{F}_1}{\tilde{C}_1 + \tilde{G}_1\frac{3}{4}\mu^2}\right) + \lambda_0\left(\frac{\mu^2\tilde{F}_1\tilde{G}_1}{\tilde{C}_1 + \tilde{G}_1\frac{3}{4}\mu^2} - \tilde{F}_1\right)\right] \tag{F.31}$$

$$\theta_{1C} = \frac{\mu}{2}\left[\tilde{\eta}_1^{\,2}(1) - \tilde{D}_1\right]\tilde{q}_1^{\,o} \Big/ \left[\tilde{C}_1 + \frac{\mu^2}{4}\tilde{G}_1\right] \tag{F.32}$$

F.4 The Horizontal-Force Coefficient

The horizontal force per unit span is given by the following relation

$$\frac{dH}{dx_0} = (L_z\varphi + L_y)\sin\psi - L_z\frac{\partial w}{\partial x_0}\cos\psi \tag{F.33}$$

where $\phi = \arctan(U_P/U_T) \tilde{=} U_P/U_T$.

Using Eqs. 3.12, 3.13 and 3.7, the average horizontal force per revolution can be written as

$$H = \frac{n_b (bR) \rho_a \ell}{2\pi} \int_{\bar{A}}^{\bar{B}} \int_0^{2\pi} \left\{ \left[U_T^2 C_{do} + a \left(U_T U_P \theta - U_P^2 \right) \right] \sin\psi \right.$$

$$\left. - a \left(\theta U_T^2 - U_P U_T \right) g_1 \eta_1' \cos\psi \right\} d\bar{x}_0 \, d\psi \qquad \text{(F.34)}$$

The substitution of Eqs. E.11, E.12, E.14, E.15 and F.20 yields, after a considerable amount of algebraic manipulation:

$$C_H = \frac{1}{4} \sigma \mu C_{do} \left(\frac{\ell}{R} \right) + \frac{\sigma a}{4} \left(\frac{\ell}{R} \right) \left[\theta_0 \lambda_0 \mu F^{16} + \theta_{1S} F^{17} \lambda_0 \right]$$

$$- \tilde{g}_1^0 \left(F^{18} \theta_{1C} - \mu \tilde{g}_1^0 F^{19} \right) \frac{\sigma a}{4} \left(\frac{\ell}{R} \right) \qquad \text{(F.35)}$$

where F^{18} and F^{19} are defined in Appendix C.

For consistency with the previous section, let

$$\left(\frac{\ell}{R} \right) = 1.0 \; ; \; \bar{A} = 0 \; ; \; \bar{B} = 1$$

and introducing the usual correction for radial flow effects, Eq. F.35 can be rewritten as

$$C_H = 0.45 \sigma \mu C_{do} + \frac{\sigma a}{4} \left[\theta_0 \lambda_0 \mu F^{16} + \theta_{1S} F^{17} \lambda_0 \right]$$

$$- \tilde{g}_1^0 \left(F^{19} \theta_{1C} - \mu \tilde{g}_1^0 F^{20} \right) \frac{\sigma a}{4} \qquad \text{(F.36)}$$

where F^{19}, F^{20} are given in Appendix C.

F.5 Trim Calculation

From Eqs. F.10 and F.36

$$-C_T\alpha_R + 0.45\,\sigma\mu C_{do} + \frac{\sigma a}{4}\left[\theta_o \lambda_o \mu F^{16} + \theta_{1s} F^{17} \lambda_o\right]$$

$$-\tilde{q}_1^o\left(F^{19}\theta_{1c} - \mu \tilde{q}_1^o F^{20}\right)\frac{\sigma a}{4} + \frac{1}{2}\left(\frac{f}{\pi R^2}\right)\mu^2 = 0 \qquad \text{(F.37)}$$

In Eq. F.37, θ_{1s} is given by Eq. F.30, C_T is given by Eq. E.17 and λ_o is given by Eq. D.10.

This system of equations is solved by an iterative process on a digital computer. First θ, α_r are obtained and from their value θ_{1s}, θ_{1c}, and λ_o are also evaluated.

APPENDIX G

DEFINITION OF THE VARIOUS EXPRESSIONS, EQUATIONS, AND QUANTITIES USED IN THE PERTURBATION METHOD

Note that almost all of the expressions given in this section have been checked using the FORMAC algebraic manipulative program.

Equation of $0(\varepsilon^{1/2})$:

$$\left.\begin{aligned} L_1(a_0,b_0) &= \mu_0 F_0(\psi_0,\theta_c) \\ L_2(a_0,b_0) &= \mu_0 H_0(\psi_0,\theta_c) \end{aligned}\right\} \qquad \text{(G.1)}$$

Equations of $0(\varepsilon)$:

$$\left.\begin{aligned} L_1(a_1,b_1) &= \mu_0 F_1(\psi_0,\theta_c,a_0,b_0) + \mu_0^2 J_1(\psi_0,\theta_c) \\ &\quad + \mu_1 F_0(\psi_0,\theta_c) + Q_1(a_0,b_0) \\ L_2(a_1,b_1) &= \mu_0 H_1(\psi_0,\theta_c,a_0,b_0) + \mu_0^2 K_1(\psi_0,\theta_c) \\ &\quad + \mu_1 H_0(\psi_0,\theta_c) + N_1(a_0,b_0) \end{aligned}\right\} \qquad \text{(G.2)}$$

Equations of $0(\varepsilon^{3/2})$:

$$\begin{aligned} L_1(a_2,b_2) &= \mu_0 F_1(\psi_0,\theta_c,a_1,b_1) + \mu_0 F_0(\theta_1,\psi_0) + \\ &\quad + \mu_0 F_2(\psi_0,a_0,b_0) + \mu_0^2 J_2(\psi_0,a_0) + \mu_1 F_1(\psi_0,\theta_c,a_0,b_0) \\ &\quad + \theta_c \mu_0 \mu_1 F^3 C_2 - \sin 2\psi_0\, g_0 C_2 F^7 \mu_0 \mu_1 + \\ &\quad + \cos 2\psi_0\, \theta_c \mu_0 \mu_1 C_2 F^3 + Q_2(a_0,b_0,a_1,b_1) \end{aligned}$$

$$\begin{aligned} L_2(a_2,b_2) &= \mu_0 H_1(\psi_0,\theta_c,a_1,b_1) + \mu_0 H_0(\psi_0,\theta_1) + \\ &\quad \mu_0 H_2(\psi_0,\theta_c,a_0,b_0) + \mu_0^2 K_2(\psi_0,a_0) + \mu_1 H_1(\psi_0,\theta_c,a_0,b_0) \\ &\quad + \sin 2\psi_0\, \theta_c g_0 \mu_0 \mu_1 C_6 L'' + N_2(a_0,b_0,a_1,b_1) \end{aligned} \qquad \text{(G.3)}$$

The operators L_1, L_2 are:

$$L_1(a,b) = \frac{\partial^2 a}{\partial \psi_0^2} + g_{D10}\frac{\partial a}{\partial \psi_0} + \omega_{F10}^2 a - X_{H0}\frac{\partial b}{\partial \psi_0} \tag{G.4}$$

$$L_2(a,b) = \frac{\partial^2 b}{\partial \psi_0^2} + g_{D20}\frac{\partial b}{\partial \psi_0} + \omega_{L10}^2 b - Y_{G0}\frac{\partial a}{\partial \psi_0} \tag{G.5}$$

$$Q_1(a_0,b_0) = C_4 a_0 \frac{\partial b_0}{\partial \psi_0} + C_1\left(\frac{\ell}{R}\right)\left[\theta_c F^{13}\left(\frac{\partial b_0}{\partial \psi_0}\right)^2 + F^{15}\frac{\partial a_0}{\partial \psi_0}\frac{\partial b_0}{\partial \psi_0}\right] \tag{G.6}$$

$$N_1(a_0,b_0) = -C_{11} a_0 \frac{\partial a_0}{\partial \psi_0} - C_7\frac{\ell}{R}\left[\left(\frac{\partial a_0}{\partial \psi_0}\right)^2 L^{18} + \theta_c L^{19}\frac{\partial a_0}{\partial \psi_0}\frac{\partial b_0}{\partial \psi_0}\right] \tag{G.7}$$

$$\begin{aligned} Q_2(a_0,b_0,a_1,b_1) = {} & C_4 a_1 \frac{\partial b_0}{\partial \psi_0} + C_4 a_0 \frac{\partial b_1}{\partial \psi_0} + 2C_1\left(\frac{\ell}{R}\right)\theta_c F^{13}\frac{\partial b_1}{\partial \psi_0}\frac{\partial b_0}{\partial \psi_0} \\ & + C_1\frac{\ell}{R}F^{15}\left[\frac{\partial a_1}{\partial \psi_0}\frac{\partial b_0}{\partial \psi_0} + \frac{\partial a_0}{\partial \psi_0}\frac{\partial b_1}{\partial \psi_0}\right] + X_1\frac{\partial b_0}{\partial \psi_0} \\ & - \eta_{11}\frac{\partial a_0}{\partial \psi_0} + X_{H0}\frac{\partial b_0}{\partial \psi_1} - g_{D10}\frac{\partial a_0}{\partial \psi_1} - 2\frac{\partial^2 a_0}{\partial \psi_0 \partial \psi_1} \end{aligned} \tag{G.8}$$

$$\begin{aligned} N_2(a_0,b_0,a_1,b_1) = {} & -C_7\left(\frac{\ell}{R}\right)\left[2L^{18}\frac{\partial a_1}{\partial \psi_0}\frac{\partial a_0}{\partial \psi_0} + \theta_c L^{19}\left(\frac{\partial a_1}{\partial \psi_0}\frac{\partial b_0}{\partial \psi_0} + \right.\right. \\ & \left.\left.\frac{\partial a_0}{\partial \psi_0}\frac{\partial b_1}{\partial \psi_0}\right] - C_{11} a_0 \frac{\partial a_1}{\partial \psi_0} - \eta_{21}\frac{\partial b_0}{\partial \psi_0} + Y_1\frac{\partial a_0}{\partial \psi_0} \\ & + Y_{G0}\frac{\partial a_0}{\partial \psi_1} - g_{D20}\frac{\partial b_0}{\partial \psi_1} - 2\frac{\partial^2 b_0}{\partial \psi_0 \partial \psi_1} - C_{11} a_1 \frac{\partial a_0}{\partial \psi_0} \end{aligned} \tag{G.9}$$

$$F_o(\psi_o,\theta_c) = C_2\left[(2F^2\theta_c - F^3\lambda_{oc})\sin\psi_o - g_o F^6\cos\psi_o\right]$$

$$H_o(\psi_o,\theta_c) = C_6\left[\left(2L'\frac{\ell d_o}{a} + \lambda_{oc}\theta_c L^2\right)\sin\psi_o + (\theta_c L'^0 - 2L''\lambda_{oc})\, g_o\cos\psi_o\right] \qquad \text{(G.10)}$$

Note that starting with Eq. G.10, the term $L^1(C_{d_o})/a$ will be neglected in all of the calculations.

$$F_1(\psi_o,\theta_c,a_o,b_o) = \left[-2\theta_c\frac{\ell}{R}C_2F''\sin\psi_o\frac{\partial b_o}{\partial\psi_o} - C_1F^9\frac{\partial a_o}{\partial\psi_o}\sin\psi_o - C_2F^6a_o\cos\psi_o + C_2\left(\frac{\ell}{R}\right)g_oF^{14}\frac{\partial b_o}{\partial\psi_o}\cos\psi_o\right] \qquad \text{(G.11)}$$

$$J_1(\psi_o,\theta_c) = -\frac{1}{2}C_2g_oF^7\sin 2\psi_o + \frac{1}{2}C_2\theta_cF^3\cos 2\psi_o + \frac{1}{2}\theta_cC_2F^3 \qquad \text{(G.12)}$$

$$H_1(\psi_o,\theta_c,a_o,b_o) = C_7L^8\theta_c\frac{\partial a_o}{\partial\psi_o}\sin\psi_o - 2g_oC_7L'^7\frac{\partial a_o}{\partial\psi_o}\cos\psi_o - C_7L'^6\theta_cg_o\frac{\partial b_o}{\partial\psi_o}\cos\psi_o + C_6L'^0a_o\theta_c\cos\psi_o - 2\lambda_{oc}C_6L''a_o\cos\psi_o \qquad \text{(G.13)}$$

$$K_1(\theta_c,\psi_o) = \frac{1}{2}g_oC_6\theta_cL''\sin 2\psi_o \qquad \text{(G.14)}$$

$$F_2(\psi_o,a_o,b_o) = a_oF^{14}C_2\frac{\ell}{R}\frac{\partial b_o}{\partial\psi_o}\cos\psi_o \qquad \text{(G.15)}$$

$$J_2(\psi_0, a_0) = -\frac{1}{2} c_2 F^7 a_0 \sin 2\psi_0 \tag{G.16}$$

$$H_2(\psi_0, \theta_c, a_0, b_0) = -2\cos\psi_0 a_0 c_7 L^{17} \frac{\partial a_0}{\partial \psi_0} - \cos\psi_0 a_0 c_7 L^{16} \frac{\partial b_0}{\partial \psi_0} \tag{G.17}$$

$$K_2(a_0, \psi_0) = \frac{1}{2} \theta_c a_0 \sin 2\psi_0 \tag{G.18}$$

$$\begin{Bmatrix} \alpha_2 \\ \beta_2 \end{Bmatrix} = (i\omega_c) \underset{\sim}{M}^{-1}(2\omega_c) \begin{Bmatrix} c_4 v_r + c_1 \left(\frac{\ell}{R}\right) i\omega_c (F^{13}\theta_c + F^{15} v_r) \\ -c_{11} v_r^2 - c_7 \left(\frac{\ell}{R}\right) v_r i\omega_c (L^{18} v_r + \theta_c L^{19}) \end{Bmatrix} \tag{G.19}$$

where

$$\underset{\sim}{M}(\Lambda) = \begin{bmatrix} \omega_{F10}^2 - \Lambda^2 + i g_{D10} \Lambda & -X_{H0} i \Lambda \\ -Y_{G0} i \Lambda & \omega_{L10}^2 - \Lambda^2 + i g_{D20} \Lambda \end{bmatrix} \tag{G.20}$$

$$\begin{Bmatrix} \alpha_3 \\ \beta_3 \end{Bmatrix} = \begin{pmatrix} \frac{\omega_c}{2\omega_{F10}^2} \left\{ c_4 i \left[(v_r)^* - v_r \right] + c_1 \frac{\ell}{R} \omega_c \left[2F^{13}\theta_c + F^{15}\left(v_r + (v_r)^*\right) \right] \right\} \\ -\frac{c_7}{2}\left(\frac{\ell}{R}\right)\frac{\omega_c^2}{\omega_{L10}^2} \left\{ 2L^{18}(v_r)^* + \theta_c L^{19} \left[v_r + (v_r)^* \right] \right\} \end{pmatrix} \tag{G.21}$$

$$P_1 = \left[-(2i\omega_c + g_{D10}) v_r + X_{H0} \right] \tag{G.22}$$

$$P_2 = \left[-2i\omega_c - g_{D20} + Y_{G0} v_r \right] \tag{G.23}$$

$$P_3 = \left[-\eta_{11} v_r + X_1 \right] i\omega_c \tag{G.24}$$

$$P_4 = \left[-\eta_{21} i\omega_c + Y_1 i\omega_c v_r \right] \tag{G.25}$$

$$P_{15} = c_4\left[-i\omega_c\alpha_2 + 2i\omega_c\alpha_3 + 2i\omega_c\beta_2(v_r)^*\right]$$

$$+ c_1\left(\frac{\ell}{R}\right)\omega_c^2\left[4F^{13}\theta_c\beta_2 + 2\alpha_2F^{15} + 2F^{15}\beta_2(v_r)^*\right] \qquad \text{(G.26)}$$

$$P_{16} = c_{11}\left[(v_r)^* i\omega_c(-\alpha_2) - 2\alpha_3 i\omega_c v_r\right] - c_7\left(\frac{\ell}{R}\right)\omega_c^2\left[4\alpha_2L^{18}(v_r)^*\right.$$

$$\left. + (v_r)^* 2\beta_2\theta_c L^{19} + 2\alpha_2\theta_c L^{19}\right] \qquad \text{(G.27)}$$

$$\begin{Bmatrix} a_{02} \\ b_{02} \end{Bmatrix} = \underset{\sim}{M}^{-1}(1) \begin{Bmatrix} P_9 \\ P_{10} \end{Bmatrix} \qquad \text{(G.28)}$$

$$P_9 = -\frac{1}{2}g_0C_2F^6 - i\theta_cF^2C_2 + \frac{i}{2}\lambda_{oc}C_2F^3 \qquad \text{(G.29)}$$

$$P_{10} = -\frac{1}{2}i\lambda_{oc}\theta_cC_6L^2 + \frac{1}{2}\theta_cg_0C_6L^{10} - \lambda_{oc}g_0C_6L^{11} \qquad \text{(G.30)}$$

$$\left.\begin{aligned} \bar{\alpha}_3 &= 2\alpha_3 \\ \bar{\beta}_3 &= 2\beta_3 \end{aligned}\right\} \qquad \text{(G.31)}$$

$$\begin{Bmatrix} a_{13} \\ b_{13} \end{Bmatrix} = \underset{\sim}{M}^{-1}(1-\omega_c) \begin{Bmatrix} P_{11} \\ P_{12} \end{Bmatrix} \qquad \text{(G.32)}$$

$$\begin{Bmatrix} a_{14} \\ b_{14} \end{Bmatrix} = \underset{\sim}{M}^{-1}(1+\omega_c) \begin{Bmatrix} P_{13} \\ P_{14} \end{Bmatrix} \qquad \text{(G.33)}$$

$$\begin{Bmatrix} a_{15} \\ b_{15} \end{Bmatrix} = \underset{\sim}{M}^{-1}(2) \begin{Bmatrix} P_{17} \\ P_{18} \end{Bmatrix} \tag{G.34}$$

where P_{11} through P_{14} and P_{17} through P_{20} are given below:

$$\begin{Bmatrix} a_{16} \\ b_{16} \end{Bmatrix} = \underset{\sim}{M}^{-1}(0) \begin{Bmatrix} P_{19} \\ P_{20} \end{Bmatrix} \tag{G.35}$$

$$\begin{aligned} P_{11} = {} & b_{02}(v_r)^* \omega_c F^{15} C_1\left(\frac{\ell}{R}\right) + a_{02}\omega_c F^{15} C_1\left(\frac{\ell}{R}\right) - i a_{02}\omega_c C_4 + \\ & + i b_{02}(v_r)^* C_4 + 2\theta_c b_{02}\omega_c F^{13} C_1\left(\frac{\ell}{R}\right) - \frac{1}{2} i\omega_c C_2\left(\frac{\ell}{R}\right) F^{14} g_0 \\ & + \frac{1}{2}(v_r)^* \omega_c C_1 F^9 - \frac{1}{2}(v_r)^* C_2 F^6 + \omega_c F^{11} C_2\left(\frac{\ell}{R}\right)\theta_c \end{aligned} \tag{G.36}$$

$$\begin{aligned} P_{12} = {} & -\theta_c b_{02}(v_r)^* \omega_c \left(\frac{\ell}{R}\right) C_7 L^{19} - \theta_c a_{02}\omega_c \left(\frac{\ell}{R}\right) C_7 L^{19} \\ & - (v_r)^* \lambda_{oc} C_6 L^{11} - \frac{1}{2}(v_r)^* \omega_c \theta_c L^8 C_7 + i(v_r)^* \omega_c g_0 L^{17} C_7 \\ & - i a_{02}(v_r)^* \omega_c C_{11} - i a_{02}(v_r)^* C_{11} - 2 a_{02}(v_r)^* \omega_c \left(\frac{\ell}{R}\right) C_7 L^{18} \\ & + \frac{1}{2} i\omega_c \theta_c g_0 L^{16} C_7 + \frac{1}{2}(v_r)^* \theta_c C_6 L^{10} \end{aligned} \tag{G.37}$$

$$\begin{aligned} P_{13} = {} & -b_{02}\omega_c v_r C_1\left(\frac{\ell}{R}\right) F^{15} - a_{02}\omega_c F^{15} C_1\left(\frac{\ell}{R}\right) + i b_{02} v_r C_4 \\ & + i a_{02}\omega_c C_4 - 2\theta_c b_{02}\omega_c F^{13} C_1\left(\frac{\ell}{R}\right) + \frac{1}{2} i\omega_c C_2\left(\frac{\ell}{R}\right) F^{14} g_0 \\ & - \frac{1}{2}\omega_c v_r C_1 F^9 - \frac{1}{2} v_r C_2 F^6 - \omega_c F^{11} C_2\left(\frac{\ell}{R}\right)\theta_c \end{aligned} \tag{G.38}$$

$$P_{14} = \theta_c\, b_{02}\, \omega_c\, v_r\, c_7 \left(\frac{\ell}{R}\right) L^{19} + \theta_c\, a_{02}\, \omega_c\, c_7 \left(\frac{\ell}{R}\right) L^{19}$$
$$- v_r\, \lambda_{0c}\, c_6 L^{11} + \frac{1}{2}\, \omega_c\, v_r\, \theta_c\, L^8\, c_7 - i\omega_c\, v_r\, g_0\, c_7\, L^{17}$$
$$- i\, a_{02}\, \omega_c\, v_r\, c_{11} - i\, a_{02}\, v_r\, c_{11} + 2\, a_{02}\, \omega_c\, v_r\, \frac{\ell}{R}\, c_7\, L^{18} \qquad \text{(G.39)}$$
$$- \frac{1}{2}\, i\omega_c\, \theta_c\, g_0\, L^{16}\, c_7 + \frac{1}{2}\, v_r\, \theta_c\, c_6\, L^{10}$$

$$P_{17} = - b_{02}\, a_{02}\, c_1 \left(\frac{\ell}{R}\right) F^{15} + i\, b_{02}\, a_{02}\, c_4 - \theta_c\, b_{02}^2\, c_1 \left(\frac{\ell}{R}\right) F^{13}$$
$$+ \frac{1}{4}\, i c_2\, F^7\, g_0 + \frac{1}{2}\, i b_{02}\, c_2 \left(\frac{\ell}{R}\right) F^{14}\, g_0 - \frac{1}{2}\, a_{02}\, c_1\, F^9 \qquad \text{(G.40)}$$
$$- \frac{1}{2}\, a_{02}\, c_2\, F^6 + \frac{1}{4}\, c_2\, \theta_c\, F^3 - b_{02}\, F^{11} c_2\, \frac{\ell}{R}\, \theta_c$$

$$P_{18} = \theta_c\, b_{02}\, a_{02}\, c_7 \left(\frac{\ell}{R}\right) L^{19} - i\, a_{02}^2\, c_{11} + a_{02}^2 \left(\frac{\ell}{R}\right) c_7\, L^{18}$$
$$- a_{02}\, \lambda_{0c}\, c_6 L^{11} - \frac{1}{4}\, i\, \theta_c\, g_0\, c_6\, L^{11} + \frac{1}{2}\, a_{02}\, \theta_c\, L^8\, c_7 \qquad \text{(G.41)}$$
$$- i a_{02}\, g_0\, L^{17}\, c_7 - \frac{1}{2}\, b_{02}\, \theta_c\, g_0\, c_7\, L^{16}\, i + \frac{1}{2}\, a_{02}\, \theta_c\, c_6\, L^{10}$$

$$P_{19} = c_1 \left(\frac{\ell}{R}\right) F^{15} \left[a_{02}\, (b_{02})^* + b_{02}\, (a_{02})^* \right] +$$
$$2\theta_c\, b_{02}\, (b_{02})^*\, c_1\, F^{13} \left(\frac{\ell}{R}\right) + \frac{c_2}{2} \left(\frac{\ell}{R}\right) F^{14}\, g_0 \left[i\, b_{02} + (i\, b_{02})^* \right] \qquad \text{(G.42)}$$
$$+ \frac{c_1\, F^9}{2} \left[a_{02} + (a_{02})^* \right] - \frac{1}{2}\, c_2\, F^6 \left[a_{02} + (a_{02})^* \right]$$
$$+ c_2\, \theta_c\, \frac{F^3}{2} + c_2 \left(\frac{\ell}{R}\right) \theta_c\, F^{11} \left[b_{02} + (b_{02})^* \right] + c_4 \left[i\, b_{02}\, (a_{02})^* + (i\, b_{02})^*\, a_{02} \right]$$

$$P_{20} = -\theta_c C_7\left(\frac{\ell}{R}\right) L^{19}\left[(b_{02})^* a_{02} + (a_{02})^* b_{02}\right] - 2(a_{02})^* a_{02} C_7\left(\frac{\ell}{R}\right) L^{18}$$

$$- C_6 L^{11}\lambda_{oc}\left[a_{02} + (a_{02})^*\right] - \frac{1}{2} C_7 L^8 \theta_c \left[a_{02} + (a_{02})^*\right]$$

$$- C_7 L^{17} g_o \left[(i a_{02}) + (i a_{02})^*\right] - \frac{C_7}{2} g_o L^{16}\theta_c \left[(i b_{02}) + (i b_{02})^*\right]$$

$$+ \frac{1}{2} C_6 L^{10}\theta_c \left[a_{02} + (a_{02})^*\right] \qquad \text{(G.43)}$$

$$P_{21} = C_2\left(\frac{\ell}{R}\right)\theta_c F^{11}\left[(b_{13})^*(1-\omega_c) + b_{14}(1+\omega_c)\right] + i\omega_c a_{16} C_4 +$$

$$i b_{02}(a_{13})^* C_4 - i(b_{02})^* a_{14} C_4 + 2\left(\frac{\ell}{R}\right)\theta_c F^{13} C_1\left[b_{02}(b_{13})^*(1-\omega_c)\right.$$

$$\left. + (b_{02})^* b_{14}(1+\omega_c)\right] - i a_{02}(b_{13})^* C_4(1-\omega_c) + i(a_{02})^* b_{14} C_4(1+\omega_c)$$

$$+ C_1\left(\frac{\ell}{R}\right) F^{15}\left[a_{02}(b_{13})^*(1-\omega_c) + (a_{02})^* b_{14}(1+\omega_c) +\right.$$

$$\left. b_{02}(a_{13})^*(1-\omega_c) + (b_{02})^* a_{14}(1+\omega_c)\right] + \frac{1}{2} C_1 F^9\left[(a_{13})^*(1-\omega_c)\right.$$

$$\left. + a_{14}(1+\omega_c)\right] - \frac{C_2}{2} F^6\left[(a_{13})^* + a_{14}\right] + \frac{1}{2} C_2\left(\frac{\ell}{R}\right) F^{14}\left[-i(b_{13})^* g_o(1-\omega_c)\right.$$

$$\left. + i b_{14} g_o(1+\omega_c) + i\left((b_{02})^* - b_{02}\right) v_r - i\omega_c\left((a_{02})^* + a_{02}\right)\right] \qquad \text{(G.44)}$$

$$P_{22} = \theta_c C_7 \frac{L^8}{2}\left[(\omega_c - 1)(a_{13})^* - (1+\omega_c) a_{14}\right] + C_7 i L^{17} g_o\left[(1-\omega_c)(a_{13})^*\right.$$

$$\left. - (1+\omega_c) a_{14}\right] + C_7 L^{17}\left[-a_{02}(1+\omega_c) v_r + (1-\omega_c) v_r (a_{02})^*\right]$$

$$+ c_7 L^{18} 2 \frac{\ell}{R} \left[a_{02} (a_{13})^* (\omega_c - 1) - (1+\omega_c)(a_{02})^* a_{14} \right]$$

$$+ c_7 L^{19} \theta_c \frac{\ell}{R} \left[b_{02}(\omega_c - 1)(a_{13})^* - (1+\omega_c)(b_{02})^* a_{14} + \right.$$

$$\left. a_{02}(b_{13})^* (\omega_c - 1) - (1+\omega_c)(a_{02})^* b_{14} \right] + c_7 \frac{L^{16}}{2} g_0 \theta_c \left[i(1-\omega_c)(b_{13})^* \right.$$

$$\left. - i(1+\omega_c) b_{14} \right] + \frac{c_7}{2} L^{16} \theta_c \left[i((b_{02})^* - b_{02}) v_r - \omega_c (a_{02} + (a_{02})^*) L \right]$$

$$+ \frac{1}{2} c_6 L^{10} \theta_c \left[(a_{13})^* + a_{14} \right] - c_6 L^{11} \lambda_{oc} \left[(a_{13})^* + a_{14} \right] -$$

$$c_{11} a_{16} \omega_c v_r i - c_{11} \omega_c i a_{02} (a_{13})^* - i (a_{02})^* \omega_c a_{14} c_{11} \qquad \text{(G.45)}$$

$$\begin{Bmatrix} \alpha_1 \\ \beta_1 \end{Bmatrix} = \frac{\underset{\sim}{M}^{-1}(1)}{2} \begin{Bmatrix} - c_2 \left[i (F^2 \theta_c - \lambda_{oc} F^3) + g_0 F^6 \right] \\ c_6 \left[- i L^2 \theta_c \lambda_{oc} + g_0 (\theta_c L^{10} - 2 L^{11} \lambda_{oc} \right] \end{Bmatrix} \qquad \text{(G.46)}$$

$$p_5 = c_1 F^9 \frac{\omega_c}{2} (v_r)^* - \frac{c_2 F^6}{2} (v_r)^* + \left(\frac{\ell}{R} \right) F^{11} \theta_c \omega_c -$$

$$c_2 \frac{g_0}{2} \left(\frac{\ell}{R} \right) F^{14} i \omega_c + \left[- \alpha_1 i \omega_c + i \beta_1 (v_r)^* \right] c_4 +$$

$$c_1 \left(\frac{\ell}{R} \right) \omega_c \left[2 \theta_c F^{13} \beta_1 + \alpha_1 F^{15} + \beta_1 F^{15} (v_r)^* \right] \qquad \text{(G.47)}$$

$$p_6 = c_7 L^{17} g_0 i \omega_c (v_r)^* + \frac{c_7 \theta_c g_0 L^{16} i \omega_c}{2} + c_{11} (v_r)^* i \alpha_1 (\omega_c - 1)$$

$$- c_7 \left(\frac{\ell}{R} \right) \left[2 L^{18} (v_r)^* \alpha_1 \omega_c + \theta_c L^{19} \omega_c \beta_1 (v_r)^* + \theta_c L^{19} \omega_c \alpha_1 \right]$$

$$- \frac{1}{2} c_7 L^8 \theta_c \omega_c (v_r)^* + \frac{c_{12}}{2} (v_r)^* \qquad \text{(G.48)}$$

where C_{12} is given by Eq. G.79.

$$F_{01} = \frac{C_2 (2F^2\theta_c - F^3 \lambda_{oc})}{\varepsilon} \tag{G.49}$$

$$F_{02} = \frac{g_o F^6 C_2}{\varepsilon} \tag{G.50}$$

$$H_{01} = \frac{C_6 \lambda_{oc} \theta_c L^2}{\varepsilon} \tag{G.51}$$

$$H_{02} = \frac{(\theta_c L^{10} - 2L^{11} \lambda_{oc}) g_o}{\varepsilon} \tag{G.52}$$

$$\bar{P}_{11} = -\frac{1}{2} i\omega_c C_2 \frac{\ell}{R} F^{14} g_o + \frac{1}{2} (v_r)^* \omega_c C_1 F^9 - \frac{1}{2} (v_r)^* C_2 F^6 + \omega_c F^{11} C_2 \frac{\ell}{R} \theta_c \tag{G.53}$$

$$\bar{P}_{12} = -(v_r)^* \lambda_{oc} C_6 L^{11} - \frac{1}{2} (v_r)^* \omega_c \theta_c L^8 C_7 + i (v_r)^* \omega_c g_o L^{17} C_7 + \frac{1}{2} i\omega_c \theta_c g_o L^{16} C_7$$
$$+ (v)^* \theta_c C_6 L^{10} \tag{G.54}$$

$$\bar{P}_{13} = \frac{1}{2} i\omega_c C_2 \left(\frac{\ell}{R}\right) F^{14} g_o - \frac{1}{2} \omega_c v_r C_1 F^9 - \frac{1}{2} v_r C_2 F^6 - \omega_c F^{11} C_2 \left(\frac{\ell}{R}\right) \theta_c \tag{G.55}$$

$$\bar{P}_{14} = -v_r \lambda_{oc} C_6 L^{11} + \frac{1}{2} \omega_c v_r \theta_c L^{18} C_7 - i\omega_c v_r g_o C_7 L^{17} \tag{G.56}$$
$$- \frac{1}{2} i\omega_c \theta_c g_o C_7 L^{16} + \frac{1}{2} v_r \theta_c C_6 L^{10}$$

$$\bar{P}_{17} = \frac{1}{4} i C_2 F^7 g_o + \frac{1}{4} C_2 \theta_c F^3 \tag{G.57}$$

$$\bar{P}_{18} = -\frac{1}{4} i\theta_c g_o C_6 L^{11} \tag{G.58}$$

$$\bar{P}_{19} = \frac{C_2 \theta_c F^3}{2} \tag{G.59}$$

$$\bar{P}_{20} = 0 \tag{G.60}$$

$$P_{23} = \left[2 \bar{b}_{15} F^{11} C_2 \left(\frac{\ell}{R}\right) \theta_c + \bar{a}_{15} C_1 F^9 - \frac{1}{2} C_2 F^6 (\bar{a}_{16} + \bar{a}_{15}) + i \bar{b}_{15} C_2 \frac{\ell}{R} g_0 F^{14} \right] \tag{G.61}$$

$$P_{24} = \left[-C_7 L^8 \theta_c \bar{a}_{15} - 2i \bar{a}_{15} g_0 L^{17} C_7 - i \bar{b}_{15} \theta_c g_0 L^{16} C_7 + \frac{1}{2} (\bar{a}_{16} + \bar{a}_{15}) C_6 L^{10} \theta_c - C_6 L^{11} \lambda_{oc} (\bar{a}_{15} + \bar{a}_{16}) \right] \tag{G.62}$$

$$P_{25} = \left\{ i\omega_c C_4 (\bar{a}_{13} - \bar{a}_{14}) + 2 C_1 F^{13} \theta_c \left(\frac{\ell}{R}\right) \omega_c \left[(\omega_c - 1) \bar{b}_{13} + (\omega_c + 1) \bar{b}_{14} \right] + i (1 - \omega_c) \bar{b}_{13} v_r C_4 + i (1 + \omega_c) C_4 \bar{b}_{14} (v_r)^* + C_1 \left(\frac{\ell}{R}\right) F^{15} \omega_c \left[(\omega_c - 1) v_r \bar{b}_{13} + (1 + \omega_c) (v_r)^* \bar{b}_{14} + (\omega_c - 1) \bar{a}_{13} + \bar{a}_{14} (1 + \omega_c) \right] - \frac{1}{2} \bar{\alpha}_3 C_2 F^6 + \frac{1}{2} i \omega_c \left[v_r - (v_r)^* \right] C_2 \frac{\ell}{R} F^{14} \right\} \tag{G.63}$$

$$P_{26} = \left\{ 2\omega_c (1 - \omega_c) v_r \bar{a}_{13} C_7 L^{18} \frac{\ell}{R} - 2\omega_c (1 + \omega_c) (v_r)^* \bar{a}_{14} C_7 L^{18} \frac{\ell}{R} + C_7 \left(\frac{\ell}{R}\right) \theta_c L^{19} \omega_c \left[(1 - \omega_c) \bar{a}_{13} - (1 + \omega_c) \bar{a}_{14} + (1 - \omega_c) v_r \bar{b}_{13} - (1 + \omega_c) \bar{b}_{14} (v_r)^* \right] + \frac{1}{2} C_7 L^{16} \theta_c i \omega_c \left[v_r - (v_r)^* \right] + \frac{1}{2} \bar{\alpha}_3 \theta_c C_6 L^{10} - \bar{\alpha}_3 \lambda_{oc} C_6 L^{11} - i v_r \bar{a}_{13} C_{11} - i (v_r)^* \bar{a}_{14} C_{11} \right\} \tag{G.64}$$

$$P_{27} = \Big[(\omega_c - 1)\, \bar{b}_{13} F^{11} C_2 \left(\frac{\ell}{R}\right) \theta_c - i\omega_c \bar{a}_{15} C_4 + 4\omega_c \bar{b}_{15} \frac{\ell}{R} \theta_c C_1 F^{13}$$
$$+ 2i(v_r)^* \bar{b}_{15} C_4 + 2(v_r)^* \omega_c \bar{b}_{15} C_1 \frac{\ell}{R} F^{15} + 2\omega_c \bar{a}_{15} C_1 \left(\frac{\ell}{R}\right) F^{15}$$
$$+ \frac{1}{2} \bar{a}_{13} C_1 F^9 (\omega_c - 1) + \frac{1}{4} i (v_r)^* C_2 F^7 - \frac{1}{2} \bar{a}_{13} C_2 F^6 +$$
$$\frac{1}{2} (1 - \omega_c) \bar{b}_{13} C_2 \left(\frac{\ell}{R}\right) g_0 i F^{14} \Big] \qquad \text{(G.65)}$$

$$P_{28} = \Big[\frac{1}{2} (1 - \omega_c) \bar{a}_{13} \theta_c L^8 C_7 + (\omega_c - 1) \bar{a}_{13} g_0 C_7 L^{17} i -$$
$$4 (v_r)^* \omega_c \bar{a}_{15} C_7 L^{18} \left(\frac{\ell}{R}\right) - 2\omega_c \bar{a}_{15} \frac{\ell}{R} \theta_c C_7 L^{19}$$
$$- 2 (v_r)^* \omega_c \bar{b}_{15} \frac{\ell}{R} \theta_c C_7 L^{19} + \frac{1}{2} i (\omega_c - 1) \bar{b}_{13} \theta_c g_0 L^{16} C_7$$
$$+ \frac{1}{2} \bar{a}_{13} \theta_c C_6 L^{10} - \bar{a}_{13} \lambda_{oc} C_6 L'' - \frac{1}{4} i (v_r)^* \theta_c C_6 L''$$
$$+ i (v_r)^* \omega_c \bar{a}_{15} C_{11} - 2i (v_r)^* \bar{a}_{15} C_{11} \Big] \qquad \text{(G.66)}$$

$$P_{29} = \Big[2\omega_c (\beta_2)^* F^{11} C_2 \frac{\ell}{R} \theta_c - i\omega_c \bar{a}_{13} C_4 + 2\omega_c \bar{b}_{13} \frac{\ell}{R} C_1 F^{13} \theta_c$$
$$- 2\omega_c^2 \bar{b}_{13} \frac{\ell}{R} \theta_c C_1 F^{13} + (v_r)^* C_4 i \bar{b}_{13} (1 - \omega_c) + C_1 F^{15} \frac{\ell}{R} (1 - \omega_c) \omega_c \bar{b}_{13} (v_r)^*$$
$$\omega_c (1 - \omega_c) \bar{a}_{13} C_1 F^{15} \frac{\ell}{R} + \omega_c (\alpha_2)^* C_1 F^9 - \frac{1}{2} (\alpha_2)^* C_2 F^6$$
$$- \omega_c (\beta_2)^* C_2 \frac{\ell}{R} g_0 F^{14} i + \frac{1}{2} i (v_r)^* \omega_c C_2 \frac{\ell}{R} F^{14} \Big] \qquad \text{(G.67)}$$

$$P_{30} = \Big[-\omega_c (\alpha_2)^* \theta_c C_7 L^8 + 2i\omega_c (\alpha_2)^* g_o L^{17} C_7 +$$

$$+ i(v_r)^{*2} \omega_c C_7 L^{17} - 2(v_r)^* \omega_c \bar{a}_{13} C_7 L^{18} \frac{\ell}{R} +$$

$$2(v_r)^* \omega_c^2 \bar{a}_{13} C_7 \left(\frac{\ell}{R}\right) L^{18} - \omega_c \bar{a}_{13} \left(\frac{\ell}{R}\right) \theta_c C_7 L^{19} +$$

$$\omega_c^2 \bar{a}_{13} \left(\frac{\ell}{R}\right) \theta_c C_7 L^{19} + (\omega_c - 1) \omega_c (v_r)^* \bar{b}_{13} \theta_c C_7 \frac{\ell}{R} L^{19} +$$

$$i\omega_c (\beta_2)^* \theta_c g_o C_7 L^{16} + \frac{1}{2} i (v_r)^* \omega_c \theta_c C_7 L^{16} + \frac{1}{2} (\alpha_2)^* \theta_c C_6 L^{10}$$

$$- (\alpha_2)^* \lambda_{oc} C_6 L^{11} - i(v_r)^* \bar{a}_{13} C_{11} + 2i(v_r)^* \omega_c \bar{a}_{13} C_{11} \Big] \qquad \text{(G.68)}$$

$$K_1 = p_1 v_r Y_{GO} + p_2 X_{HO} \qquad \text{(G.69)}$$

$$K_2 = -\left(p_3 v_r Y_{GO} + p_4 X_{HO}\right) / K_1 \qquad \text{(G.70)}$$

$$K_3 = -\left(p_{15} v_r Y_{GO} + p_{16} X_{HO}\right) / K_1 \qquad \text{(G.71)}$$

$$K_6 = -\left(p_{21} v_r Y_{GO} + p_{22} X_{HO}\right) / K_1 \qquad \text{(G.72}$$

$$K_5 = -\left(p_5 v_r Y_{GO} + p_6 X_{HO}\right) / K_1 \qquad \text{(G.73)}$$

$$K_4 = -\left(v_r Y_{GO} p_9 + X_{HO} p_{10}\right) / K_1 \qquad \text{(G.74)}$$

$$K_7 = -\left(v_r Y_{GO} p_{23} + X_{HO} p_{24}\right) / K_1 \qquad \text{(G.75)}$$

$$K_8 = -\left(v_r Y_{GO} p_{25} + X_{HO} p_{26}\right) / K_1 \qquad \text{(G.76)}$$

$$K_9 = -\left(v_r Y_{GO} p_{27} + X_{HO} p_{28}\right) / K_1 \qquad \text{(G.77)}$$

$$K_{10} = -\left[v_r Y_{G0}\,(p_{2g})^* + X_{H0}\,(p_{30})^*\right] / K_1 \qquad \text{(G.78)}$$

$$C_{12} = C_6\left(L^{10}\theta_c - 2\lambda_{0c} L^{11}\right) \qquad \text{(G.79)}$$

$$K_{2\theta_1} = -\frac{1}{K_1}\left[i\omega_c v_r Y_{G0}\left(\frac{C_2 C_4 F^1}{\omega_{F10}^2} - 2C_1 F^{10}\right)\right.$$
$$\left. + X_{H0} i\omega_c\left(-C_7 L^{13}\lambda_{0c} - \frac{C_{11} C_2}{\omega_{F10}^2} F^1 v_r + C_7 L^7 v_r\right)\right] \qquad \text{(G.80)}$$

$$K_{2\lambda_1} = -\frac{1}{K_1}\left[i\omega_c v_r Y_{G0}\left(-\frac{C_2 C_4 F^2}{\omega_{F10}^2} + C_1 F^{11}\right)\right.$$
$$\left. + X_{H0} i\omega_c\left(-C_7 L^{13}\theta_c + \frac{C_2 C_{11}}{\omega_{F10}^2} F^2 v_r - 2v_r C_7 L^8\right)\right] \qquad \text{(G.81)}$$

APPENDIX H

THE SOLUTION OF EQUATIONS 5.101 AND 5.102

For convenience, Eqs. 5.101 and 5.102 can be rewritten as

$$\frac{d\xi}{d\psi_o} = (d_1 + \mu^2 K_{qR})\xi - (d_2 - \mu^2 K_{qI})\eta + \xi_o$$

$$\frac{d\eta}{d\psi_o} = (d_2 + \mu^2 K_{qI})\xi + (d_1 - K_{qR}\mu^2)\eta + \eta_o \qquad \text{(H.1)}$$

where

$$d_1 = (K_{2\theta_1})_R (\theta - \theta_c) + (K_{2\lambda_1})_R (\lambda_o - \lambda_{oc}) + \mu^2 \bar{K}_{6R} \qquad \text{(H.2)}$$

$$d_2 = (K_{2\theta_1})_I (\theta - \theta_c) + (K_{2\lambda_1})_I (\lambda_o - \lambda_{oc}) + \mu^2 \bar{K}_{6I} \qquad \text{(H.3)}$$

and

$$\xi_o = \mu K_{4R} + \mu^3 K_{7R} \qquad \text{(H.4)}$$

$$\eta_o = \mu K_{4I} + \mu^3 K_{7I} \qquad \text{(H.5)}$$

The homogeneous system is given by Eq. H.1 with $\xi_o = \eta_o = 0$. The solution of the homogeneous system denoted by subscript h can be written as

$$\xi_h = D_1 e^{s_1\psi_o} + D_2 e^{s_2\psi_o}$$

$$\eta_h = D_1\sigma_1 e^{s_1\psi_o} + D_2\sigma_2 e^{s_2\psi_o} \qquad \text{(H.6)}$$

where D_1 and D_2 are arbitrary constants and

$$\sigma_1 = \frac{S_1 - (d_1 + \mu^2 K_{qR})}{-d_2 + \mu^2 K_{qI}} \tag{H.7}$$

$$\sigma_2 = \frac{S_2 - (d_1 + \mu^2 K_{qR})}{-d_2 + \mu^2 K_{qI}} \tag{H.8}$$

and S_1, S_2 are the roots of the characteristic equation given by

$$S^2 - 2 d_1 S + \left[d_1^2 + d_2^2 + \mu^4 |K_q|^2 \right] = 0 \tag{H.9}$$

Therefore

$$S_{1,2} = (K_{2\theta_1})_R (\theta - \theta_c) + (K_{2\lambda_1})_R (\lambda_0 - \lambda_{0c}) + \mu^2 \bar{K}_{6R} \pm \sqrt{\mu^4 |K_q|^2 - \left[(K_{2\theta_1})_I (\theta - \theta_c) + (K_{2\lambda_1})_I (\lambda_0 - \lambda_{0c}) + (\omega_c - 1) + \mu^2 \bar{K}_{6I} \right]^2} \tag{H.10}$$

The particular solution of Eq. 5.103 is given by

$$\xi_p = - \frac{\xi_0 (d_1 - K_{qR} \mu^2) + \eta_0 (-d_2 + \mu^2 K_{qI})}{\Delta} \tag{H.11}$$

$$\eta_p = \frac{-\eta_0 (d_1 + \mu^2 K_{qR}) + \xi_0 (d_2 + \mu^2 K_{qI})}{\Delta}$$

$$\Delta = (d_1 + \mu^2 K_{qR})(d_1 - K_{qR} \mu^2) + (d_2 + \mu^2 K_{qI})(d_2 - \mu^2 K_{qI}) \tag{H.12}$$

The complete solution is given by

$$\xi = \xi_h + \xi_p$$

$$\eta = \eta_h + \eta_p \tag{H.13}$$

so that from Eqs. H.6, H.13, and 5.100, the solution can be written as

$$\bar{\chi}_2 = \xi + i\eta = D_1(1+i\sigma_1)\, e^{s_1\psi_0} + D_2(1+i\sigma_2)\, e^{s_2\psi_0} + (\xi_p + i\eta_p)$$

$$= \bar{D}_1\, e^{s_1\psi_0} + \bar{D}_2\, e^{s_2\psi_0} + \xi_p + i\eta_p \qquad \text{(H.14)}$$

and

$$A_0 \tilde{=} \frac{\bar{\chi}_2}{\epsilon^{1/2}}\, e^{-i\nu\epsilon\psi_0} \qquad \text{(H.15)}$$

APPENDIX I

COORDINATE TRANSFORMATIONS AND PROOF OF THE EQUIVALENCE OF ROTATIONS

I.1 Coordinate Transformations

In this section, the various coordinate transformations for the various coordinate systems mentioned in Subsection 8.3.2 will be given, together with the various approximations involved.

The relations between the $\underset{\sim}{i}$, $\underset{\sim}{j}$, $\underset{\sim}{k}$ unit vectors and the $\underset{\sim}{i}_1$, $\underset{\sim}{j}_1$, $\underset{\sim}{k}_1$ unit vectors is shown in Fig. 29a.

$$\begin{Bmatrix} \underset{\sim}{i}_1 \\ \underset{\sim}{j}_1 \\ \underset{\sim}{k}_1 \end{Bmatrix} = \underbrace{\begin{bmatrix} \cos\beta & 0 & \sin\beta \\ 0 & 1 & 0 \\ -\sin\beta & 0 & \cos\beta \end{bmatrix}}_{[R_1(\beta)]} \begin{Bmatrix} \underset{\sim}{i} \\ \underset{\sim}{j} \\ \underset{\sim}{k} \end{Bmatrix} = \begin{bmatrix} 1 & 0 & \beta \\ 0 & 1 & 0 \\ -\beta & 0 & \beta \end{bmatrix} \begin{Bmatrix} \underset{\sim}{i} \\ \underset{\sim}{j} \\ \underset{\sim}{k} \end{Bmatrix} \tag{I.1}$$

The relations between the i_1, j_1, k_i and the i_2, j_2, k_2 coordinate systems (see Fig. 29b) is given by

$$\begin{Bmatrix} \underset{\sim}{i}_2 \\ \underset{\sim}{j}_2 \\ \underset{\sim}{k}_2 \end{Bmatrix} = \underbrace{\begin{bmatrix} 1 & 0 & 0 \\ 0 & \cos(\theta+\Phi) & \sin(\theta+\Phi) \\ 0 & -\sin(\theta+\Phi) & \cos(\theta+\Phi) \end{bmatrix}}_{[R_2(\theta,\Phi)]} \begin{Bmatrix} \underset{\sim}{i}_1 \\ \underset{\sim}{j}_1 \\ \underset{\sim}{k}_1 \end{Bmatrix} \tag{I.2}$$

The last two coordinate transformations are orthonormal. Thus, the inverse transformations can be obtained by using $[R_1(\beta)]^T$ and $[R_2(\theta,\Phi)]^T$, respectively.

If one assumes that the undeformed blade coincides with the i_2 direction, the position of the elastic axis in the deformed state can be specified by two displacements v_{e2}, w_{e2} [in the y_2 and z_2 directions, respectively, and for simplicity $u = 0$]. These displacements for the same loading conditions

will be related to v_e, w_e (see Fig. 27) by

$$v_{2e} \cong v_e \cos(\theta+\Phi) + w_e \sin(\theta+\Phi)$$
$$w_{2e} \cong -v_e \sin(\theta+\Phi) + w_e \cos(\theta+\Phi) \qquad \text{(I.3)}$$

Then for

$$\tan^{-1}\left(\frac{\partial v_{e2}}{\partial x_2}\right) \cong \frac{\partial v_{e2}}{\partial x_2} \quad , \quad \tan^{-1}\left(\frac{\partial w_{e2}}{\partial x_2}\right) \cong \frac{\partial w_{e2}}{\partial x_2}$$

a coordinate system $\underset{\sim}{I}_1$, $\underset{\sim}{J}_1$, $\underset{\sim}{K}_1$ can be defined.

A coordinate system $\underset{\sim}{I}_1$, $\underset{\sim}{J}_1$, $\underset{\sim}{K}_1$ can be attached to the cross section of the of the deformed blade at the elastic axis such that $\underset{\sim}{I}_1$ is tangential to the deformed elastic axis, $\underset{\sim}{J}_1$ coincides with the chord and $\underset{\sim}{K}_1$ is normal to both $\underset{\sim}{I}_1$ and $\underset{\sim}{J}_1$. For $\tan^{-1}\left(\frac{\partial v_{e2}}{\partial x_2}\right) \cong \frac{\partial v_{e2}}{\partial x_2}$, $\tan^{-1}\left(\frac{\partial w_{e2}}{\partial x_2}\right) \cong \frac{\partial w_{e2}}{\partial x_2}$

$$\begin{Bmatrix} \underset{\sim}{I}_1 \\ \underset{\sim}{J}_1 \\ \underset{\sim}{K}_1 \end{Bmatrix} = \underbrace{\begin{bmatrix} 1 & \frac{\partial v_{e2}}{\partial x_2} & \frac{\partial w_{e2}}{\partial x_2} \\ -\frac{\partial v_{e2}}{\partial x_2} & 1 & 0 \\ -\frac{\partial w_{e2}}{\partial x_2} & 0 & 1 \end{bmatrix}}_{[R_7]} \begin{Bmatrix} \underset{\sim}{i}_2 \\ \underset{\sim}{j}_2 \\ \underset{\sim}{k}_2 \end{Bmatrix} \qquad \text{(I.4)}$$

Also, for β small: $\partial/\partial x = \partial/\partial x_2 = \partial/\partial x_n$.

In the inverse transformation, it will be assumed that

$$1 + \left(\frac{\partial v_{e2}}{\partial x_2}\right)^2 + \left(\frac{\partial w_{e2}}{\partial x_2}\right)^2 \cong 1$$

Then the inverse transform is again given by using $[R_7]^T$.

Finally, the pertinent relations for the transformation between the $\underset{\sim}{i}$, $\underset{\sim}{j}$, $\underset{\sim}{k}$, $\underset{\sim}{I}_2$, $\underset{\sim}{J}_2$, $\underset{\sim}{K}_2$, and $\underset{\sim}{I}_3$, $\underset{\sim}{J}_3$, $\underset{\sim}{K}_3$ systems defined in Subsection 8.3.2 are given below

$$\begin{Bmatrix} \underset{\sim}{I}_2 \\ \underset{\sim}{J}_2 \\ \underset{\sim}{K}_2 \end{Bmatrix} = \begin{bmatrix} 1 & \frac{\partial v}{\partial x} & \frac{\partial w}{\partial x} \\ -\frac{\partial v}{\partial x} & 1 & 0 \\ -\frac{\partial w}{\partial x} & 0 & 1 \end{bmatrix} \begin{Bmatrix} \underset{\sim}{i} \\ \underset{\sim}{j} \\ \underset{\sim}{k} \end{Bmatrix} \tag{I.5}$$

$$\begin{Bmatrix} \underset{\sim}{I}_3 \\ \underset{\sim}{J}_3 \\ \underset{\sim}{K}_3 \end{Bmatrix} = \begin{bmatrix} 1 & 0 & 0 \\ 0 & \cos(\theta+\Phi) & \sin(\theta+\Phi) \\ 0 & -\sin(\theta+\Phi) & \cos(\theta+\Phi) \end{bmatrix} \begin{Bmatrix} \underset{\sim}{I}_2 \\ \underset{\sim}{J}_2 \\ \underset{\sim}{K}_2 \end{Bmatrix} \tag{I.6}$$

In the inverse transform of Eq. I.5, again it will be assumed that

$$\left(\frac{\partial w}{\partial x}\right)^2 + \left(\frac{\partial v}{\partial x}\right)^2 + 1 \cong 1 \tag{I.7}$$

It is important to note that unless this assumption is made on the various coordinate transformations involving slopes, the nonlinear problem

becomes almost untreatable.

I.2 Proof of the Equivalence of Rotations

In this subsection, it will be shown that with the assumptions that β, Φ are small and that

$$1 + \left(\frac{\partial w}{\partial x}\right)^2 + \left(\frac{\partial v}{\partial x}\right)^2 \cong 1 \tag{I.7}$$

The final orientation of the blade cross section in space will be independent of the order in which the deformations occur. It will also be shown that it is immaterial if the rotations θ and Φ of the cross section take place about the feathering axis ($\underset{\sim}{i}_1$ axis), $\underset{\sim}{i}$ axis or the $\underset{\sim}{I}_2$ axis.

First, let us assume the following hypothetical displacement patterns:

(1) The undeformed point on the elastic axis is located in the $\underset{\sim}{i}_1$, $\underset{\sim}{j}_1$, $\underset{\sim}{k}_1$ system.

(2) The v_{e2}, w_{e2} deformations occur in the $\underset{\sim}{i}_2$, $\underset{\sim}{j}_2$, $\underset{\sim}{k}$ system.

(3) The final orientation of the blade cross section in space is given by $\underset{\sim}{I}_1$, $\underset{\sim}{J}_1$, $\underset{\sim}{K}_1$ unit vectors.

Measuring the final orientation of the $\underset{\sim}{I}_1$, $\underset{\sim}{J}_1$, $\underset{\sim}{K}_1$ system by the $\underset{\sim}{i}$, $\underset{\sim}{j}$, $\underset{\sim}{k}$ vectors, the following relation can be written:

$$\begin{Bmatrix} \underset{\sim}{I}_1 \\ \underset{\sim}{J}_1 \\ \underset{\sim}{K}_1 \end{Bmatrix} = [R_4] \begin{Bmatrix} \underset{\sim}{i} \\ \underset{\sim}{j} \\ \underset{\sim}{k} \end{Bmatrix} \tag{I.8}$$

The transformation matrix $[R_4]$, obtained by going through the various coordinate transformations and using Eqs. I.1, I.2, I.4, and I.3, is given by Eq. I.9 on page .

In the second stage, the following pattern of transformations is assumed:

(1) A point on the elastic axis is assumed to have the displacements v, w (Eqs. 8.4 and 8.5). The new orientation of the blade is given by the $\underset{\sim}{I}_2$, $\underset{\sim}{J}_2$, $\underset{\sim}{K}_2$ system.

(2) The cross section is rotated by an angle of $(\theta + \Phi)$ about the $\underset{\sim}{I}_2$ axis. The final orientation of the cross section in space is given by the $\underset{\sim}{I}_3$, $\underset{\sim}{J}_3$, $\underset{\sim}{K}_3$ system.

Then the following relations can be written

$$\begin{Bmatrix} \underset{\sim}{I}_3 \\ \underset{\sim}{J}_3 \\ \underset{\sim}{K}_3 \end{Bmatrix} = [R_5] \begin{Bmatrix} \underset{\sim}{i} \\ \underset{\sim}{j} \\ \underset{\sim}{k} \end{Bmatrix} \tag{I.9}$$

Performing the coordinate transformation, it is found that $[R_5]$ is given by Eq. I.10, page .

Comparing the two matrices $[R_4]$ and $[R_5]$, it can be seen that all of the elements agree, except $R_4(1,1)$, $R_4(2,3)$, and $R_4(3,3)$ when compared with the same terms of R_5. The discrepancies between the two matrices always involve only second-order terms which according to Eq. I.7 are negligible compared to 1.

By varying the displacement pattern similar results are obtained. This is not surprising since these are all the result of the assumptions β small and Eq. I.7, which is equivalent to taking

$$\cos\left(\frac{\partial w}{\partial x}\right) = \cos\left(\frac{\partial v}{\partial x}\right) \cong 1$$

It should be noted that this approximation is related only to calculating the orientation in space of the deformed blade. This is required for the evaluation of the aerodynamic loading terms. It has not been used in calculating the inertia loads which therefore are consistently accurate up to $0(\varepsilon_D^3)$.

$$[R_4] = \begin{bmatrix} 1 - \beta\left(\frac{\partial w_e}{\partial x}\right) & \frac{\partial v_e}{\partial x} & \beta + \frac{\partial w_e}{\partial x} \\ -\frac{\partial v_e}{\partial x}\cos(\theta+\Phi) - \left(\beta + \frac{\partial w_e}{\partial x}\right)\sin(\theta+\Phi) & \cos(\theta+\Phi) & -\beta\left[\frac{\partial v_e}{\partial x}\cos(\theta+\Phi) + \frac{\partial w_e}{\partial x}\sin(\theta+\Phi)\right] + \sin(\theta+\Phi) \\ -\frac{\partial v_e}{\partial x}\sin(\theta+\Phi) - \left(\frac{\partial w_e}{\partial x} + \beta\right)\cos(\theta+\Phi) & -\sin(\theta+\Phi) & \beta\left(\frac{\partial v_e}{\partial x}\right)\sin(\theta+\Phi) + \left(1 - \beta\left(\frac{\partial w_e}{\partial x}\right)\cos(\theta+\Phi)\right) \end{bmatrix}$$

Eq. I.9

$$[R_5] = \begin{bmatrix} 1 & \frac{\partial v_e}{\partial x} & \beta + \frac{\partial w_e}{\partial x} \\ -\frac{\partial v_e}{\partial x}\cos(\theta+\Phi) - \left(\frac{\partial w_e}{\partial x} + \beta\right)\sin(\theta+\Phi) & \cos(\theta+\Phi) & \sin(\theta+\Phi) \\ \frac{\partial v_e}{\partial x}\sin(\theta+\Phi) - \left(\beta + \frac{\partial w_e}{\partial x}\right)\cos(\theta+\Phi) & -\sin(\theta+\Phi) & \cos(\theta+\Phi) \end{bmatrix}$$

Eq. I.10

APPENDIX J

COMPLETE EXPRESSIONS FOR THE ACCELERATIONS

Terms marked by ↗ are negligible according to the considerations of Subsection 8.4.1.

$$
\begin{aligned}
a_x = {} & \ddot{U} + X_I \left\{ -\frac{\partial^3 v}{\partial X_o \partial t^2} \left(\cos\theta - \Phi \sin\theta \right) + 2 \frac{\partial^2 v}{\partial X_o \partial t} \left[\dot{\theta} \left(\sin\theta + \Phi \cos\theta \right) \right. \right. \\
& \left. + \dot{\Phi} \sin\theta + \Phi \dot{\Phi} \cos\theta \right] + \frac{\partial v}{\partial X_o} \left[\dot{\theta}^2 \cos\theta - \dot{\theta}^2 \Phi \sin\theta \right] \\
& + \frac{\partial v}{\partial X_o} \left(2\dot{\theta}\dot{\Phi} + \dot{\Phi}^2 \right) \left(\cos\theta - \Phi \sin\theta \right) + \frac{\partial v}{\partial X_o} \left[\ddot{\theta} \sin\theta + \ddot{\Phi} \sin\theta \right. \\
& \left. + \Phi \ddot{\theta} \cos\theta + \Phi \ddot{\Phi} \cos\theta \right) - \frac{\partial^3 W}{\partial X_o \partial t^2} \left(\sin\theta + \Phi \cos\theta \right) \\
& - \frac{\partial^2 W}{\partial X_o \partial t} 2 \left(\dot{\theta} \cos\theta - \dot{\theta} \Phi \sin\theta + \dot{\Phi} \cos\theta - \Phi \dot{\Phi} \sin\theta \right) \\
& + \frac{\partial W}{\partial X_o} \dot{\theta}^2 \left(\sin\theta + \Phi \cos\theta \right) + \frac{\partial W}{\partial X_o} \left(\sin\theta + \Phi \cos\theta \right) \left(2\dot{\theta}\dot{\Phi} + \dot{\Phi}^2 \right) \\
& - \frac{\partial W}{\partial X_o} \ddot{\theta} \left(\cos\theta - \Phi \sin\theta \right) - \frac{\partial W}{\partial X_o} \ddot{\Phi} \left(\cos\theta - \Phi \sin\theta \right) \\
& - \Omega^2 \left(X_o + e_1 + v \right) - 2\Omega \dot{v} + \Omega^2 X_I \left[\left(\frac{\partial v}{\partial X_o} \cos\theta + \frac{\partial W}{\partial X_o} \sin\theta \right) \right. \\
& \left. + \Phi \left(-\frac{\partial v}{\partial X_o} \sin\theta + \frac{\partial W}{\partial X_o} \cos\theta \right) \right] + 2\Omega X_I \left[\dot{\theta} \left(\sin\theta + \Phi \cos\theta \right) \right. \\
& \left. + \dot{\Phi} \left(\sin\theta + \Phi \cos\theta \right) \right]
\end{aligned}
\tag{J.1}
$$

In this report, whenever a_x is used its meaning will be Eq. J.1 without the terms marked by ↗.

$$a_y = \ddot{v} + 2\Omega\dot{u} - \Omega^2 v + X_I \Big\{ -(\cos\theta - \Phi\sin\theta)(\dot{\theta}^2 + 2\dot{\theta}\dot{\Phi} + \dot{\Phi}^2)$$

$$-(\sin\theta + \Phi\cos\theta)\ddot{\theta} - (\sin\theta + \Phi\cos\theta)\ddot{\Phi} - \Omega^2(\cos\theta - \Phi\sin\theta)$$

$$+ 2\Omega\Big[-\frac{\partial^2 v}{\partial x_o \partial t}(\cos\theta - \Phi\sin\theta) + \frac{\partial v}{\partial x_o}(\sin\theta + \Phi\cos\theta)\dot{\theta}$$

$$+ \frac{\partial v}{\partial x_o}(\sin\theta + \Phi\cos\theta)\dot{\Phi} - \frac{\partial^2 w}{\partial x_o \partial t}(\sin\theta + \Phi\cos\theta)$$

$$- \frac{\partial w}{\partial x_o}(\cos\theta - \Phi\sin\theta)\dot{\theta} - \frac{\partial w}{\partial x_o}(\cos\theta - \Phi\sin\theta)\dot{\Phi} \Big] \Big\} \qquad \text{(J.2)}$$

$$a_z = \ddot{w} - X_I(\sin\theta + \Phi\cos\theta)(\dot{\theta}^2 + 2\dot{\theta}\dot{\Phi} + \dot{\Phi}^2)$$

$$+ X_I(\cos\theta - \Phi\sin\theta)\ddot{\theta} + X_I(\cos\theta - \Phi\sin\theta)\ddot{\Phi} \qquad \text{(J.3)}$$

APPENDIX K

DERIVATION OF THE MOMENT LOADS PER UNIT SPAN ABOUT THE FEATHERING AXIS

K.1 Derivation of q_{il}

In order to derive the quantity q_{il}, the quantities q_x and q_z are required. From the geometry of Fig. 28

$$q_x = M_a + \left[- P_{yI} \left(\bar{z}_1 - w \right) + P_{zI} \left(y_1 - v \right) \right] \tag{K.1}$$

where moments in the nose-up direction, for the cross section are considered positive.

From Eqs. 8.11, 8.12, 8.20, and 8.23

$$q_x = M_a + \Big\langle \Big[\left(\ddot{v} + 2\Omega \dot{u} - \Omega^2 v \right) \sin\theta + \Phi \left(\ddot{w} + 2\Omega \dot{u} - \Omega^2 w \right) \cos\theta \Big] X_I m$$

$$+ X_I^2 m \Big\{ \Big[- \ddot{\Phi} \sin^2\theta - \Omega^2 \left(\cos\theta \sin\theta - \Phi \sin^2\theta \right)$$

$$- 2\Omega \left(\frac{\partial^2 v}{\partial x_o \partial t} \cos\theta \sin\theta + \frac{\partial^2 w}{\partial x_o \partial t} \sin^2\theta \right) \Big] + \Big[- \Omega^2 \left(\Phi \cos^2\theta - \Phi^2 \sin\theta \cos\theta \right)$$

$$- 2\Omega \left(\frac{\partial^2 v}{\partial x_o \partial t} \cos^2\theta + \frac{\partial^2 w}{\partial x_o \partial t} \sin\theta \cos\theta \right) \Phi \Big] + \Big[2\Omega\Phi \left(\frac{\partial^2 v}{\partial x_o \partial t} \sin^2\theta \right.$$

$$\left. - \frac{\partial^2 w}{\partial x_o \partial t} \sin\theta \cos\theta \right) + 2\Omega \dot{\Phi} \left(\frac{\partial v}{\partial x_o} \sin^2\theta - \frac{\partial w}{\partial x_o} \cos\theta \sin\theta \right) \Big]$$

$$+ \Big[2\Omega\Phi^2 \left(\frac{\partial^2 v}{\partial x_o \partial t} \sin\theta \cos\theta - \frac{\partial^2 w}{\partial x_o \partial t} \cos^2\theta \right) + 2\Omega \Phi \dot{\Phi} \left(\frac{\partial v}{\partial x_o} \sin\theta \cos\theta \right.$$

$$- \frac{\partial w}{\partial x_o}\cos^2\theta\Big)\Big] + \Big[-\dot\theta^2\cos\theta\sin\theta - 2\dot\theta\dot\Phi\sin\theta\cos\theta - \ddot\theta\Big(\sin^2\theta$$

$$+ \Phi\cos\theta\sin\theta\Big) + 2\Omega\Big(\frac{\partial v}{\partial x_o}\sin^2\theta - \frac{\partial w}{\partial x_o}\cos\theta\sin\theta\Big)\dot\theta$$

$$+ 2\Omega\Phi\dot\theta\frac{\partial v}{\partial x_o}\cos\theta\sin\theta\Big] + \Big[-\dot\theta^2\Phi\cos^2\theta - 2\dot\theta\dot\Phi\Phi\cos^2\theta - \ddot\theta\Phi\Big(\sin\theta\cos\theta$$

$$+ \Phi\cos^2\theta\Big) + 2\Omega\Phi\Big(\frac{\partial v}{\partial x_o}\sin\theta\cos\theta - \frac{\partial w}{\partial x_o}\cos^2\theta\Big)\dot\theta + 2\Omega\Phi^2\dot\theta\frac{\partial v}{\partial x_o}\cos^2\theta\Big]\Big\rangle$$

$$+ \Big\langle -mx_I\ddot W\Big(\cos\theta - \Phi\sin\theta\Big) - mx_I^2\Big\{\Big(\ddot\Phi\cos^2\theta - \Phi\dot\Phi^2\sin\theta\cos\theta\Big)$$

$$+ \ddot\theta\Big(\cos^2\theta - \Phi\cos\theta\sin\theta\Big)\Big\}\Big\rangle \qquad \text{(K.2)}$$

The terms in Eq. K.2, marked by arrows, are of $0(\varepsilon_D^3)$, according to considerations (1) through (6) Subsection 8.4.1, and therefore are negligible. Thus

$$q_x = M_a - mx_I\Omega^2\Big(\sin\theta + \Phi\cos\theta\Big)v + mx_I\Big[\ddot v\Big(\sin\theta + \Phi\cos\theta\Big)$$

$$- \ddot W\cos\theta + 2\Omega\dot v\Big(\sin\theta + \Phi\cos\theta\Big)\Big]$$

$$- mx_I^2\Big\{\Big[\ddot\Phi + \Omega^2\sin\theta\cos\theta + \Omega^2\Phi\cos 2\theta + 2\Omega\Big(\frac{\partial^2 v}{\partial x_o\partial t}\sin\theta\cos\theta$$

$$+ \frac{\partial^2 w}{\partial x_o\partial t}\sin^2\theta\Big)\Big] - 2\Omega\Phi\frac{\partial^2 v}{\partial x_o\partial t}\cos 2\theta$$

$$+ \Big[\ddot\theta + \dot\theta^2\sin\theta\cos\theta - 2\Omega\Big(\frac{\partial v}{\partial x}\sin\theta - \frac{\partial w}{\partial x}\cos\theta\Big)\dot\theta\sin\theta\Big]\Big\}$$

(K.3)

Due to the model selected to represent the blade cross section, terms due to the polar moment of inertia of the cross section itself are missing. The missing terms are:

(a) The regular angular inertia term given by

$$-k_o^2 m\left(\ddot{\theta} + \ddot{\Phi}\right) \tag{K.4}$$

(b) The missing part of the propeller moment effect, derived separately in Section K.3 of this appendix, given by

$$-mk_o^2\Omega^2\left[\sin\theta\cos\theta + \Phi\cos 2\theta\right] \tag{K.5}$$

From Eqs. K.3 through K.5

$$q_x = M_a - mX_I\Omega^2\left(\sin\theta + \Phi\cos\theta\right)v + mX_I\Omega^2\left[\overset{**}{v}\left(\sin\theta + \Phi\cos\theta\right) - \overset{**}{w}\cos\theta + 2\overset{*}{v}\left(\sin\theta + \Phi\cos\theta\right)\right]$$

$$- m\left(k_o^2 + X_I^2\right)\overset{**}{\Phi}\Omega^2 - m\left(k_o^2 + X_I^2\right)\Omega^2\left(\sin\theta\cos\theta + \Phi\cos 2\theta\right)$$

$$- mX_I^2\Omega^2\left[2\left(\frac{\partial^2 v}{\partial x_o \partial\psi}\sin\theta\cos\theta + \frac{\partial^2 w}{\partial x_o\partial\psi}\sin^2\theta\right) - 2\frac{\partial^2 v}{\partial x_o\partial\psi}\Phi\cos 2\theta\right]$$

$$- m\left(k_o^2 + X_I^2\right)\overset{**}{\theta}\Omega^2 - mX_I^2\Omega^2\left[\overset{*}{\theta}{}^2\sin\theta\cos\theta\right.$$

$$\left. - 2\left(\frac{\partial v}{\partial x_o}\sin\theta - \frac{\partial w}{\partial x_o}\cos\theta\right)\overset{*}{\theta}\sin\theta\right] \tag{K.6}$$

Next, q_z will be derived. From the geometry of Figs. 27 and 28

$$q_z = -P_x\left(y_1 - v\right) \tag{K.7}$$

where a positive q_z is one which gives compression in the nose fiber of the blade. From Eqs. K.7 and 8.18

$$q_z = m x_I \Omega^2 \Big[\ddot{v} \left(\cos\theta - \Phi \sin\theta \right) - (x_o + e_1)\left(\cos\theta - \Phi \sin\theta \right)$$

$$- v\left(\cos\theta - \Phi \sin\theta \right) - 2\dot{v}\left(\cos\theta - \Phi \sin\theta \right) \Big]$$

$$+ m x_I^2 \Omega^2 \Bigg\{ \Bigg[-\frac{\partial^3 v}{\partial x_o \partial \psi^2} \cos^2\theta - \frac{\partial^3 w}{\partial x_o \partial \psi^2} \sin\theta\cos\theta + \Big(\frac{\partial v}{\partial x_o} \cos^2\theta$$

$$+ \frac{\partial w}{\partial x_o} \sin\theta\cos\theta \Big) + 2\dot{\Phi} \sin\theta\cos\theta \Bigg] + \Bigg[\Phi \Big(\frac{\partial^3 v}{\partial x_o \partial \psi^2} \sin\theta\cos\theta$$

$$- \frac{\partial^2 w}{\partial x_o \partial \psi^2} \cos^2\theta + \frac{\partial w}{\partial x_o} \cos^2\theta - \frac{\partial v}{\partial x_o} \sin\theta\cos\theta \Big) + 2\dot{\Phi} \Big(\frac{\partial^2 v}{\partial x_o \partial \psi} \sin\theta\cos\theta$$

$$- \frac{\partial^2 w}{\partial x_o \partial \psi} \cos^2\theta \Big) + \ddot{\Phi} \Big(\frac{\partial v}{\partial x_o} \sin\theta\cos\theta - \frac{\partial w}{\partial x_o} \cos^2\theta \Big) \Bigg]$$

$$+ \Bigg[2 \Big(\frac{\partial^2 v}{\partial x_o \partial \psi} \sin\theta\cos\theta - \frac{\partial^2 w}{\partial x_o \partial \psi} \cos^2\theta \Big) \dot{\theta} + \ddot{\theta} \Big(\frac{\partial v}{\partial x_o} \sin\theta\cos\theta$$

$$- \frac{\partial w}{\partial x_o} \cos^2\theta \Big) + 2\dot{\theta} \Big(\sin\theta\cos\theta + \Phi \cos^2\theta \Big) \Bigg]$$

$$+ \Bigg[\Phi \Big(\frac{\partial^3 v}{\partial x_o \partial \psi^2} \sin\theta\cos\theta - \frac{\partial^2 w}{\partial x_o \partial \psi^2} \sin^2\theta \Big) - \Phi \Big(\frac{\partial v}{\partial x_o} \cos\theta\sin\theta$$

$$+ \frac{\partial w}{\partial x_o} \sin^2\theta \Big) - 2\Omega \dot{\Phi} \Phi \sin^2\theta \Bigg] + \Bigg[-\Phi^2 \sin\theta \Big(\frac{\partial^3 v}{\partial x_o \partial \psi^2} \sin\theta$$

$$- \frac{\partial^3 W}{\partial x_0 \partial \psi^2} \cos\theta + \frac{\partial W}{\partial x_0} \cos\theta - \frac{\partial v}{\partial x_0} \sin\theta \Big)$$

$$- 2\Phi \overset{*}{\Phi} \sin\theta \Big(\frac{\partial^2 v}{\partial x_0 \partial \psi} \sin\theta - \frac{\partial^2 W}{\partial x_0 \partial \psi} \cos\theta \Big)$$

$$- \Phi \overset{**}{\Phi} \sin\theta \Big(\frac{\partial v}{\partial x_0} \sin\theta - \frac{\partial W}{\partial x_0} \cos\theta \Big)$$

$$+ \Big[- 2\Phi \sin\theta \overset{*}{\theta} \Big(\frac{\partial^2 v}{\partial x_0 \partial \psi} \sin\theta - \frac{\partial^2 W}{\partial x_0 \partial \psi} \cos\theta \Big)$$

$$- \Phi \sin\theta \overset{**}{\theta} \Big(\frac{\partial v}{\partial x_0} \sin\theta - \frac{\partial W}{\partial x_0} \cos\theta \Big)$$

$$- 2 \overset{*}{\theta} \Phi \sin\theta \Big(\sin\theta + \Phi \cos\theta \Big) \Big] \Big\} \qquad \text{(K.8)}$$

The quantities marked by the arrows ↗ are $O(\varepsilon_D^3)$ or higher and are therefore negligible. Thus

$$q_{/z} = - m\Omega^2 x_I \Big[\Big(x_0 + v + e_1 \Big) \cos\theta - \Big(x_0 + e_1 \Big) \Phi \sin\theta \Big]$$

$$+ m x_I \Omega^2 \Big(\overset{**}{v} \cos\theta - 2 \overset{*}{v} \cos\theta \Big) + m x_I^2 \Omega^2 \Big\{ \Big[\frac{\partial v}{\partial x_0} \cos^2\theta$$

$$+ \frac{\partial W}{\partial x_0} \sin\theta\cos\theta - \frac{\partial^3 v}{\partial x_0 \partial \psi^2} \cos^2\theta - \frac{\partial^3 W}{\partial x_0 \partial \psi^2} \sin\theta\cos\theta$$

$$+ 2 \overset{*}{\Phi} \sin\theta\cos\theta \Big] + \Big[\Phi \Big(2 \frac{\partial^3 v}{\partial x_0 \partial \psi^2} \sin\theta\cos\theta - \frac{\partial^3 W}{\partial x_0 \partial \psi^2} \cos 2\theta \Big)$$

$$+ \Phi \frac{\partial w}{\partial x_o} \cos 2\theta - 2\Phi \frac{\partial v}{\partial x_o} \sin\theta\cos\theta + 2\overset{*}{\Phi}\left(\frac{\partial^2 v}{\partial x_o \partial \psi} \sin\theta\cos\theta \right.$$

$$\left. - \frac{\partial^2 w}{\partial x_o \partial \psi} \cos^2\theta \right) + \overset{**}{\Phi}\left(\frac{\partial v}{\partial x_o} \sin\theta\cos\theta - \frac{\partial w}{\partial x_o} \cos^2\theta \right) \Big]$$

$$+ \Big[\left(2 \frac{\partial^2 v}{\partial x_o \partial \psi} \sin\theta\cos\theta - \frac{\partial^2 w}{\partial x_o \partial \psi} \cos^2\theta \right) \overset{*}{\theta}$$

$$+ \overset{**}{\theta}\left(\frac{\partial v}{\partial x_o} \sin\theta\cos\theta - \frac{\partial w}{\partial x_o} \cos^2\theta \right) + 2\overset{*}{\theta}\left(\sin\theta\cos\theta \right.$$

$$\left. + \Phi \cos^2\theta \right) \Big] \Big\} \qquad \text{(K.9)}$$

In order to evaluate q_{il}, βq_z is required. In this analysis, β is a small quantity, again of $0(\varepsilon_D)$ and when evaluating βq_z, using Eq. K.9, many terms can be neglected. The result can be written as

$$q_{z\beta} = - m\Omega^2 x_I \Big[(e_1 + x_o)\beta\cos\theta \Big] - 2 m x_I \Omega^2 \overset{*}{v}\beta\cos\theta$$

$$+ m x_I^2 \Omega^2 \Big[\left(\frac{\partial v}{\partial x_o} \cos^2\theta + \frac{\partial w}{\partial x_o} \sin\theta\cos\theta \right)\beta$$

$$- \frac{\partial^2 v}{\partial x_o \partial \psi^2} \cos^2\theta\beta - \frac{\partial^3 w}{\partial x_o \partial \psi^2} \beta \sin\theta\cos\theta \Big]$$

$$+ 0\left(\varepsilon_D^3\right)$$

(K.10)

The expression for q_{il} can be obtained from Eqs. K.6, K.10, and 8.35.

K.2 Derivation of $M_{P_{il}}$

From Eqs. 8.17 and 8.18

$$\beta P_x = -m\Omega^2 \left[\ddot{v}\beta - (X_o + e_1 + v)\beta - 2\beta\dot{v} \right]$$

$$- m X_I \Omega^2 \left\{ -\frac{\partial^3 v}{\partial x_o \partial \psi^2} \beta \cos\theta - \frac{\partial^3 w}{\partial x_o \partial \psi^2} \beta \sin\theta + \beta \left(\frac{\partial v}{\partial x_o} \cos\theta \right.\right.$$

$$\left.\left. + \frac{\partial w}{\partial x_o} \sin\theta \right) + 2\dot{\Phi}\beta \sin\theta \right\} - m X_I \Omega^2 \left\{ \beta\Phi \left[\frac{\partial^3 v}{\partial x_o \partial \psi^2} \sin\theta \right.\right.$$

$$\left.\left. - \frac{\partial^3 w}{\partial x_o \partial \psi^2} \cos\theta + \left(\frac{\partial w}{\partial x_o} \cos\theta - \frac{\partial v}{\partial x_o} \sin\theta \right) \right] + 2\dot{\Phi}\beta \left(\frac{\partial^2 v}{\partial x_o \partial \psi} \sin\theta \right.\right.$$

$$\left.\left. - \frac{\partial^2 w}{\partial x_o \partial \psi} \cos\theta \right) + \ddot{\Phi}\beta \left(\frac{\partial v}{\partial x_o} \sin\theta - \frac{\partial w}{\partial x_o} \cos\theta \right) \right\} - m X_I \Omega^2 \left\{ 2\beta \left(\frac{\partial^2 v}{\partial x_o \partial \psi} \sin\theta \right.\right.$$

$$\left.\left. - \frac{\partial^2 w}{\partial x_o \partial \psi} \cos\theta \right) \dot{\theta} + \ddot{\theta}\beta \left(\frac{\partial v}{\partial x_o} \sin\theta - \frac{\partial w}{\partial x_o} \cos\theta \right) - 2\dot{\theta}\beta \left(\sin\theta + \Phi\cos\theta \right) \right\}$$

$$\beta P_x = -m\Omega^2 \left[-(X_o + e_1)\beta - 2\dot{v}\beta \right] - m X_I \Omega^2 \left\{ -\frac{\partial^3 v}{\partial x_o \partial \psi^2} \beta \cos\theta \right.$$

$$\left. - \frac{\partial^3 w}{\partial x_o \partial \psi^2} \beta \sin\theta + \beta \left(\frac{\partial v}{\partial x_o} \cos\theta + \frac{\partial w}{\partial x_o} \sin\theta \right) \right\}$$

(K.11)

From Eqs. K.11, 8.23, and 8.24

$$\left(P_z - \beta P_x\right) v \approx v L_z - m\Omega^2\left(\overset{**}{W} v + X_I \overset{**}{\Phi} v\cos\theta\right)$$

$$- m X_I \overset{**}{\theta}\Omega^2 v\left(\cos\theta - \Phi\sin\theta\right) + m\Omega^2\left[-(X_0+e_1)\beta v\right.$$

$$\left. - 2\beta \overset{*}{V} v\right] + m X_I \Omega^2\left\{- v\frac{\partial^3 v}{\partial X_0 \partial \psi^2}\beta\cos\theta\right.$$

$$\left. - v\frac{\partial^3 W}{\partial X_0 \partial \psi^2}\beta\sin\theta + \beta v\left(\frac{\partial v}{\partial X_0}\cos\theta + \frac{\partial W}{\partial X_0}\sin\theta\right)\right\}$$

$$= v L_z - m\Omega^2\left(\overset{**}{W} v + X_I \overset{**}{\Phi} v\cos\theta\right) - m X_I \overset{**}{\theta} v\Omega^2\cos\theta$$

$$- m\Omega^2\left(X_0 + e_1\right)\beta v \qquad \text{(K.12)}$$

From Eqs. 8.20 and 8.21, neglecting $u\beta = 0(\varepsilon_D^3)$

$$P_y\left(W - \beta X_0\right) = L_y\left(W - \beta X_0\right) - m\left(W - \beta X_0\right)\Omega^2\left(\overset{**}{V} + 2\overset{*}{U} - v\right)$$

$$- \Omega^2 m X_I\left\{\left[-\overset{**}{\Phi}\sin\theta\left(W - \beta X_0\right) - \cos\theta\left(W - \beta X_0\right)\right.\right.$$

$$\left.\left. + \Phi\sin\theta\left(W - \beta X_0\right) - 2\left(W - \beta X_0\right)\left(\frac{\partial^2 v}{\partial X_0 \partial \psi}\cos\theta - \frac{\partial^2 W}{\partial X_0 \partial \psi}\sin\theta\right)\right]\right.$$

$$\left. + \left[2\Phi\left(\frac{\partial^2 v}{\partial X_0 \partial \psi}\sin\theta - \frac{\partial^2 W}{\partial X_0 \partial \psi}\cos\theta\right)\left(W - \beta X_0\right)\right.\right.$$

$$+ 2\overset{*}{\Phi}\left(w-\beta x_o\right)\left(\frac{\partial v}{\partial x_o}\sin\theta - \frac{\partial w}{\partial x_o}\cos\theta\right)\Big]$$

$$+\Big[-\left(\overset{*2}{\theta} + 2\overset{*}{\theta}\overset{*}{\Phi}\right)\left(w-\beta x_o\right)\cos\theta - \overset{**}{\theta}\left(\sin\theta + \Phi\cos\theta\right)\left(w-\beta x_o\right)$$

$$+ 2\left(\frac{\partial v}{\partial x_o}\sin\theta - \frac{\partial w}{\partial x_o}\cos\theta\right)\overset{*}{\theta}\left(w-\beta x_o\right)$$

$$+ 2\Phi\overset{*}{\theta}\frac{\partial v}{\partial x_o}\cos\theta\left(w-\beta x_o\right)\Big] \qquad \text{(K.13)}$$

From Eqs. 8.33, K.12, and K.13

$$M\rho_{ii} = vL_z - m\Omega^2\left(\overset{**}{w}v + x_I\overset{**}{\Phi}v\cos\theta\right)$$

$$- mx_I\overset{**}{\theta}\Omega^2 v\cos\theta - m\Omega^2\left(x_o+e_1\right)\beta v - L_y\left(w-\beta x_o\right)$$

$$+ m\left(w-\beta x_o\right)\left(\overset{**}{v} - v\right)\Omega^2 + mx_I\Omega^2\Big\{-\cos\theta\left(w-\beta x_o\right)$$

$$+ \Phi\sin\theta\left(w-\beta x_o\right) - \overset{**}{\Phi}\sin\theta\left(w-\beta x_o\right)$$

$$- 2\left(w-\beta x_o\right)\left(\frac{\partial^2 v}{\partial x_o\partial\psi}\cos\theta - \frac{\partial^2 w}{\partial x_o\partial\psi}\sin\theta\right)\Big\}$$

(K.14)

In Eqs. K.11 through K.14, all of the terms marked by arrows are negligible $0(\varepsilon_D^3)$ quantities.

K.3 Derivation of the Propeller Moment

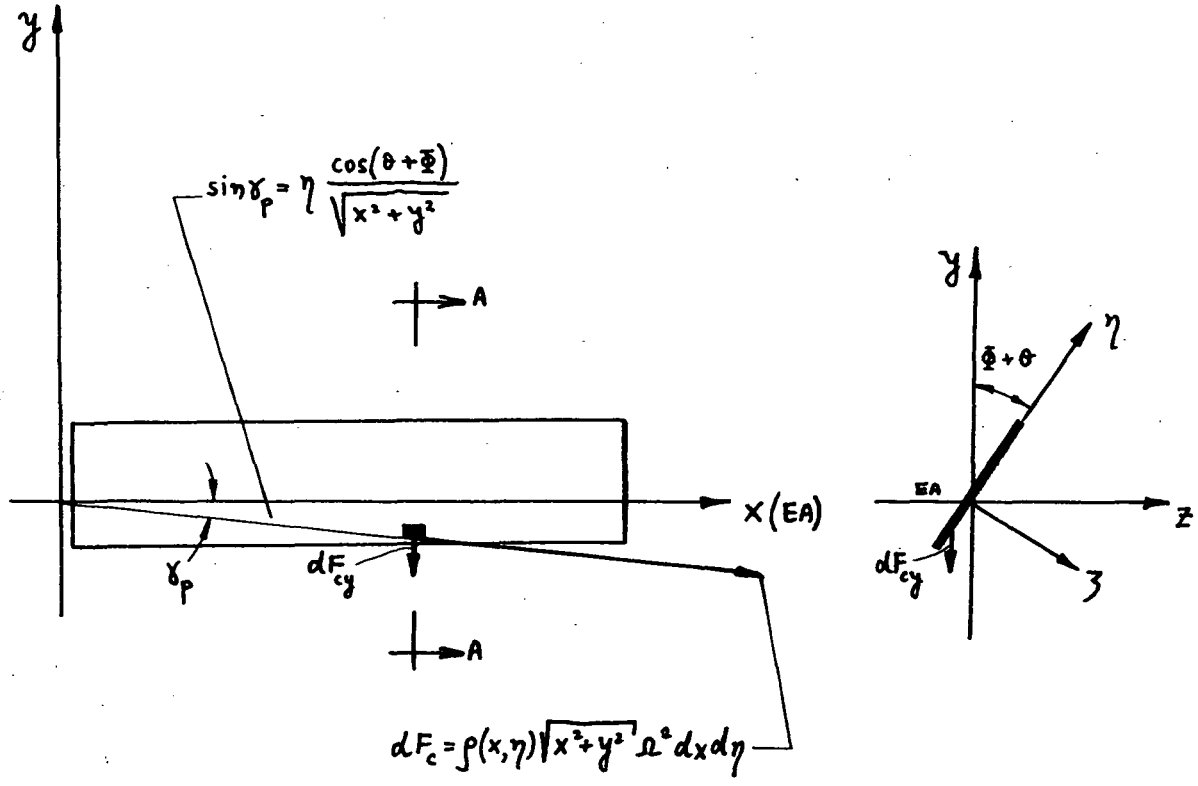

FIG. K.1 GEOMETRY FOR PROPELLER MOMENT EVALUATION

The geometry of the problem is shown in Fig. K.1; η is the chordwise coordinate (see Fig. 28).

Assume that the mass of the blade is compressed in a plate-like structure with $\rho(x,y)$ denoting the mass per unit area.

From the geometry, the centrifual force acting on an element of mass

is given by

$$dF = \rho(x,\eta)\sqrt{x^2+y^2}\ \Omega^2\, dx\, d\eta$$

Its component in the y-direction is

$$dF_{cy} = \sqrt{x^2+y^2}\ \Omega^2 \rho(x,\eta)\sin\gamma_p\, dx\, d\eta$$

$$= \rho(x,\eta)\,\eta\ \frac{\cos(\theta+\Phi)}{\sqrt{x^2+y^2}}\ \Omega^2\sqrt{x^2+y^2}\ dx\, d\eta$$

The propeller moment per unit length of the blade is given by

$$dM_{PROP} = -\int_{t.e}^{l.e} \rho(x,\eta)\,\eta^2\cos(\theta+\Phi)\sin(\theta+\Phi)\,\Omega^2\, d\eta\, dx$$

$$= -\int_{t.e}^{l.e} m\eta^2\cos(\theta+\Phi)\sin(\theta+\Phi)\, d\eta \qquad \text{(K.15)}$$

Using $$\int_{t.e}^{l.e} m\eta^2 d\eta = k_o^2 m + m x_I^2$$

and $$\cos(\theta+\Phi)\sin(\theta+\Phi) = (\cos\theta - \Phi\sin\theta)(\sin\theta + \Phi\cos\theta)$$

$$= \sin\theta\cos\theta - \Phi\sin^2\theta + \Phi\cos^2\theta - \Phi^2\sin\theta\cos\theta$$

$$dM_{PROP} = -m k_o^2\Omega^2\left[\sin\theta\cos\theta + \Phi\cos 2\theta\right]$$

$$- m x_I^2\left[\sin\theta\cos\theta + \Phi\cos 2\theta\right] \qquad \text{(K.16)}$$

Comparing Eqs. K.16 with the appropriate term in Eq. K.3, it can be seen that the last term of Eq. K.16 is included in Eq.3 while the first term of Eq. K.16 is missing and must be added to Eq. K.3.

APPENDIX L

THE ELASTIC COUPLING EFFECT

The elastic coupling effect is due to the angle of pitch setting θ which causes the bending perpendicular to the hub plane to be coupled with the bending parallel to the hub plane. In order to be able to represent the stiffness of the blade by rotating flap and lag frequencies, which is the usual practice in rotary wing-stability analyses, it is necessary to replace $\cos^2\theta$ by $(1 - \sin^2\theta)$ in Eq. 8.72. The appropriate expressions in Eqs. 8.72 can then be rewritten as

$$(EI)_y \cos^2\theta + (EI)_z \sin^2\theta = (EI)_y + \left[(EI)_z - (EI)_y\right] \sin^2\theta \qquad (L.1)$$

$$(EI)_y \sin^2\theta + (EI)_z \cos^2\theta = -\left[(EI)_z - (EI)_y\right] \sin^2\theta + (EI)_z \qquad (L.2)$$

It is convenient to define

$$E_{c1} = \left[(EI)_z - (EI)_y\right] \sin^2\theta \qquad (L.3)$$

and

$$E_{c2} = \left[(EI)_z - (EI)_y\right] \sin\theta\cos\theta \qquad (L.4)$$

When applying Galerkin's method in order to eliminate the spatial variable in the flap and lag equations, it is necessary to evaluate the following expressions

$$\overline{E}_{c2} = \frac{\frac{1}{\ell}\int_0^1 E_{c2}\, \gamma_1''\, \eta_1''\, d\bar{x}_0}{I_b \Omega^2} \qquad (L.5)$$

$$\overline{E}_{c1} = \frac{\frac{1}{\ell}\int_0^1 E_{c1} (\eta_1'')^2\, d\bar{x}_0}{I_b \Omega^2} = \frac{\frac{1}{\ell}\int_0^1 E_c (\gamma_1'')^2\, d\bar{x}_0}{I_b \Omega^2} \qquad (L.6)$$

Note that throughout this report it will always be assumed that the first elastic mode in flap is the same as in lag (i.e., $\gamma_1 = \eta_1$); thus Eq. L.6 is satisfied.

In rotary wing work, it is useful to express $\bar{E}_{c1}$, $\bar{E}_{c2}$ by rotating or nonrotating first flap and lag frequencies.

From elementary consideration

$$\frac{\frac{1}{\ell_o}\int_0^1 (EI)_y (\eta_1'')^2 d\bar{x}_o}{I_b \Omega^2} = \bar{\omega}_{FIN}^2 \bar{M}_{F1} \tag{L.7}$$

$$\frac{\frac{1}{\ell_o}\int_0^1 (EI)_z (\gamma_1'') d\bar{x}_o}{I_b \Omega^2} = \bar{\omega}_{LIN}^2 \bar{M}_{L1} \tag{L.8}$$

Using Eqs. L.7 and L.8, together with the relation $\gamma_1 = \eta_1$, Eqs. L.5 and L.6 can be rewritten as

$$\bar{E}_{c1} = \bar{M}_{F1} \sin^2\theta \left[\bar{\omega}_{LIN}^2 - \bar{\omega}_{FIN}^2\right] = \bar{M}_{L1} \sin^2\theta \left[\bar{\omega}_{LIN}^2 - \bar{\omega}_{FIN}^2\right] \tag{L.9}$$

$$\bar{E}_{c2} = \bar{M}_{F1} \sin\theta\cos\theta \left[\bar{\omega}_{LIN}^2 - \bar{\omega}_{FIN}^2\right] = \bar{M}_{L1} \sin\theta\cos\theta \left[\bar{\omega}_{LIN}^2 - \bar{\omega}_{FIN}^2\right] \tag{L.10}$$

In order to be consistent with the approach used in this report, Eqs. L.9 and L.10 must be expressed in terms of the rotating flap and lag frequencies of the blade. The rotating flap and lag frequencies of the blade will be calculated using Eqs. A.2 and A.4. The use of these equations implies that the rotating flap and lag frequencies of the beam are defined as those which would occur at a pitch setting of $\theta = 0$.

Equations A.2, A.4, L.7, and L.8 yield

$$\bar{\omega}_{FIN}^2 \bar{M}_{F1} + \frac{\ell_o^3 \int_0^1 (\eta_1')^2 \left(\int_{\bar{x}_o}^1 m(\bar{x}_1 + \bar{e}_1) d\bar{x}_o \right)}{I_b} = \bar{\omega}_{F1}^2 \bar{M}_{F1} \tag{L.11}$$

$$\bar{\omega}_{LIN}^2 \bar{M}_{L1} + \frac{\ell^3 \int_0^1 \left[\int_{\bar{x}_0}^1 m(\bar{x}_1 + \bar{e}_1) d\bar{x}_1 \right] (\gamma_1')^2 d\bar{x}_0}{I_b} - \bar{M}_{L1} = \bar{M}_{L1} \bar{\omega}_{L1}^2 \qquad \text{(L.12)}$$

With the assumption that $\gamma_1 = \eta_1$ and Eq. M.6, Eqs. L.11 and L.12 can be rewritten as:

$$\bar{\omega}_{FIN}^2 = \bar{\omega}_{F1}^2 - \frac{\bar{B}^6}{\bar{M}_{F1}} \qquad \text{(L.13)}$$

$$\bar{\omega}_{LIN}^2 = \bar{\omega}_{L1}^2 + 1 - \frac{\bar{B}^6}{\bar{M}_{L1}} \qquad \text{(L.14)}$$

Thus, Eqs. L.9, L.10, L.13, and L.14 finally yield

$$\bar{\omega}_{LIN}^2 - \bar{\omega}_{FIN}^2 = \bar{\omega}_{L1}^2 - \bar{\omega}_{F1}^2 + 1 \qquad \text{(L.15)}$$

and

$$\bar{E}_{C1} = \bar{M}_{F1} \sin^2\theta \left[\bar{\omega}_{L1}^2 - \bar{\omega}_{F1}^2 + 1 \right] = \bar{M}_{L1} \sin^2\theta \left[\bar{\omega}_{L1}^2 - \bar{\omega}_{F1}^2 + 1 \right] \qquad \text{(L.16)}$$

$$\bar{E}_{C2} = \bar{M}_{F1}^2 \sin\theta\cos\theta \left[\bar{\omega}_{L1}^2 - \bar{\omega}_{F1}^2 + 1 \right] = \bar{M}_{L1} \sin\theta\cos\theta \left[\bar{\omega}_{L1}^2 - \bar{\omega}_{F1}^2 + 1 \right] \qquad \text{(L.17)}$$

Using the approximation $\sin\theta \tilde{=} \theta$, $\cos\theta \tilde{=} 1$, the elastic coupling effect can be rewritten as

$$\bar{E}_{C1} = \bar{M}_{F1} \theta^2 \left(\bar{\omega}_{L1}^2 - \bar{\omega}_{F1}^2 + 1 \right) = \bar{M}_{L1} \theta^2 \left(\bar{\omega}_{L1}^2 - \bar{\omega}_{F1}^2 + 1 \right) \qquad \text{(L.18)}$$

$$\bar{E}_{C2} = \bar{M}_{F1} \theta \left(\bar{\omega}_{L1}^2 - \bar{\omega}_{F1}^2 + 1 \right) = \bar{M}_{L1} \theta \left(\bar{\omega}_{L1}^2 - \bar{\omega}_{F1}^2 + 1 \right) \qquad \text{(L.19)}$$

Finally, it is important to note that the treatment of the elastic coupling in this appendix implies the use of the so-called Southwell coefficient for rotating beam problems (Ref. 40). As pointed out by Bramwell in Ref. 20, this treatment can lead to considerable error, depdning upon the assumed mode shapes in the flap and lag degrees of freedom.

For the mode shape defined by Eq. 7.1, it can be shown that the present treatment of the elastic coupling is a good approximation for $\bar{\omega}_{F1} \geq 1.2$.

APPENDIX M

DEFINITION OF THE ADDITIONAL GENERALIZED MASS INTEGRALS AND INTEGRALS ENCOUNTERED IN THE AIRLOAD EVALUATION

In order to evaluate the various integrals required for the application of Galerkin's method on the flap and lag equations, various integrals which represent generalized masses must be considered. These expressions are defined in Eqs. M.1 through M.14 below. For the feathering equation, Galerkin's method is not used; still, spanwise integrals similar to those occurring in the flap and lag equations are encountered. These are defined in Eqs. M.14 through M.18 given below.

$$\bar{B}^1 = \frac{1}{I_b}\ell^3 \int_0^1 \left[\int_{\bar{x}_0}^1 m(\bar{x}_1 + \bar{e}_1)\, d\bar{x}_1 \right] \eta_1' \, d\bar{x}_0 \tag{M.1}$$

$$\bar{B}^2 = \frac{\ell^3}{I_b} \int_0^1 \left[\int_{\bar{x}_0}^1 m(\bar{x}_1 + \bar{e}_1)\, d\bar{x}_1 \right] \gamma_1' \eta_1' \, d\bar{x}_0 \tag{M.2}$$

$$\bar{B}^3 = \frac{\ell^3}{I_b} \int_0^1 \left(\int_{\bar{x}_0}^1 m \gamma_1 \, d\bar{x}_1 \right) \eta_1' \, d\bar{x}_0 \tag{M.3}$$

$$\bar{B}^4 = \frac{\ell^3}{I_b} \int_0^1 \left(\int_{\bar{x}_0}^1 m \eta_1 \, d\bar{x}_1 \right) \eta_1' \, d\bar{x}_0 \tag{M.4}$$

$$\bar{B}^5 = \frac{\ell^3}{I_b} \int_0^1 \left(\int_{\bar{x}_0}^1 m \bar{x}_1 \, d\bar{x}_1 \right) \eta_1' \, d\bar{x}_0 \tag{M.5}$$

$$\bar{B}^6 = \frac{\ell^3}{I_b} \int_0^1 \left(\int_{\bar{x}_0}^1 m \bar{x}_1 \, d\bar{x}_1 \right) (\eta_1')^2 \, dx_0 \tag{M.6}$$

$$\bar{B}^7 = \frac{\ell^3}{I_b} \int_0^1 m \gamma_1 \eta_1 \, d\bar{x}_0 \tag{M.7}$$

$$\overline{B}^{8} = \frac{\ell^3}{I_b} \int_0^1 \left(\int_{\bar{x}_0}^1 m \gamma_1 \, d\bar{x}_1 \right) \gamma_1' \, d\bar{x}_0 \qquad \text{(M.8)}$$

$$\overline{B}^{9} = \frac{\ell^3}{I_b} \int_0^1 \left(\int_{\bar{x}_0}^1 m \bar{x}_1 \, d\bar{x}_1 \right) (\gamma_1')^2 \, d\bar{x}_0 \qquad \text{(M.9)}$$

$$\overline{B}^{10} = \frac{\ell^3}{I_b} \int_0^1 \left(\int_{\bar{x}_0}^1 m (\bar{x}_1 + \bar{e}_1) \, d\bar{x}_1 \right) \gamma_1' \, d\bar{x}_0 \qquad \text{(M.10)}$$

$$\overline{B}^{11} = \frac{\ell^3}{I_b} \int_0^1 \bar{x}_0 m \gamma_1 \, d\bar{x}_0 \qquad \text{(M.11)}$$

$$\overline{B}^{12} = \frac{\ell^3}{I_b} \int_0^1 m \bar{x}_0 \eta_1 \, d\bar{x}_0 \qquad \text{(M.12)}$$

$$\overline{B}^{13} = \frac{\ell^3}{I_b} \int_0^1 m \eta_1 \, d\bar{x}_0 \qquad \text{(M.13)}$$

$$\overline{B}^{14} = \frac{\ell^3}{I_b} \int_0^1 m \bar{x}_0 \, d\bar{x}_0 \qquad \text{(M.14)}$$

$$\overline{B}^{15} = \frac{\ell^3}{I_b} \int_0^1 m \bar{x}_0 \left[\int_0^{\bar{x}_0} (\eta_1')^2 \, d\bar{x}_1 \right] d\bar{x}_0 \qquad \text{(M.15)}$$

$$\overline{B}^{16} = \frac{\ell^3}{I_b} \int_0^1 m \bar{x}_0 \left[\int_0^{\bar{x}_0} (\gamma_1')^2 \, d\bar{x}_1 \right] d\bar{x}_0 \qquad \text{(M.16)}$$

$$\overline{B}^{17} = \frac{\ell^3}{I_b} \int_0^1 m \eta_1 \left[\int_0^{\bar{x}_0} (\eta_1')^2 \, d\bar{x}_1 \right] d\bar{x}_0 \qquad \text{(M.17)}$$

$$\overline{B}^{18} = \frac{\ell^3}{I_b} \int_0^1 m \eta_1 \left[\int_0^{\bar{x}_0} (\gamma_1')^2 \, d\bar{x}_1 \right] d\bar{x}_0 \qquad \text{(M.18)}$$

The integrals due to the integrations of the airloads associated with the feathering equation are given below:

$$T^1 = \int_{\bar{A}}^{\bar{B}} \bar{x}^2 \, d\bar{x}_0 \qquad \text{(M.19)}$$

$$T^2 = \int_{\bar{A}}^{\bar{B}} \bar{x} \, d\bar{x}_0 \qquad \text{(M.20)}$$

$$T^3 = \int_{\bar{A}}^{\bar{B}} \bar{x}_0^2 \, \bar{x} \, d\bar{x}_0 \qquad \text{(M.21)}$$

APPENDIX N

QUANTITIES REQUIRED FOR THE CALCULATION OF THE STATIC EQUILIBRIUM POSITION AND DEFINITION OF THE FLUTTER DERIVATIVES

N.1 Quantities Required for the Calculation of the Static Equilibrium Position

The quantities associated with the calculation of the static equilibrium condition are defined below.

$$S_{11} = \overline{M}_{F1}\,\bar{\omega}_{F1}^{2} + \overline{E}_{C1} \tag{N.1}$$

$$S_{12} = -\overline{E}_{C2} \tag{N.2}$$

$$S_{13} = -\frac{\gamma}{2}\left(\frac{\ell}{R}\right)^{2} F' \tag{N.3}$$

$$S_{21} = -\overline{E}_{C2} \tag{N.4}$$

$$S_{22} = \overline{M}_{L1}\,\bar{\omega}_{L1}^{2} - \overline{E}_{C1} \tag{N.5}$$

$$S_{23} = \overline{B}'^{0}\beta_{P} - \overline{B}''\beta_{P} - \frac{\gamma}{2}\left(\frac{\ell}{R}\right)^{2}\lambda_{0}L' \tag{N.6}$$

$$S_{31} = -\overline{B}'^{2}\beta_{P}\theta - \frac{C_{d0}}{\alpha}F'\frac{\gamma}{2}\left(\frac{\ell}{R}\right)^{2} - \lambda_{0}\left(F^{2}\theta - \lambda_{0}F^{3}\right)\frac{\gamma}{2}\left(\frac{\ell}{R}\right)^{2} \tag{N.7}$$

$$S_{32} = -B''\left(\beta+\beta_{P}\right) + \frac{\gamma}{2}\left(\frac{\ell}{R}\right)^{2}L^{4}\theta - \frac{\gamma}{2}\left(\frac{\ell}{R}\right)^{2}L'\lambda_{0} - \beta\,\overline{e}_{1}\,\overline{C}_{1} \tag{N.8}$$

$$S_{33} = I\left(1+\bar{\omega}_o^2\right) - \beta_p\left(\beta+\beta_p\right) - \frac{\gamma}{2}\frac{\ell}{R}\, b\, \bar{X}_A\, T' + \frac{\gamma}{2}\left(\frac{\ell}{R}\right)^2 T^3 \beta_p \theta 2 - \frac{\gamma}{2}\left(\frac{\ell}{R}\right)^2 \lambda_o \beta_p T' 2 \qquad \text{(N.9)}$$

$$C_1 = -\bar{B}'\left(\beta+\beta_p\right) + \frac{\gamma}{2}\left(\frac{\ell}{R}\right)^2\left(F'\theta - F^2\lambda_o\right) \qquad \text{(N.10)}$$

$$C_2 = \bar{B}''\beta_p\theta - \bar{B}'^0\beta_p\theta + \frac{\gamma}{2}\left(\frac{\ell}{R}\right)^2\left\{\lambda_o\left[L'\theta - L^2\lambda_o\right] + \frac{C_{do}}{a}L^4\right\} \qquad \text{(N.11)}$$

$$C_3 = -I\theta + \beta_p\left(\beta+\beta_p\right)\theta + \frac{\gamma}{2}\frac{\ell}{R}\, b\, \bar{X}_A\left(T'\theta - T^2\lambda_o\right) - \frac{\gamma}{2}\left(\frac{\ell}{R}\right)^2\theta\beta_p\left[T^3\theta - T'\lambda_o\right] + \frac{\gamma}{2}\left(\frac{\ell}{R}\right)^2\left[\lambda_o\beta_p\left(\theta T' - \lambda_o T^2\right) + \frac{C_{do}}{a}T^3\beta_p\right] \qquad \text{(N.12)}$$

$$F_{SN} = \bar{B}^2 h_1^\circ \Phi_o \qquad \text{(N.13)}$$

$$L_{SN} = \bar{B}^7 g_1^\circ \Phi_o - \bar{B}^2 g_1^\circ \Phi_o \qquad \text{(N.14)}$$

$$T_{SN} = \bar{B}^7 h_1^\circ g_1^\circ + \bar{B}'^2 g_1^\circ \Phi_o\left(\beta+\beta_p\right) + \bar{M}_{F1}\left(g_1^\circ\right)^2\Phi_o - \bar{M}_{L1}\Phi_o\left(h_1^\circ\right)^2 - \frac{\gamma}{2}\left(\frac{\ell}{R}\right)^2 L^4 h_1^\circ \Phi_o + \bar{B}'^2\beta_p g_1^\circ\Phi_o - \frac{\gamma}{2}\left(\frac{\ell}{R}\right)^2 g_1^\circ\Phi_o\left(F'\theta - F^2\lambda_o\right) \qquad \text{(N.15)}$$

N.2 Definition of the Flutter Derivatives

In defining the flutter derivatives, it is important to note that some are due only to elastic or inertia forces, while others can be due to both aerodynamic and inertia forces. In order to be able to keep track of the relative importance of the aerodynamic and inertia effects, the flutter derivatives in which these effects combine, will be split into two parts; the aerodynamic part will be denoted by the superscript A and the inertia part by the superscript I.

The various flutter derivatives required for treating the flap equation are given below.

$$F_{\chi_2} = \frac{\bar{B}^7 \Phi_0}{\bar{M}_{F1}}$$

$$F^I_{\chi_2} = \frac{1}{\bar{M}_{F1}} \left[2 \bar{P}_{111} q_1^0 + 2 \bar{B}^3 (\beta + \beta_p) \right]$$

$$F^A_{\chi_2} = -\frac{\gamma}{2} \left(\frac{\ell}{R} \right)^3 \frac{1}{\bar{M}_{F1}} \left[2 F^{10} (\theta + \Phi_0) - \lambda_0 F^{11} - L^7 \Phi_0 \right] \qquad \text{(N.16)}$$

$$F_{\chi_2} = F^I_{\chi_2} + F^A_{\chi_2}$$

$$F_{\chi_2} = \frac{1}{\bar{M}_{F1}} \left(\bar{E}_{C2} + \bar{B}^2 \Phi_0 \right)$$

$$F_{\chi_1} = -\frac{\gamma}{2} \left(\frac{\ell}{R} \right)^3 \frac{F^8}{\bar{M}_{F1}}$$

$$F_{\chi_1} = \frac{\bar{E}_{C1}}{\bar{M}_{F1}}$$

$$F_{\dot{\varphi}}^{*} = \frac{\bar{B}^7 h_1^0}{\bar{M}_{F1}}$$

$$F_{\varphi}^{*} = \frac{\gamma}{2}\left(\frac{\ell}{R}\right)^2\left[\left(\frac{\ell}{R}\right)^2 L^7 h_1^0 - 2\frac{\ell}{R} F'\beta_P + \left(\frac{3}{2} - \bar{x}_A\right) bF^2\right]\frac{1}{\bar{M}_{F1}}$$

$$F_{\varphi}^{I} = \bar{B}^2 h_1^0 \frac{1}{\bar{M}_{F1}}$$

(N.16)

$$F_{\varphi}^{A} = \frac{\gamma}{2}\left(\frac{\ell}{R}\right)^2 \frac{F'}{\bar{M}_{F1}}$$

$$F_{\varphi} = F_{\varphi}^{I} + F_{\varphi}^{A}$$

$$\bar{g}_{D1} = \left(2\bar{\omega}_{F1}\eta_{SF1} - F_{\dot{x}_1}^{*}\right)$$

The various flutter derivatives required for treating the lag equation are given below.

$$L_{\dot{x}_1}^{*} = -\frac{\bar{B}^7 \Phi_0}{\bar{M}_{L1}}$$

$$L_{\dot{x}_1}^{I} = \left[-2\bar{B}^7(\beta+\beta_P) - 2(\bar{M}_\eta)_{111} g_1^0\right]\frac{1}{\bar{M}_{L1}}$$

(N.17)

$$L_{\dot{x}_1}^{A} = \frac{\gamma}{2}\left(\frac{\ell}{R}\right)^3\left[L^7(\theta+\Phi_0) - 2L^8\lambda_0\right]\frac{1}{\bar{M}_{L1}}$$

$$L_{\dot{x}_1}^{*} = L_{\dot{x}_1}^{I} + L_{\dot{x}_1}^{A}$$

$$L_{\chi_1} = \left(\bar{B}^7 \Phi_o + \bar{E}_{c2} - \bar{B}^2 \Phi_o \right) \frac{1}{\bar{M}_{L1}}$$

$$L^{I}_{\dot{\chi}_2} = 2 \bar{B}^8 \theta \beta_p \frac{1}{\bar{M}_{L1}}$$

$$L^{A}_{\dot{\chi}_2} = -\frac{\gamma}{2}\left(\frac{\ell}{R}\right)^3 \left[\lambda_o (\theta + \Phi_o) L^{13} + 2 \frac{C d_o}{a} L^{14} + L^{14} \theta \Phi_o \right] \frac{1}{\bar{M}_{L1}}$$

$$L_{\dot{\chi}_2} = L^{I}_{\dot{\chi}_2} + L^{A}_{\dot{\chi}_2}$$

$$L_{\chi_2} = \frac{\bar{E}_{c1}}{\bar{M}_{L1}}$$

$$L_{\dot{\varphi}} = \left(-\bar{B}^7 g_1^\circ - \bar{B}^{11} \beta_p \right) \frac{1}{\bar{M}_{L1}} \qquad \text{(N.17)}$$

$$L^{A}_{\dot{\varphi}} = -\frac{\gamma}{2}\left(\frac{\ell}{R}\right)^3 L^{14} \theta h_1^\circ \frac{1}{\bar{M}_{L1}} + \frac{\gamma}{2}\left(\frac{\ell}{R}\right)^2 \left(\frac{3}{2} - \bar{X}_A\right) \frac{b L^2 \lambda_o}{\bar{M}_{L1}}$$

$$L^{I}_{\varphi} = \left[-\bar{B}^2 g_1^\circ + \bar{B}^7 g_1^\circ - \bar{B}^{10} \beta_p + \bar{B}^{11} \beta_p \right] \frac{1}{\bar{M}_{L1}}$$

$$L^{A}_{\varphi} = \frac{\gamma}{2}\left(\frac{\ell}{R}\right)^2 \frac{\lambda_o L'}{\bar{M}_{L1}}$$

$$L_{\varphi} = L^{I}_{\varphi} + L^{A}_{\varphi}$$

$$\bar{g}_{D2} = 2 \bar{\omega}_{L1} \eta_{SL1} - L_{\dot{\chi}_2}$$

Finally, the flutter derivatives associated with the feathering equation are given below:

$$T_{\varphi}^{**} = -\bar{M}_{L1}\left(h_1^{\circ}\right)^2 - 2\bar{B}^{12}g_1^{\circ}\beta_P - \bar{M}_{F1}\left(g_1^{\circ}\right)^2 - \beta_P^2 \tag{N.18}$$

$$I_E = I - T_{\varphi}^{*} \tag{N.19}$$

$$T_{\varphi}^{I} = \bar{B}^{12}g_1^{\circ}\left(\beta+\beta_P\right) + \bar{M}_{F1}\left(g_1^{\circ}\right)^2 + \beta_P\left(\beta+\beta_P\right) + \bar{B}^{12}g_1^{\circ}\beta_P - \bar{M}_{L1}\left(h_1^{\circ}\right)^2 \tag{N.20}$$

$$T_{\varphi}^{A} = \frac{\gamma}{2}\frac{\ell}{R}b\bar{x}_A T' + \frac{\gamma}{2}\left(\frac{\ell}{R}\right)^2\left[-L^4 h_1^{\circ} - 2T^3\beta_P\theta + 2\lambda_o\beta_P T' + \lambda_o F^2 g_1^{\circ}\right] \tag{N.21}$$
$$- \frac{\gamma}{2}\left(\frac{\ell}{R}\right)^2\left(F'\theta - F^2\lambda_o\right)g_1^{\circ}$$

$$T_{\varphi} = T_{\varphi}^{I} + T_{\varphi}^{A} \tag{N.22}$$

$$K_E = I\left(1+\bar{\omega}_o^2\right) - T_{\varphi} \tag{N.23}$$

$$\bar{K}_E = \frac{K_E}{I_E} \tag{N.24}$$

$$T_{\ddot{x}_1}^{**} = \frac{1}{I_E}\left(\bar{B}^7 h_1^{\circ} + \bar{B}^{12}\beta_P\theta\right) \tag{N.25}$$

$$T_{\ddot{x}_1}^{*I} = \frac{2}{I_E}\left[-\bar{B}^{12}\beta_P\left(\beta+\beta_P\right) - \bar{B}^{15}\beta_P g_1^{\circ} - \bar{M}_{F1}g_1^{\circ}\left(\beta+\beta_P\right) - \bar{B}^{17}\left(g_1^{\circ}\right)^2\right] \tag{N.26}$$

$$T_{\ddot{x}_1}^{*A} = -\frac{1}{I_E}\frac{\gamma}{2}\left(\frac{\ell}{R}\right)^2 b\bar{x}_A F^2 + \frac{1}{I_E}\frac{\gamma}{2}\left(\frac{\ell}{R}\right)^3\left\{h_1^{\circ}L^7 + F'\beta_P\theta + \beta_P\left[F'\left(\theta+\Phi_o\right) - 2\lambda_o F^2\right]\right\} \tag{N.27}$$
$$+ \frac{\gamma}{2}\left(\frac{\ell}{R}\right)^2\frac{1}{I_E}\left\{\frac{1}{R}\beta_P\Phi_o F' + \left(\frac{\ell}{R}\right)g_1^{\circ}\Phi_o F^8 + \frac{\ell}{R}g_1^{\circ}\left[F^8\left(\theta+\Phi_o\right) - 2\lambda_o F^9\right]\right\}$$

$$T_{\chi_1}^{*} = T_{\chi_1}^{A} + T_{\chi_1}^{I} \tag{N.28}$$

$$T_{\chi_1}^{I} = \frac{1}{I_E}\left[\bar{B}^{7} h_1^{\circ} + \bar{B}^{12}\Phi_0(\beta+\beta_P) + \bar{M}_{F1}\, 2 g_1^{\circ}\Phi_0 + \bar{B}^{12}\beta_P(\theta+\Phi_0)\right] \tag{N.29}$$

$$T_{\chi_1}^{A} = \frac{1}{I_E}\frac{\gamma}{2}\left(\frac{\ell}{R}\right)^2\left\{\lambda_0\left[F^2(\theta+\Phi_0) - \lambda_0 F^3\right] + \frac{C_{d_0}}{a}F' - (F'\theta - F^2\lambda_0)\Phi_0\right\} \tag{N.30}$$

$$T_{\chi_1} = T_{\chi_1}^{I} + T_{\chi_1}^{A} \tag{N.31}$$

$$T_{\chi_2}^{*} = \frac{1}{I_E}\left(-\bar{B}^{11}\beta_P - \bar{B}^{7} g_1^{\circ}\right) \tag{N.32}$$

$$T_{\chi_2}^{I} = \frac{2}{I_E}\left(-\bar{B}^{16}\beta_P h_1^{\circ} - \bar{B}^{18} g_1^{\circ} h_1^{\circ}\right) \tag{N.33}$$

$$T_{\chi_2}^{A} = \frac{1}{I_E}\frac{\gamma}{2}\left(\frac{\ell}{R}\right)^2 b\,\bar{x}_A\left\{L'\Phi_0 - \left[2L'(\theta+\Phi_0) - L^2\lambda_0\right]\right\}$$

$$+\frac{1}{I_E}\frac{\gamma}{2}\left(\frac{\ell}{R}\right)^3\left\{\left[2(\theta+\Phi_0)L^{14} - \lambda_0 L^{13}\right]h_1^{\circ} - \left[\lambda_0(\theta+\Phi_0)L' + 2\frac{C_{d_0}}{a}L^4\right]\beta_P\right\} \tag{N.34}$$

$$-\frac{\chi}{2}\left(\frac{\ell}{R}\right)^2\frac{1}{I_E}\left\{\left[\lambda_0 F''(\theta+\Phi_0) + 2\frac{C_{d_0}}{a}F'^{0}\right]g_1^{\circ} + \frac{\ell}{R}\left(\beta_P\theta L^{14} + g_1^{\circ}\theta F^{10}\right)\Phi_0\right\}$$

$$T_{\chi_2}^{*} = T_{\chi_2}^{I} + T_{\chi_2}^{A} \tag{N.35}$$

$$T_{\chi_2}^{I} = \frac{1}{I_E}\left[\bar{B}^{11}(\beta+\beta_P) + \bar{B}^{7} g_1^{\circ} - 2\bar{M}_{L1} h_1^{\circ}\Phi_0 + \bar{e}_1\bar{C}_1\beta\right] \tag{N.36}$$

$$T_{\chi_2}^{A} = -\frac{1}{I_E}\frac{\gamma}{2}\left(\frac{\ell}{R}\right)^2\left[L^4\left(\theta+\Phi_0\right) - L^1\lambda_0 + L^{14}h_1\Phi_0\right] \tag{N.37}$$

$$T_{\chi_2} = T_{\chi_2}^{I} + T_{\chi_2}^{A} \tag{N.38}$$

$$T_{\varphi}^{*} = \frac{1}{I_E}\left\{\frac{\gamma}{2}\left(\frac{\ell}{R}\right)^2 b\bar{X}_A\left[L^1h_1^0 - 2T^1\beta_p\theta\right] + b^2\frac{\gamma}{2}\frac{\ell}{R}T^2\left(1-\bar{X}_A\right)\left(\bar{X}_A - .5\right)\right\} \tag{N.39}$$

$$+ \frac{\gamma}{2}\left(\frac{\ell}{R}\right)^2\frac{1}{I_E}\left\{\left(\frac{3}{2}-\bar{X}_A\right)b\left[-L^1h_1^0 - F^2g_1^0\Phi_0 - T^1\beta_p\theta\right.\right.$$

$$\left.\left. + \lambda_0\left(T^2\beta_p + F^3g_1^0\right) + \frac{\ell}{R}g_1^0\beta_p F^2\right] - \left(\beta_p\theta L^{14} + g_1^0\theta F^{10}\right)h_1^0 - L^{14}\left(h_1^0\right)^2\right\}$$

$$\bar{q}_{D3} = -T_{\varphi}^{*} \tag{N.40}$$

APPENDIX O

ALGEBRAIC EXPRESSIONS FOR THE VARIOUS QUANTITIES USED IN THE NONLINEAR EQUATIONS OF MOTION

$$T_{N\ddot{X}_1} = \frac{1}{I_E}\left(\bar{B}^7 X_2\right) \tag{O.1}$$

$$T_{N\ddot{X}_2} = -\frac{\bar{B}^7 X_1}{I_E} \tag{O.2}$$

$$T_{N\ddot{\varphi}} = \left[-\bar{M}_{L1}\left(X_2 2h_1^{\circ} + X_2^2\right) - 2\bar{B}^{12} X_1 \beta_p - \bar{M}_{F1}\left(2g_1^{\circ} X_1 + X_1^2\right)\right]\frac{1}{I_E} \tag{O.3}$$

$$F_{NL}\left(\ddot{X}_1, \ddot{X}_2, X_2, \varphi, \ddot{\varphi}\right) = \frac{1}{\bar{M}_{F1}}\left\{2\bar{B}^7 \ddot{X}_2 \ddot{\varphi} + X_2 \bar{B}^2 \varphi + 2\bar{P}_{111} X_1 \ddot{X}_2\right.$$

$$+ \frac{\varepsilon}{2}\left[-2\frac{\ell}{R} F^{10} \varphi \ddot{X}_2 + \left(\frac{\ell}{R}\right)^2 \theta F^{13}\left(\ddot{X}_2\right)^2 + \left(\frac{\ell}{R}\right)^2 \ddot{X}_1 \ddot{X}_2 F^{15} + \frac{\ell}{R} L^7\left(\ddot{X}_2 \varphi + \ddot{\varphi} X_2\right)\right]\left(\frac{\ell}{R}\right)^2$$

$$\left. + F_{NS}\right\} \tag{O.4}$$

$$L_{NL}\left(X_1, \ddot{X}_1, X_2, \ddot{X}_2, \varphi, \ddot{\varphi}\right) = \frac{1}{\bar{M}_{L1}}\left\{-\bar{B}^7 2\ddot{X}_1 \ddot{\varphi} + \bar{B}^7 X_1 \varphi - 2\left(\bar{M}_\eta\right)_{111} X_1 \ddot{X}_1\right.$$

$$-\bar{B}^2 X_1 \varphi + \frac{\varepsilon}{2}\left(\frac{\ell}{R}\right)^2\left[\frac{\ell}{R}\varphi \ddot{X}_1 L^7 - \frac{\ell}{R} L^{13} \lambda_0 \varphi \ddot{X}_2 - \frac{\ell}{R} L^{14}\theta\left(\ddot{X}_2 \varphi + X_2 \ddot{\varphi}\right)\right.$$

$$\left. - \left(\frac{\ell}{R}\right)^2 L^{19}\theta \ddot{X}_1 \ddot{X}_2 - \left(\frac{\ell}{R}\right)^2 L^{18}\left(\ddot{X}_1\right)^2 + \frac{\ell}{R}\left(\frac{3}{2} - \bar{X}_A\right) b L^8 \ddot{\varphi} \ddot{X}_1\right] + L_{SN}\left.\right\} \tag{O.5}$$

$$T_{NL}(x_1,\dot{x}_1^*,x_2,\dot{x}_2^*,\varphi,\dot{\varphi}^*) = \frac{1}{I_E}\Big\langle -\bar{M}_{L1}\,2\,x_2\,\dot{x}_2^*\,\dot{\varphi}^* - \bar{M}_{L1}\,h_1^o\,2\,\dot{x}_2^*\,\dot{\varphi}^* + \Big\{\bar{B}^{17}x_1x_2 + \bar{B}^{12}(x_1\varphi$$

$$- 2\,\dot{x}_1^*\dot{\varphi}^*)(\beta+\beta_P) + \bar{M}_{F1}\big[2g_1^o x_1\varphi + x_1^2\varphi + x_1^2\Phi_o - 2\dot{x}_1^*\dot{\varphi}^*(g_1^o + x_1)\big] + \bar{B}^{12}\beta_P x_1\varphi$$

$$- \bar{M}_{L1}h_1^o x_2\varphi - \bar{M}_{L1}x_2\big[x_2(\Phi_o+\varphi) + h_1^o\varphi\big]\Big\} - 2\Big\{\bar{B}^{15}\beta_P x_1\dot{x}_1^* + \bar{B}^{16}x_2\dot{x}_2^*\beta_P$$

$$+ \bar{M}_{F1}x_1\dot{x}_1^*(\beta+\beta_P) + \bar{B}^{17}2g_1^o x_1\dot{x}_1^* + x_1^2\dot{x}_1^*\bar{B}^{17} + \bar{B}^{18}\big[h_1^o x_1 + x_2(g_1^o+x_1)\big]\dot{x}_2^*\Big\}$$

$$+ \beta\bar{B}^{12}2\dot{x}_1^*\dot{\varphi}^* + \frac{\gamma}{2}\frac{\ell}{R}b\Big\{\bar{x}_A\Big[-\frac{\ell}{R}2L^1\varphi\dot{x}_2^* + \theta(\dot{x}_2^*)^2\Big(\frac{\ell}{R}\Big)^2L^{13} + \Big(\frac{\ell}{R}\Big)^2F^{11}\dot{x}_1^*\dot{x}_2^*$$

$$+ \frac{\ell}{R}L^1(\dot{x}_2^*\varphi + x_2\dot{\varphi}^*)\Big] + \Big[b(1-\bar{x}_A)(\bar{x}_A-0.5)\Big(-\frac{\ell}{R}L^2\dot{x}_2^*\dot{\varphi}^*\Big)\Big]\Big\}$$

$$- \frac{\gamma}{2}\Big(\frac{\ell}{R}\Big)^2\Big\{L^4\varphi x_2 - \Big(\frac{\ell}{R}\Big)L^7\dot{x}_1^*x_2 - \Big(\frac{\ell}{R}\Big)\Big[2(\theta+\Phi_o+\varphi)L^{14} - \lambda_o L^{13}\Big]x_2\dot{x}_2^*$$

$$- \frac{\ell}{R}2\varphi L^{14}h_1^o\dot{x}_2^*\Big\} + \frac{\gamma}{2}\Big(\frac{\ell}{R}\Big)^2\Big\{\frac{\ell}{R}\dot{x}_1^*\beta_P F^1\varphi - \frac{\ell}{R}\lambda_o\varphi\dot{x}_2^*L^1\beta_P + \lambda_o F^2\varphi x_1\Big\}$$

$$- \frac{\gamma}{2}\Big(\frac{\ell}{R}\Big)^2\Big\{\Big(\frac{3}{2}-\bar{x}_A\Big)bL^1x_2\dot{\varphi}^* + (F^1\theta - F^2\lambda_o)x_1\varphi + L^{14}h_1^o(\dot{x}_2^*\varphi + x_2\dot{\varphi}^*)$$

$$+ L^{14}x_2\big[\dot{x}_2^*(\varphi+\Phi_o) + (x_2+h_1^o)\dot{\varphi}^*\big] - \frac{\ell}{R}\beta_P F^1(\Phi_o+\varphi)\varphi\dot{x}_1^* - \frac{\ell}{R}\Big[g_1^o\dot{x}_1^*\varphi F^8$$

$$+ x_1\dot{x}_1^*F^8(\Phi_o+\varphi)\Big] + \frac{\ell}{R}\dot{x}_1^*\dot{x}_2^*(h_1^o+x_2)L^{19} + \Big(\frac{3}{2}-\bar{x}_A\Big)b\dot{\varphi}^*\big[F^2(g_1^o x_1$$

$$+ x_1\Phi_o + x_1\varphi) - \frac{\ell}{R}(h_1^o+x_2)\dot{x}_2^*L^{13} - \frac{\ell}{R}\beta_P\theta L^1\dot{x}_2^*\big]\Big\}$$

$$+ \frac{\gamma}{2}\Big(\frac{\ell}{R}\Big)^2\Big\{\frac{\ell}{R}\dot{x}_1^*g_1^o\varphi F^8 + \frac{\ell}{R}x_1\dot{x}_1^*\big[F^8(\theta+\Phi_o+\varphi) - 2\lambda_o F^9\big] - \frac{\ell}{R}\lambda_o F^{11}\varphi\dot{x}_2^*g_1^o$$

$$- \frac{\ell}{R}\Big[\lambda_o F^{11}(\theta+\Phi_o+\varphi) + 2\,\frac{c_{do}}{a}F^{10}\Big]x_1\dot{x}_2^* - \frac{\ell}{R}(\dot{x}_2^*\varphi + x_2\dot{\varphi}^*)\big[\beta_P\theta L^{14}$$

$$+ (g_1^o+x_1)\theta F^{10}\big] - \frac{\ell}{R}(\dot{x}_2^*\Phi_o + \dot{\varphi}^*h_1^o)x_1\theta F^{10} + \Big(\frac{3}{2}-\bar{x}_A\Big)b\dot{\varphi}^*\big[F^3\lambda_o x_1$$

$$+ \frac{\ell}{R}F^9x_1\dot{x}_1^*\big] - \frac{\ell}{R}\theta\dot{x}_1^*\dot{x}_2^*\big[\beta_P F^{10} + (g_1^o+x_1)L^{18}\big]\Big\} + T_{SN}\Big\rangle \qquad (0.6)$$

APPENDIX P

COEFFICIENTS OF THE CHARACTERISTIC EQUATION

The coefficients of the characteristic equation obtained by expanding Eq. 10.6 are given below. These coefficients were obtained by using the FORMAC algebraic manipulative system.

$$\vartheta_6 = - T_{\chi_1}^{**} L_{\varphi}^{**} F_{\chi_2}^{**} - L_{\chi_1}^{**} F_{\chi_2}^{**} - L_{\varphi}^{**} T_{\chi_2}^{**} - L_{\chi_1}^{**} F_{\varphi}^{**} T_{\chi_2}^{**} - F_{\varphi}^{**} T_{\chi_1}^{**} + 1 \tag{P.1}$$

$$\begin{aligned}\vartheta_5 = {} & \bar{q}_{D1} + \bar{q}_{D2} + \bar{q}_{D3} - L_{\varphi}^{**} T_{\chi_2}^{**} \bar{q}_{D1} - L_{\chi_1}^{**} \bar{q}_{D3} F_{\chi_2}^{**} - T_{\chi_1}^{*} L_{\varphi}^{**} F_{\chi_2}^{**} \\ & - T_{\chi_1}^{**} L_{\varphi}^{*} F_{\chi_2}^{**} - L_{\chi_1}^{*} F_{\chi_2}^{**} - T_{\chi_1}^{**} L_{\varphi}^{**} F_{\chi_2}^{*} - L_{\chi_1}^{**} F_{\chi_2}^{*} - L_{\varphi}^{*} T_{\chi_2}^{**} \\ & - L_{\chi_1}^{*} F_{\varphi}^{**} T_{\chi_2}^{**} - L_{\chi_1}^{**} F_{\varphi}^{*} T_{\chi_2}^{**} - L_{\varphi}^{**} T_{\chi_2}^{*} - L_{\chi_1}^{**} F_{\varphi}^{**} T_{\chi_2}^{*} \\ & - \bar{q}_{D2} F_{\varphi}^{**} T_{\chi_1}^{**} - F_{\varphi}^{*} T_{\chi_1}^{**} - F_{\varphi}^{**} T_{\chi_1}^{*}\end{aligned} \tag{P.2}$$

$$\begin{aligned}\vartheta_4 = {} & \bar{\omega}_{F1}^2 + F_{\chi_1} + \bar{K}_E - L_{\chi_2} + \bar{\omega}_{L1}^2 - L_{\varphi}^{*} T_{\chi_2}^{**} \bar{q}_{D1} - L_{\varphi}^{**} T_{\chi_2}^{*} \bar{q}_{D1} \\ & + \bar{q}_{D3} \bar{q}_{D1} + \bar{q}_{D2} \bar{q}_{D1} - L_{\varphi}^{**} T_{\chi_2}^{**} \bar{\omega}_{F1}^2 - L_{\varphi}^{**} T_{\chi_2}^{**} F_{\chi_1}\end{aligned}$$

$$- L_{\chi_1} \bar{g}_{D3} F_{\chi_2}^{**} - L_{\chi_1}^{**} \bar{K}_E F_{\chi_2}^{**} - T_{\chi_1} L_{\varphi}^{**} F_{\chi_2}^{**} - T_{\chi_1}^{*} L_{\varphi}^{*} F_{\chi_2}^{**}$$

$$- T_{\chi_1}^{**} L_{\varphi} F_{\chi_2}^{**} - L_{\chi_1} F_{\chi_2}^{**} - L_{\chi_1}^{**} \bar{g}_{D3} F_{\chi_2}^{*} - T_{\chi_1}^{*} L_{\varphi}^{**} F_{\chi_2}^{*}$$

$$- T_{\chi_1}^{**} L_{\varphi}^{*} F_{\chi_2}^{*} - L_{\chi_1}^{*} F_{\chi_2}^{*} - T_{\chi_1}^{**} L_{\varphi}^{**} F_{\chi_2} - L_{\chi_1}^{**} F_{\chi_2} - L_{\varphi} T_{\chi_2}^{**}$$

$$- L_{\chi_1} T_{\varphi}^{**} T_{\chi_2}^{**} - L_{\chi_1}^{*} F_{\varphi}^{*} T_{\chi_2}^{**} - L_{\chi_1}^{**} F_{\varphi} T_{\chi_2}^{**} - L_{\varphi}^{*} T_{\chi_2}^{*}$$

$$- L_{\chi_1}^{*} F_{\varphi}^{**} T_{\chi_2}^{*} - L_{\chi_1}^{**} F_{\varphi}^{*} T_{\chi_2}^{*} - L_{\varphi}^{**} T_{\chi_2} - L_{\chi_1}^{**} F_{\varphi}^{**} T_{\chi_2}$$

$$+ \bar{g}_{D2} \bar{g}_{D3} + F_{\varphi}^{**} T_{\chi_1}^{**} L_{\chi_2} - \bar{\omega}_{L1}^{2} F_{\varphi}^{**} T_{\chi_1}^{**} - \bar{g}_{D2} F_{\varphi}^{*} T_{\chi_1}^{**}$$

$$- F_{\varphi} T_{\chi_1}^{**} - \bar{g}_{D2} F_{\varphi}^{**} T_{\chi_1}^{*} - F_{\varphi}^{*} T_{\chi_1}^{*} - F_{\varphi}^{**} T_{\chi_1} \qquad \text{(P.3)}$$

$$\vartheta_3 = - L_{\varphi} T_{\chi_2}^{**} \bar{g}_{D1} - L_{\varphi}^{*} T_{\chi_2}^{*} \bar{g}_{D1} - L_{\varphi}^{**} T_{\chi_2} \bar{g}_{D1} + \bar{g}_{D1} \bar{g}_{D2} \bar{g}_{D3}$$

$$+ \bar{K}_E \bar{g}_{D1} - L_{\chi_2} \bar{g}_{D1} + \bar{\omega}_{L1}^{2} \bar{g}_{D1} - L_{\varphi}^{*} T_{\chi_2}^{**} \bar{\omega}_{F1}^{2}$$

$$- L_{\varphi}^{**} T_{\chi_2}^{*} \bar{\omega}_{F1}^{2} + \bar{g}_{D3} \bar{\omega}_{F1}^{2} + \bar{g}_{D2} \bar{\omega}_{F1}^{2} - L_{\varphi}^{*} T_{\chi_2}^{**} F_{\chi_1}$$

$$- L_{\varphi}^{**} T_{\chi_2}^{*} F_{\chi_1} + \bar{g}_{D3} F_{\chi_1} + \bar{g}_{D2} F_{\chi_1} - L_{\chi_1} \bar{g}_{D3} F_{\chi_2}^{**}$$

$$- L_{\chi_1}^{*} \bar{K}_E F_{\chi_2}^{**} - T_{\chi_1} L_{\varphi}^{*} F_{\chi_2}^{**} - T_{\chi_1}^{*} L_{\varphi} F_{\chi_2}^{**} - L_{\chi_1}^{*} \bar{g}_{D3} F_{\chi_2}^{*}$$

$$- L_{\chi_1}^{**} \bar{K}_E F_{\chi_2}^{*} - T_{\chi_1} L_{\varphi}^{**} F_{\chi_2}^{*} - T_{\chi_1}^{*} L_{\varphi}^{*} F_{\chi_2}^{*} - T_{\chi_1}^{**} L_{\varphi} F_{\chi_2}^{*}$$

$$- L_{\chi_1} F_{\chi_2}^{*} - L_{\chi_1}^{**} \bar{g}_{D3} F_{\chi_2} - T_{\chi_1}^{*} L_{\varphi}^{**} F_{\chi_2} - T_{\chi_1}^{**} L_{\varphi}^{*} F_{\chi_2}$$

$$- L_{\chi_1}^{*} F_{\chi_2} - L_{\chi_1} F_{\varphi}^{*} T_{\chi_2}^{**} - L_{\chi_1}^{*} F_{\varphi} T_{\chi_2}^{**} - L_{\varphi} T_{\chi_2}^{*} - L_{\chi_1} F_{\varphi}^{**} T_{\chi_2}^{*}$$

$$- L_{\chi_1}^{*} F_{\varphi}^{*} T_{\chi_2}^{*} - L_{\chi_1}^{**} F_{\varphi} T_{\chi_2}^{*} - L_{\varphi}^{*} T_{\chi_2} - L_{\chi_1}^{*} F_{\varphi}^{**} T_{\chi_2}$$

$$- L_{\chi_1}^{**} F_{\varphi}^{*} T_{\chi_2} - L_{\chi_2} \bar{g}_{D3} + \bar{\omega}_{L1}^{2} \bar{g}_{D3} + \bar{g}_{D2} \bar{K}_E + F_{\varphi}^{**} T_{\chi_1}^{*} L_{\chi_2}$$

$$+ F_{\varphi}^{**} T_{\chi_1}^{*} L_{\chi_2} - \bar{\omega}_{L1}^{2} F_{\varphi}^{*} T_{\chi_1}^{**} - \bar{g}_{D2} F_{\varphi} T_{\chi_1}^{**} - \bar{\omega}_{L1}^{2} F_{\varphi}^{**} T_{\chi_1}^{*}$$

$$- \bar{g}_{D2} F_{\varphi}^{*} T_{\chi_1}^{*} - F_{\varphi} T_{\chi_1}^{*} - \bar{g}_{D2} F_{\varphi}^{**} T_{\chi_1} - F_{\varphi}^{*} T_{\chi_1} \qquad \text{(P.4)}$$

$$\nu_2 = - L_P T_{\chi_2}^{*} \bar{g}_{D1} - L_{\varphi}^{*} T_{\chi_2} \bar{g}_{D1} - L_{\chi_2} \bar{g}_{D3} \bar{g}_{D1} + \bar{\omega}_{L1}^{2} \bar{g}_{D3} \bar{g}_{D1}$$

$$+ \bar{g}_{D2} \bar{K}_E \bar{g}_{D1} - L_{\varphi} T_{\chi_2}^{**} \bar{\omega}_{F1}^{2} - L_{\varphi}^{*} T_{\chi_2}^{*} \bar{\omega}_{F1}^{2} - L_{\varphi}^{**} T_{\chi_2} \bar{\omega}_{F1}^{2}$$

$$+ \bar{g}_{D2} \bar{g}_{D3} \bar{\omega}_{F1}^{2} + \bar{K}_E \bar{\omega}_{F1}^{2} - L_{\chi_2} \bar{\omega}_{F1}^{2} + \bar{\omega}_{F1}^{2} \bar{\omega}_{L1}^{2} - L_{\varphi} T_{\chi_2}^{**} F_{\chi_1}$$

$$- L_{\dot{\varphi}}^{*} T_{\dot{\chi}_2}^{*} F_{\chi_1} - L_{\dot{\varphi}}^{**} T_{\chi_2} F_{\chi_1} + \bar{g}_{D2} \bar{g}_{D3} F_{\chi_1} + \bar{K}_E F_{\chi_1} - L_{\chi_2} F_{\chi_1}$$

$$+ \bar{\omega}_{L1}^2 F_{\chi_1} - L_{\chi_1} \bar{K}_E F_{\dot{\chi}_2}^{**} - T_{\chi_1} L_{\varphi} F_{\dot{\chi}_2}^{**} - L_{\chi_1} \bar{g}_{D3} F_{\dot{\chi}_2}^{*}$$

$$- L_{\dot{\chi}_1}^{*} \bar{K}_E F_{\dot{\chi}_2}^{*} - T_{\chi_1} L_{\dot{\varphi}}^{*} F_{\dot{\chi}_2}^{*} - T_{\dot{\chi}_1}^{*} L_{\varphi} F_{\dot{\chi}_2}^{*} - L_{\dot{\chi}_1}^{*} \bar{g}_{D3} F_{\chi_2}$$

$$- L_{\dot{\chi}_1}^{**} \bar{K}_E F_{\chi_2} - T_{\chi_1} L_{\dot{\varphi}}^{**} F_{\chi_2} - T_{\dot{\chi}_1}^{*} L_{\dot{\varphi}}^{*} F_{\chi_2} - T_{\dot{\chi}_1}^{**} L_{\varphi} F_{\chi_2}$$

$$- L_{\chi_1} F_{\chi_2} - L_{\chi_1} F_{\varphi} T_{\dot{\chi}_2}^{**} - L_{\chi_1} F_{\dot{\varphi}}^{*} T_{\dot{\chi}_2}^{*} - L_{\dot{\chi}_1}^{*} F_{\varphi} T_{\dot{\chi}_2}^{*} - L_{\varphi} T_{\chi_2}$$

$$- L_{\chi_1} F_{\dot{\varphi}}^{**} T_{\chi_2} - L_{\dot{\chi}_1}^{*} F_{\varphi} T_{\chi_2} - L_{\dot{\chi}_1}^{**} F_{\varphi} T_{\chi_2} - L_{\chi_2} \bar{K}_E + \bar{K}_E \bar{\omega}_{L1}^2$$

$$+ F_{\varphi} T_{\dot{\chi}_1}^{**} L_{\chi_2} + F_{\dot{\varphi}}^{*} T_{\dot{\chi}_1}^{*} L_{\chi_2} + F_{\dot{\varphi}}^{**} T_{\chi_1} L_{\chi_2} - \bar{\omega}_{L1}^2 F_{\varphi} T_{\dot{\chi}_1}^{**}$$

$$- \bar{\omega}_{L1}^2 F_{\dot{\varphi}}^{*} T_{\dot{\chi}_1}^{*} - \bar{g}_{D2} F_{\varphi} T_{\dot{\chi}_1}^{*} - \bar{\omega}_{L1}^2 F_{\dot{\varphi}}^{**} T_{\chi_1} - \bar{g}_{D2} F_{\dot{\varphi}}^{*} T_{\chi_1}$$

$$- F_{\varphi} T_{\chi_1} \qquad \text{(P.5)}$$

$$\nu_1 = - L_{\varphi} T_{\chi_2} \bar{g}_{D1} - L_{\chi_2} \bar{K}_E \bar{g}_{D1} + \bar{\omega}_{L1}^2 \bar{K}_E \bar{g}_{D1} - L_{\varphi} T_{\dot{\chi}_2}^{*} \bar{\omega}_{F1}^2$$

$$- L_{\dot{\varphi}}^{*} T_{\chi_2} \bar{\omega}_{F1}^2 - L_{\chi_2} \bar{g}_{D3} \bar{\omega}_{F1}^2 + \bar{\omega}_{L1}^2 \bar{g}_{D3} \bar{\omega}_{F1}^2 + \bar{g}_{D2} K_E \bar{\omega}_{F1}^2$$

$$- L_\varphi T^*_{\chi_2} F_{\chi_1} - L_\varphi T_{\chi_2} F_{\chi_1} - L_{\chi_2} \bar{g}_{D3} F_{\chi_1} + \bar{\omega}^2_{L1} g_{D3} F_{\chi_1}$$

$$+ \bar{g}_{D2} \bar{K}_E F_{\chi_1} - L_{\chi_1} \bar{K}_E F^*_{\chi_2} - T_{\chi_1} L_\varphi F^*_{\chi_2} - L_{\chi_1} \bar{g}_{D3} F_{\chi_2}$$

$$- L^*_{\chi_1} \bar{K}_E F_{\chi_2} - T_{\chi_1} L^*_\varphi F_{\chi_2} - T^*_{\chi_1} L_\varphi F_{\chi_2} - L_{\chi_1} F_\varphi T^*_{\chi_2}$$

$$- L_{\chi_1} F^*_\varphi T_{\chi_2} - L^*_{\chi_1} F_\varphi T_{\chi_2} + F_\varphi T^*_{\chi_1} L_{\chi_2} + F^*_\varphi T_{\chi_1} L_{\chi_2}$$

(P.6)

$$- \bar{\omega}^2_{L1} F_\varphi T^*_{\chi_1} - \bar{g}_{D2} F_\varphi T_{\chi_1} - \bar{\omega}^2_{L1} F^*_\varphi T_{\chi_1}$$

$$\vartheta_0 = - L_\varphi T_{\chi_2} \bar{\omega}^2_{F1} - L_{\chi_2} \bar{K}_E \bar{\omega}^2_{F1} + \bar{\omega}^2_{L1} \bar{K}_E \bar{\omega}^2_{F1} - L_\varphi T_{\chi_2} F_{\chi_1}$$

$$- L_{\chi_2} \bar{K}_E F_{\chi_1} + \bar{\omega}^2_{L1} \bar{K}_E F_{\chi_1} - L_{\chi_1} \bar{K}_E F_{\chi_2} - T_{\chi_1} L_\varphi F_{\chi_2}$$

(P.7)

$$- L_{\chi_1} F_\varphi T_{\chi_2} + F_\varphi T_{\chi_1} L_{\chi_2} - \bar{\omega}^2_{L1} F_\varphi T_{\chi_1}$$

APPENDIX R

EVALUATION OF THE EXACT DIVERGENCE BOUNDARY IN FLAP-PITCH

The exact divergence boundary can be obtained from Eq. 9.22 after suppressing the lag degree of freedom by taking $h_1^o = 0$.

Then from the first of Eqs. 9.22:

$$g_1^o = \left(C_1 \quad S_{13}\,\Phi_o\right)\frac{1}{S_{11}} \tag{R.1}$$

From the last of Eqs. 9.22

$$S_{31}\left(C_1 - S_{13}\,\Phi_o\right)\frac{1}{S_{11}} + S_{33}\,\Phi_o = T_{SN} + C_3 \tag{R.2}$$

Using Eqs. N.15 and R.2, one obtains, after some algebraic manipulation, a third-order polynomial for Φ_o. Thus

$$\left(\frac{1}{S_{11}^2}\,S_{13}^2\,\bar{M}_{F1}\right)\Phi_o^3 - \frac{1}{S_{11}}\,S_{13}\left(i_3 + \frac{C_1}{S_{11}}\,\bar{M}_{F1}\right)\Phi_o^2$$

$$+\left[\left(\frac{C_1 i_3 + S_{13}\,S_{31}}{S_{11}}\right) - S_{33}\right]\Phi_o + \left(C_3 - \frac{S_{31}}{S_{11}}\,C_1\right) = 0 \tag{R.3}$$

where

$$i_3 = \bar{B}^{12}\left(\beta + \beta_p\right) + \frac{\gamma}{2}\left(\frac{\ell}{R}\right)^2 F^2 \lambda_o + \bar{B}^{12}\beta_p + \frac{\bar{M}_{F1}\,C_1}{S_{11}} \tag{R.4}$$

Equation R.3 can be easily solved using Subroutine DPRQD available in the IBM Scientific Subroutine Package. Thus, Φ_o, g_1^o are known. The exact divergence boundary is obtained from Eq. 10.4, and can be written as

$$\nu_o = 0 = S_{11}\left(S_{33} - \frac{\partial T_{SN}}{\partial \Phi_o}\right) - S_{13}\left(S_{31} - \frac{\partial T_{SN}}{\partial g_1^o}\right) \tag{R.5}$$